DELAYING SHEAR STRENGTH DECAY IN REINFORCED CONCRETE FLEXURAL MEMBERS UNDER LARGE LOAD REVERSALS

by

Charles F. Scribner

James K. Wight

Report on Research Conducted under Grant
No. ENV75-13900 from the National Science Foundation

Report UMEE 78R2
Department of Civil Engineering
The University of Michigan
Ann Arbor, MI 48109

May 1978

Any opinions, findings, conclusions or recommendations expressed in this publication are those of the author(s) and do not necessarily reflect the views of the National Science Foundation.

ABSTRACT

Eight half-size and four full-size T-shaped reinforced concrete exterior beam-column subassemblies were tested to determine the effect of intermediate longitudinal shear reinforcement on the hysteretic behavior of flexural members subjected to repeated reversed loading. Specimens were tested by appyling a constant axial load to the fixed column portion of the specimen and applying a cyclic shear load to the beam. The beam typical loading history was chosen to simulate the disortion which might take place at a typical connection in a ductile moment-resisting frame during a severe earthquake.

Specimens were designed with a variety of longitudinal beam reinforcement and tested using four different shear spans such that maximum shear stresses varied from 2 $\sqrt{f'_c}$ to 6 $\sqrt{f'_c}$. Half the specimens contained beam web reinforcement as specified by seismic provisions of the ACI Building Code (318-71) and half the specimens contained two layers of intermediate longitudinal shear reinforcement in addition to the Code-specified ties.

Several conclusions were drawn on the basis of test results. The repeatability of member hysteretic behavior was related to maximum beam shear stress. Intermediate longitudinal shear reinforcement provided significant

increases in member energy dissipation and repeatability of hysteretic response for beams with shear stresses between 3 $\sqrt{f'_c}$ and 6 $\sqrt{f'_c}$. Beams with shear stresses below this range performed satisfactorily without intermediate longitudinal shear reinforcement and beams with shear stresses higher than 6 $\sqrt{f'_c}$ did not perform totally satisfactorily, regardless of the type of shear reinforcement used.

Buckling of compression reinforcement was found to be a significant factor in the loss of load-carrying capacity for more than half the specimens tested. It was found that stirrup size and strength were more important than stirrup spacing in preventing the buckling of longitudinal reinforcement.

ACKNOWLEDGMENTS

This report was submitted by Dr. Scribner to The University of Michigan in partial fulfillment of the requirements for the degree Doctor of Philosophy (Civil Engineering). Professor Wight provided guidance and assistance throughout this investigation as chairman of the doctoral committee. The authors would like to thank Professor William J. Anderson, Glen V. Berg, Robert D. Hanson and Frank E. Richart, Jr. (members of his doctoral committee) for reviewing the report and offering helpful suggestions.

The authors would like to thank technicians George Geisendorfer, Harold Chalmers, and Lou North for the technical assistance they provided in solving a variety of problems associated with testing of the specimens, and fellow graduate student Martin E. Batts for his help in testing.

Dr. Scribner would also like to thank his fiancee, Ms. Susan J. Walker, and his minister, Rev. Ronald Cary, for the encouragement they gave him during his work on this project.

This investigation was supported by Horace H. Rackham School of Graduate Studies Grant FRR-387098, the Department of Civil Engineering, and National Science Foundation Grant ENV75-13900. The conclusions arrived at in this paper are solely those of the author and do not necessarily represent the views of any of the sponsors.

PREFACE

It is suggested that the reader be selective in choosing which chapters to read, depending on the depth of his interest in this subject. A general understanding of the work can be obtained by considering only Chapter 6 or Chapters 1 and 6. Those interested in a more specific explanation of the details of specimen fabrication and testing are advised to read Chapter 2 as well.

A detailed explanation and discussion of the mathematical aspects of test findings is contained in Chapter 5. Those interested in this aspect of the study may also wish to read Chapter 4, which discusses the calculation of various important relationships.

Chapter 3 contains a detailed description of the manner of deterioration of all specimens. Because of the depth of detail which it contains, it is suggested that only the most avid reader consider this chapter.

The term "beam-column joint" is intended to refer to a beam-to-column joint, rather than to a joint in a beam-column member. This terminology has been used because of the precedent established in previous reports discussing this subject.

TABLE OF CONTENTS

TABLE OF CONTENTS (CONT'D)

LIST OF TABLES

LIST OF TABLES (CONT'D)

LIST OF ILLUSTRATIONS

LIST OF ILLUSTRATIONS (CONT'D)

LIST OF ILLUSTRATIONS (CONT'D)

LIST OF ILLUSTRATIONS (CONT'D)

LIST OF ILLUSTRATIONS (CONT'D)

LIST OF ILLUSTRATIONS (CONT'D)

LIST OF ILLUSTRATIONS (CONT'D)

LIST OF APPENDICES

NOTATION

a = the beam shear span used in testing, measured from the face of the column to the point of loading ram attachment (in.)

A_b = the area of a reinforcing bar (sq. in.)

A_{cv} = the net beam-column joint area resisting input shear forces = $b' \cdot d_e$ (sq. in.)

A_g = gross cross-sectional area of column (sq. in.)

A_i = total area of intermediate longitudinal beam reinforcement (sq. in.)

A_s = area of tension reinforcement (sq. in.)

A_s' = area of compression reinforcement (sq. in.)

A_v = area of vertical web reinforcement within a distance s (sq. in.)

A_{vi} = area of supplementary web reinforcement within a distance s (sq. in.)

b = overall beam or column width (in.)

$b'=b_c$ = width of beam or beam-column joint measured to outside of ties (in.)

C_1 = a constant relating R_u, the coefficient of flexural resistance, to the ρ/ρ_{bal} ratio

d = effective beam depth measured from extreme compression fiber to the centroid of tension reinforcement (in.)

d' = distance from extreme compression fiber to the centroid of compression reinforcement (in.)

d_b = nominal diameter of reinforcing bar (in.)

d_c = depth of beam measured to outside of ties (in.)

d_e = effective depth of beam-column joint resisting shear, measured from one face of the column to the centroid of column longitudinal reinforcement near the opposite face of the column (in.)

d_1, d_2 = distance from extreme compression fiber to centroid of layers of intermediate longitudinal reinforcement (in.)

E = total energy dissipated by a specimen during testing divided by the energy dissipated during the first inelastic cycle

E_c = initial slope of concrete stress vs. strain curve (psi.)

E_s = modulus of elasticity of steel (psi.)

E_{sh} = initial slope of steel stress vs. strain curve during strain hardening (psi.)

f'_c = specified compressive strength of concrete (psi.)

f_h = tensile stress developed by a standard hook (psi)

f_y = tensile yield stress of reinforcing steel (psi.)

G_c = shear modulus of concrete (psi.)

h = overall depth of beam portion of specimen (in.)

I'_w = modified work index = $\Sigma(P_n/P_y \times \frac{\Delta n}{\Delta y})(1 - d_c/a)$

L = length of column section held between simple supports (in.)

ℓ' = length between beam hinging zone and point of load ram attachment (in.)

L_b = total length of beam portion of specimen (in.)

L_i = total length between points of attachment of ith LVDT (in.)

ℓ_s = minimum straight lead embedment length from critical section to beginning of bar hook (in.)

M_{bal} = moment capacity of column section at balanced axial load (in-kips)

M_{col} = moment capacity of column section for axial load used during test (in-kips)

M_u = ultimate moment capacity of a section (in-kips)

n = the number of ties to be used to satisfy shear strength requirements in a beam-column joint

N_u = gross column axial load (lbs.)

P_a = column axial load used during testing (lbs.)

P_n = maximum beam shear load in nth cycle of loading (lbs.)

P_y = beam load at yield of main longitudinal reinforcement (lbs.)

r^2 = the ratio of explained variation to total variation for statistical regression

R_u = coefficient of flexural resistance for beam section (psi.)

s = spacing of web reinforcement (in.)

T_s = tension force in beam tension reinforcement at beam-column joint (lbs.)

V = measured shear force in beam (lbs.)

v_c = shear stress carried by concrete at any beam or column cross section (psi.)

V_{col} = gross shear force in column (lbs.)

v_j = nominal beam-column joint shear stress

V_m = maximum shear force in a member (lbs.)

V_s = shear force which can be considered to be carried by web reinforcement in a member (lbs.)

V_u = ultimate shear force in a member (lbs.)

v_u = ultimate shear stress at any cross section of beam or column (psi.)

v'_u = ultimate beam shear stress acting over beam core area (psi.) = $V_u/b_c d_c$

α = maximum beam shear stress measured in the first quarter-cycle of inelastic loading, as a multiple of $\sqrt{f'_c}$

= stress multiplication factor to account for strain hardening in steel strained past yield (as used in Appendix C only)

β = joint type correction factor = 1.0 for Type 2 joint

γ = joint classification correction factor = 1.0 for joints considered in this research project

γ_1 = elastic shear strain between beam hinging zone and point of loading ram attachment (deg.)

Δ_1 = deflection of beam load point due to flexural rotation in beam hinging zone (in.)

Δ_2 = deflection of beam load point due to shear deformation in beam hinging zone (in.)

Δ_3 = deflection of beam load point due to flexural deformation between the beam hinging zone and the load point (in.)

Δ_4 = deflection of beam load point due to shear deformation between the beam hinging zone and the load point (in.)

Δ_5 = deflection of beam load point due to rigid body rotation of beam-column joint (in.)

Δ_6 = indicated deflection of beam load point resulting from deformation of the test frame used to hold specimen (in.)

Δ_n = maximum deflection of beam load point in nth cycle of loading (in.)

Δ_y = deflection of beam load point at yield of main longitudinal reinforcement (in.)

ε_c = compressive strain of concrete at any selected point (in./in.)

ε_{sh} = strain in steel at the beginning of strain hardening (in./in.)

ε_y = strain in steel at the beginning of yield (in./in.)

θ_3 = the angle of overall shear strain within the beam hinging zone (deg.)

θ_4 = the angle of flexural rotation of a beam section at the end of the beam hinging zone nearest the point of loading ram attachment (deg.)

ρ = area ratio of non prestressed tension reinforcement, A_s/bd

ρ_v = area ratio of web reinforcement, A_v/bs

ϕ = capacity reduction factor = 0.85 for shear

ψ = anchorage effectiveness coefficient (taken as 1.0 for all specimens)

CHAPTER 1

INTRODUCTION

1.1 General

Of all the dynamic loads which the structural engineer must consider in design, earthquake loads are the most complex and unpredictable. Because it is generally impossible or economically impractical to design all members in a frame structure to resist earthquake loads elastically, repeated inelastic flexure within some members must be anticipated. Present building codes (1, 21, 36) recognize this necessity and attempt to deal with the problem in two ways. First, to minimize the severity of possible structural damage, a "strong column - weak beam" design philosophy is endorsed which should insure that most inelastic flexural rotations take place in beams and girders rather than in columns or beam-column joints. Second, an attempt is made to insure stable hysteretic behavior by requiring increased web reinforcement in areas of the beams and girders which are likely to undergo inelastic flexure.

Recent tests of a variety of beams and beam-column subassemblies have shown that members may suffer severe shear stiffness decay and loss of energy dissipation capacity during repeated reversed inelastic loading, even

though they are reinforced in accordance with modern seismic codes. The purpose of this investigation was to study a method of reinforcement to improve the stability of response of reinforced concrete flexural members subjected to repeated reversed loading.

1.2 Review of Related Research

Burns and Siess (10, 11) were among the first researchers to consider the problem of repeated inelastic flexure of concrete members. Their tests demonstrated the ability of closed ties and compression reinforcement to increase rotational ductility and confine core concrete. Of the eighteen specimens they tested, however, only three were subjected to reversed loading. It cannot be said that these tests represented a good approximation to earthquake loading.

The Tokachi-Oki earthquake of 1968, in which several structures experienced column shear failures, sparked renewed interest in this problem, primarily in the area of compression members subjected to shear reversals. Wight and Sozen (39) investigated twelve specimens having varying axial load, transverse reinforcement and imposed displacement level. Following the work of Hisada et al. (19) and others (20, 24, 40), they were able to conclude that repeated inelastic loading caused a progressive decrease in a member's shear strength and stiffness which could be delayed by close spacing of transverse reinforce-

ment. Their tests also showed that axial compressive loading slowed the rate of strength deterioration.

The behavior of beam-column joints also attracted the attention of several researchers. As an integral part of any column, the beam-column joint was seen as a section whose failure would produce structural damage as severe as that accompanying column failure. Hanson and Conner (15) were among the first to consider beam-column joint action experimentally. Research by Megget and Park (28), Uzumeri and Seckin (37), Margues and Jirsa (27), and others (22, 30) has led to increased understanding of a variety of complex problems associated with the beam-column joint. Based on this research, ACI-ASCE Committee 352 (35) formulated recommendations for design of beam-column joints in monolithic reinforced concrete structures as a design standard. Subsequent work by Lee et al. (25) and by Meinheit and Jirsa (29) has shown that, although modifications of these recommendations may be necessary, beam-column joints can be designed to resist effectively seismic forces transmitted by both beams and columns.

Several researchers have attempted to examine and define the cyclic flexural behavior of members without axial load. Brown and Jirsa (9) tested twelve specimens with varying reinforcement ratio, shear span to depth ratio, stirrup spacing and loading history and found that

failure of all specimens was initiated by shear deformations which occurred along planes nearly perpendicular to the specimen longitudinal axis. Shear strength decay was also more pronounced with increases in maximum shear stress. In a related study, Jirsa (23) concluded that at certain shear stress levels vertical stirrups at any spacing could not prevent shear strength decay.

Paulay was the first to consider the use of unique and previously untried reinforcement designs to combat shear strength decay. Considering the problem of shear failure in coupling beams of shear walls (32, 33), he successfully used diagonal reinforcement to achieve high ductility and stability during load reversals for deep spandrel beams carrying very high shear stresses.

Popov, Bertero, and Krawinkler (34) considered a similar problem when they subjected deep beams with shear stresses greater than $6\sqrt{f'_c}$ to repeated reversed flexure. As in previous tests, deterioration in shear resistance was the major cause of failure. In a following study, Bertero, Popov, and Wang (6) tested similar specimens which contained elaborate diagonal bracing in the beam to control the location of plastic hinging and reduce shear deterioration. This cross-reinforcing technique was as effective as Paulay's had been in promoting stability, but it was suggested that this reinforcement detail was too complex and potentially expensive for general use.

1.3 Objectives and Scope

The primary objective of this research project was to evaluate experimentally the effect of intermediate longitudinal reinforcement in preventing shear strength and stiffness deterioration in concrete flexural members subjected to repeated reversed inelastic loading. A secondary objective was to study the action of the beam-column joint supporting a flexural member during such conditions.

Eight half-size and four full-size beam-column sub-assemblies were constructed and tested to meet these objectives. Variables in the study, in addition to the inclusion of four intermediate longitudinal bars in half the specimens, included shear span to depth ratio which varied from 3.6 to 5.0, main longitudinal reinforcement ratios ranging from 1.27 percent to 2.62 percent, and transverse reinforcement ratios which varied from 0.63 percent to 1.1 percent. Specimens were designed to cover the range of shear stress values from $2\sqrt{f'_c}$ to greater than $6\sqrt{f'_c}$.

CHAPTER 2

SPECIMEN DESIGN AND EXPERIMENTAL INVESTIGATION

2.1 General

Twelve reinforced concrete beam-column subassemblies were designed and fabricated for the testing program. The test specimens, shown schematically in Fig. 2.1, simulated an external beam-column connection in a reinforced concrete moment resisting frame. Each specimen was subjected to forces intended to simulate the forces an actual beam-column subassembly might experience during an earthquake. An axial load was placed on the column portion of the specimen at the beginning of the test and was held constant for the duration of the test. The column was held by rollers at its extreme ends as shear forces were statically applied to a point near the beam end by a double-action hydraulic ram. Downward shears and displacements were considered positive as illustrated in Fig. 2.1.

2.2 Specimen Design

The test specimen and cross-sections of the beam and column are shown in Fig. 2.1 with corresponding dimensions listed in Table 2.1. A complete description

TABLE 2.1

PHYSICAL DIMENSIONS OF SPECIMENS*

Specimen Number	L (in)	L_b (in)	a (in)	h (in)	b (in)	d (in)	d_1 (in)	d_2 (in)	d' (in)	Number - Bar Designation				
										A_s	A'_s	A_i	A_v	A_{vi}
1	60.	54.	41.5	10.	8.	8.6	-	-	1.3	2-#6	2-#5	-	#2	-
2	60.	54.	41.5	10.	8.	8.6	6.2	3.8	1.3	2-#6	2-#5	4-#2	#2	#2
3	60.	54.	41.5	12.	8.	10.1	-	-	1.8	3-#6	3-#5	-	#2	-
4	60.	54.	41.5	12.	8.	10.1	7.2	4.8	1.8	3-#6	3-#5	4-#3	#2	#2
5	60.	54.	31.0	10.	8.	8.6	-	-	1.3	2-#6	2-#5	-	#2	-
6	60.	54.	31.0	10.	8.	8.6	6.2	3.8	1.3	2-#6	2-#5	4-#2	#2	#2
7	60.	54.	41.5	12.	8.	10.1	-	-	1.8	3-#6	3-#5	-	#3	-
8	60.	54.	41.5	12.	8.	10.1	7.2	4.8	1.8	3-#6	3-#5	4-#3	#2	-
9	96.	72.	60.	14.	10.	12.1	-	-	1.8	4-#8	4-#7	-	#3	-
10	96.	72.	60.	14.	10.	12.1	9.0	5.0	1.8	4-#8	4-#7	4-#4	#3	#2
11	96.	72.	48.	14.	10.	12.1	-	-	1.8	4-#8	4-#7	-	#3	-
12	96.	72.	48.	14.	10.	12.1	9.0	5.0	1.8	4-#8	4-#7	4-#4	#3	#2

*Dimensions illustrated in Fig. 2.1.

of shear reinforcement details is given in Appendix A. The twelve specimens may be divided into two groups on the basis of column size. Specimens 1 through 8 will hereafter be referred to as Group I and Specimens 9 through 12 will be called Group II. Due to the difference in specimen size between the two groups, two testing frames were used. Typical test frame configurations for Group I and Group II specimens are shown in Figs. 2.2 and 2.3 respectively.

In general, the specimens can be considered in pairs, regardless of column size. Odd numbered specimens contained beam shear reinforcement near the face of the column as required by Appendix A of the ACI Building Code (1). The corresponding even numbered member of the pair (the next higher numbered specimen) contained supplementary longitudinal shear reinforcement as well as the code-specified ties. Specimens 7 and 8 represent the only deviation from this condition. Specimen 7 was similar to Specimen 3 and was designed to determine the effect of Grade 60 web reinforcement on shear strength degradation. Specimen 8 was essentially a replica of Specimen 4 with the exception that it contained no ties around intermediate longitudinal reinforcement.

Some pairs of specimens contained identical reinforcement and were tested at different shear spans to determine the effect of different shear stresses on

specimen hysteretic performance. Pairs of specimens having identical reinforcement and different testing shear spans included Specimens 1 and 5, 2 and 6, 9 and 11, and Specimens 10 and 12.

Recommendations of ACI-ASCE Committee 352 (35) were used as a guide in designing joint shear reinforcement. However, the extra shear transmitted to the joint by the supplementary longitudinal reinforcement in the beams of even numbered specimens was ignored. The results from these specimens satisfied a secondary objective of the research effort: to determine whether a joint designed to resist the shear input by a conventional doubly reinforced member could accept the forces contributed by auxiliary longitudinal reinforcement.

All columns of a given size were reinforced identically, in accordance with Appendix A of ACI 318-71. Ties required by this specification provided shear reinforcement in excess of the amount required to resist design shear forces. A complete discussion of specific design procedures for a selected specimen is given in Appendix C.

2.3 Specimen Loading

A typical loading schedule is shown in Fig. 2.4. Each specimen was subjected to at least one cycle of positive and negative loading to one-half the computed positive yield load. This preliminary cycle allowed

members of the test team to check the response of the data gathering equipment and verify the security of the attachments between the specimen and the testing frame. The specimen was then subjected to large scale reversed loadings. Displacement ductility, defined here as the ratio of the displacement at the beam load point at any stage in testing to the corresponding displacement at initial yield of the beam longitudinal steel under positive shear, was used as the loading control parameter. The typical loading routine consisted of six cycles to displacement ductilities of +4 and -3, followed by six more cycles to displacement ductilities of +6 and -5. Failure prior to completion of the nominal loading routine was considered to have occurred when the beam offered little resistance to displacement or when torsional instability developed in the beam.

Due to the nature of data acquisition equipment, it was necessary to hold the deflection constant at certain points (load points) in each cycle to allow recording of displacement transducer, strain gage and dial gage data. Load points were chosen at significant changes of slope of the load-displacement curve, at integral values of displacement ductility, or at any other point considered significant.

2.4 Material Properties

Average steel yield stresses are listed in Table 2.2.

TABLE 2.2

MATERIAL PROPERTIES

(Averaged for specimens cast simultaneously)

Specimen Number	f'_c (psi)	f_y (ksi)			
		A_s	A'_s	A_i	A_v
1	4970	48.9	51.7	-	42.6
2	"	"	"	48.2	"
3	"	"	"	-	"
4	4970	48.9	51.7	55.4	"
5	3980	52.7	52.7	-	"
6	"	"	"	48.2	42.6
7	"	"	"	-	75.4
8	3980	52.7	52.7	55.4	42.6
9	4940	60.2	49.3	-	54.0
10	"	"	"	57.0	"
11	"	"	"	-	"
12	4940	60.2	49.3	57.0	54.0

Grade 40 steel was used for all beam longitudinal reinforcement and all vertical shear reinforcement except for that used in Specimen 7. In that specimen, Grade 60 ties were used in the plastic hinging region. Grade 60 bars were used for all column longitudinal reinforcement and joint ties. Complete results of steel coupon tests are given in Appendix D.

Average concrete compressive strengths are also listed in Table 2.2. As noted in Appendix D, the concrete mix was designed to yield a 28 day strength of 4000 psi.

2.5 Data Acquisition

Details of data acquisition equipment are given in Appendix B. Data was gathered from four sources during testing: (1) a load cell and displacement transducer attached to the loading ram, (2) displacement transducers over the beam plastic hinging region, (3) electrical resistance strain gages attached to longitudinal and shear reinforcement and (4) dial gages.

Beam load and displacement at the point of loading ram attachment were continuously plotted on an X-Y recorder. The load vs. deflection curve not only served as the main guide to progress of the test, but also gave an immediate indication of specimen integrity.

Linear variable displacement transducers (LVDTs)

were positioned over the beam plastic hinging region as shown in Fig. 2.5. The plastic hinging region was assumed to extend a distance from the face of the column equal to the overall beam depth. These transducers allowed simultaneous measurement of shearing and flexural deformations in the hinging region.

Electrical resistance strain gages were bonded to reinforcement at various points in the specimen. The location of gages was similar in all specimens, as shown in Fig. 2.6. Strain gage locations were selected to augment load-deformation data as well as document the action of shear reinforcement.

Two micrometer dial gages were positioned to detect rigid body rotations of the beam-column joint with respect to the loading frame for all specimens. Three additional dial gages were used when testing Specimen 3 to determine the elastic deflection of the testing frame used to hold Group I specimens. A schematic diagram of dial gage locations on the frame and specimen is shown in Fig. 2.7. The frame used to hold Group II specimens for testing was considered rigid, so only dial gages 1 and 2 were used for Group II tests.

CHAPTER 3

TEST RESULTS

3.1 Typical Results

Several types of data were recorded during the testing of each specimen. Load vs. deflection curves are perhaps the most important for three reasons: (1) the maximum shear experienced by the specimen during any load cycle is easily determined, (2) the degradation of load capacity and stiffness is easily seen, and (3) the area within the curve for each cycle of loading is proportional to energy dissipation during that cycle. Load vs. deflection curves for all specimens are shown in Figs. 3.1(a) through 3.1(ℓ). A tabulation of important reinforcement ratios and parameters obtained from these curves, including maximum first-cycle shear, number of cycles before failure, and total energy dissipation is given in Table 3.1.

The importance of load vs. deflection curves may be illustrated by comparing the curve for Specimen 1, which showed primarily flexural response, with the curve for Specimen 3, which experienced severe decay of strength and mid-cycle stiffness (Figs. 3.1(a) and 3.1(c) respectively). Specimen 1 maintained high energy dissipation per cycle and mid-cycle stiffness through all cycles of loading. In

TABLE 3.1

SELECTED TESTING PARAMETERS AND TEST RESULTS

Specimen Number	Max. Shear* (α)	Total Energy Dissipation (in-kips)	No. of Cycles	$\rho = A_s/bd$	A_i/A_s	$\rho_v = A_v/bs$	a (in)	a/d
1	2.06	366	14**	0.0127	0	0.0063	41.5	4.8
2	2.24	394	14**	0.0127	0.23	0.0063	41.5	4.8
3	3.06	311	8	0.0163	0	0.0050	41.5	4.1
4	3.45	544	11	0.0163	0.33	0.0050	41.5	4.1
5	3.35	316	12	0.0127	0	0.0063	31.0	3.6
6	3.44	327	13.5	0.0127	0.23	0.0063	31.0	3.6
7	3.60	407	12	0.0163	0	0.0110	41.5	4.1
8	3.84	506	14	0.0163	0.33	0.0050	41.5	4.1
9	4.92	1270	7.5	0.0262	0	0.0073	60.0	5.0
10	5.09	1360	7.5	0.0262	0.25	0.0073	60.0	5.0
11	6.16	723	5	0.0262	0	0.0073	48.0	4.0
12	6.23	942	7	0.0262	0.25	0.0073	48.0	4.0

*Maximum shear measured at maximum positive displacement in first load cycle; as a multiple of $\sqrt{f'_c}$.

**Specimen behavior stable at conclusion of testing.

contrast, for Specimen 3 there was a loss of stiffness (shown by "pinching" of the curve at mid-cycle) and a loss of load capacity as early as the second cycle of loading. Both losses became progressively more severe as loading continued.

Linear variable displacement transducers (LVDTs) were positioned to detect flexural rotation and shear strain in the beam hinging zone, a region assumed to extend along the beam from the column face a distance equal to overall beam depth. The location of LVDTs is shown in Fig. 2.5, with a deformed joint shown in Fig. 3.2. Using the notation shown in Fig. 3.2, the following relations were assigned:

$$L_1 = EA' \qquad (3.1\ a)$$

$$L_2 = GB' \qquad (3.1\ b)$$

$$L_3 = A'G \qquad (3.1\ c)$$

$$L_4 = EB' \qquad (3.1\ d)$$

Then, from trigonometry, the deformed angular relationships become,

$$A'EG = \cos^{-1}\left(\frac{H^2 + L_1^2 - L_3^2}{2HL_1}\right) \qquad (3.2\ a)$$

$$EGB' = \cos^{-1}\left(\frac{H^2 + L_2^2 - L_4^2}{2HL_2}\right) \qquad (3.2\ b)$$

and assuming an initial right angle at the beam-column intersection,

$$\theta_1 = \frac{\pi}{2} - A'EG \qquad (3.3\ a)$$

$$\theta_2 = EGB' - \frac{\pi}{2} \qquad (3.3\ b)$$

Finally, using Eqs. (3.2) and (3.3), it can be shown that:

$$\theta_3 = \tan^{-1}\left(\frac{L_1 \sin\theta_1 + L_2 \sin\theta_2}{L_1 \cos\theta_1 + L_2 \cos\theta_2}\right) \qquad (3.4)$$

$$\theta_4 = \sin^{-1}\left(\frac{L_1 \cos\theta_1 - L_2 \cos\theta_2}{H}\right) \qquad (3.5)$$

The angle θ_3 was taken as the shear strain within the hinging zone and the angle θ_4 was taken as the angle of flexural rotation within the zone. The relationship between computed hinge shear strains, hinge rotations, beam loads and load point displacements for Specimen 1 are shown in Figs. 3.3(a) through 3.3(d). The characteristics of these relationships are typical for a specimen exhibiting primarily flexural behavior, as Specimen 1 did. The uniform proportionality between beam load point displacement and hinge flexural rotation, shown in Fig. 3.3(a), and between beam load point displacement and hinge shear strain (Fig. 3.3(b)), indicate that displacements due to shear strain and flexural rotation constituted a nearly constant percentage of total load point displacement at maximum displacement during all load cycles. Similar conclusions regarding hinging zone reponse stability for this specimen

may be drawn from analysis of Figs. 3.3(c) and 3.3(d).

Depending on the type of reinforcement used in each specimen, ten or fourteen electrical resistance strain gages were bonded to the reinforcement as discussed in Chapter 2. Strain gage data helped to explain various visually observed responses and quantified some critical aspects of behavior. This is illustrated by the plot of beam shear vs. stirrup strain (as measured by strain gage #1) shown in Fig. 3.4 for the center joint tie of Specimen 1. First cracking in the joint occurred between the load points designated as A and B. At some load between these two points, the tensile strength of the concrete was exceeded and the stress carried by the concrete was suddenly taken by the steel, as shown by the large strain which accompanied the load increase between points A and B. The strain in the stirrup never reached the yield strain during the test. This indication of stable joint behavior is in agreement with visual observations of joint behavior which are discussed below.

Strain gage data was also important in confirming conclusions which had been based on other data. One example is the plot of beam load vs. bar strain in the top longitudinal reinforcement shown in Fig. 3.5 for Specimen 1. The bar yield strain and the load point at which yield had been assumed based on load vs. displacement curve shape are both indicated in this figure. Clearly, the strain gage data confirms the assumed yield of longitudinal tension

reinforcement at load point A.

Strain in the second, third, and fourth beam ties from the face of the column was also monitored. The plot of beam load vs. stirrup strain (measured by Gage #9) of Specimen 1 is shown in Fig. 3.6. The approximate load accompanying the first inclined crack to cross this tie can be estimated based on the break in the curve. During repeated loading, the strain in the tie never reached yield.

3.2 Description of Individual Specimen Behavior

Common Behavior

Several aspects of behavior were common to nearly all specimens. Column behavior is one example. The regions of the columns away from the joint withstood all input forces without any cracking or degradation of the concrete.

Beam behavior outside the hinging zone was also similar for all specimens. Although inclined cracks were noted in most beams between the point of loading and the hinging zone, all such cracks formed in the first or second load cycle and remained stable throughout loading. No significant motion was detected along the majority of these cracks.

Behavior of the beam-column joints was also similar for all specimens. All joints developed at least one diagonal crack and spalling of the cover concrete occurred in Specimens 7 and 8. However, no relative motion was observed along any inclined cracks. Grade 60 shear

reinforcement was used in all joints and typically the measured stirrup strain never exceeded the yield strain, as shown in Fig. 3.4 for Specimen 1.

All specimens experienced failure or major deterioration as a result of cracks which formed in the hinging region, although the nature, extent, and rate of degradation varied greatly from one specimen to another. Figure 3.7 illustrates the general nature of cracking which resulted from reversed loading. Vertical cracks which formed in the positive half-cycle of loading (Fig. 3.7(a)) were intersected by similar types of cracks originating from the opposite side of the beam during loading reversal (Fig. 3.7(b)). In general, vertical cracks which formed during a loading half-cycle closed only under large reversed load because tension reinforcement had been strained past its yield point. As a result, stiffness at mid-cycle was less than at high positive or negative loads because some cracks remained open. As larger loads were applied, cracks closed and shear was again carried by friction between adjacent sections, web reinforcement, and a smaller contribution from dowel action of the longitudinal reinforcement. Intersecting inclined cracks also caused deterioration of the hinging zone by dividing the region into a matrix of prismatic blocks. The integrity of the region was influenced primarily by the ability of the reinforcement to decrease the mobility, and consequent degradation, of the individual blocks.

Reinforcement and loading parameters which had a major effect on specimen behavior are listed in Table 3.1. For convenience, the maximum measured first-cycle shear stress as a multiple of $\sqrt{f'_c}$ (α), the ratio of intermediate longitudinal reinforcement area to tension reinforcement area (A_i/A_s), and the web reinforcement ratio (ρ_v) will be reproduced to aid the discussion of behavior for each specimen.

Specimen 1 (α = 2.06, A_i/A_s = 0.0, ρ_v = 0.0063)

Primary damage occurred in the region of the beam adjacent to the beam-column joint. The specimen is shown in Fig. 3.8 at the conclusion of testing. Two vertical flexural cracks which formed during the positive half-cycles of loading joined with similar cracks formed during the negative loading half-cycles to form two continuous vertical cracks in the hinging zone. These flexural cracks, which formed at the face of the column and at approximately d/2 from the column face, opened to widths visually estimated at more than 1/2 in. Shear stress in the beam was not large enough to cause significant relative motion of contiguous blocks, however. Some inclined cracks also formed in the hinging region, but crack widths and motions along these cracks were insignificant.

The observed damage, the load vs. deflection curve (Fig. 3.1(a)), and the load point displacement vs. hinge rotation relationship (Fig. 3.3(a)) indicated that the specimen responded primarily in a flexural mode. The

specimen retained substantial load capacity and mid-cycle stiffness at the end of twelve cycles of large scale deflection, so two additional load cycles were imposed to determine if any additional degradation would occur. Spalling occurred near the bottom reinforcement in the thirteenth load cycle but the bottom bars did not buckle at the maximum positive displacements. Load capacity was not affected by the additional loading and the test was terminated after fourteen cycles.

Specimen 2 (α = 2.24, A_i/A_s = 0.23, ρ_v = 0.0063)

Maximum moments and accompanying shears were slightly higher in this specimen than in Specimen 1 due to the presence of intermediate longitudinal bars in the beam. The pattern and progress of vertical and inclined cracking in the hinging zone were nearly identical for Specimens 1 and 2, as can be seen by comparing the appearance of the two specimens at the conclusion of testing shown in Figs. 3.8 and 3.9 respectively. Motion along cracks in the hinging region was small and hinge shear strain remained nearly proportional to load point displacement for all cycles of loading as shown in Fig. 3.10.

Cracks which formed in the beam between the hinging zone and the load point can be seen in Fig. 3.9. As previously noted, no deterioration was observed near cracks in this area of the beam.

Specimen 3 (α = 3.06, A_i/A_s = 0.0, ρ_v = 0.0050)

This specimen suffered severe shear strength decay under large scale deflection reversals. Although vertical cracks formed in the hinging zone near the face of the column in the first cycle of loading as shown in Fig. 3.11, diagonal cracks which formed in subsequent cycles were responsible for major deterioration. The appearance of the beam hinging zone and beam-column joint at the conclusion of testing is shown in Fig. 3.12. The dominant inclined crack originated at the intersection of the column face and the beam's lower side, crossing the beam at an angle of approximately 60 degrees measured counterclockwise from the beam centerline. Severe concrete crushing took place near this crack as adjacent blocks ground against each other during the cyclic loading. A second inclined crack ran parallel to the first at a separation distance of approximately d/2. Crushing and grinding near this crack were less extensive than for the main inclined crack. A third major inclined crack intersected the first two with degradation similar to that along the smaller of the parallel cracks. No serious degradation occurred near the vertical crack at the face of the column.

Loading was stopped after the bottom longitudinal reinforcement buckled in the eighth cycle of displacement. The inability of the beam to resist shear at that stage of loading was shown by the small slope of the load vs. displacement curve (Fig. 3.1(c)). The progressively increasing

shear stiffness decay which occurred in the hinging zone can also be seen in the plot of beam load point displacement vs. hinge shear strain, Fig. 3.13. This relationship confirms the visual observation that shear deformation in the hinging region constituted an increasingly larger percentage of total deformation as the number of load cycles increased. The beam twisted approximately 10 degrees counterclockwise (as viewed from the beam free end) about its longitudinal axis during the eighth repetition of negative load. Because both shear and torsional forces are resisted by shearing stresses in the concrete and tension in web reinforcement, this twisting was an indication of severe shear strength loss.

The hinging region of the beam after removal of broken and loose concrete is shown in Fig. 3.14. The bowed shape of buckled bottom reinforcement and the rounding of the main blocks in the hinging zone can be clearly seen.

Specimen 4 (α = 3.45, A_i/A_s = 0.33, ρ_v = 0.0050)

This specimen was able to withstand eleven cycles of reversed loading before buckling of longitudinal reinforcement and twist of the beam about its longitudinal axis made further loading impractical. Crack patterns for Specimens 3 and 4, shown in Figs. 3.11 and 3.15 respectively, were similar after the first half cycle of loading. Cracks tended to be uniformly distributed in Specimen 4 as loading progressed, in contrast to the widely spaced cracks which

developed in Specimen 3. As shown in Fig. 3.16, at the conclusion of testing cracking produced a large number of small blocks in the zone of beam plastic hinging for Specimen 4. In addition, deterioration was not confined to the area around one crack, but was distributed among several cracks. The hinging zone of the beam after removal of broken and loose concrete is shown in Fig. 3.17. Concrete had been crushed so extensively in this region that almost all broken blocks could be removed.

The plot of load point displacement vs. hinge shear strain for Specimen 4 is shown in Fig. 3.18. This plot illustrates the ability of the beam to maintain its shear stiffness during cyclic loading, as hinge shear strain remained nearly proportional to displacement at points of maximum displacement for the duration of the test.

Specimen 5 (α = 3.35, A_i/A_s = 0.0, ρ_v = 0.0063)

Specimen 5 was reinforced identically to Specimen 1, but experienced larger beam shear stresses as a result of a smaller shear span to depth ratio used for loading (see Table 3.1). Shear strength and mid-cycle stiffness decreased gradually with every cycle of loading. Although one bottom longitudinal reinforcing bar buckled during the tenth cycle of loading at maximum positive displacement, the rate of decrease in measured shear at maximum displacement remained uniform. The test of this specimen was stopped after twelve load cycles in accordance with the typical loading procedure.

The progress and nature of cracking and deterioration which the specimen experienced can be visualized by observing the beam hinging zone after one cycle of loading (Fig. 3.19) and after twelve cycles of loading (Fig. 3.20). All major cracks were formed in the first inelastic load cycle. As in nearly all specimens, a vertical crack formed at the face of the column. Two more vertical or very steeply inclined cracks occurred at approximately d/2 and 3d/4 from the column face. The concrete adjacent to the crack at d/2 from the column face suffered the greatest deterioration during the course of testing. Although crack widths approached approximately 1/2 in. during maximum deflections in the final cycles of loading, lateral motion along these cracks was estimated at less than 1/4 in. Cracks divided the hinging region into prismatic blocks on the order of the size of half the beam core largest dimension as shown in Fig. 3.20.

The response of the hinging zone was stable throughout loading. The plot of load point displacement vs. hinge shear strain, shown in Fig. 3.21, illustrates the similarity of the behavior of Specimen 5 to the behavior of Specimen 1 in this regard. Although mid-cycle behavior was slightly less stable for Specimen 5, the contribution of displacement due to shear strain to the total displacement remained uniform.

Specimen 6 (α = 3.44, A_i/A_s = 0.23, ρ_v = 0.0063)

Reinforcement in this specimen was identical to that used for Specimen 5 except that this specimen contained intermediate longitudinal reinforcement in the beam hinging zone. The specimen was able to withstand twelve inelastic load cycles with a 33% reduction of maximum measured shear between the first and twelfth cycles. Because the beam was in good condition after the typical loading routine, additional load cycles were imposed at the maximum available ram displacement (+2.8 in., -2.5 in.). This severe loading caused torsional instability to develop in the beam during the thirteenth cycle of negative loading, resulting in a twist of the beam about its longitudinal axis. In the following cycle the bottom reinforcement buckled at maximum positive displacement and loading was terminated. The final 1 1/2 cycles of deflection were not considered in calculating energy dissipation for the specimen and are not shown on the load vs. deflection curve, Fig. 3.1(f).

Nearly all cracks in the hinging zone were formed during the first cycle of loading and overall crack pattern remained unchanged throughout testing. Crack distribution after one and twelve load cycles is illustrated in Fig. 3.22. Three characteristics of the cracking which occurred are intimated in Fig. 3.22(b): (1) cracks formed with maximum widths estimated at less than 1/2 in., (2) motion between adjacent blocks was much smaller and degradation of concrete near cracks was less severe than for Specimen

5, and (3) cracks were more uniformly distributed through the hinging zone than they had been in Specimen 5. Blocks formed by the cracks in this region were approximately half as large as those formed in the hinging zone of Specimen 5.

Despite the many differences in physical breakup of the hinging zones of Specimens 5 and 6, overall behavior was nearly identical. The relationship of hinge shear strain and load point displacement for Specimen 6, shown in Fig. 3.23, is nearly indistinguishable from the corresponding relationship for Specimen 5.

Specimen 7 (α = 3.60, A_i/A_s = 0.0, ρ_v = 0.011)

This specimen was designed to determine the effectiveness of a larger percentage and a higher strength of web reinforcement in preventing shear strength deterioration. The specimen was reinforced identically to Specimen 3, except Grade 60, No. 3 ties were used in the beam hinging zone instead of Grade 40, No. 2 ties.

Nearly all cracks which developed in the beam hinging zone were inclined as shown in the photo taken at the third cycle of maximum negative displacement (Fig. 3.24). Crack widths of approximately 1/2 in. were noted in the cover concrete at maximum displacements during the final load cycles, but the crack widths were significantly reduced within the beam core due to the stronger web reinforcement used in this specimen. The effectiveness of the web reinforcement in preserving the hinging zone integrity was visually confirmed when loose cover concrete was removed

from that area, as shown in Fig. 3.25. This specimen was peculiar among all specimens tested in that major deterioration took place in the beam at the face of the column and extended into the beam-column joint. The stability of the hinging zone could be inferred from the characteristics of the plot of beam shear vs. stirrup strain (measured by strain gage #9) in the third tie from the column face (Fig. 3.26). The behavior of this stirrup was typical in that measured stirrup strain never reached the stirrup yield strain.

Although all specimens showed deterioration of bond along main reinforcement between the face of the column and the beginning of the bar hook, Specimens 7 and 8 showed the most dramatic loss of bond in this region. Beam shear vs. strain in the bottom longitudinal reinforcement of Specimen 7 at the face of the column and at the beginning of the hook are shown in Figs. 3.27 and 3.28 respectively. The characteristics of these plots indicate that a deterioration of bond along the lower main reinforcement spread from the column face into the beam-column joint. Tensile strains at the face of the column were large in the first cycle, but decreased with additional load cycles. Strains near the bar hook became larger in each consecutive load cycle. Cover concrete over reinforcement in this area swelled upward and eventually spalled off between the face of the column and the main bar hooks. However, the damage was mainly superficial because the bar hook was able to

develop the yield stress in the bottom reinforcement throughout the test. Maximum strains in the center beam-column joint tie were significantly larger than the stirrups' yield strain, as shown in the plot of beam shear load vs. the strain detected by Gage 1, Fig. 3.29. Overall strain in this tie tended to increase slightly with each loading reversal and strains increased significantly when displacements of the +6 and -5 times yield displacement were imposed (cycles 7 through 11). Behavior of the beam-column joint was considered acceptable throughout loading.

Specimen 8 (α = 3.84, A_i/A_s = 0.33, ρ_v = 0.0050)

Identical to Specimen 4 except that it contained no auxiliary ties around intermediate longitudinal bars, Specimen 8 exhibited stable behavior for fourteen cycles of reversed loading. The relationship of load to deflection in the thirteenth and fourteenth cycles is not shown on the specimen's load vs. deflection curve, Fig. 3.1(h), and no strain gage data or LVDT data was recorded for these cycles. The appearance of the specimen at the conclusion of testing is shown in Fig. 3.30. The uniform distribution of cracks and the resulting small blocks which formed in the hinging zone are evident in Fig. 3.30.

As occurred in the test of Specimen 7, deterioration entered the beam-column joint and severe spalling of concrete cover resulted. From the seventh cycle of load until the conclusion of loading, yield strain was exceeded in the instrumented beam-column joint tie as shown in Fig.

3.31. Strains near the hooks in both top and bottom longitudinal beam reinforcement also exceeded yield strain for cycles seven through twelve. The beam shear load vs. bar strain relationships for top longitudinal reinforcement at the beginning of the bar hook and at the face of the column are shown in Figs. 3.32 and 3.33 respectively. These plots indicate that the loss of bond which occurred along reinforcement in this specimen between these two points of strain measurement was similar to the bond deterioration which occurred along the anchorage region of main longitudinal reinforcement in Specimen 7.

The extent of spalling can be seen in Fig. 3.34, which shows the beam hinging zone and beam-column joint after removal of broken and loose concrete. Because no strain gages were attached to intermediate longitudinal bars near the hooks in the beam-column joint, it is impossible to say what magnitude of load these hooks resisted. However, large loads were probably acting at the hooks because strain gages attached to intermediate longitudinal bars within the beam hinging zone indicated that both intermediate longitudinal bars had been strained far in excess of their yield strain from the first cycle until the conclusion of testing.

Specimen 9 (α = 4.92, A_i/A_s = 0.0, ρ_v = 0.0073)

Specimen 9 was able to withstand seven and one half cycles of reversed loading. Buckling of bottom longitudinal bars during the seventh load cycle made further large

scale positive deflection impractical. In addition, the out-of-plane bending and the twist of the beam about its longitudinal axis which occurred during the seventh negative deflection limited negative load capacity.

The crack pattern which existed during the fifth cycle of negative deflection is shown in Fig. 3.35. The spalling near bottom longitudinal bars shown in this photo occurred at the beginning of the fifth load cycle and grew progressively worse until the termination of loading. Major cracks were inclined at an angle of approximately 45 degrees to the beam centerline and were separated by distances approximately equal to half the beam effective depth. Maximum crack widths were visually estimated at 1/2 in. Two major cracks originated in the hinging zone and continued into the portion of the beam adjacent to the hinging zone, but the opening of these cracks was estimated as less than half that of the major cracks in the hinging region. Interblock motion parallel to cracks was small, with largest motions estimated at approximately 1/4 in. occurring along cracks nearest the column face during the final two load cycles. Inclined beam cracks which formed entirely outside the hinging zone showed insignificant opening.

Beam behavior was essentially stable until the final load cycle when buckling of bottom reinforcement caused erratic hinging zone motion measurement. Prior to the buckling of these bars, hinge shear strain remained nearly

uniformly related to total displacement, as shown in Fig. 3.36. However, uniform shear strain was accompanied by decreasing shear loads at maximum displacements as shown in Fig. 3.37, indicating that the large shear stresses experienced by the beam had a dibilitating effect which was not completely evident in the load point displacement vs. hinge shear strain relationship.

The cracks which developed in the beam-column joint, shown in Fig. 3.35, were typical for all Group II (Specimens 9 through 12) specimens in that cracks width and deterioration were negligible. Both top and bottom longitudinal bars developed yield stress near their hooks without causing spalling. The strain gage attached to the joint tie in Specimen 9 did not give reliable strain readings, but the fact that no joint tie reached its yield stress in any other Group II specimen is indicative of similar behavior in this specimen.

Specimen 10 (α = 5.09, A_i/A_s = 0.25, ρ_v = 0.0073)

Load vs. deflection behavior for Specimens 9 and 10 (shown in Figs. 3.1(i) and 3.1(j) respectively) was nearly identical. Energy dissipation for the two specimens was nearly equal as well.

The crack pattern which existed at maximum positive displacement during the first load cycle is shown in Fig. 3.38. The crack pattern was peculiar because, in addition to the inclined cracks which were expected both inside and outside the hinging zone, a crack also formed approximately

1 in. inside of and parallel to the bottom reinforcement and extended from the face of the column a distance of approximately 3d/4 into the beam. This unusual crack was accompanied by spalling of the cover concrete near the bottom longitudinal bars, indicating the possible buckling of at least one main bar. However, cover concrete spalled more completely in a later load cycle and at that time it was possible to see that no bars had buckled in the first six load cycles.

During repeated reversed loading major cracks originated from each side of the beam near the column face and crossed the beam at inclinations of approximately 45 degrees to the beam centerline. Maximum crack widths and motion along these cracks (each estimated at approximately 1/2 in.) occurred during the last two cycles of loading. Degradation of concrete adjacent to these cracks was severe, especially near the bottom reinforcement, where both crushing and grinding occurred. Unlike the damage which occurred in Specimen 9, deterioration was confined to the hinging zone and no damaging cracks occurred outside that region.

The specimen is shown in Fig. 3.39 at the conclusion of testing. Load capacity of the beam remained stable until the bottom reinforcement buckled in the seventh load cycle at maximum positive displacement. Loading reversal led to beam twist which limited negative load capacity and caused loading to be stopped. The shape of buckled bottom

reinforcement, shown in Fig. 3.40, indicates that the stirrups did not confine or prevent buckling. This was typical for Group II specimens, as each specimen in Group II suffered buckling of bottom reinforcement and in each case the zone of bar buckling spanned more than one stirrup interval.

The load point displacement vs. hinge shear strain relationship for this specimen, Fig. 3.41, was not significantly different from the corresponding relationship for Specimen 9. Specimen 10 experienced a 36% increase in maximum positive hinge shear strain after six cycles of load compared to a corresponding 33% increase which occurred in Specimen 9.

Specimen 11 (α = 6.16, A_i/A_s = 0.0, ρ_v = 0.0073)

Specimen 11 was able to withstand only five cycles of inelastic loading, the least number of cycles for any specimen tested. The crack pattern which developed in the beam of Specimen 11 in the first cycle of loading, shown in Fig. 3.42, did not change significantly throughout loading. Inclined cracks originated from both sides of the beam throughout the hinging zone and significant cracks extended into the beam outside the hinging zone. Very wide cracks existed at maximum negative deflection after only four cycles of loading, as shown in Fig. 3.43.

The strains in the fourth tie from the column face, illustrated in Fig. 3.44, are typical of the large strains which were present in all ties in the hinging zone during

inelastic loading. Strain exceeded stirrup yield strain in the first cycle of loading and increased in each of the following three cycles. Gage output was erratic during the fifth and sixth load cycles due to local bending or other factors.

The severe deterioration of hinging zone shear stiffness which resulted from repeated reversal loading is illustrated by the load point displacement vs. hinge shear strain plot, Fig. 3.45. As shown, maximum shear strain in the hinging zone in the sixth cycle is three times as large as the maximum first cycle strain. The significance of this stiffness loss is magnified by the fact that beam shear strength also dropped sharply with each successive load cycle.

Specimen 12 (α = 6.23, A_i/A_s = 0.25, ρ_v = 0.0073)

This specimen was able to survive seven cycles of loading under very high shear stresses. The pattern of cracking after one load cycle, shown in Fig. 3.46, was similar to that of Specimen 11. However, cracks in Specimen 12 were more closely spaced than cracks in Specimen 11 and crack openings were always smaller in Specimen 12. Cracking and damage were not confined to the hinging region. As shown in Fig. 3.47, large crack widths had been developed after six cycles of loading, with significant cracks extending a distance 2d from the column face.

Stability of the hinging zone was only slightly better in this specimen than in Specimen 11. As shown in the plot of load point displacement vs. hinge shear strain, Fig. 3.48, maximum hinge shear strain increased with each load cycle. Shear loads at maximum displacement for this specimen decreased less rapidly than for Specimen 11, indicating slightly better overall behavior.

All ties in the hinging zone were strained past their yield. The plot of beam shear vs. stirrup strain in the third tie from the column face (Fig. 3.49) is typical for all ties.

CHAPTER 4

COMPARISON OF THEORETICAL AND EXPERIMENTAL RESULTS

4.1 Introduction

A comparison of theoretical and experimental results for several aspects of specimen behavior is presented in this chapter to verify testing equipment calibration as well as to illustrate the accuracy of certain analytical models.

Four general aspects of specimen behavior are compared. First, calculated and measured yield and maximum moments are compared. Second, the load vs. displacement relationship for the beam is calculated for the first quarter-cycle of inelastic loading and compared to the actual measured response for Specimens 3, 6 and 7. Third, maximum beam shear stress experienced by each specimen is compared to the allowable shear stress as calculated according to ACI 318-71 (1). Fourth, the beam-column joint is examined and the range of loads which accompanied the first joint crack is compared to allowable joint shear as calculated according to ASCE-ACI Committee recommendations (35). The range of maximum measured joint shear stresses is also discussed and compared to allowable values.

The relationship between the shear span to depth

ratio (a/d), the reinforcement ratio as a percentage of balanced reinforcement ratio (ρ/ρ_{bal}), and the maximum beam shear stress level is examined. The proof of interdependance of these three factors serves as the basis for conclusions regarding the effect of each factor on energy dissipation potential for a given specimen during repeated reversed flexure.

4.2 Comparison of Calculated and Measured Moments

A computer program developed by Wight and Sozen (39) was used to calculate yield and maximum moments for each beam section. A linear strain variation across the section was assumed for this model. In addition, the stress-strain relationships for the longitudinal steel (including strain hardening) and concrete were considered as input factors. A compilation of all material parameters critical to the moment-curvature model, including typical stress-strain curves for steel and concrete, is given in Appendix D.

A comparison of computed and measured moments, yield and maximum, experienced during the first cycle of inelastic loading is given in Table 4.1. As the table illustrates, agreement between computed and measured moments for these two conditions was satisfactory, differing by an average of five percent for yield and three percent for maximum moment.

TABLE 4.1

COMPUTED AND MEASURED YIELD AND MAXIMUM* MOMENTS

Specimen Number	Yield Moment, in-k		Maximum Moment, in-k	
	Calculated	Actual	Calculated	Actual
1	328	369	436	415
2	344	369	456	456
3	564	598	718	722
4	589	681	747	818
5	347	360	437	459
6	360	372	446	471
7	606	622	710	751
8	635	706	743	809
9	1974	2052	2472	2508
10	2058	2148	2520	2592
11	1974	1968	2472	2501
12	2058	2208	2520	2539

*Maximum moment taken as that attained at maximum positive displacement during first inelastic load cycle.

4.3 Comparison of Calculated and Measured Deflections

One important comparison that can be made in conjunction with the testing of any type of specimen is the comparison of the calculated and measured load vs. deflection relationship for a wide range of deflection values. A comparison of this type not only demonstrates the interaction of the various components of deformation at any particular deflection, but also illustrates the change in relative contribution of deformation components to the total deflection as the deflection level changes.

Several different components of deflection were considered in calculating the total deflection at various load points in the first quarter-cycle of inelastic loading, including flexural rotations inside and outside the hinging zone, shear deformations inside and outside the hinging zone, rigid body rotation of the beam-column joint, and deflection of the test frame for Specimens 1 through 8. Shear and flexural deformations are depicted for a typical beam in Fig. 4.1. This figure illustrates the way in which four deflection sources were assumed to contribute to total deformation.

The major portion of total deflection, flexural rotation in the plastic hinging zone, was monitored through the use of LVDTs positioned over this region

which measured the rotation with respect to the face of the column of a section at the end of the hinging zone. The setup of LVDTs and calculation of this rotation are discussed in Chapter 3 and illustrated in Fig. 3.2. Measurement of this rotation was considered essential for an accurate calculation of total deflection because it was anticipated that bond slip and local bending of main reinforcement would introduce significant errors in any calculation of rotations near the face of the column based on section properties alone (bond slip is discussed Section 4.5). The calculated deflections due to measured flexural rotations in the hinging zone are shown in column 2 of Table 4.2.

Shear strain within the hinging zone was also measured by LVDTs. All elastic methods of calculating shear strains within this region were considered unacceptable because of the typically nonlinear shear stress vs. shear strain behavior which existed in this region during inelastic loading. The measured shear strain within the hinging zone was used to calculate the deflection component given in column 3 of Table 4.2.

Deformations due to flexural curvature between the hinging zone and the beam load point were calculated using the moment-area theorem. The analytical model used to calculate yield and maximum moments was also used to calculate the curvature diagram from the known

TABLE 4.2(a)

CALCULATED DEFLECTION COMPONENTS FOR FIRST INELASTIC QUARTER-CYCLE OF LOAD - SPECIMEN 3

Measured Displacement, (in) (1)	Δ_1 (in) (2)	Δ_2 (in) (3)	Δ_3 (in) (4)	Δ_4 (in) (5)	Δ_5 (in) (6)	Δ_6 (in) (7)	Total Calculated Displacement (in) (8)
0.0	0.0	0.0	0.0	0.0	0.0	0.0	0.0
0.29	0.08	0.03	0.034	0.003	0.04	0.034	0.22
0.61	0.19	0.07	0.056	0.004	0.13	0.063	0.51
1.17	0.52	0.20	0.064	0.005	0.14	0.062	0.99
1.57	0.83	0.30	0.066	0.005	0.16	0.064	1.42
2.27	1.27	0.44	0.071	0.005	0.18	0.070	2.04

TABLE 4.2(b)

CALCULATED DEFLECTION COMPONENTS FOR FIRST INELASTIC QUARTER-CYCLE OF LOAD - SPECIMEN 6

Measured Displacement (in) (1)	Δ_1 (in) (2)	Δ_2 (in) (3)	Δ_3 (in) (4)	Δ_4 (in) (5)	Δ_5 (in) (6)	Δ_6 (in) (7)	Total Calculated Displacement (in) (8)
0.0	0	0	0	0	0	0	0
0.16	0.06	0.02	0.04	0.002	0.03	0.02	0.17
0.26	0.09	0.03	0.05	0.003	0.04	0.03	0.24
0.39	0.15	0.06	0.07	0.004	0.05	0.04	0.37
0.88	0.50	0.21	0.08	0.004	0.07	0.04	0.90
1.42	0.82	0.36	0.09	0.005	0.08	0.04	1.40

TABLE 4.2(c)

CALCULATED DEFLECTION COMPONENTS FOR FIRST INELASTIC QUARTER-CYCLE OF LOAD - SPECIMEN 7

Measured Displacement (in) (1)	Δ_1 (in) (2)	Δ_2 (in) (3)	Δ_3 (in) (4)	Δ_4 (in) (5)	Δ_5 (in) (6)	Δ_6 (in) (7)	Total Calculated Displacement (in) (8)
0	0	0	0	0	0	0	0
0.26	0.08	0.03	0.07	0.003	0.04	0.03	0.25
0.63	0.20	0.08	0.13	0.006	0.14	0.06	0.62
1.15	0.53	0.21	0.14	0.006	0.16	0.06	1.11
1.70	0.87	0.34	0.15	0.006	0.20	0.07	1.64
2.26	1.24	0.47	0.16	0.007	0.22	0.07	2.17

moment diagram. Deflections attributable to this source are shown in column 4 of Table 4.2.

Deflections due to shear strain between the hinging zone and the point of load application were calculated using elastic analysis as:

$$\Delta_4 = \gamma_1 \ell' = \frac{V\ell'}{bdG_c} \qquad (4.1)$$

where

γ_1 = elastic shear strain

ℓ' = length of beam section between the hinging zone and the beam load point

V = measured beam shear

G_c = concrete shear modulus = $0.4\ E_c$

E_c = concrete modulus of elasticity obtained from cylinder tests.

Calculated values for this deformation source are given in column 5 of Table 4.2.

In addition to considering deflections resulting from deformations in the beam itself, it was necessary to consider motion of the column section which resisted flexural and shear forces from the beam. The column axial load was assumed to eliminate any significant longitudinal motion of the column. No assumptions were made, however, about the rotation of the beam-column joint except that such rotation would be elastic. Two dial gages were positioned to detect rotations through-

out loading (Fig. 2.7, gages 1 and 2). In calculating the amount of measured deflection caused by rotation of the beam-column joint, it was assumed that the joint rotated as a rigid body. Calculated contributions to total deflection from this source are given in column 6 of Table 4.2.

A final contribution to total measured deflection in the case of Specimens 1 through 8 was the deformation of the test frame itself. Dial gages were positioned at three points as shown in Fig. 2.7 to measure the frame deflection during the first quarter-cycle of inelastic loading for Specimen 3. Elastic frame action was assumed for all subsequent loading. The frame used to hold Specimens 9 through 12 was assumed rigid for all load levels.

A tabulation of calculated deflection components and measured total deflection for Specimens 3, 6 and 7 is given in Table 4.2. The relationship of the various components of deflection to total deflection is shown in Fig. 4.2 for Specimen 3 and in Fig. 4.3 for Specimen 7 during the first quarter-cycle of inelastic loading. These figures indicate that the composition of deflection components remained relatively constant during the first cycle of loading until the yield deflection of the beam was reached, after which flexure and shear within the hinging zone constituted an increasing portion of the

total deflection. Figures 4.4 and 4.5 also illustrate the relationship of measured and calculated deflection for Specimens 3 and 7 over this same deflection interval. The relationship of deflection components for Specimen 3 during the sixth cycle of inelastic loading between the point of zero load and maximum positive load is shown in Fig. 4.6. This relationship illustrates the increasing amount of deflection attributable to shear in the hinging zone during later cycles of loading for Specimen 3, a specimen which showed significant deterioration of shear stiffness during repeated reversed loading.

4.4 Comparison of Maximum Measured and Allowable Shears

A comparison of measured maximum shears and allowable shear stresses calculated according to ACI 318-71, including the calculated shear strength contributed by web reinforcement, is presented in Table 4.3. Because the spacing of stirrups in the section of the beam near the beam-column joint was governed by a maximum allowable spacing of d/4 (ACI 318-71, Appendix A), rather than by strength, the calculated shear strength of the beam in the plastic hinging zone always exceeded the maximum shear experienced. For seven specimens the calculated strength of the web reinforcement alone exceeded the maximum measured shear. However, as discussed in Section 5.2, this fact did not guarantee satisfactory behavior in members subjected to large shear reversals.

TABLE 4.3

SHEAR STRENGTH AND SHEAR REINFORCEMENT PARAMETERS

Specimen Number	Maximum* Shear (k)	Maximum* Shear Stress (psi)	Tie Size and Spacing	Allowable v_c (psi)	Allowable v_s (psi)	Allowable v_t (psi)
1	10.0	144	#2@2"	141	268	409
2	11.0	158	#2@2"	141	268	409
3	17.4	213	#2@2.5"	144	213	357
4	19.7	241	#2@2.5"	144	213	357
5	14.8	212	#2@2"	129	268	397
6	15.2	221	#2@2"	129	268	397
7	18.1	221	#3@2.5"	130	505**	635
8	19.5	238	#2@2.5"	130	213	343
9	41.8	342	#3@3"	147	394	541
10	43.2	353	#3@3"	147	394	541
11	52.1	426	#3@3"	150	394	544
12	52.9	432	#3@3"	150	394	544

*Maximum shear measured at maximum positive displacement in first inelastic load cycle.

**ACI Code limits allowable stirrup stress to a normal value of 15 $\sqrt{f'_c}$. Actual v_s = 830 psi.

4.5 Response of Beam-Column Joint

It was possible to study the behavior of the beam-column joint by analyzing the relationship of beam load to strain in the central joint tie. Although no specimen suffered severe damage of concrete in the beam-column joint core, two specimens experienced spalling of joint cover concrete.

Joint shear stress was calculated based on recommendations of ASCE-ACI Committee 352. Figure 4.7 illustrates the assumed forces in a typical exterior beam-column joint. Shear stress in the joint core at any section A-A was calculated as follows:

$$v_j = \frac{T_s - V_{col}}{A_{cv}} \qquad (4.2)$$

where

v_j = the nominal joint shear stress

T_s = tension force in beam tension reinforcement

V_{col} = resisting shear force in column

A_{cv} = net joint core area resisting input shears

The area A_{cv} was calculated as the product of the depth to the centroid of column steel (shown as d_e in Fig. 4.7) and the effective width to the outside of joint ties. Allowable concrete shear stress was calculated as follows:

$$v_c = 3.5\beta\gamma\sqrt{f'_c}\,(1 + 0.002\, N_u/A_g) \qquad (4.3)$$

where

γ = 1.0 (lateral confinement factor)

β = 1.0 (joint classification correction factor)

f'_c = compressive strength of concrete, psi

N_u = column axial load

A_g = gross area of column cross section

Table 4.4 contains a summary of calculated shear stress in the beam-column joint at first cracking. Cracking was indicated by a large increase in strain in the central joint tie as measured by gage 1 in all specimens. This situation is discussed in Chapter 3 and illustrated for Specimen 1 in Fig. 3.4. It is probable that minor cracks formed prior to the stress levels given in column 2 of Table 4.4, as only cracks which crossed the instrumented stirrup were definitely documented.

A tabulation of maximum calculated joint shear stress is shown in column 3 of Table 4.4. Measured cracking shear stress was generally well in excess of computed allowable concrete shear stress. Maximum allowable shear stress was exceeded in three specimens, but the performance of all joints was satisfactory. This was expected, as a previous study by Lee et al. (25) indicated that satisfactory joint behavior could be predicted for joints having shear stresses greater than allowable, provided that the ratio of total column moment capacity to beam moment capacity remained large

TABLE 4.4

BEAM-COLUMN JOINT SHEAR STRENGTH AND REINFORCEMENT

Specimen Number (1)	v_j, psi first crack (2)	v_j, psi maximum (3)	v_c, psi allowable (4)	v_u, psi allowable* (5)	Stirrups required (6)	Stirrups used (7)	$\frac{\Sigma M_{column}}{M_{beam}}$ (8)
1	321	641	341	1,410	3-#3 gr. 60	3-#3 gr. 60	3.66
2	473	881	341	1,410	4-#3 gr. 60	3-#3 gr. 60	3.33
3	468	1,019	341	1,410	5-#3 gr. 60	5-#3 gr. 60	2.10
4	576	1,419	341	1,410	7-#3 gr. 60	5-#3 gr. 60	1.86
5	432	744	305	1,262	3-#3 gr. 60	3-#3 gr. 60	3.27
6	361	914	305	1,262	4-#3 gr. 60	3-#3 gr. 60	3.18
7	457	1,034	305	1,262	5-#3 gr. 60	5-#3 gr. 60	2.00
8	627	1,359	305	1,262	7-#3 gr. 60	5-#3 gr. 60	1.85
9	549	1,274	341	1,406	4-#4 gr. 60	4-#4 gr. 60	2.75
10	620	1,575	341	1,406	5-#4 gr. 60	4-#4 gr. 60	2.66
11	585	1,325	341	1,406	4-#4 gr. 60	4-#4 gr. 60	2.76
12	618	1,487	341	1,406	5-#4 gr. 60	4-#4 gr. 60	2.72

* $20\sqrt{f'_c}$

(greater than 2). The ratio of total column moment capacity to beam moment capacity for all specimens is given in Table 4.4. This table also includes a documentation of the number of ties used in each joint and the number required to satisfy strength provisions of the Committee 352 recommendations. The same number of joint ties were used for specimens with intermediate reinforcement as for comparable specimens without supplementary reinforcement. This was done to determine if inclusion of supplementary longitudinal reinforcement would require a special joint design. All joints performed satisfactorily.

A final characteristic of specimen behavior related to action in the beam-column joint was bond failure along main reinforcement between the face of the column and the beginning of the hooks anchoring the bars in the joint. Strain gages were attached to main reinforcement to determine the progress of bond failure in this segment. Bond failure and its effect on overall specimen performance were most noticeable in Specimens 7 and 8. Figures 3.32 and 3.33 show the beam load vs. strain relationship for top reinforcement near the bar hook and at the face of the column respectively in Specimen 8. For the first six cycles of inelastic loading, all with limiting displacement of $+4\Delta_y$ and $-3\Delta_y$, strain near the bar hook remained at a uniform level. These cycles were

followed by several cycles of loading at increased displacement ductilities and bar strains, during which the strains near the hook increased dramatically during the first two larger cycles before beginning to restabilize. This behavior is in substantial agreement with the conclusions of Ismail and Jirsa (22) and of Hawkins et al. (18). Both research groups concluded that an important factor affecting bond stress degradation was the peak axial stress applied to the bar during any cycle of loading. Hawkins et al. attributed this action to new cracking and Bauschinger effects developing during the first cycles at any given load level. Figures 3.32 and 3.33 verify the contention that repetition of load cycles with constant peak stress produces a gradual deterioration of stress transfer capacity after an initial large decrease.

4.6 Interaction of Reinforcement Ratio, Shear Span and Shear Stress

Although some researchers have considered the shear span to depth ratio to be a controlling factor in determining whether a particular concrete member will have large energy dissipation potential during reversed loading, the results from specimens tested during this research project did not support this contention. It was found that maximum shear stress was the most important factor in determining a member's ability to withstand repeated

inelastic loading.

The shear span to depth ratio and maximum shear stress are, however, interdependent. Wang and Salmon (38) and others have shown that the coefficient of flexural resistance for a member can be expressed as follows:

$$R_u = M_u/bd^2 \qquad (4.4)$$

where

R_u = coefficient of flexural resistance

M_u = member ultimate moment

It has been shown that, for singly reinforced beams with a given concrete design strength and steel yield stress, this coefficient of resistance is nearly linearly related to the ratio of the reinforcement ratio to the balanced reinforcement ratio, ρ/ρ_{bal}. As a result, the following expression can be written:

$$R_u = C_1\rho/\rho_{bal} \qquad (4.5)$$

where

C_1 = a constant

A similar type of relationship can be developed for doubly reinforced members if the ratio of compression to tension reinforcement remains relatively constant. Using the relationship between moment and shear which is appropriate for this test series,

$$M_u = V_u a \qquad (4.6)$$

where "a" is the shear span, it is possible to write the following expressions:

$$R_u = \frac{M_u}{bd^2} = \frac{V_u\ (a/d)}{bd} \qquad (4.7)$$

and

$$\frac{V_u}{bd} = C_1 \rho/\rho_{bal}\ (d/a) \qquad (4.8)$$

Therefore, the shear stress (V_u/bd) a member experiences is directly proportional to the ratio ρ/ρ_{bal} and inversely proportional to the shear span to depth ratio, a/d. Because the specimens tested covered a range of reinforcement ratios and shear span to depth ratios, they served as a practical test of this conclusion. The relationship of these three factors is shown in Fig. 4.8. The excellent linearity of the least squares regression for this relationship is indicated by a coefficient of determination of $r^2 = 0.967$.

CHAPTER 5

DISCUSSION OF TEST RESULTS

5.1 Introduction

The twelve specimens tested during the course of this research project varied in several respects. The most obvious variable was specimen size, with Group II specimens (Specimens 9 through 12) having been much larger than Group I specimens (Specimens 1 through 8) and having required much larger input forces. Other major variables included the ratio of shear span to beam depth (a/d), the size and type of shear reinforcement, and the ratio of the percentage of tension reinforcement to the theoretical percentage of reinforcement at balanced conditions (ρ/ρ_{bal}).

Because of the large number of variables involved, analysis of these test results is more complicated than a comparable analysis of test results involving only one or two variables. It is necessary to establish criteria for evaluating the response of disparate specimens to determine the relative effect of a given parameter and to determine the overall effectiveness of a given specimen in performing its structural function. This problem was addressed by Gosain et al. (13) in formulating a

"work index" which normalized energy dissipation for a single cycle of load reversal based on displacement ductility (Δ/Δ_y), the ratio of maximum load in a given cycle to the section's monotonic yield load (P_n/P_y), the level of axial load carried by the section, and the shear span to depth ratio (a/d). Because complete load vs. deflection curves were recorded for the specimens evaluated here, such approximations of cyclic energy dissipation were not necessary. Various methods of normalizing and evaluating energy dissipation are discussed below and compared to results obtained by applying the work index approach. The effect of various specimen parameters on normalized energy dissipation is also considered.

The mode of failure exhibited by each specimen was also an important consideration. Concrete members subjected to repeated reversed loading may cease to provide flexural and shear resistance due to a variety of causes, including a progressive destruction of the concrete in the region where plastic hinging occurs, shear slippage in the plastic hinging region, and buckling of compression reinforcement. The contribution of section characteristics which either encouraged or prevented these failures is discussed below for three levels of maximum shear stress. Because buckling of compression reinforcement was a prime cause of loss of load carrying ability in six specimens and a significant factor in the

strength decay of three other specimens, this situation will be discussed in detail for all shear stress levels.

5.2 Energy Dissipation Evaluation

In order to compare successfully the energy dissipation performance of specimens which differ in size, flexural stiffness, and displacement history prior to failure, it is necessary to normalize energy dissipation. Two criteria must be used in evaluating any normalization process. First, the approach must eliminate differences in specimen moment capacity resulting from size and reinforcement differences. Second, the approach must not eliminate behavior characteristics which result from changes in dimensionless relationships, such as reinforcement ratio, shear span to depth ratio, and web reinforcement ratio.

As described in Chapter 2, after an initial elastic cycle the typical loading routine used for all specimens consisted of six cycles of inelastic deformation with an imposed displacement ductility of four in the positive direction and three in the negative direction. This was followed by larger displacement cycles, usually to displacement ductilities of plus six and negative five until failure of the specimen or to a maximum total of 12 cycles. A complete listing of energy dissipation per cycle for all specimens is given in Table E.1, Appendix E.

Energy dissipation can be normalized by dividing the total energy dissipation of any specimen after any number of cycles by that specimen's energy dissipation in a single cycle. Because all specimens were subjected to displacement ductilities of equal magnitude in the first six inelastic cycles of loading, the energy dissipation of any one of these cycles is a logical choice for a normalization factor. First-cycle energy dissipation was chosen as the normalization factor in evaluating relative energy dissipation for this test series because the first-cycle energy dissipation is the most predictable and representative of the specimens strength and stiffness. As shown in Chapter 4, the beam load vs. load point displacement relationship can be calculated reasonably well for the first quarter-cycle of inelastic loading based on the beam section properties and the properties of the materials comprising the section. This process is much more complicated and much less reliable for all cycles after the first cycle because of unpredictable variations in slippage of main reinforcement, the extent of spalling which has taken place in previous load cycles, and the mobilization of concrete blocks along cracks in or near the zone of plastic hinge formation.

The use of second-cycle energy dissipation was briefly considered as a normalization factor because the second cycle load vs. displacement curve has no elastic

TABLE 5.1

ENERGY DISSIPATION RELATIONSHIPS

Specimen Number	Energy Dissipation, in-k			Second Cycle / First Cycle Dissipation Ratio	Normalized Energy Dissipation Total/First Cycle	Modified* Work Index, I_w'
	First Cycle	Second Cycle	Total			
1	23.9	19.4	366	0.81	15.3	53.2
2	24.6	19.1	394	0.78	16.0	53.7
3	55.8	41.8	311	0.75	5.6	19.9
4	59.4	46.1	544	0.78	9.2	27.8
5	33.9	25.7	315	0.76	9.3	30.5
6	30.6	23.5	327	0.77	10.7	38.3
7	54.5	39.4	407	0.72	7.5	31.4
8	57.3	42.2	506	0.74	8.8	31.4
9	232	184	1269	0.79	5.5	20.8
10	233	187	1358	0.80	5.8	21.1
11	205	160	723	0.78	3.5	10.5
12	205	176	942	0.86	4.6	13.1

*Modified Work Index = $I_w' = (\Sigma\ P_n/P_y \times \frac{\Delta_n}{\Delta_y})\ (1 - d_c/a)$: see Gosain et al. (13).

portion and is more comparable in shape to the following cycles than to the first cycle. A problem occurs in the use of second cycle energy as a normalizing factor, however, because of the previously noted differential decay rate of individual specimens. Consider the relationship of first and second cycle energy dissipation given in column 5 of Table 5.1. The ratio of second to first cycle energy varies from 0.72 to 0.86, with no clearly defined relationship existing between this ratio and the normalized energy dissipation for the specimens.

The total, first cycle, and normalized total energy dissipated by each specimen is also given in Table 5.1. By using these normalized relationships as a basis of comparison it is possible to assess the effect of various dimensionless parameters on the potential of the specimens to resist stiffness and strength decay under repeated reversed loading.

The effect of varying amounts of web reinforcement is a major factor to consider because web reinforcement must perform three functions in insuring ductile behavior of a member subjected to load reversals. It must (1) carry the majority of shear forces in the member, (2) limit the mobility of concrete blocks formed by intersecting inclined cracks in the plastic hinging region, and (3) provide stability to longitudinal reinforcement to delay or prevent buckling of compression reinforcement.

It is possible to nondimensionalize the amount and strength of web reinforcement in a specimen by dividing the effective force contribution of web reinforcement crossing a crack inclined at 45 degrees to the beam centerline ($V_s = A_v f_y d/s$) by the maximum shear force experienced by the specimen during the first cycle of loading (V_m). The relationship of normalized energy dissipation to the ratio V_s/V_m is shown in Fig. 5.1. Two observations may be made based on this figure. First, there is a trend toward increased energy dissipation with an increase in the V_s/V_m ratio. Second, the performance of Specimen 7 indicates that a high V_s/V_m ratio does not guarantee high energy dissipation, because the specimen may fail in a mode which cannot be controlled by web reinforcement of any size. In the case of Specimen 7, sliding along nearly vertical cracks in the beam at the face of the column was the major cause of stiffness loss. This sort of deterioration can not be prevented by vertical ties only, even if their spacing is very small.

Shear span to depth ratio has also been considered a significant factor in influencing the ability of a specimen to resist stiffness and strength decay during load reversals. The relationship between normalized energy dissipation and shear span to depth ratio is shown in Fig. 5.2. It is apparent that no significant or defineable relationship exists between energy dissipation

and shear span to depth ratio in the range considered when other beam parameters are allowed to vary.

The significance of shear span to depth ratio is best shown when it is considered in conjunction with the ratio of main longitudinal reinforcement area to the balanced area of reinforcement (ρ/ρ_{bal}), as was illustrated in Fig. 4.8.

To observe the relationship of these parameters to energy dissipation, consider first the relationship between energy dissipation and the ρ/ρ_{bal} ratio shown in Fig. 5.3. The general trend evident here is that an increase in energy dissipation potential accompanys lower percentages of tension reinforcement. However, shear span to depth ratio varied within relatively narrow limits for these tests (from 3.6 to 5.0). The relative fixity of the a/d ratio tends to magnify the effect of the ρ/ρ_{bal} ratio on energy dissipation when in reality the ρ/ρ_{bal} ratio would not appear to be as significant if other parameters were allowed to vary within a wider range.

It is possible to show the combined effect of the a/d and ρ/ρ_{bal} ratios by plotting the relationship of normalized energy dissipation to the maximum shear stress parameter, α, or its reciprocal as shown in Figs. 5.4 and 5.5 respectively. The use of the reciprocal of shear stress level improves the linearity of this relation.

In general, lower shear stresses had a compound effect of allowing more cycles of displacement before failure with high energy dissipation per cycle.

Figure 5.5 emphasizes the relationship of energy dissipation to shear stress for specimens with and without supplementary longitudinal reinforcement intended to reduce shear strength deterioration. It is evident in Fig 5.5 that intermediate longitudinal reinforcement increased the level of shear stress at maximum first-cycle load for each section considered and in each case increased energy dissipation potential in excess of what might be expected based on greater ultimate load alone. Any energy dissipation increase based on strength increase alone would have been eliminated by normalization. It is possible to define this relationship further by performing a least squares regression to describe the manner of variation between shear stress level and energy dissipation for specimens with and without supplementary reinforcement. If we refer to normalized energy dissipation as E, then for normally reinforced specimens this relationship becomes:

$$E = 33.7\ (1/\alpha) - 2.1 \qquad (5.1)$$

with the coefficient of determination ($r^2 = 0.83$) indicating the efficacy of the regression. For specimens with intermediate longitudinal shear reinforcement,

$$E = 40.5\ (1/\alpha) - 1.9 \qquad (5.2)$$

with $r^2 = 0.98$. A final regression may be performed on data related to normally reinforced specimens by disregarding the results of tests for Specimen 3, which performed particularly poorly and may not have been totally representative of all specimens having similar section properties. Performing the regression without consideration of Specimen 3, the relationship for normally reinforced specimens becomes,

$$E = 35.9\ (1/\alpha) - 2.0 \qquad (5.3)$$

with $r^2 = 0.99$.

It is appropriate to compare the results of tests performed here with the results of other tests of similar specimens having a wide range of shear span to depth ratios, web reinforcement ratios, and significant variations in other critical variables. A ready comparison is available by considering the work of Gosain et al. (13), where the work index was used as a basis of comparison for specimen energy dissipation. The relationship of calculated work index to total measured energy dissipation as normalized by first cycle energy dissipation is shown in Fig. 5.6. The linearity of this relationship shows good agreement in evaluation of overall specimen performance, with some minor scatter caused by the inability of the work index to represent precisely

the energy dissipation performance of a specimen by considering only deflection ductility, shear span to depth ratio and maximum load per cycle.

The relationship of the tests discussed here to other similar tests conducted by other research groups may be shown by plotting all tests in some uniform manner. In Fig. 5.7 the test results obtained in this investigation are presented in a form identical to that used by Gosain (see Gosain et al., Fig. 10). The statistical mean performance of all specimens considered by Gosain is shown in Fig. 5.7, as are the limits of 90% statistical confidence for the regression. Although the results of tests considered here all fall within the projected norm (at 90% statistical confidence) for specimens of this type, the results of the twelve specimens tested indicate that most specimens, particularly Specimens 1 and 2, did not develop a work index as high as expected. It must be recalled that Specimens 1 and 2 were exhibiting stable behavior at the end of testing and might have been able to dissipate significantly greater amounts of energy.

In addition energy dissipation for all specimens might have been higher if a different displacement history had been used during testing. Although, as noted in Chapter 1, several research groups have subjected concrete flexural members to repeated reversed

loading, there has been a conspicuous lack of agreement as to what constitutes a displacement history that is representative of severe earthquake loading. This presents a serious problem when comparing the energy dissipations for specimens which have undergone different displacement histories, regardless of the method used to normalize energy dissipation. For the specimens considered in this test series, the rate of decay of maximum load and mid-cycle stiffness varied with the imposed displacement ductility. The load vs. displacement relationship for Specimen 4, shown in Fig. 3.1 (d), illustrates particularly well the effect of maximum imposed displacement ductility on strength and stiffness decay. As shown in this figure, overall stiffness and maximum load were relatively stable during the first six cycles of loading (maximum displacement ductility of +4 and -3), but both stiffness and maximum load decayed rapidly when maximum displacement ductilities of +6 and -5 were imposed during the seventh through eleventh load cycles. It is impossible to say exactly how much energy would have been dissipated by this specimen if displacement cycles comparable to the first six had been continued to failure, but it is logical to speculate that total energy dissipation in that case would have been as high or higher than that achieved during the actual imposed load history.

5.3 Buckling of Compression Reinforcement

Nine of the twelve specimens tested experienced buckling of compression reinforcement. In six of these cases, buckling was severe enough to cause cessation of loading, while in the remaining three cases loading was suspended because of strength loss due to several factors including buckling. Buckling severely limited energy dissipation potential of the specimens by decreasing their flexural capacity. In addition, buckling of longitudinal reinforcement was accompanied by twisting about the beam longitudinal axis in four specimens (Nos. 3, 6, 9, and 10).

Several researchers have proposed that buckling of longitudinal reinforcement may be prevented or made inconsequential in relation to other failure mechanisms common to reinforced concrete members subjected to repeated reversed loading by using a limiting stirrup spacing in the region where buckling is anticipated. The results of the present tests indicate that this is not an entirely adequate solution. A compilation of the behavior of these specimens in regard to buckling is given in Table 5.2. As shown in this table, the length of the buckled bar sections always exceeded the spacing between stirrups and in general was equal to three to four stirrup intervals. This condition may be explained

TABLE 5.2

COMPILATION OF CHARACTERISTICS OF BUCKLED REINFORCEMENT

Specimen Number	Buckling Influence	Buckled Bar Size	Size and Spacing of Confining Ties	Hinging Zone or Buckled Deformation Length
1	None		#2 @ 2"	7"
2	None		#2 @ 2"	7"
3	Major	#5	#2 @ 2.5"	10"
4	Major	#5	#2 @ 2.5"	8"
5	Negligible		#2 @ 2"	7"
6	Major	#5	#2 @ 2"	7"
7	Negligible		#3 @ 2.5"	10"
8	Negligible		#2 @ 2"	9"
9	Major	#7	#3 @ 3"	12"
10	Major	#7	#3 @ 3"	11"
11	Minor	#7	#3 @ 3"	10"
12	Major	#7	#3 @ 3"	10"

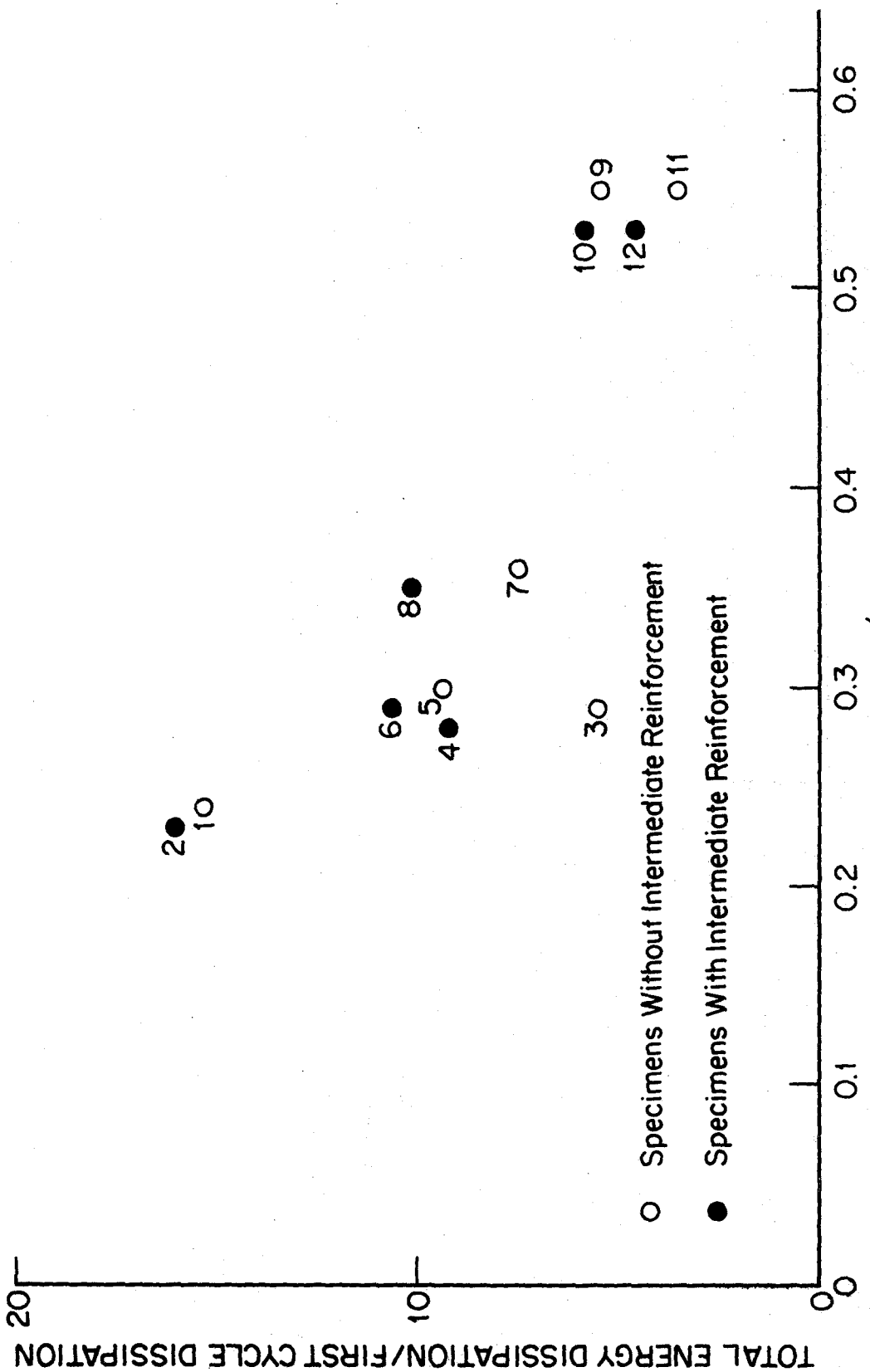

Fig. 5.3. Normalized Energy Dissipation vs. ρ/ρ_{bal} for Twelve Specimens.

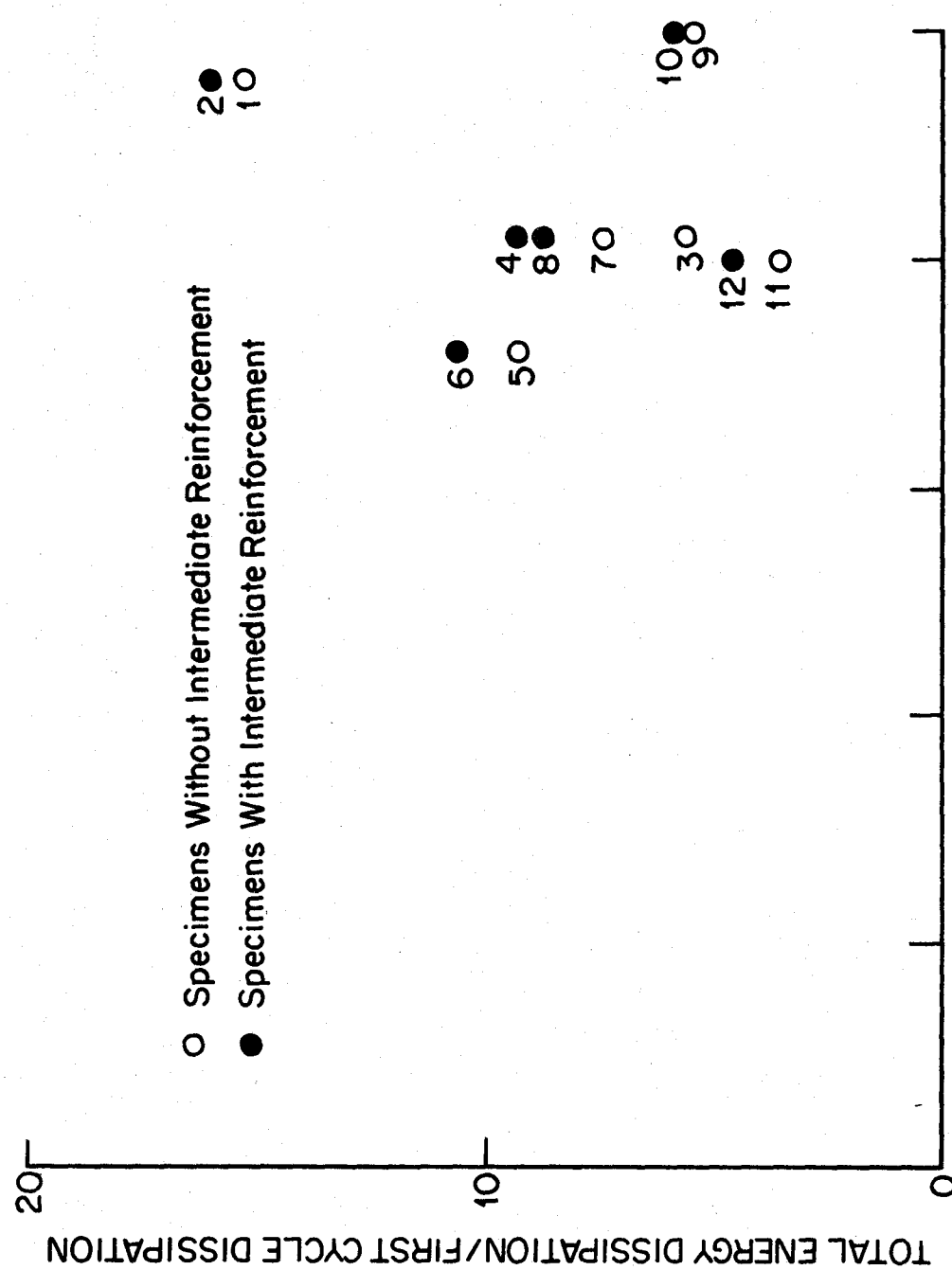

Fig. 5.2. Relationship of Normalized Energy Dissipation to Shear Span to Depth Ratio (a/d).

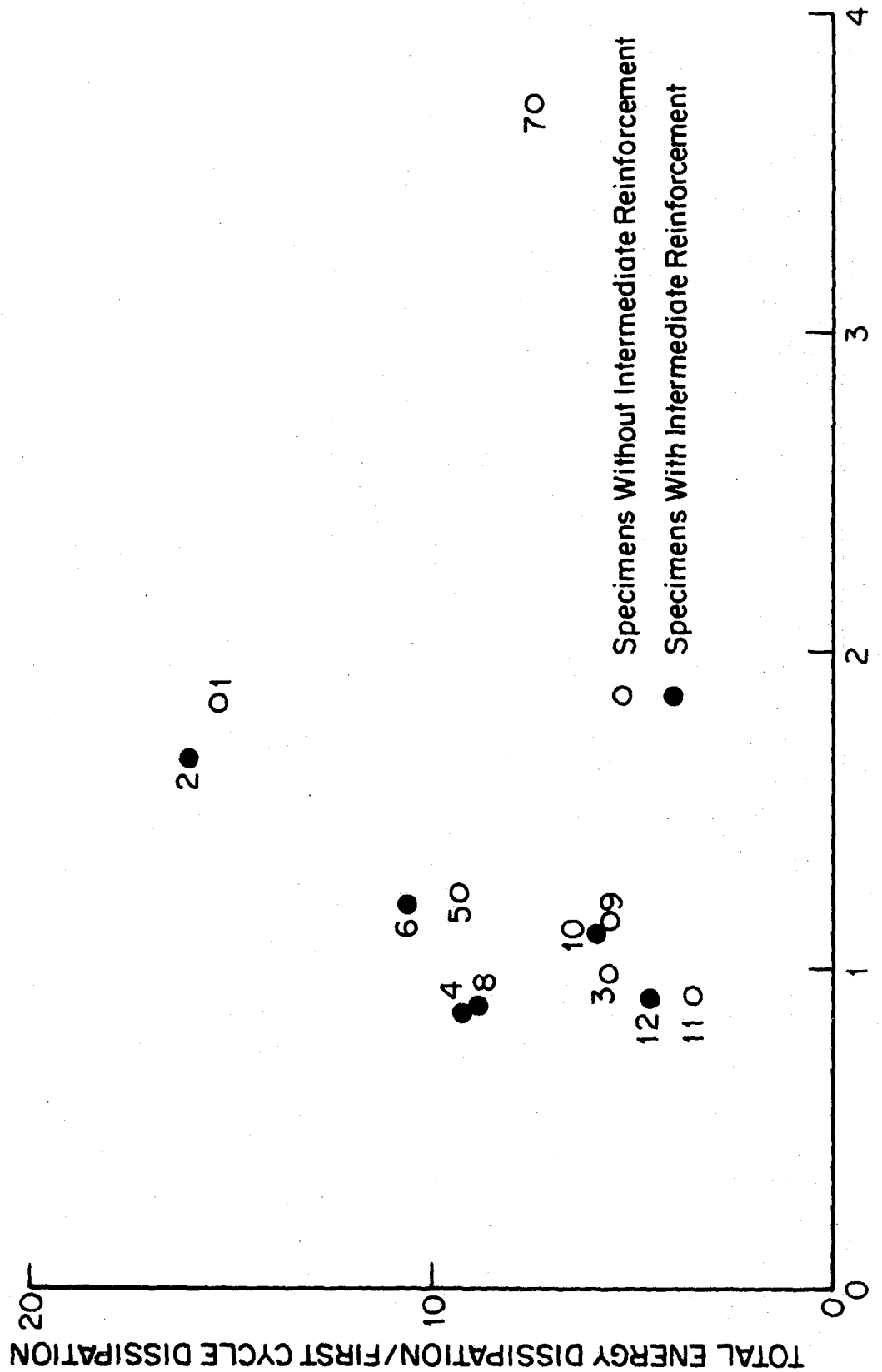

Fig. 5.1. Relationship of Normalized Energy Dissipation to v_s/v_m Ratio.

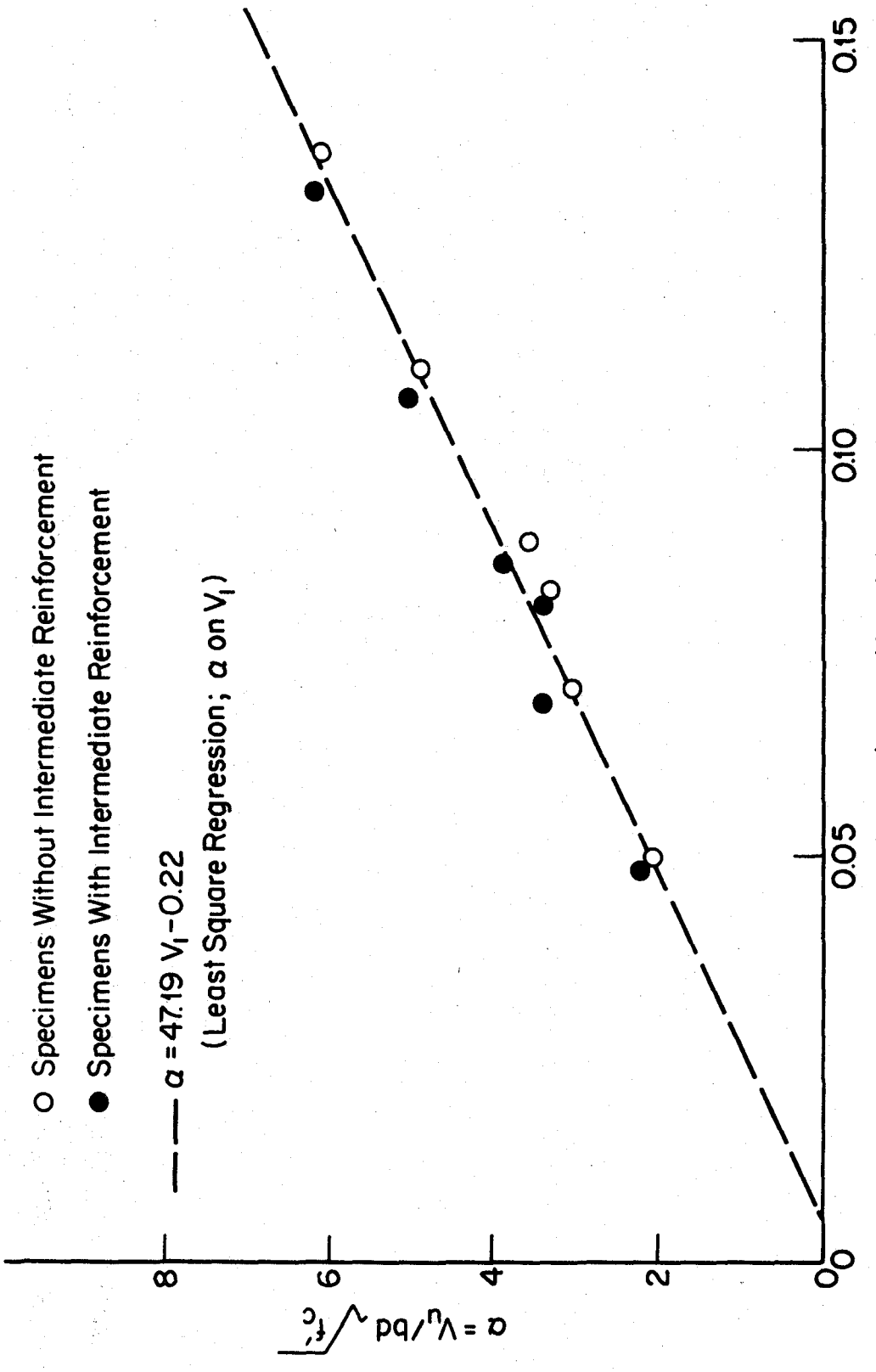

Fig. 4.8. Relationship of Maximum Shear Stress to $(\rho/\rho_{bal})(d/a)$

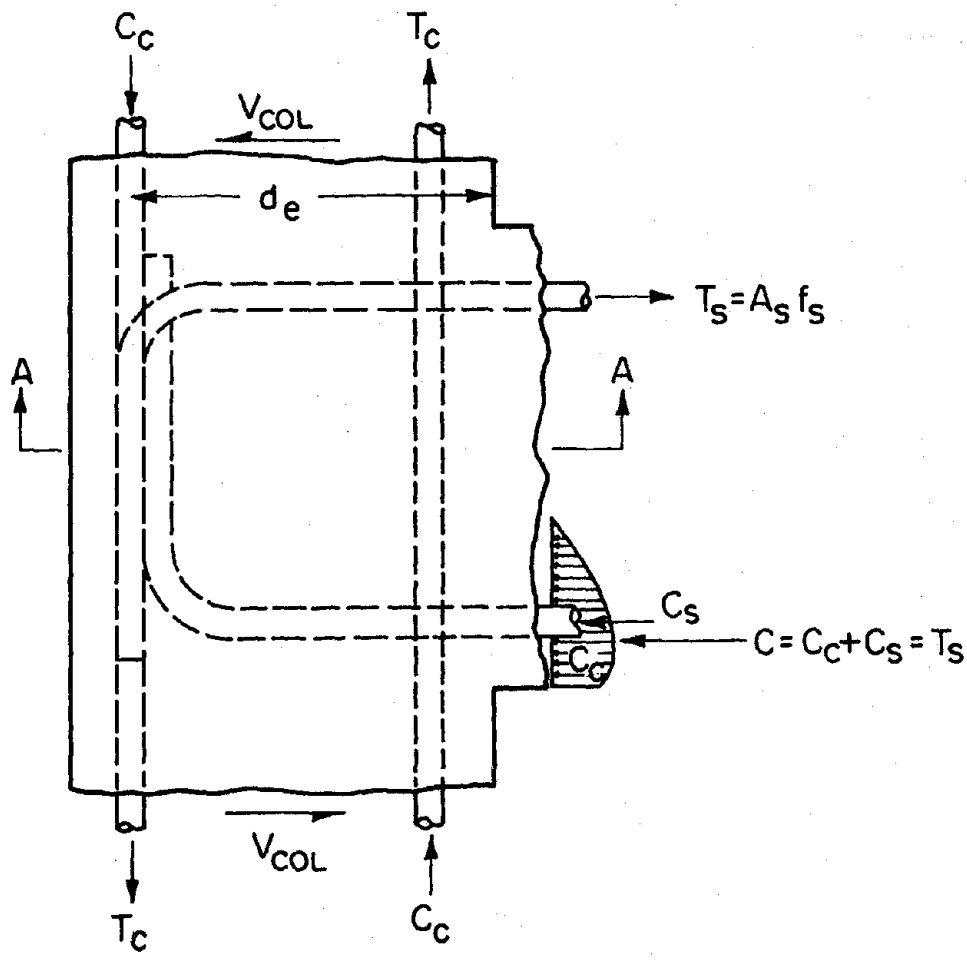

Fig. 4.7. Idealization of Forces at Beam-Column Joint.

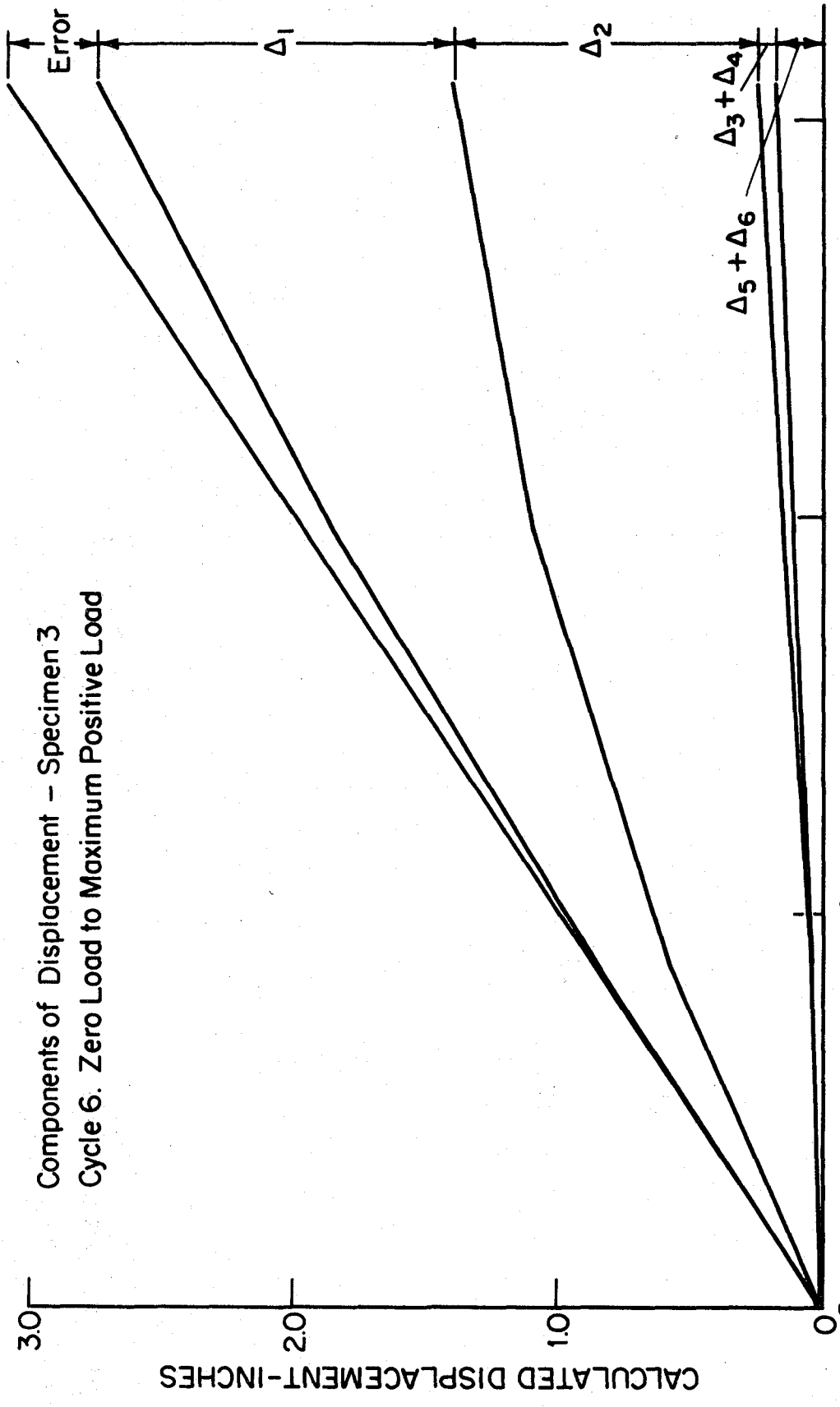

Fig. 4.6. Components of Displacement - Sixth Cycle of Inelastic Loading - Specimen 3.

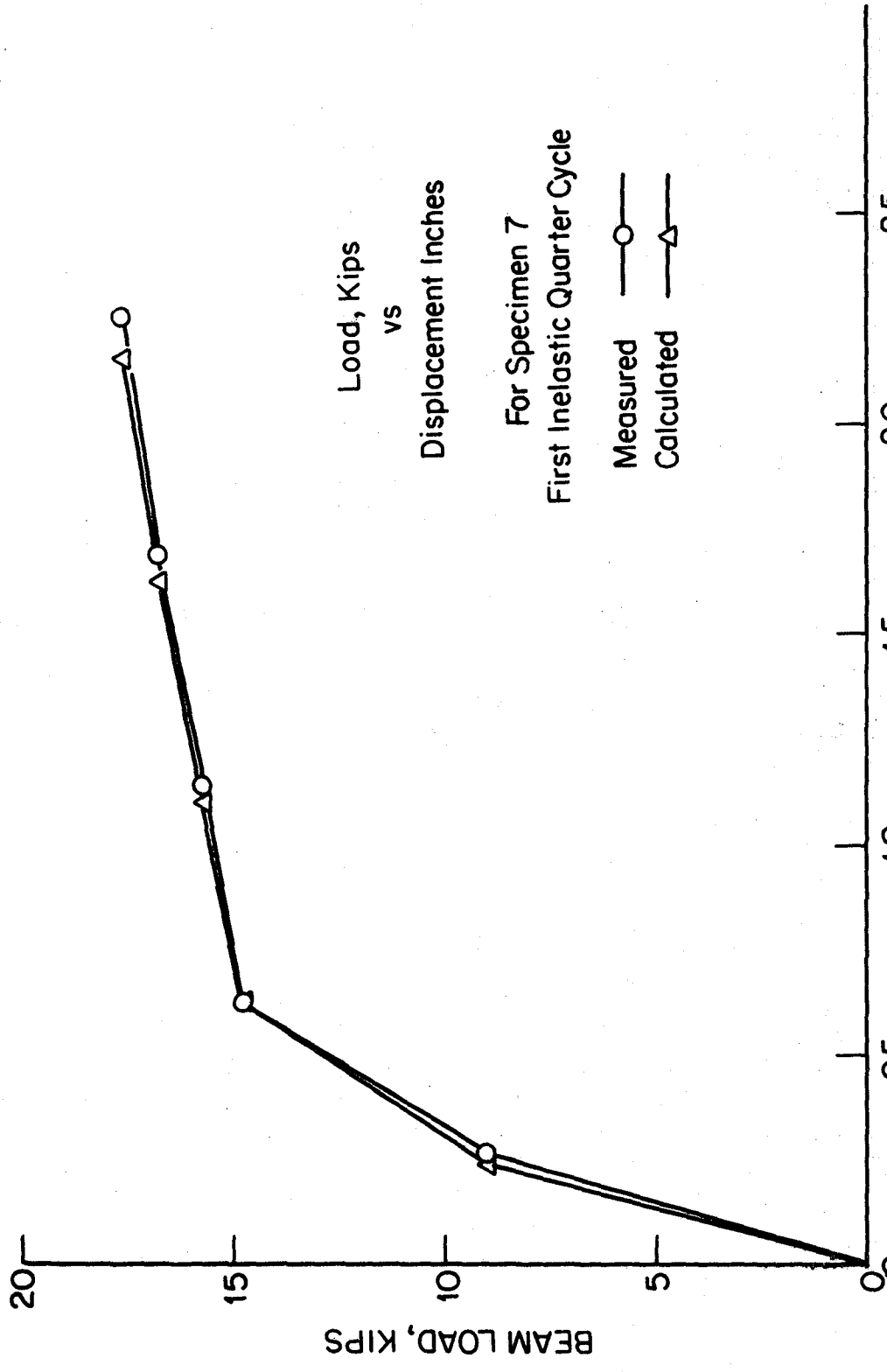

Fig. 4.5. Beam Load vs. Measured and Calculated Displacement for Specimen 7.

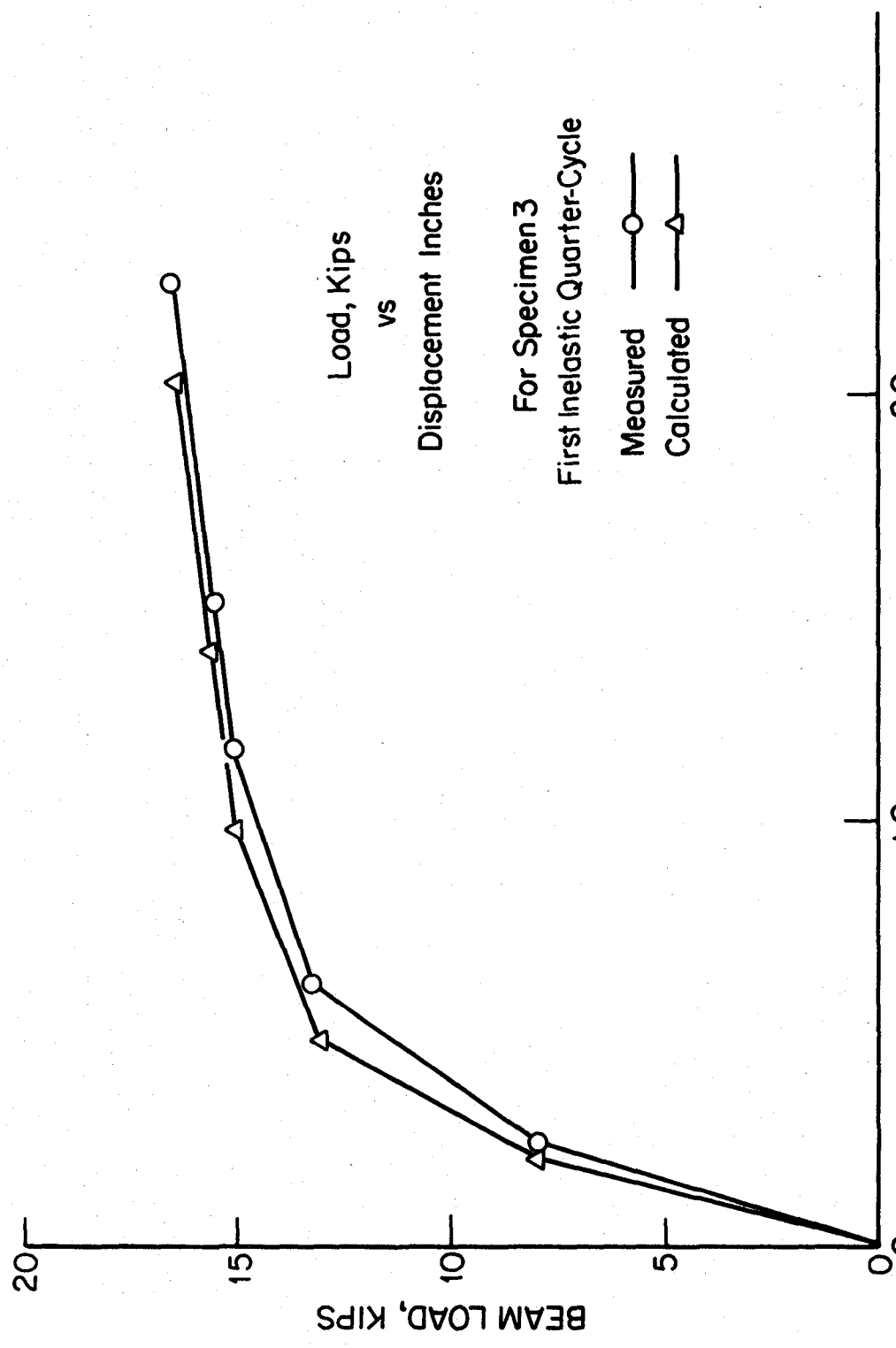

Fig. 4.4. Beam Load vs. Measured and Calculated Displacement for Specimen 3.

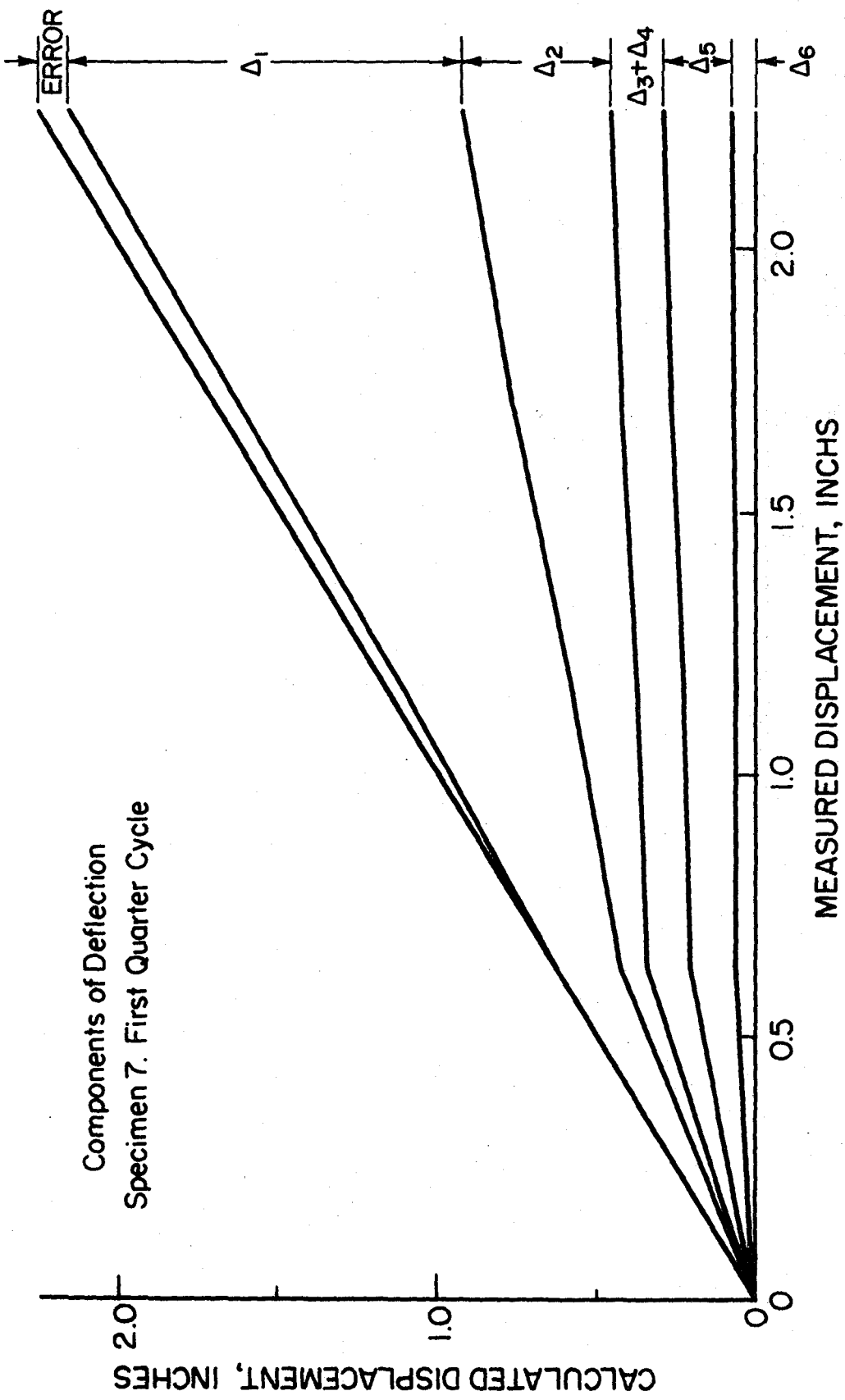

Fig. 4.3. Components of Deflection during First Quarter-Cycle of Inelastic Loading - Specimen 7.

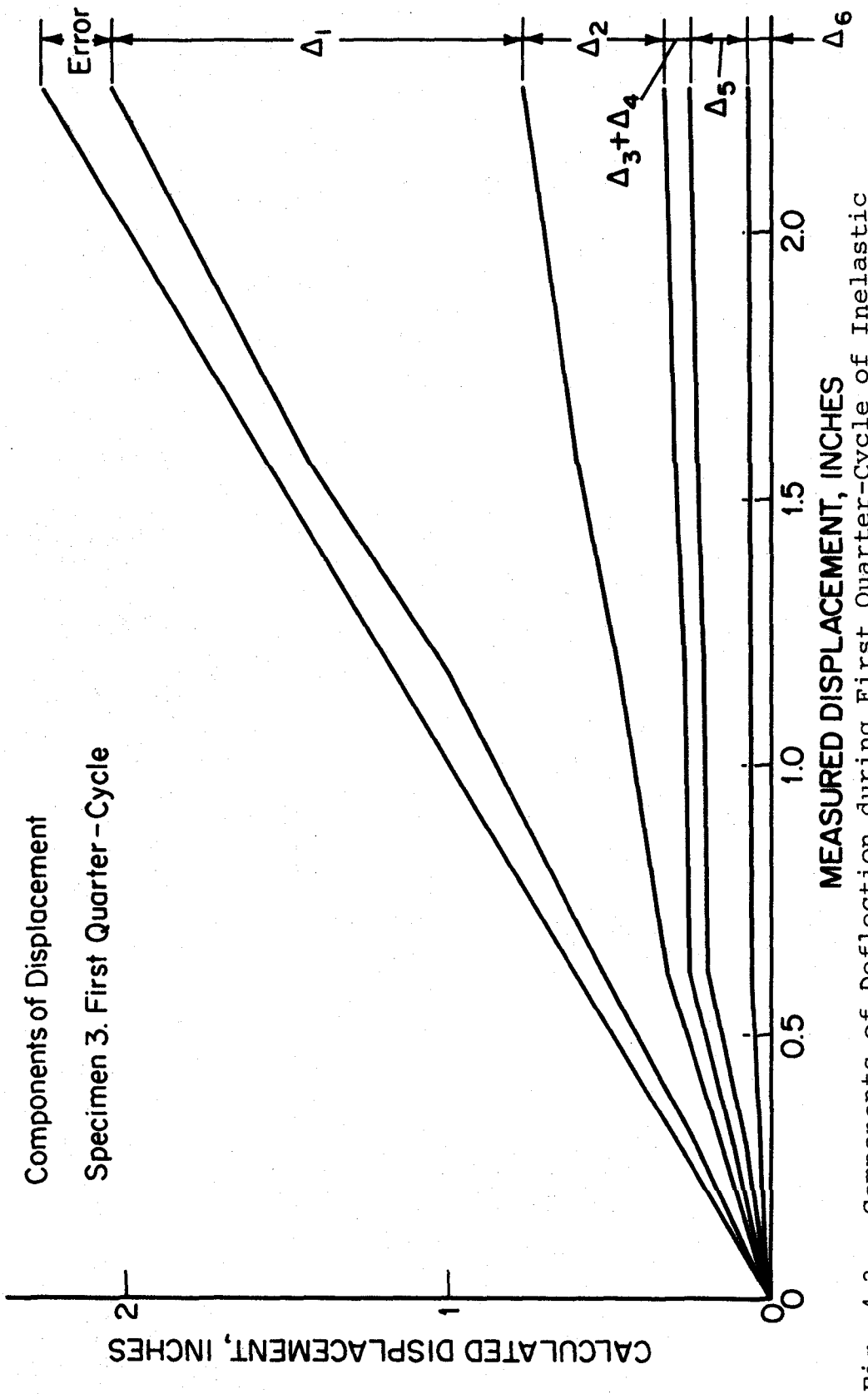

Fig. 4.2. Components of Deflection during First Quarter-Cycle of Inelastic Loading - Specimen 3.

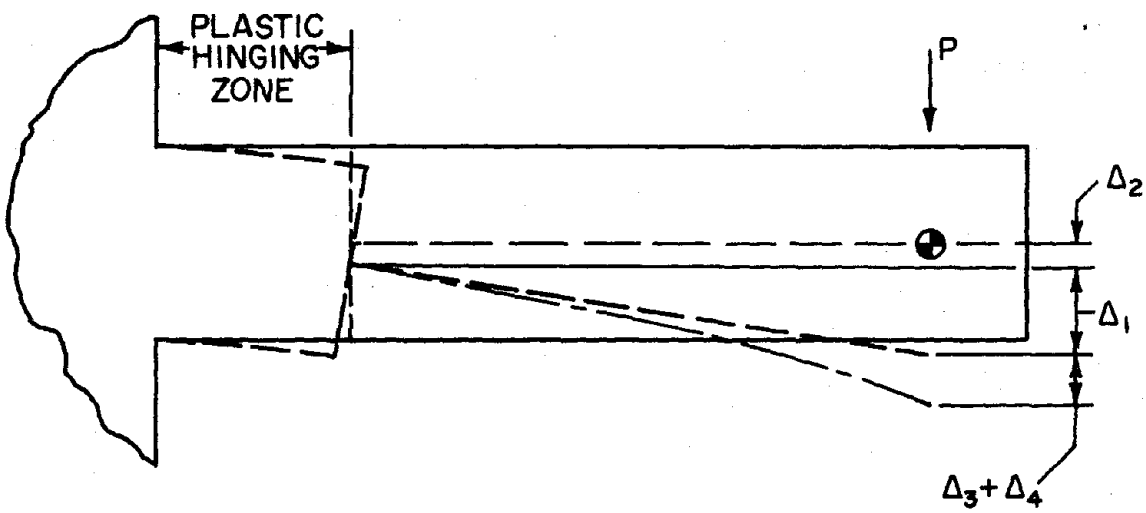

Δ_1 = Deflection due to flexural rotation within the hinging zone

Δ_2 = Deflection due to shear strain in the hinging zone

Δ_3 = Deflection due to flexural deformation outside the hinging zone

Δ_4 = Deflection due to shear strain outside the hinging zone

Fig. 4.1. Assumed Components of Deflection from Deformation within the Beam.

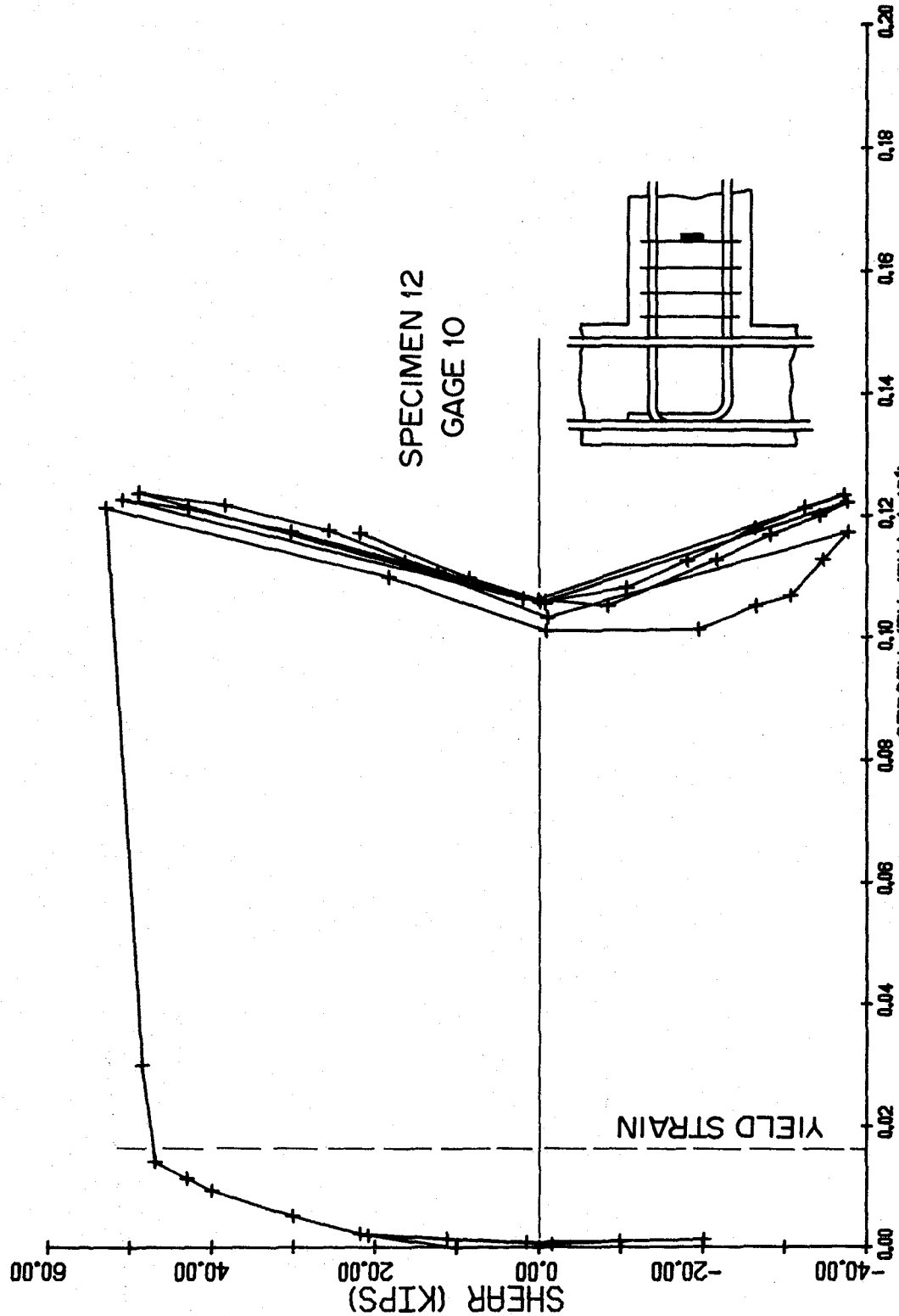

Fig. 3.49. Beam Shear Load vs. Strain in Hinging Zone Tie - Specimen 12.

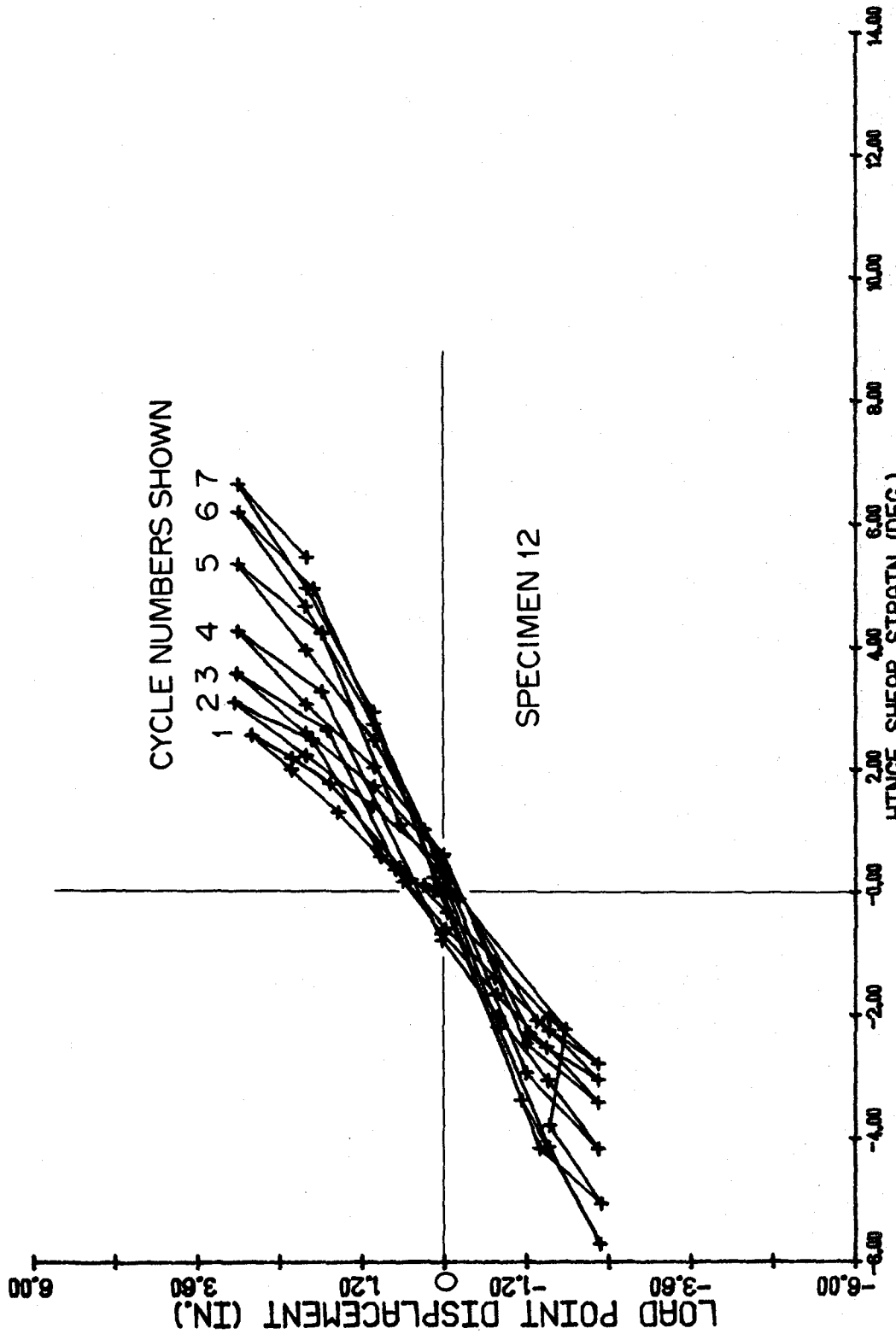

Fig. 3.48. Beam Load Point Displacement vs. Hinge Shear Strain - Specimen 12.

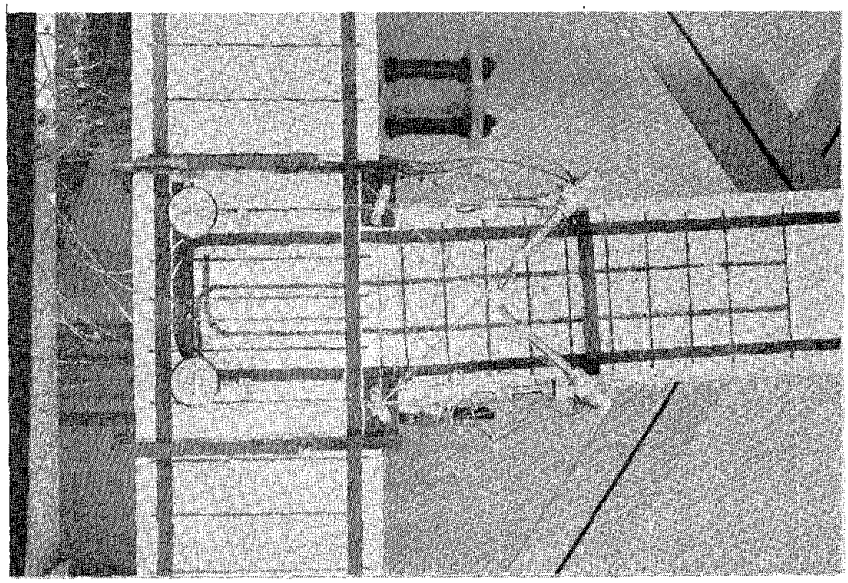

Fig. 3.46. Specimen 12 after One Inelastic Load Cycle.

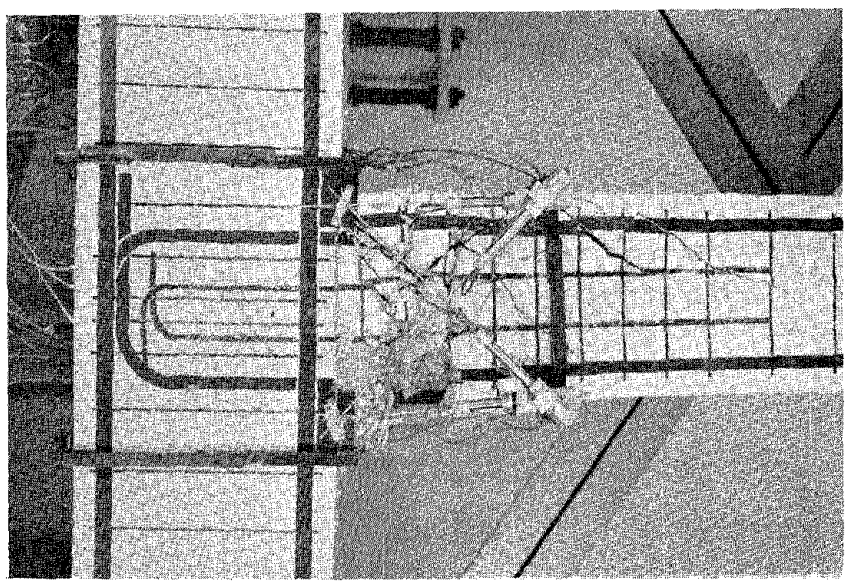

Fig. 3.47. Specimen 12 during Sixth Inelastic Load Cycle.

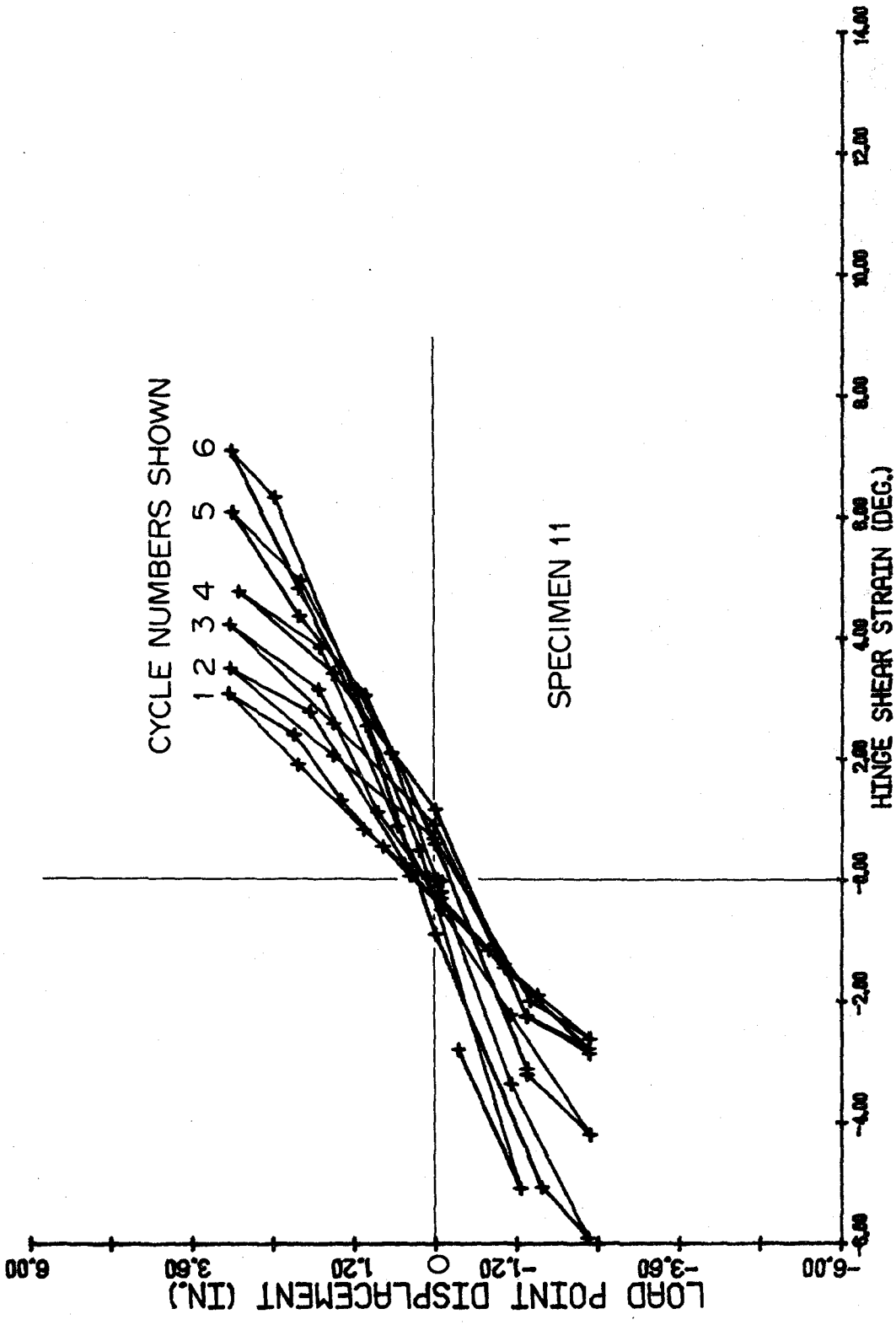

Fig. 3.45. Beam Load Point Displacement vs. Hinge Shear Strain - Specimen 11.

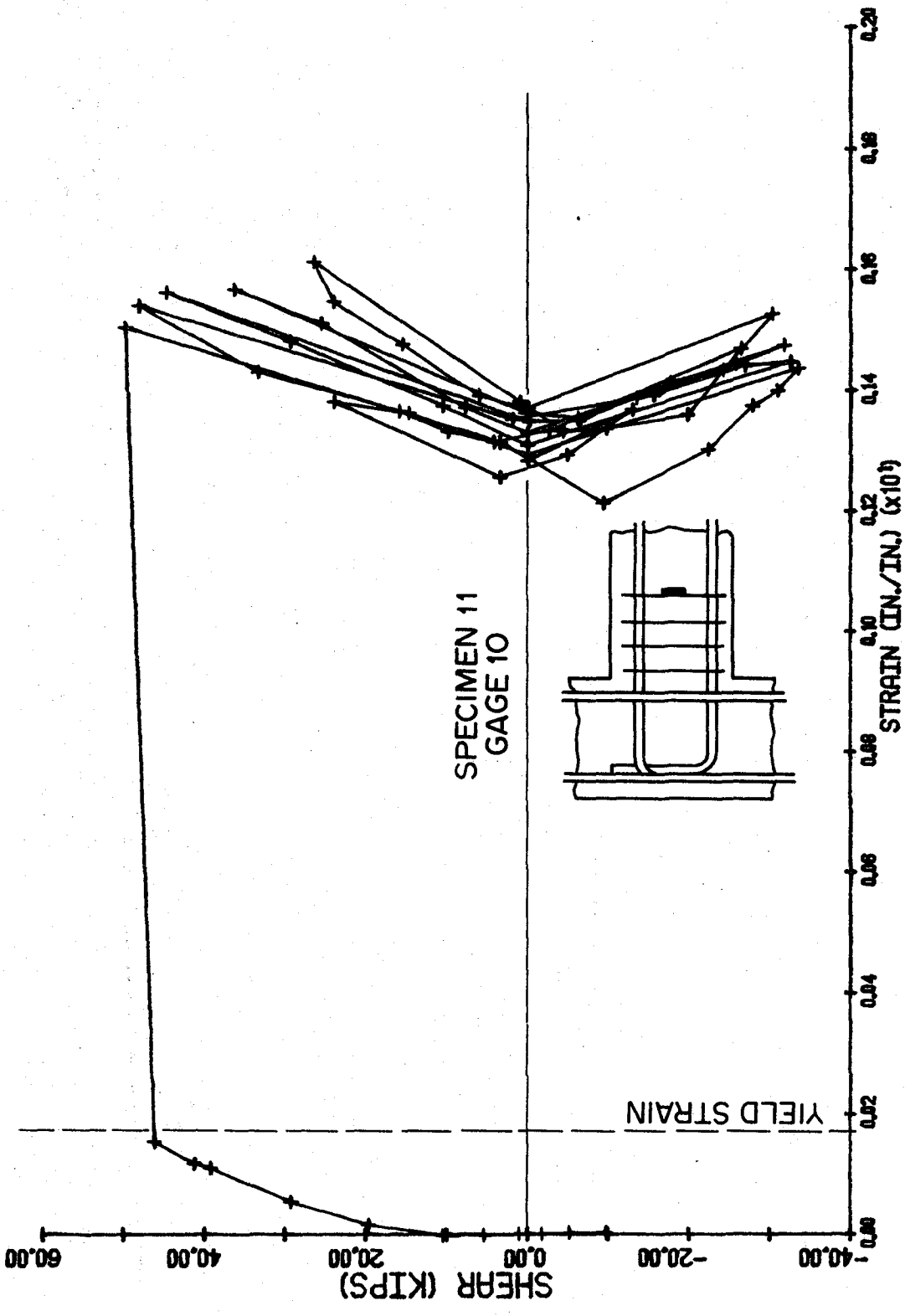

Fig. 3.44. Beam Shear Load vs. Strain in Hinging Zone Tie - Specimen 11.

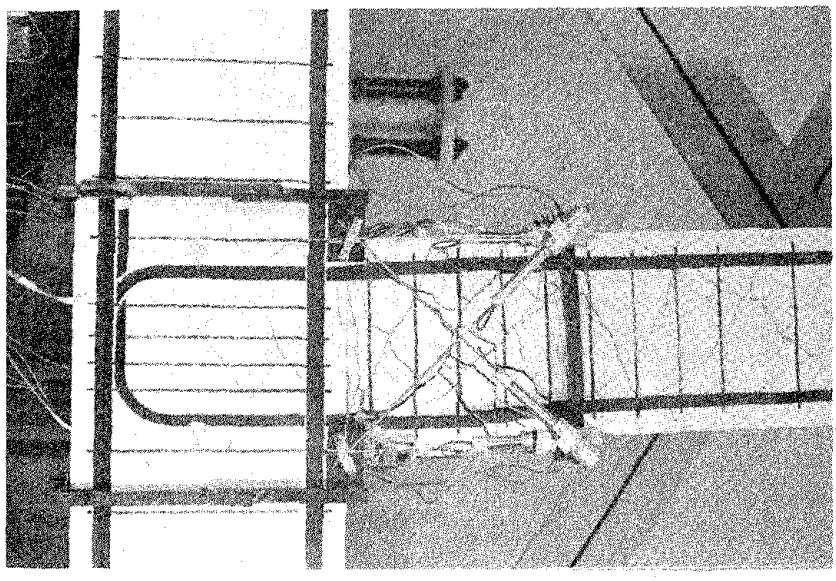

Fig. 3.42. Specimen 11 during First Cycle of Inelastic Loading.

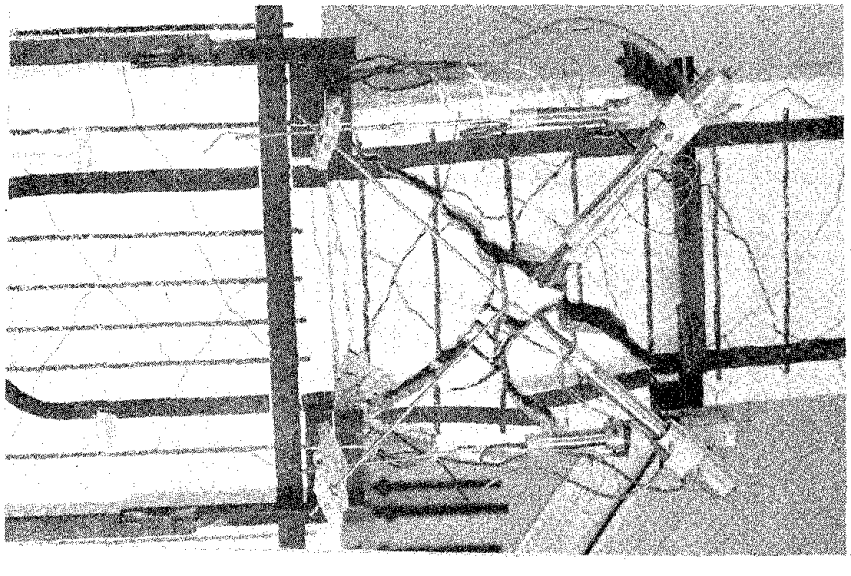

Fig. 3.43. Specimen 11 at Maximum Negative Displacement in Fourth Inelastic Load Cycle.

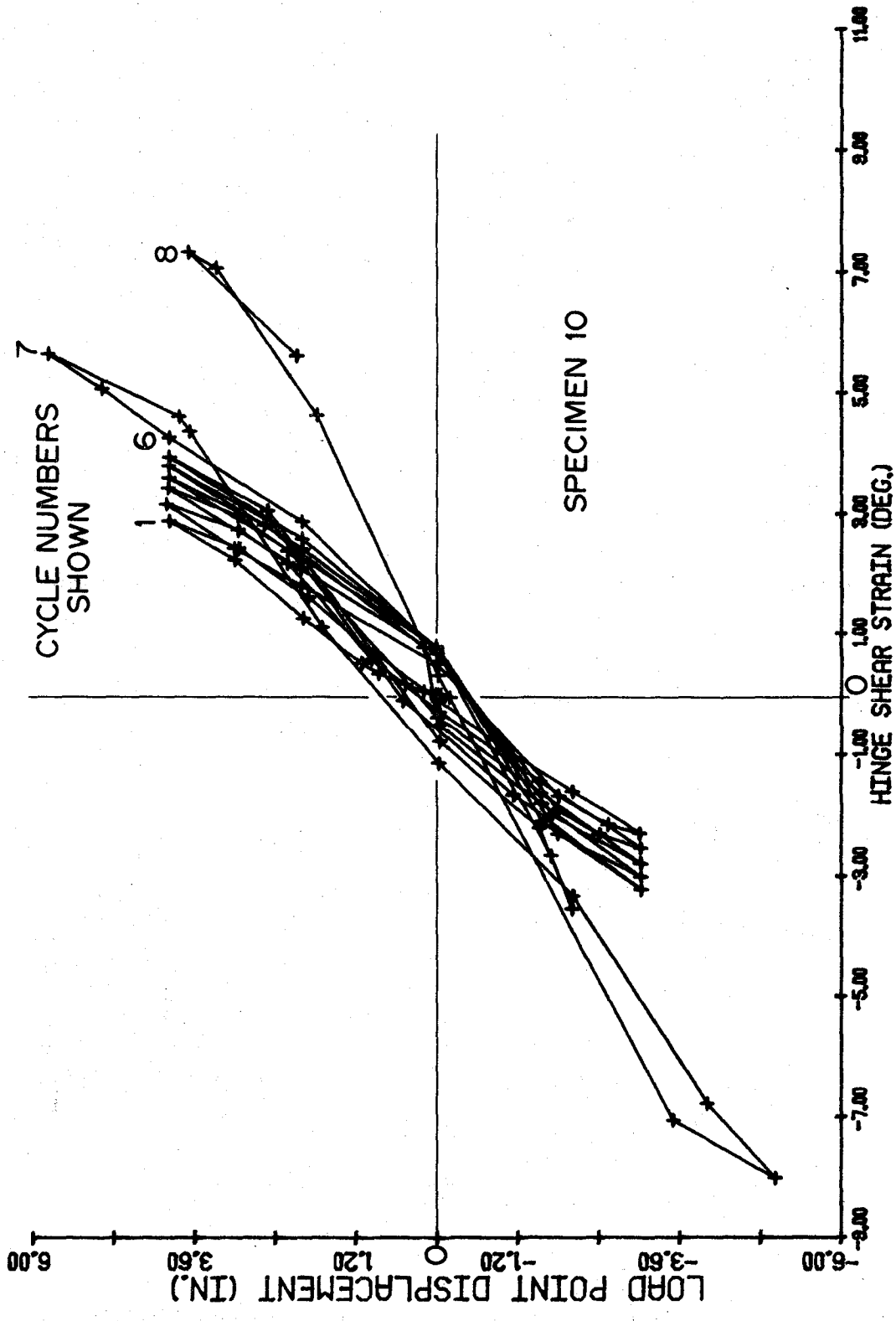

Fig. 3.41. Beam Load Point Displacement vs. Hinge Shear Strain - Specimen 10.

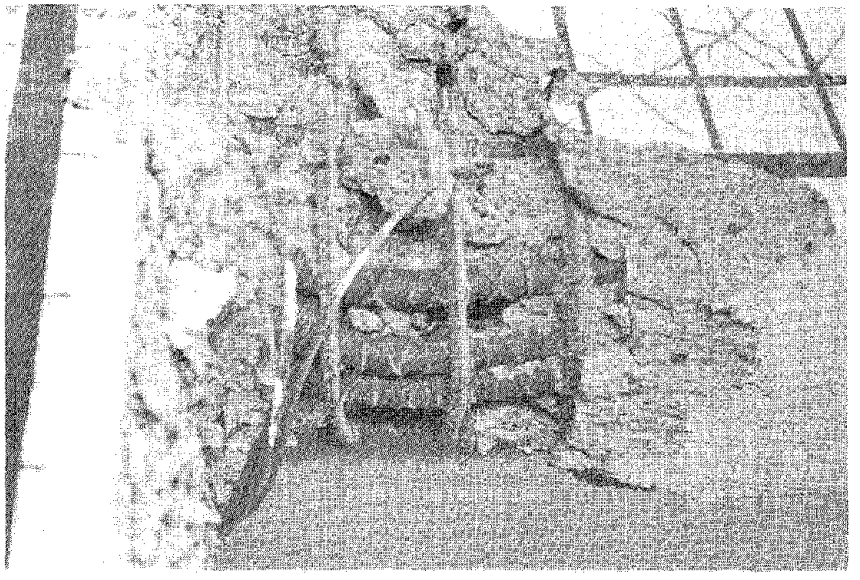

Fig. 3.40. Buckled Shape of Bottom Longitudinal Reinforcement - Specimen 10.

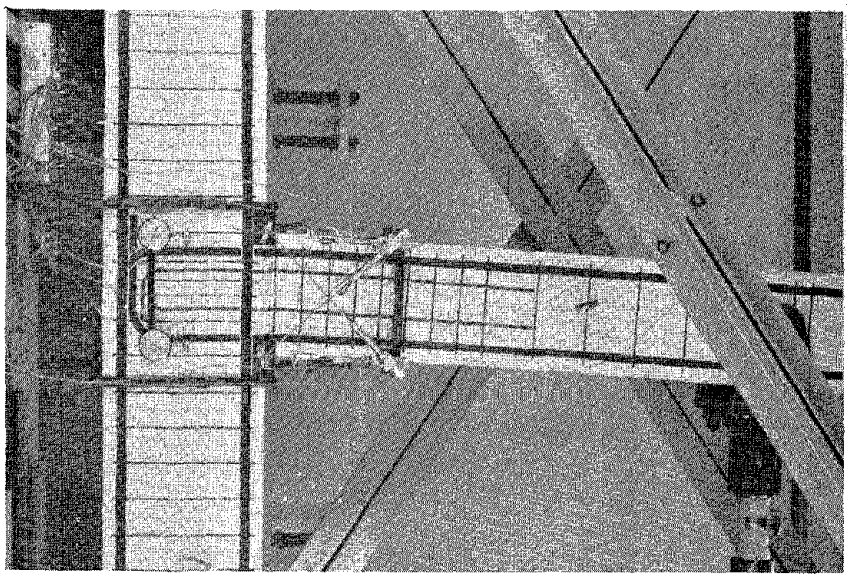

Fig. 3.38. Specimen 10 at Maximum Positive Displacement in First Inelastic Load Cycle.

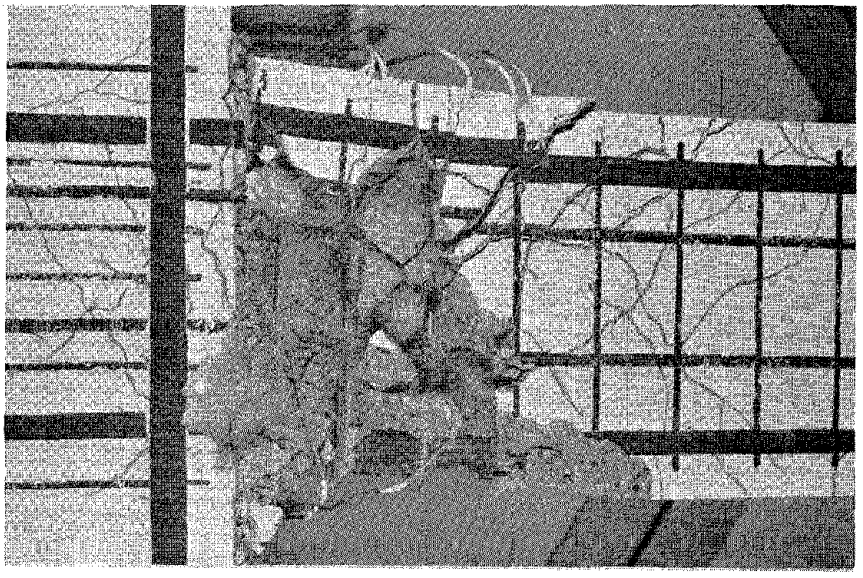

Fig. 3.39. Specimen 10 at the Conclusion of Loading.

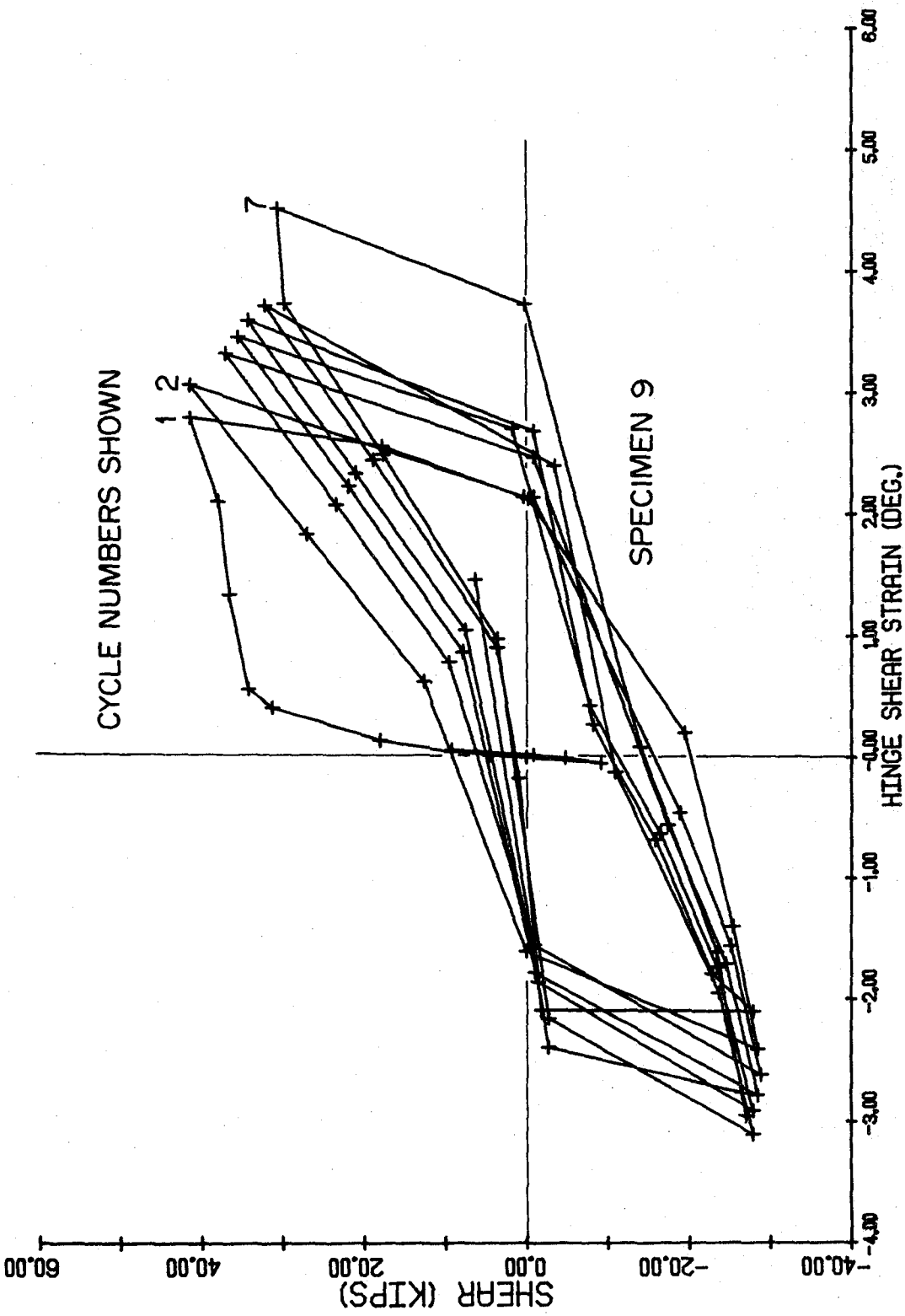

Fig. 3.37. Beam Shear Load vs. Hinge Shear Strain - Specimen 9.

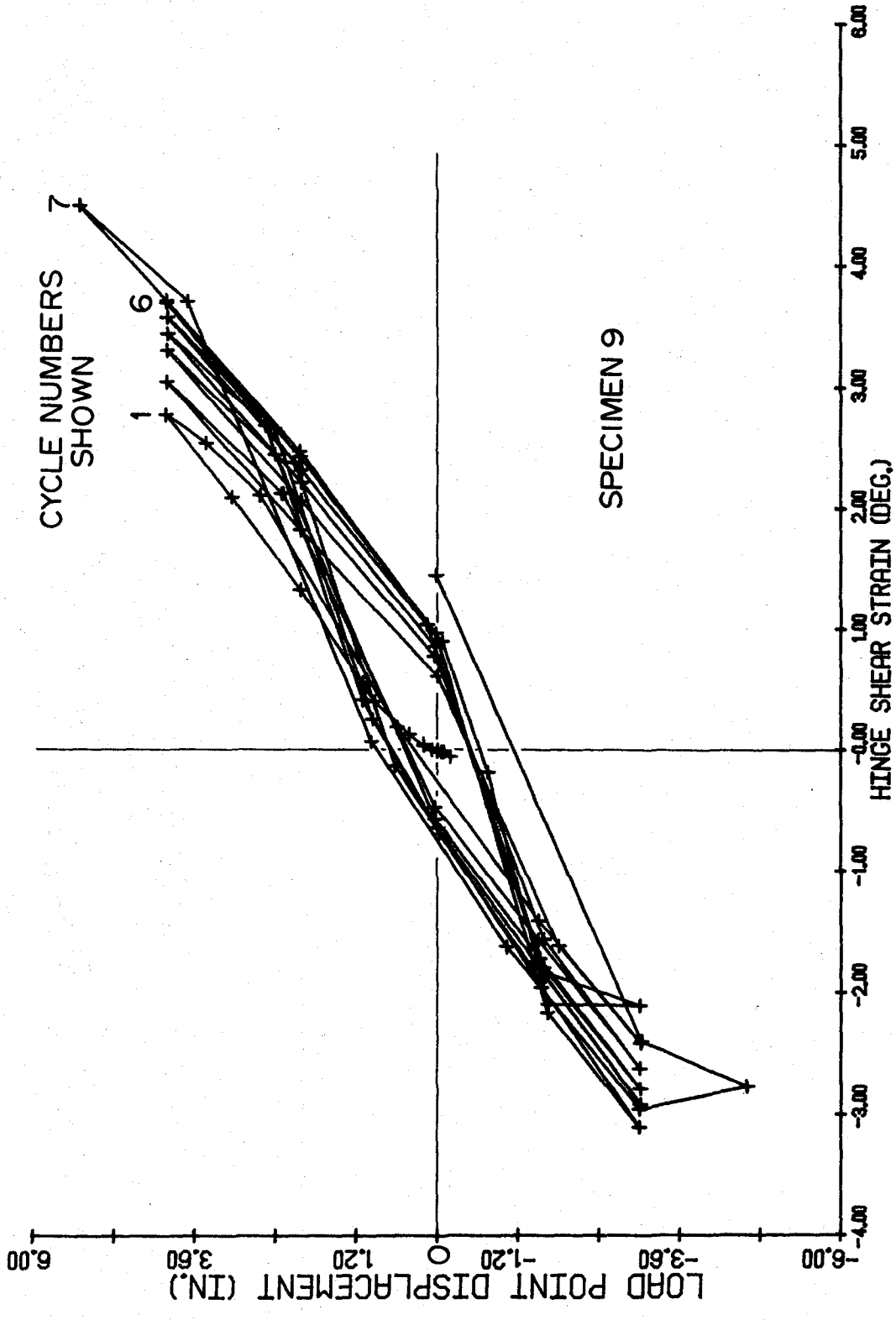

Fig. 3.36. Beam Load Point Displacement vs. Hinge Shear Strain - Specimen 9.

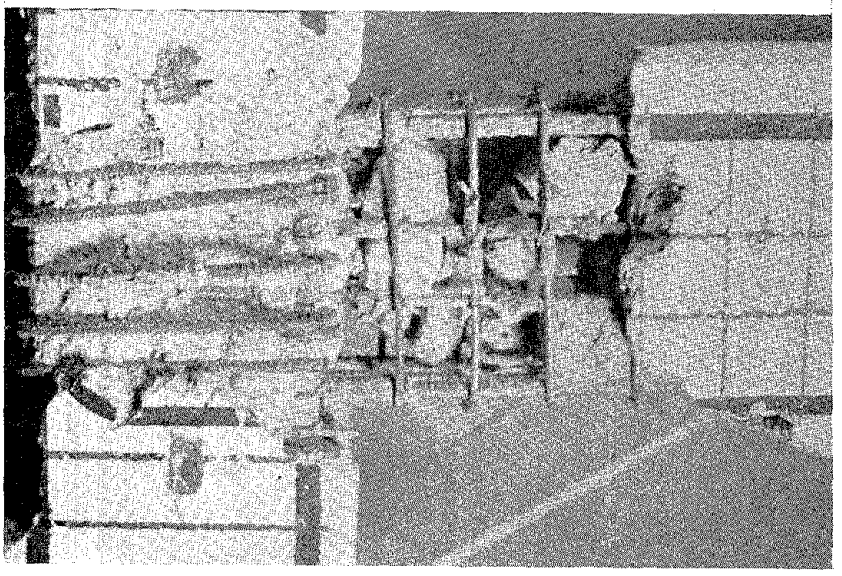

Fig. 3.34. Hinging Region and Beam-Column Joint of Specimen 8 after Removal of Loose Concrete.

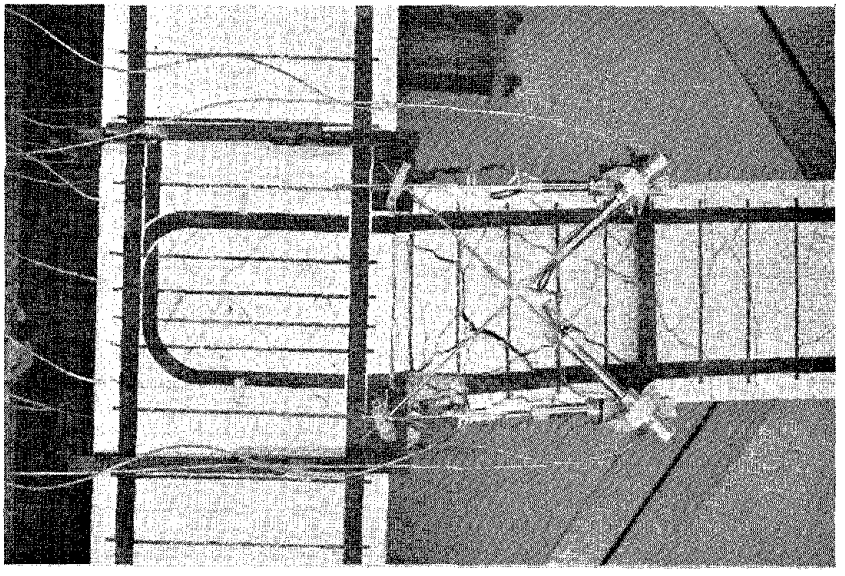

Fig. 3.35. Specimen 9 during Fifth Cycle of Loading.

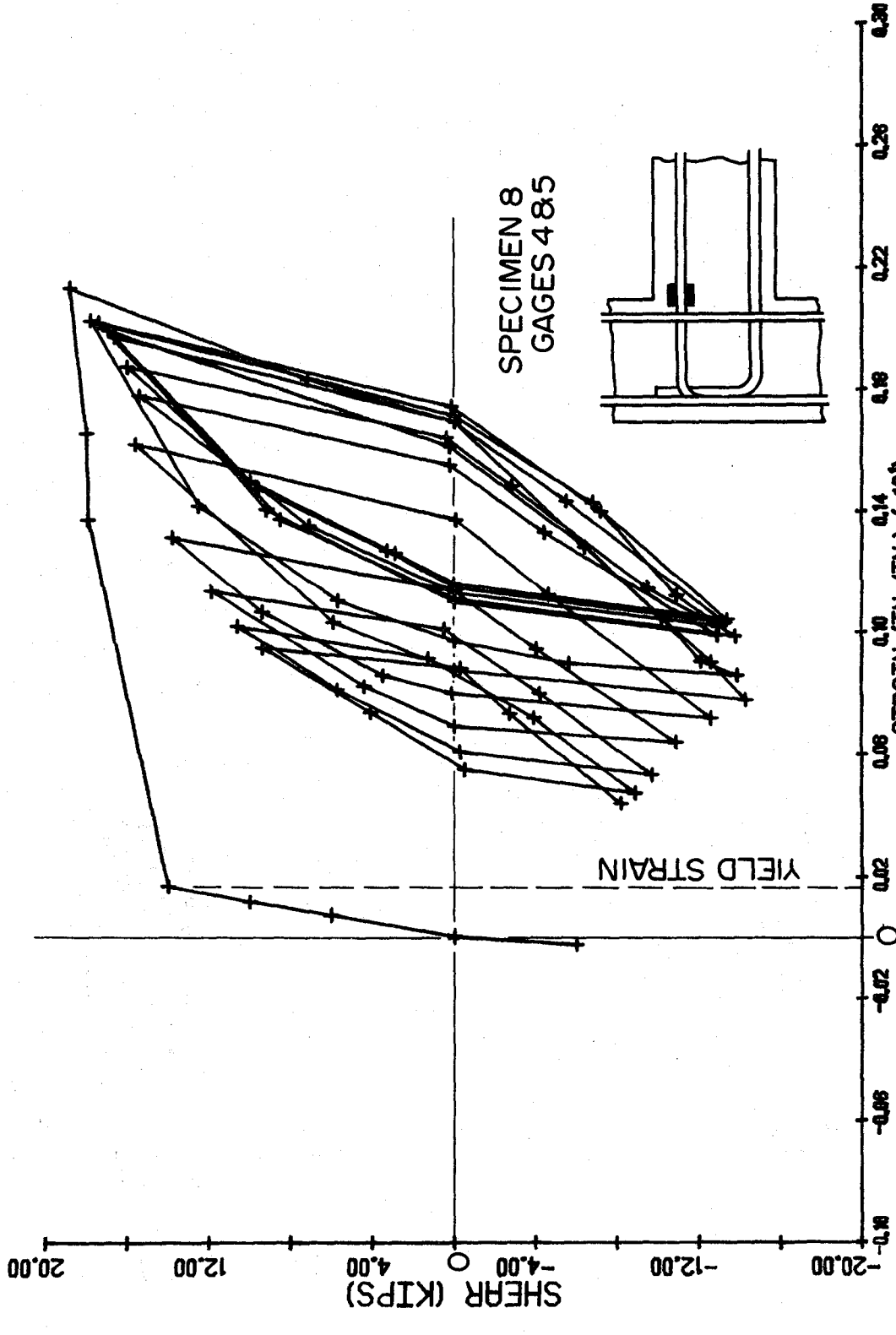

Fig. 3.33. Beam Shear Load vs. Strain at the Face of the Column in Top Longitudinal Reinforcement - Specimen 8.

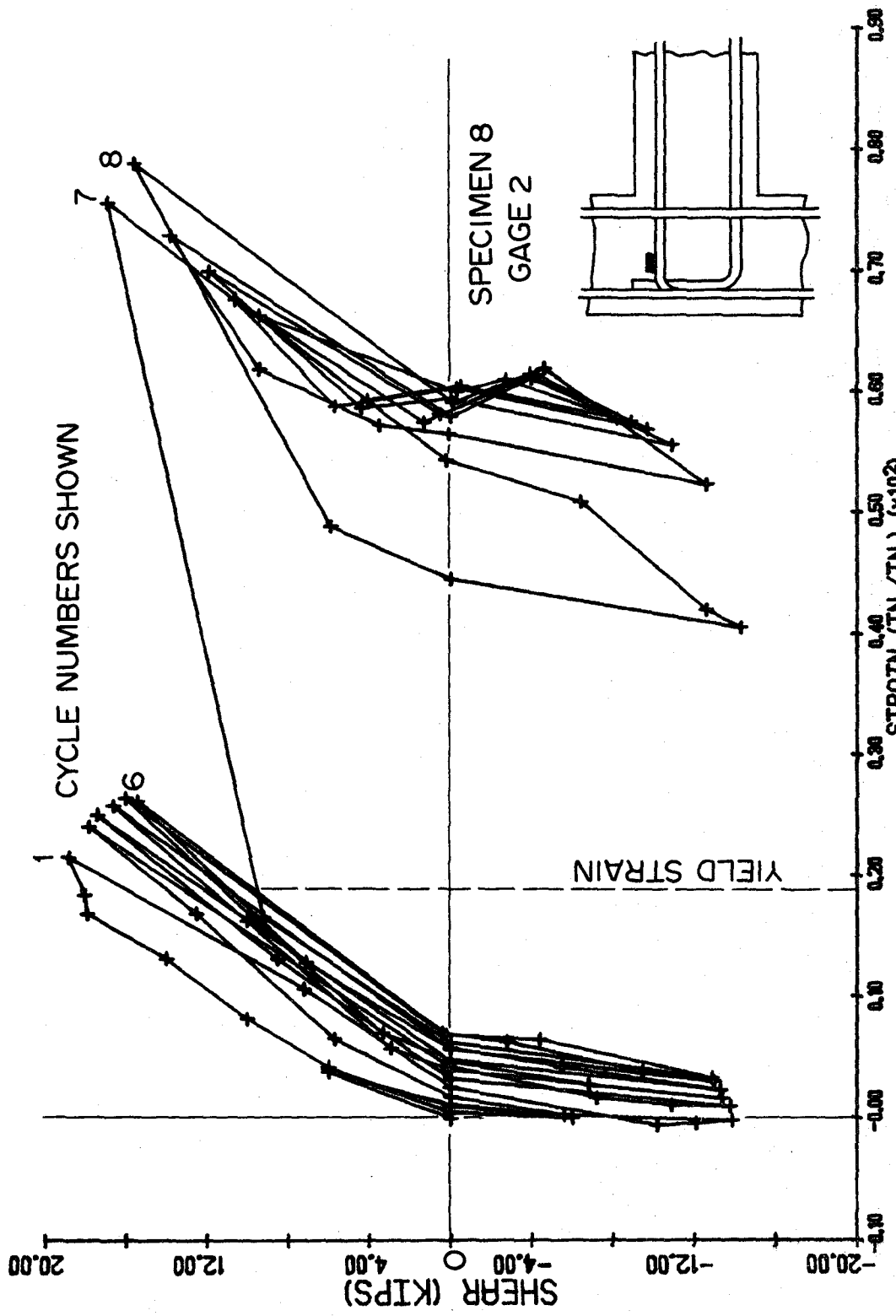

Fig. 3.32. Beam Shear Load vs. Strain at the Beginning of the Hook in Top Longitudinal Reinforcement - Specimen 8.

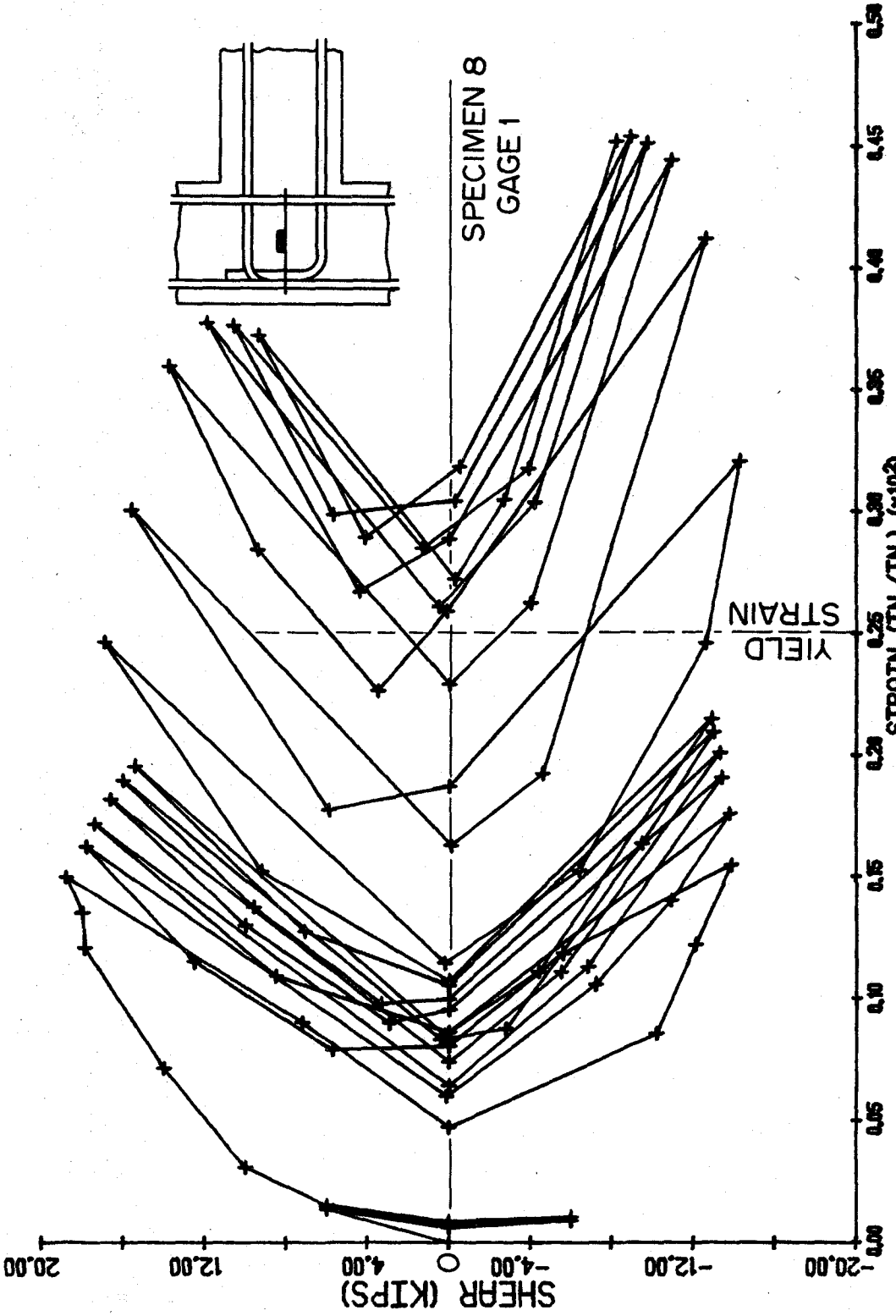

Fig. 3.31. Beam Shear Load vs. Strain in Intermediate Beam-Column Joint Tie -Specimen 8.

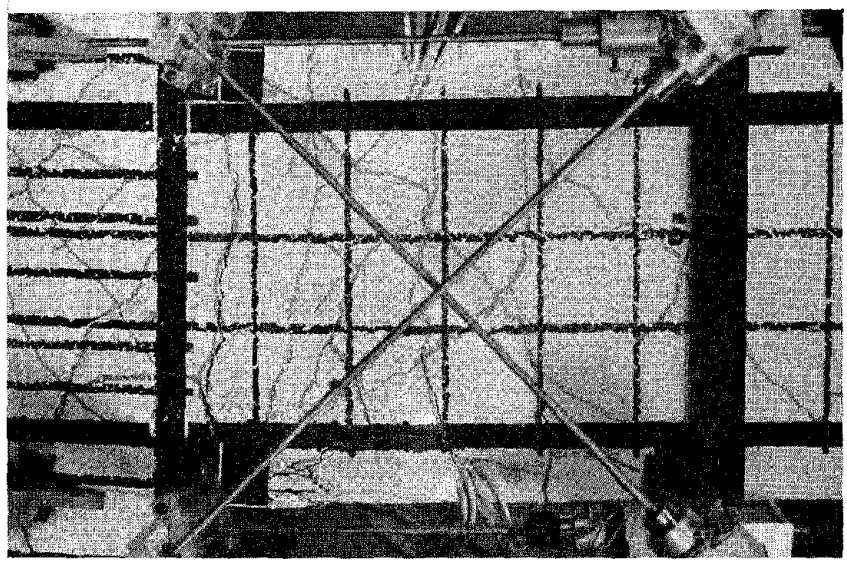

Fig. 3.30(a). Hinging Zone of Specimen 8 at the Conclusion of One Cycle of Testing.

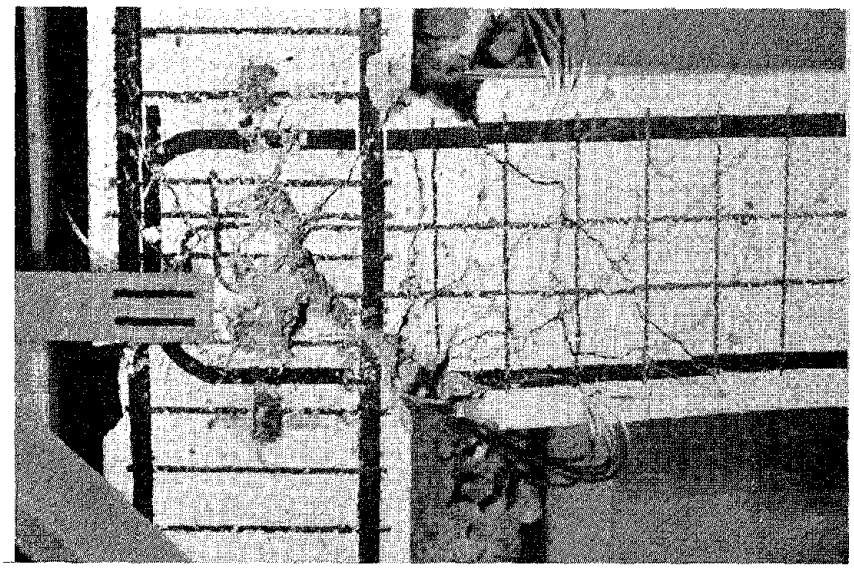

Fig. 3.30(b). Specimen 8 at the Conclusion of Testing.

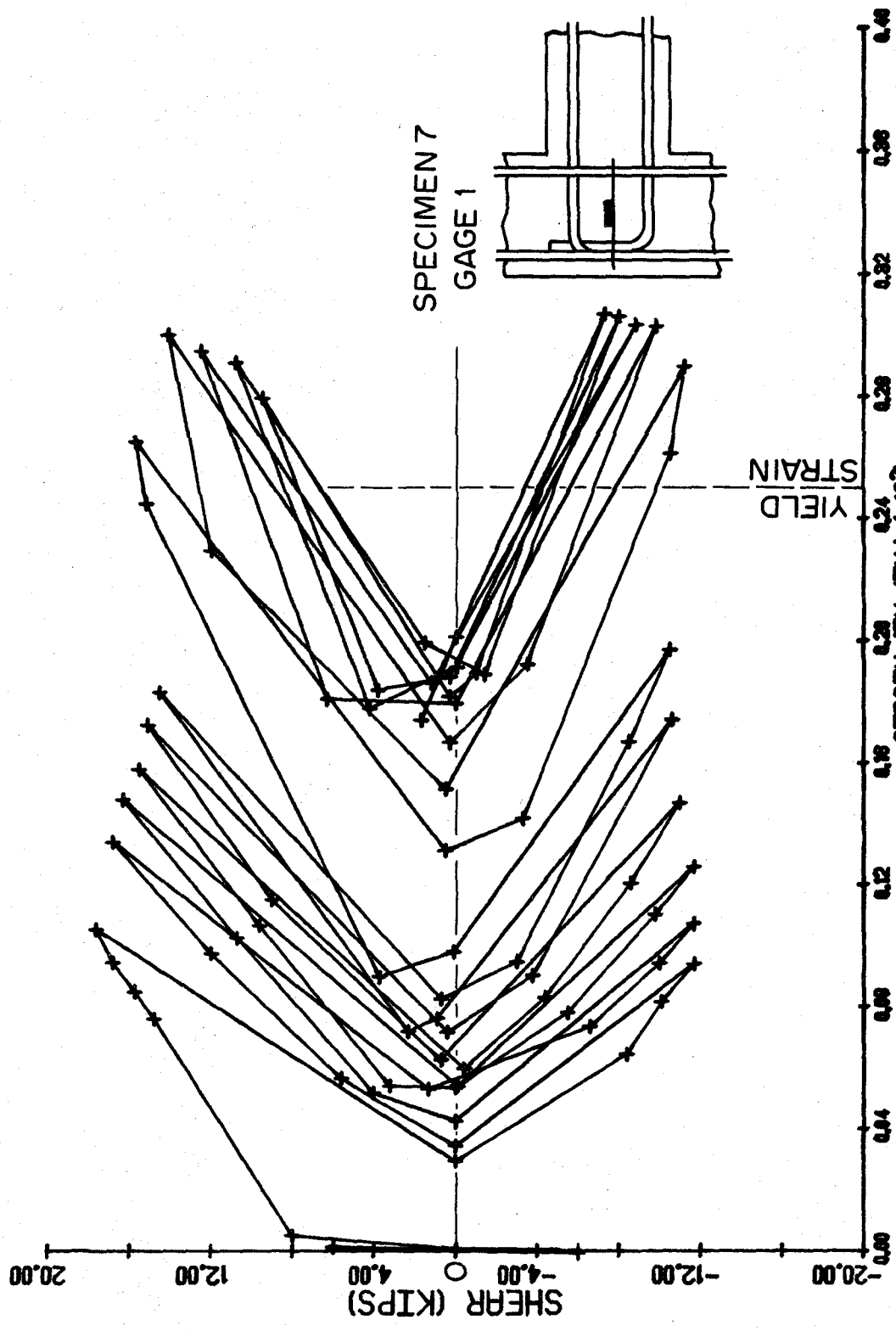

Fig. 3.29. Beam Shear Load vs. Strain in Intermediate Beam-Column Joint Tie - Specimen 7.

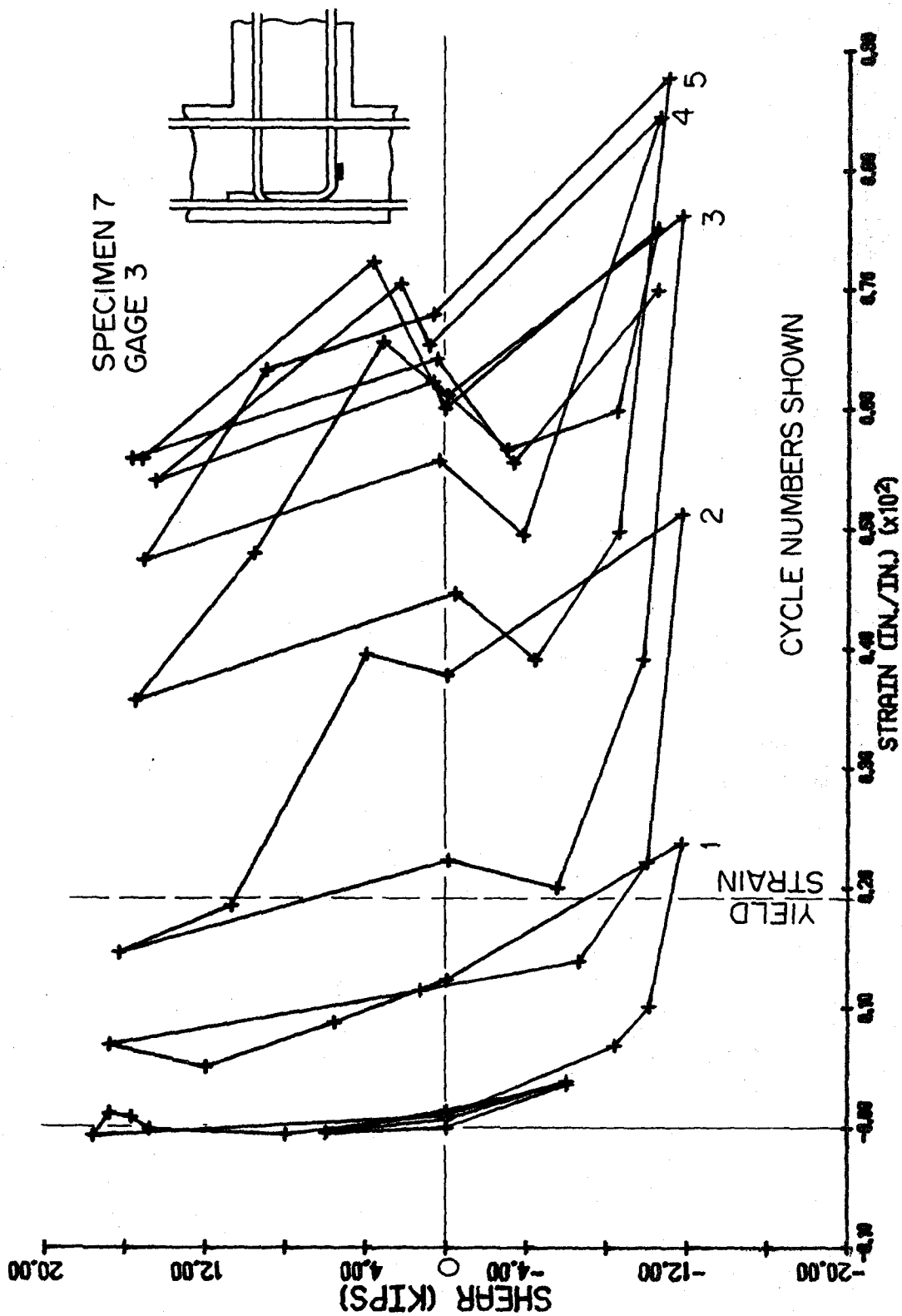

Fig. 3.28. Beam Shear Load vs. Strain at the Beginning of the Hook in Bottom Longitudinal Reinforcement - Specimen 7.

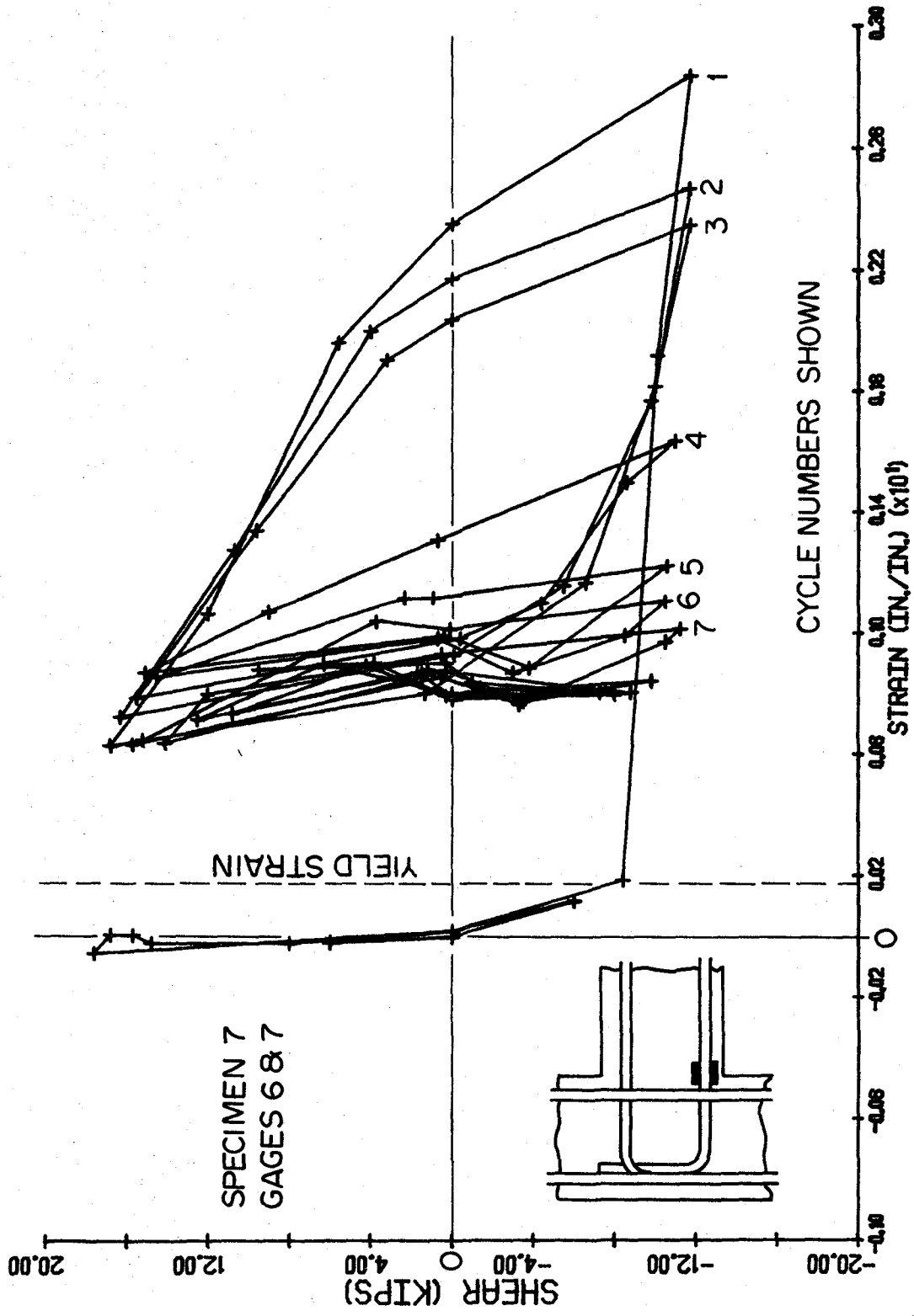

Fig. 3.27. Beam Shear Load vs. Strain at the Face of the Column in Bottom Longitudinal Reinforcement - Specimen 7.

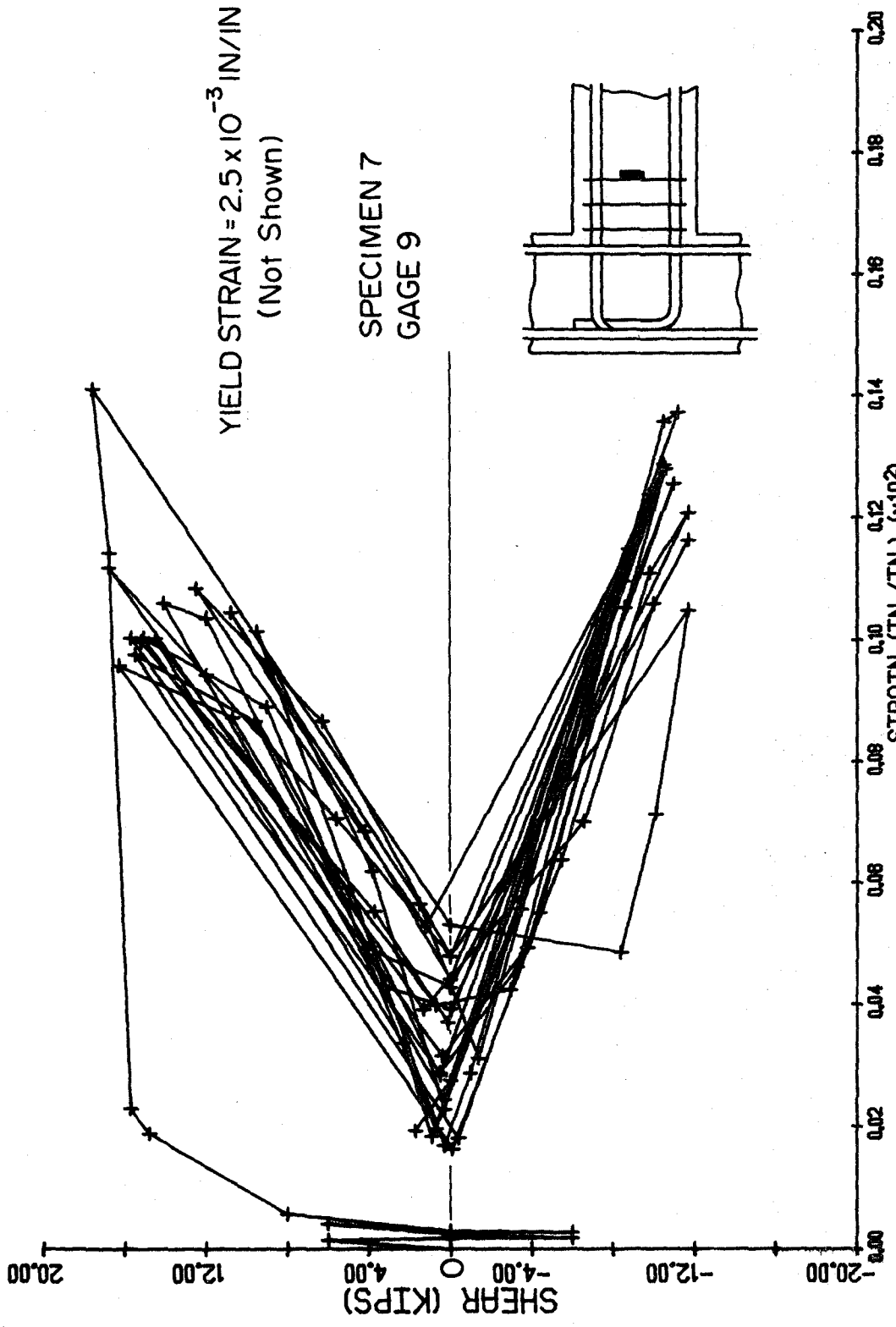

Fig. 3.26. Beam Shear Load vs. Strain in Hinging Zone Tie - Specimen 7.

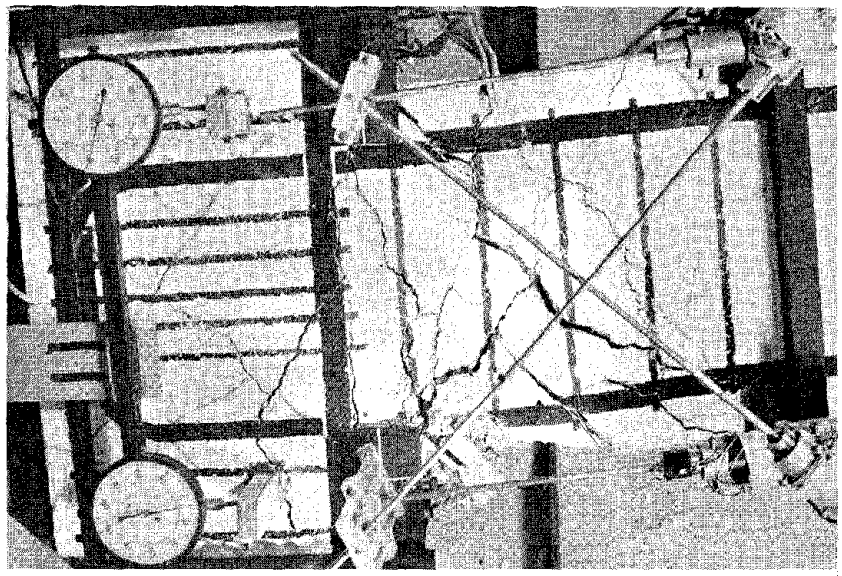

Fig. 3.24. Specimen 7 at Maximum Negative Displacement in Third Load Cycle.

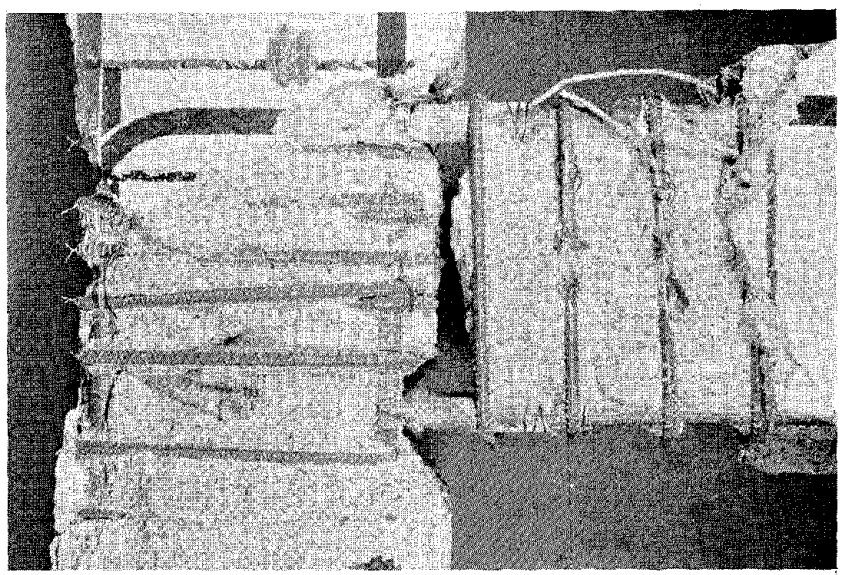

Fig. 3.25. Specimen 7 after Removal of Loose Concrete.

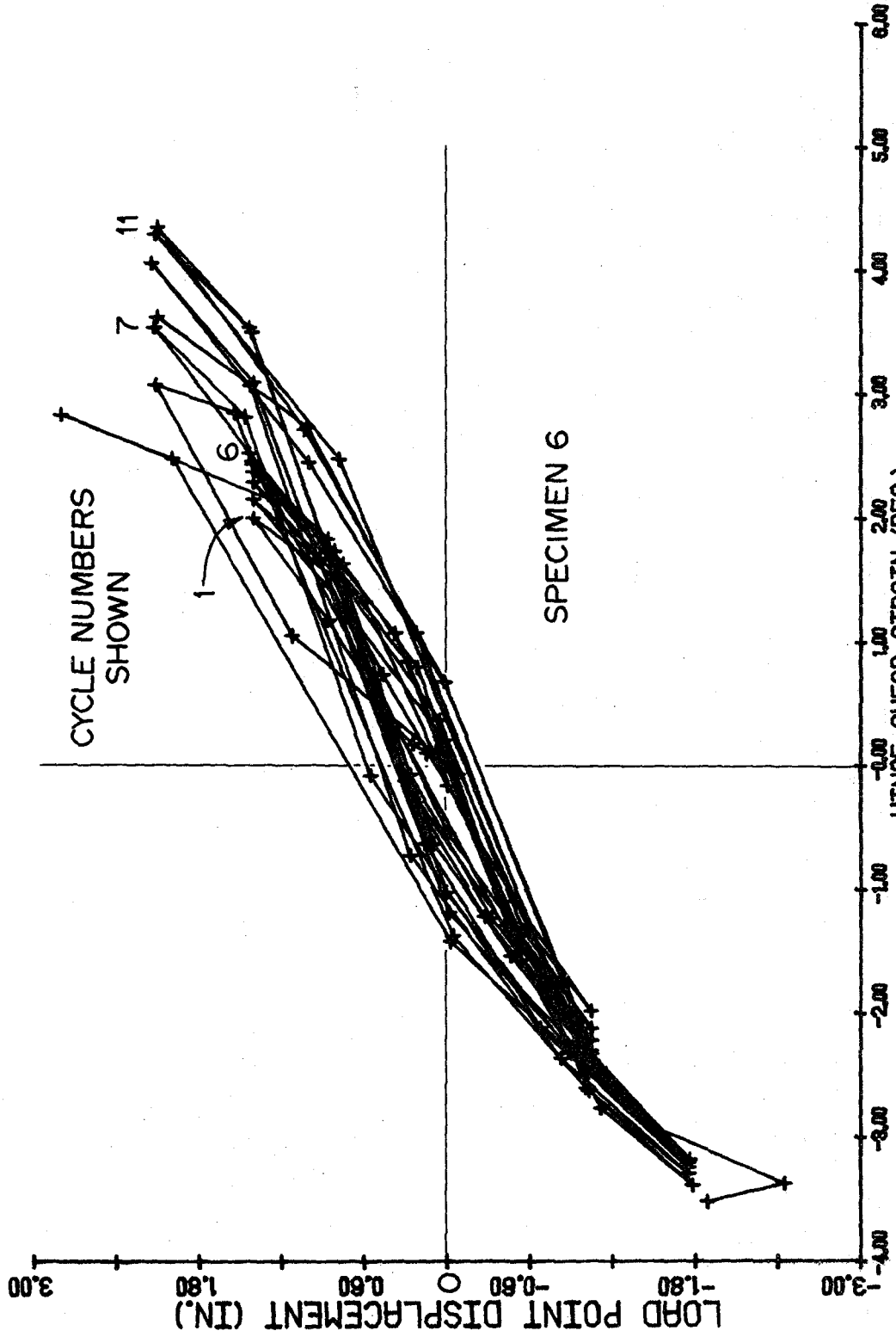

Fig. 3.23. Beam Load Point Displacement vs. Hinge Shear Strain - Specimen 6.

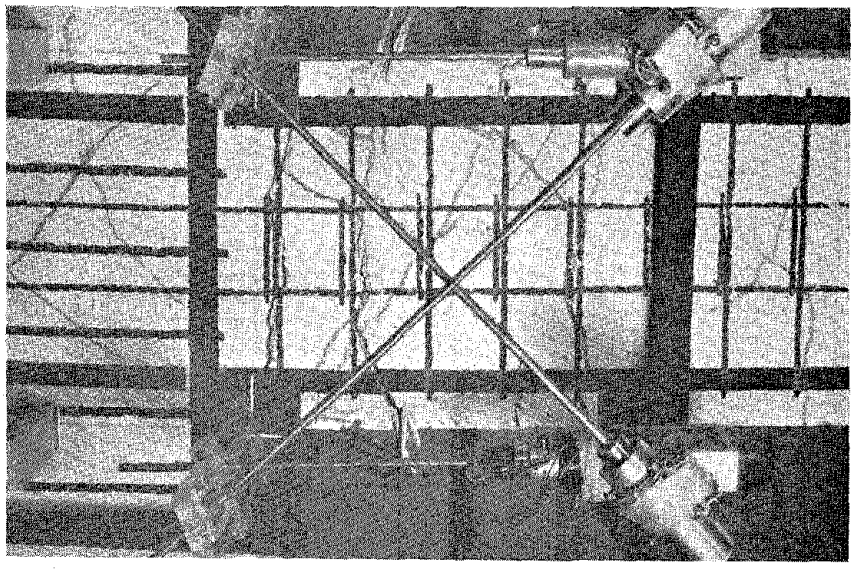

Fig. 3.22(a). Specimen 6 at the Conclusion of One Cycle of Loading.

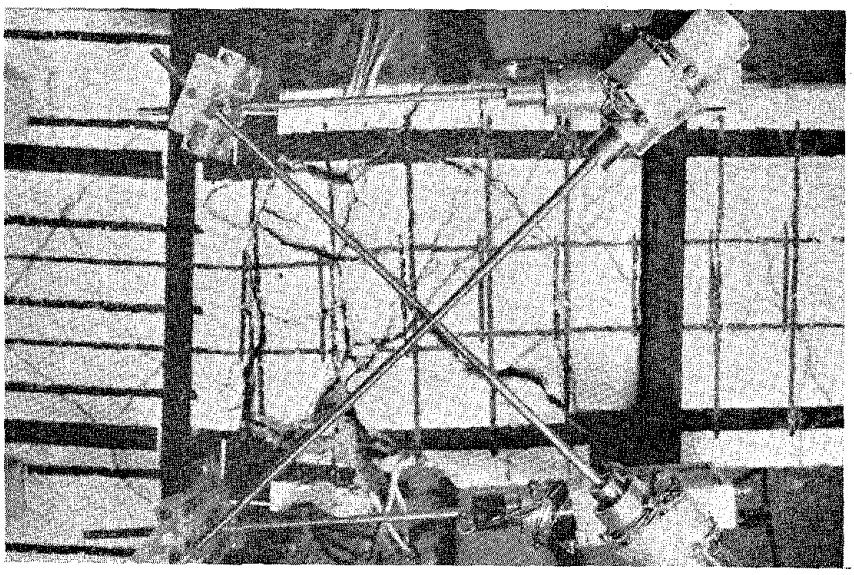

Fig. 3.22(b). Specimen 6 at the Conclusion of Twelve Cycles of Loading.

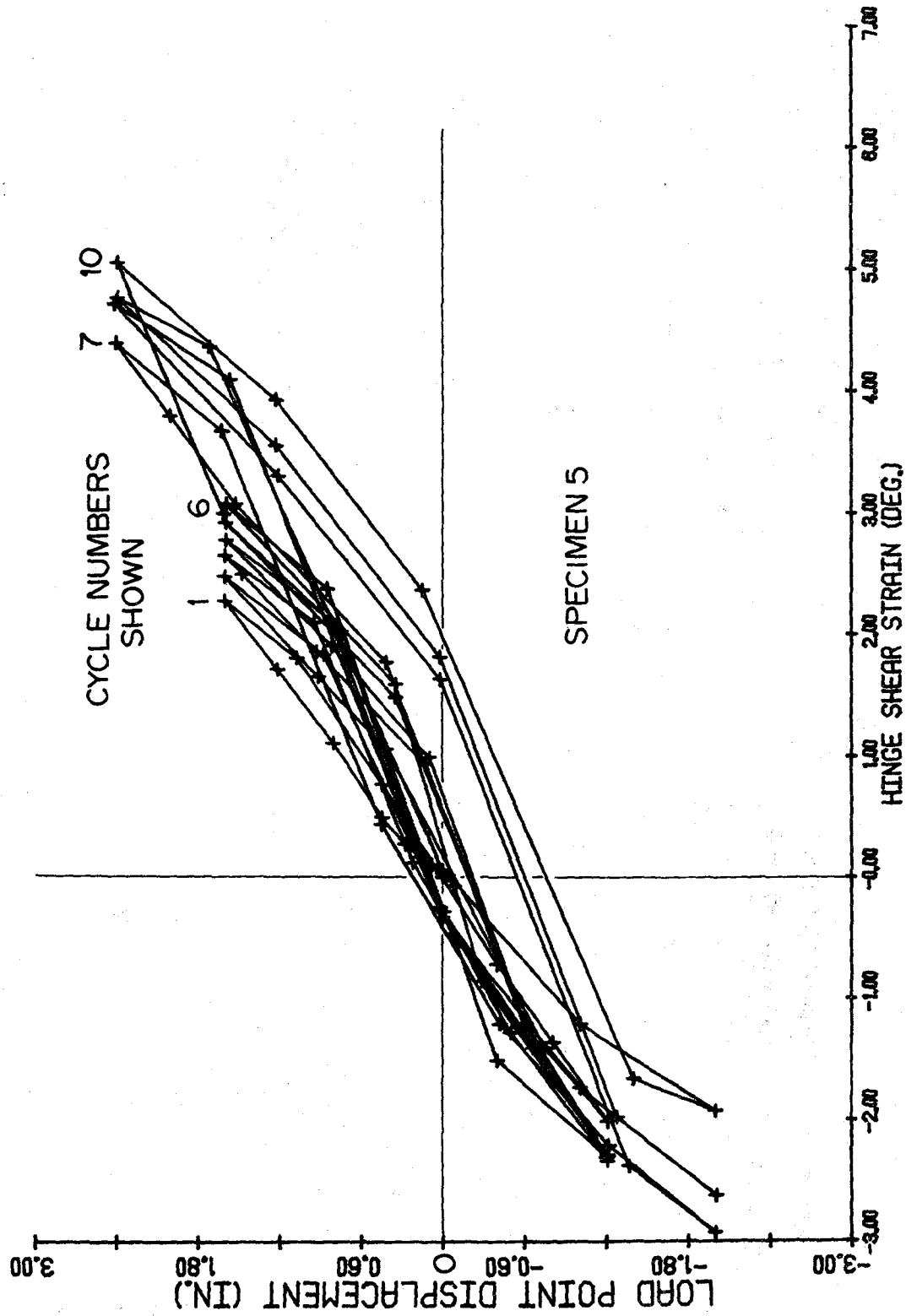

Fig. 3.21. Beam Load Point Displacement vs. Hinge Shear Strain - Specimen 5.

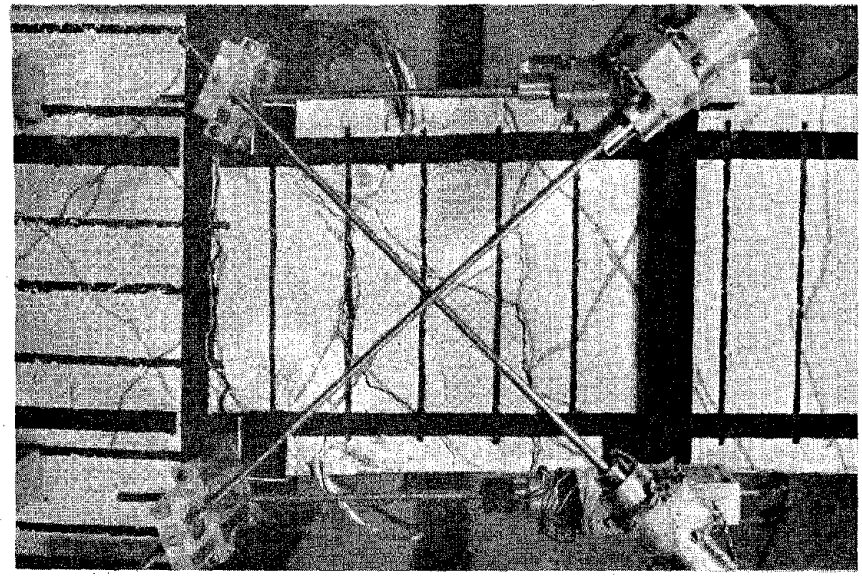

Fig. 3.19. Specimen 5 at the Conclusion of One Cycle of Loading.

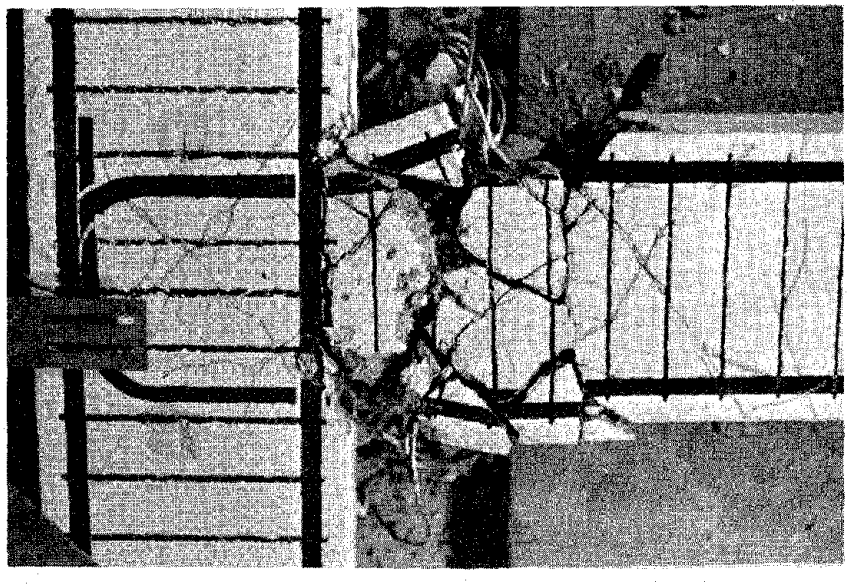

Fig. 3.20. Specimen 5 at the Conclusion of Testing.

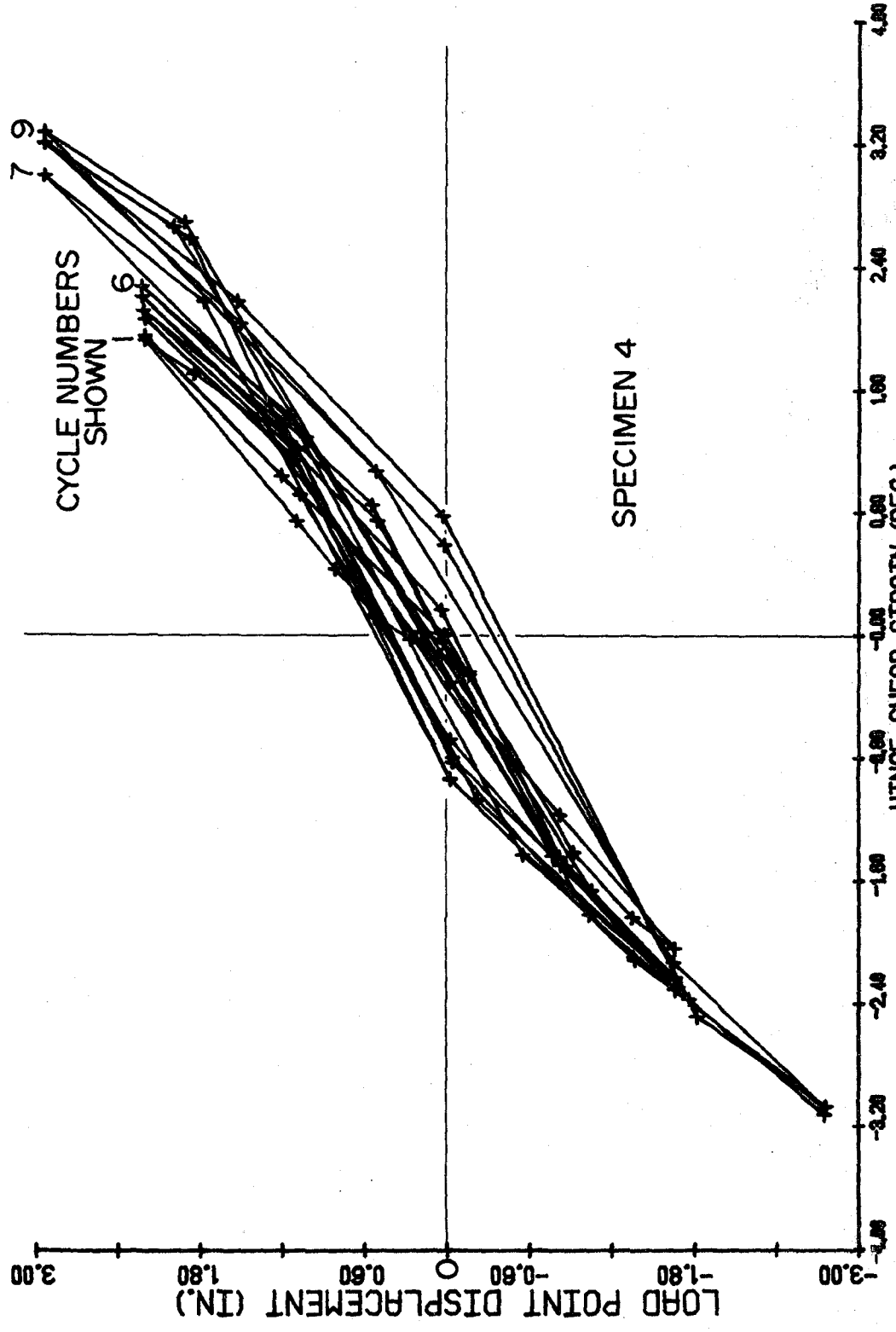

Fig. 3.18. Beam Load Point Displacement vs. Hinge Shear Strain - Specimen 4.

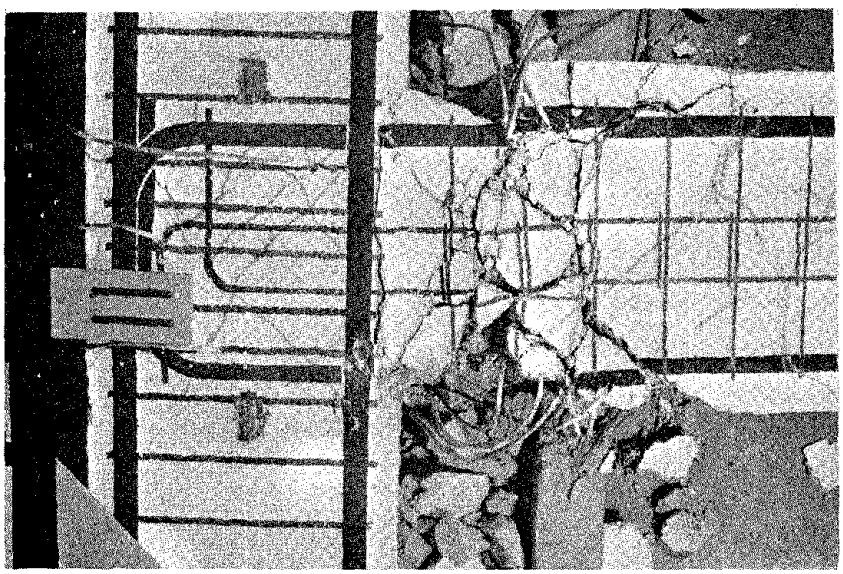

Fig. 3.16. Specimen 4 at Conclusion of Test.

Fig. 3.17. Hinging Region of Specimen 4 after Removal of Loose Concrete.

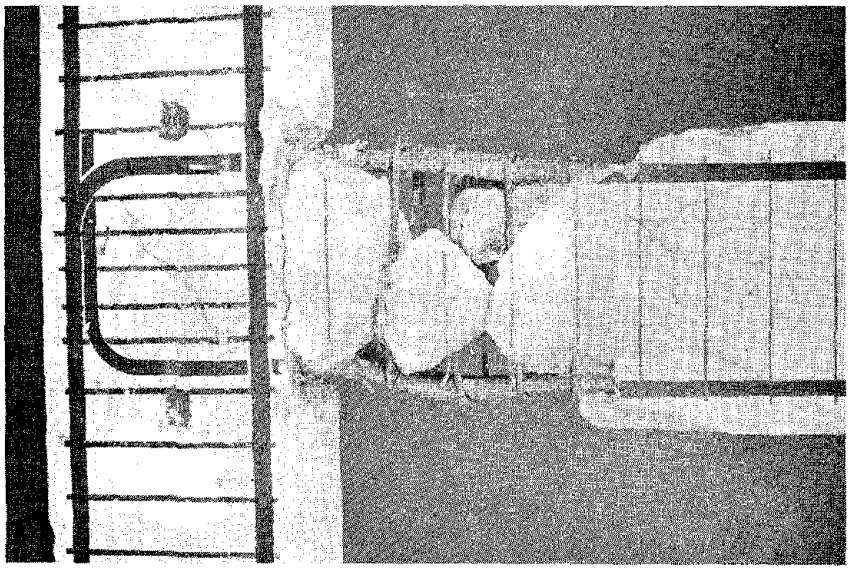

Fig. 3.14. Hinging Region of Specimen 3 after Removal of Loose Concrete.

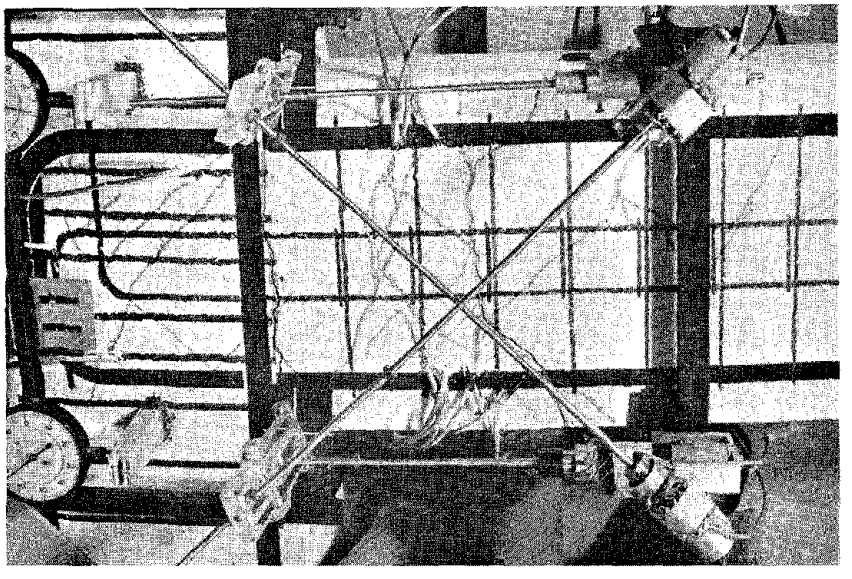

Fig. 3.15. Specimen 4 at Conclusion of One Cycle of Loading.

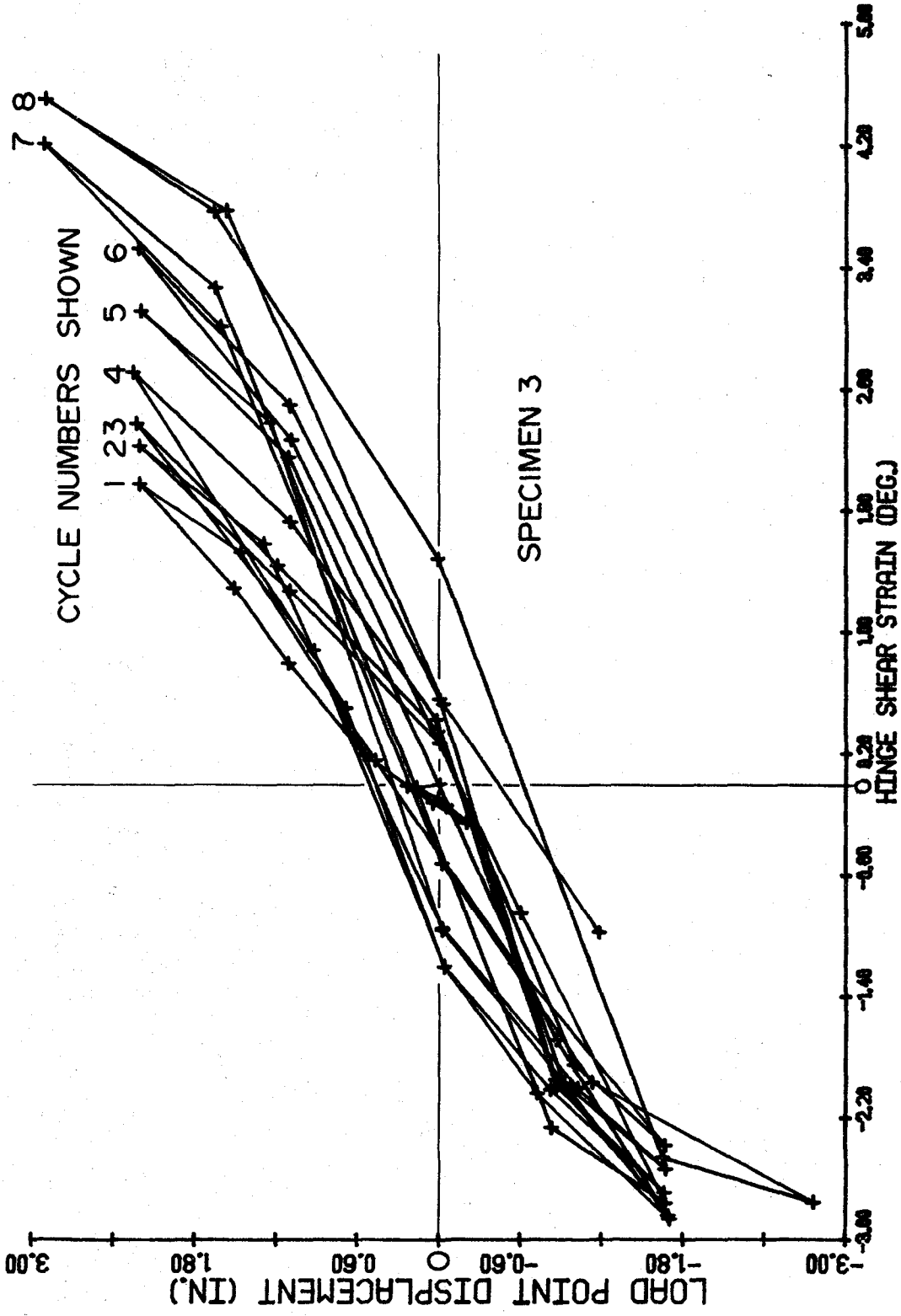

Fig. 3.13. Beam Load Point Displacement vs. Hinge Shear Strain - Specimen 3.

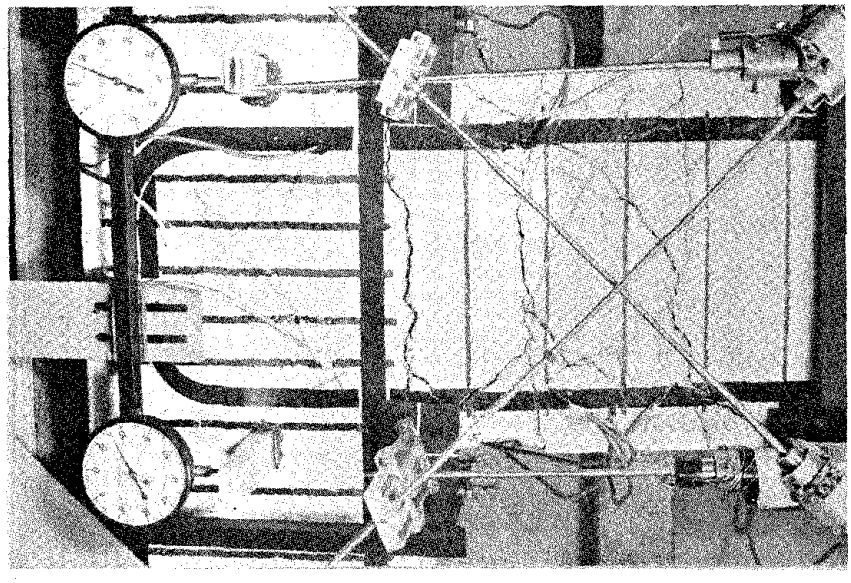

Fig. 3.11. Specimen 3 at the Conclusion of One Cycle of Loading.

Fig. 3.12. Specimen 3 at the Conclusion of Test.

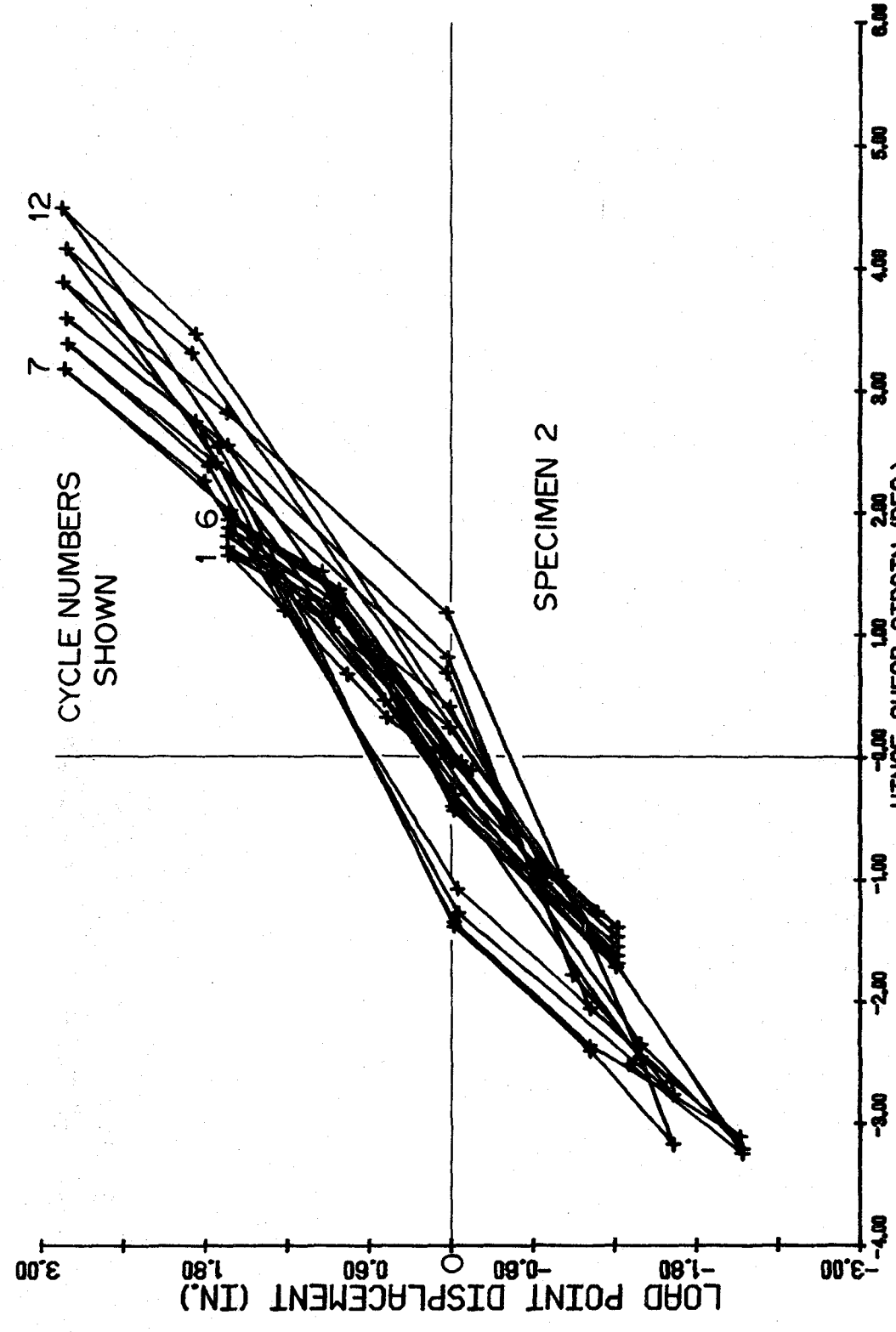

Fig. 3.10. Beam Load Point Displacement vs. Hinge Shear Strain - Specimen 2.

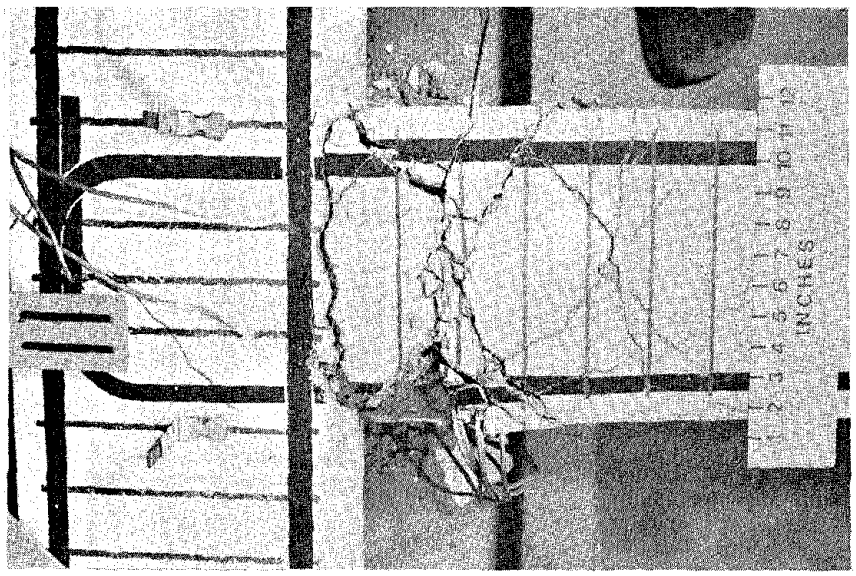

Fig. 3.8. Specimen 1 at Conclusion of Test.

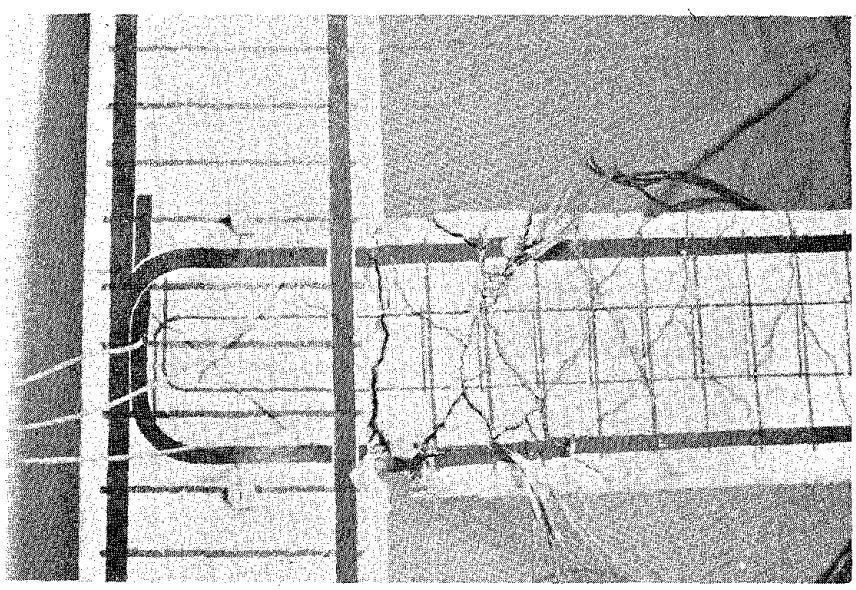

Fig. 3.9. Specimen 2 at Conclusion of Test.

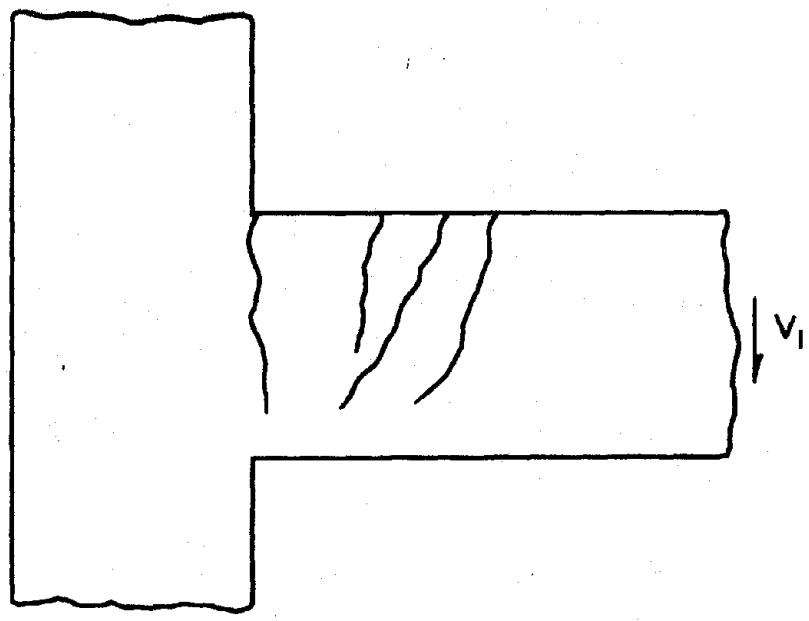

Fig. 3.7(a). Formation of Cracks during Positive Loading Half-Cycle - Specimen 1.

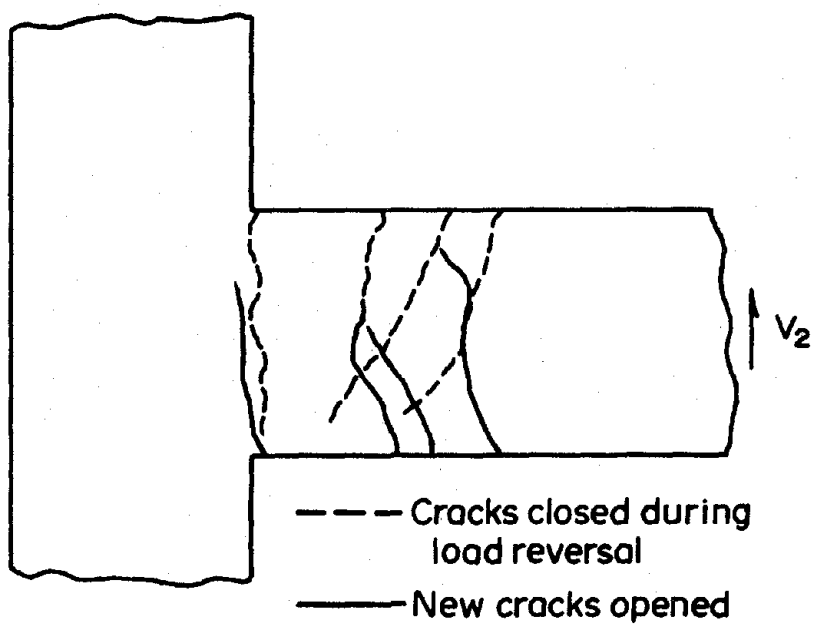

Fig. 3.7(b). Formation of Cracks during Negative Loading Half-Cycle - Specimen 1.

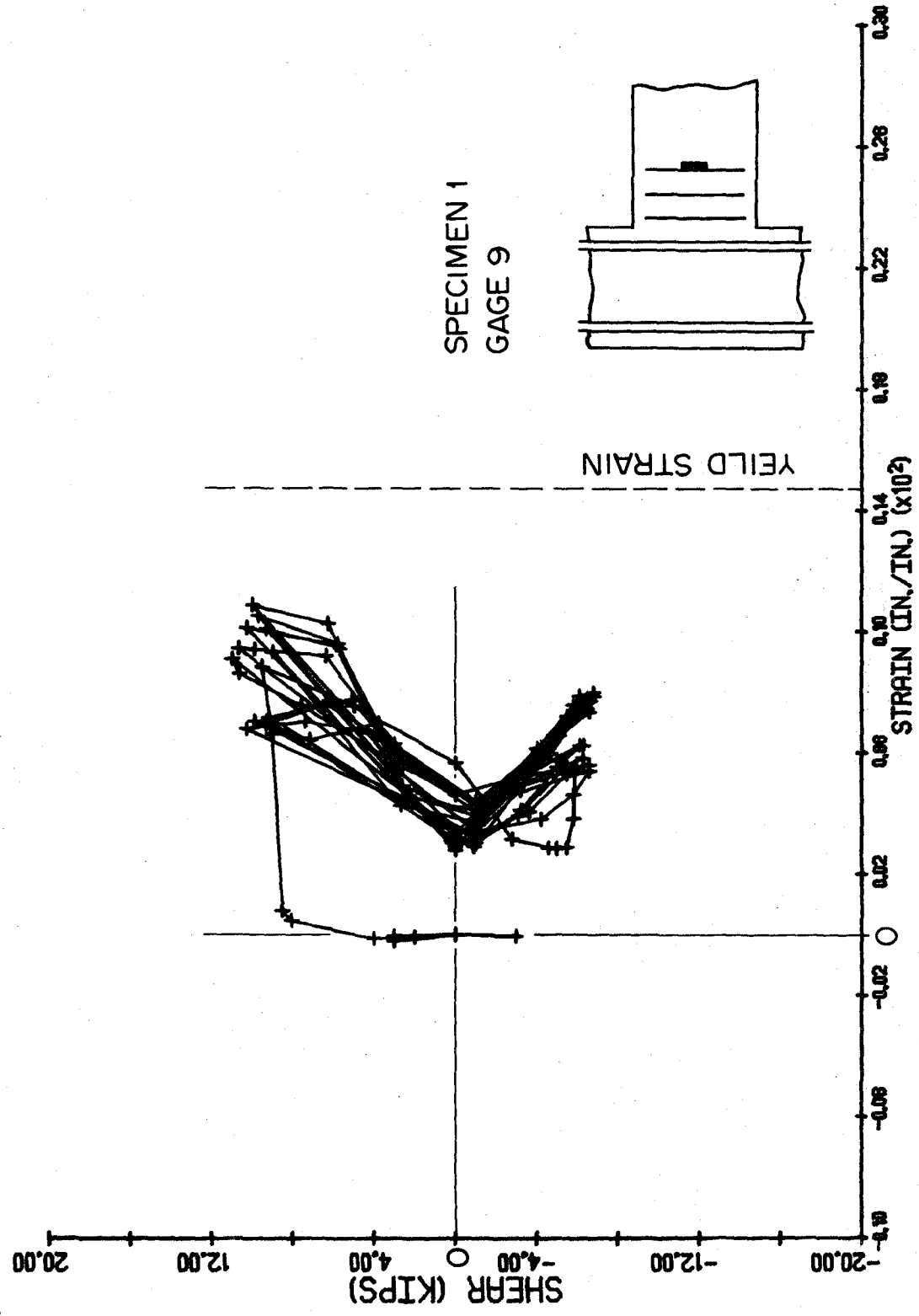

Fig. 3.6. Beam Shear Load vs. Strain in Tie in Hinging Zone.

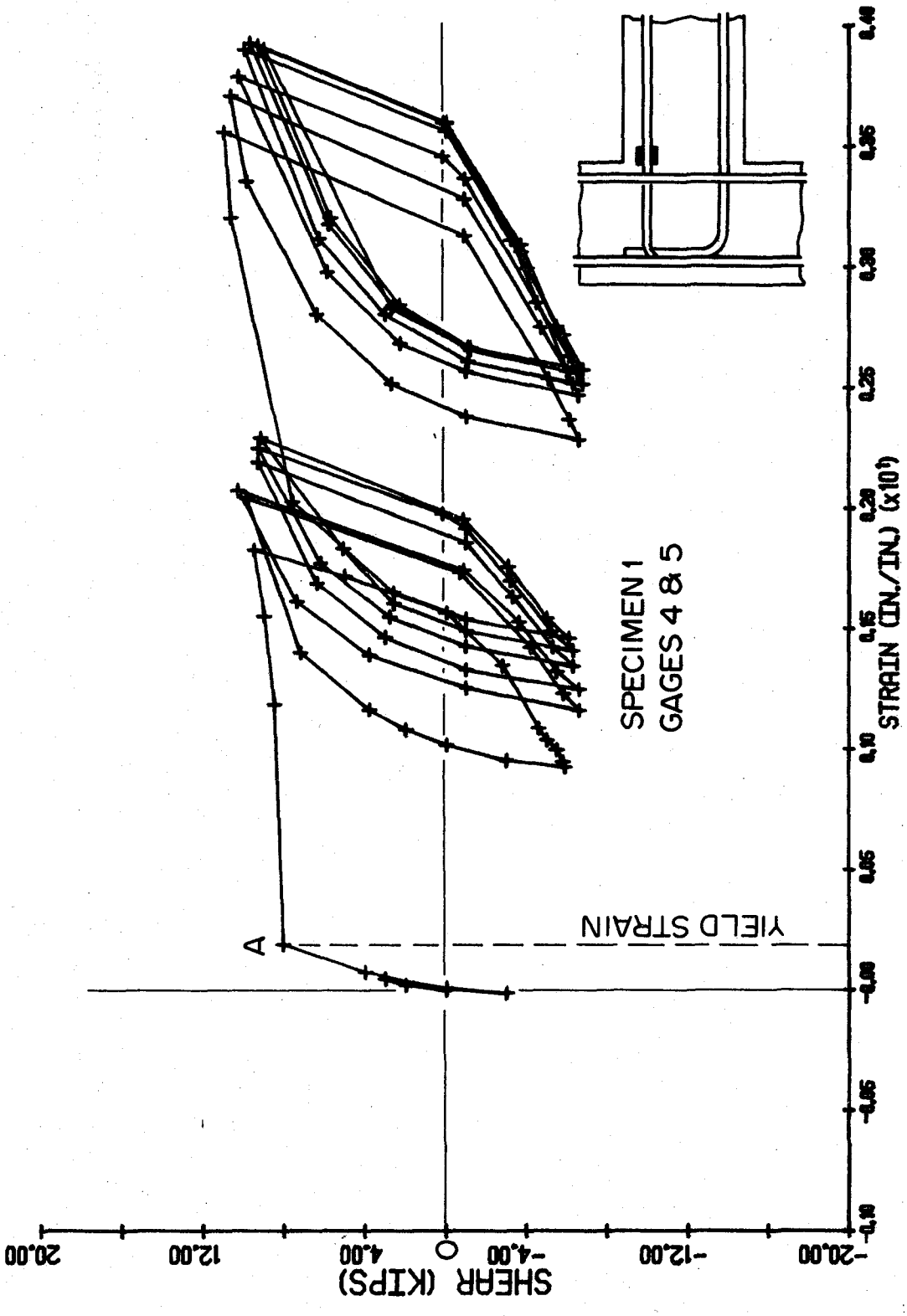

Fig. 3.5. Beam Shear Load vs. Strain in Top Longitudinal Reinforcement - Specimen 1.

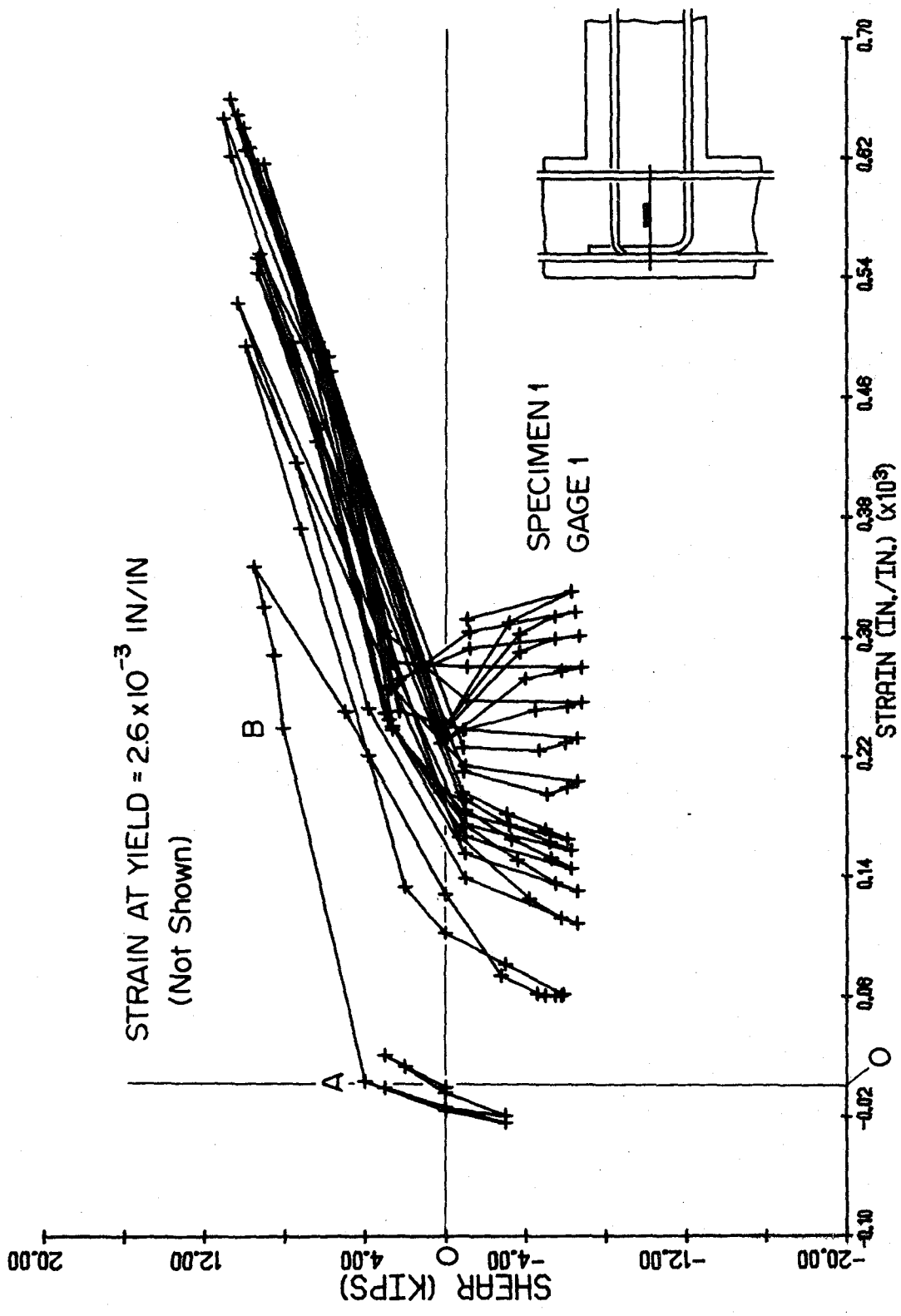

Fig. 3.4. Beam Shear Load vs. Strain in Central Beam-Column Joint Tie - Specimen 1.

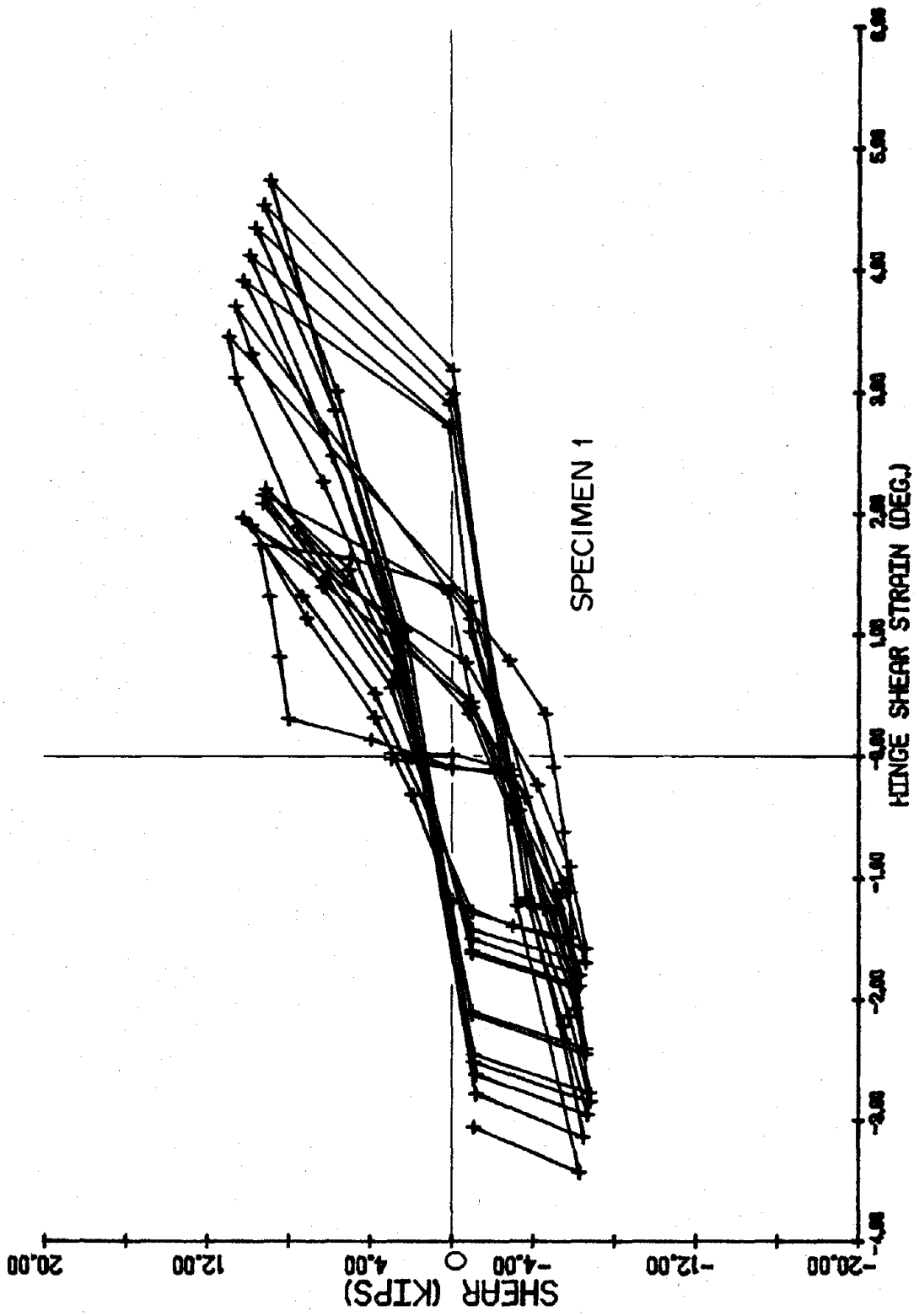

Fig. 3.3(d). Beam Shear Load vs. Hinge Shear Strain - Specimen 1.

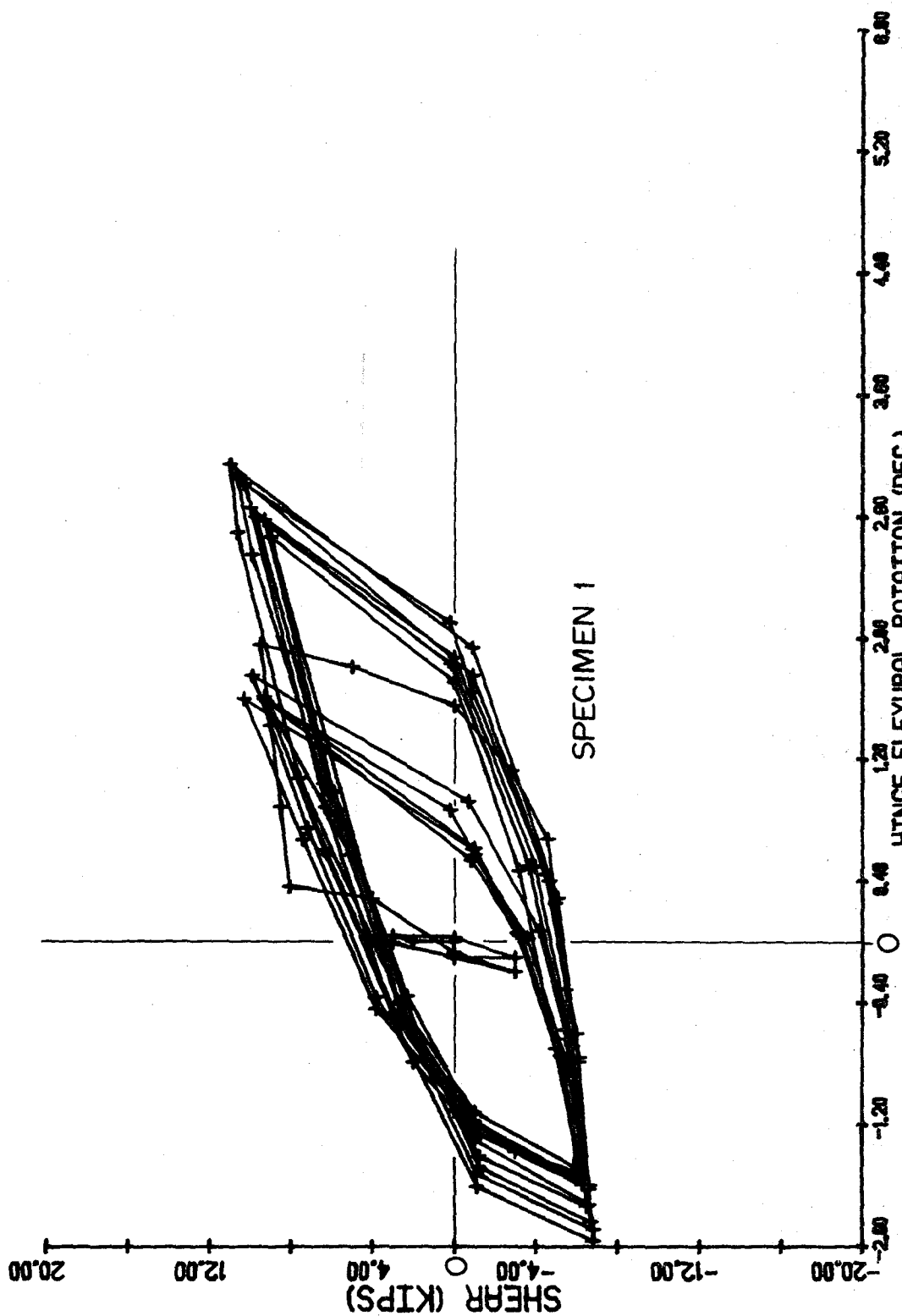

Fig. 3.3(c). Beam Shear Load vs. Hinge Flexural Rotation - Specimen 1.

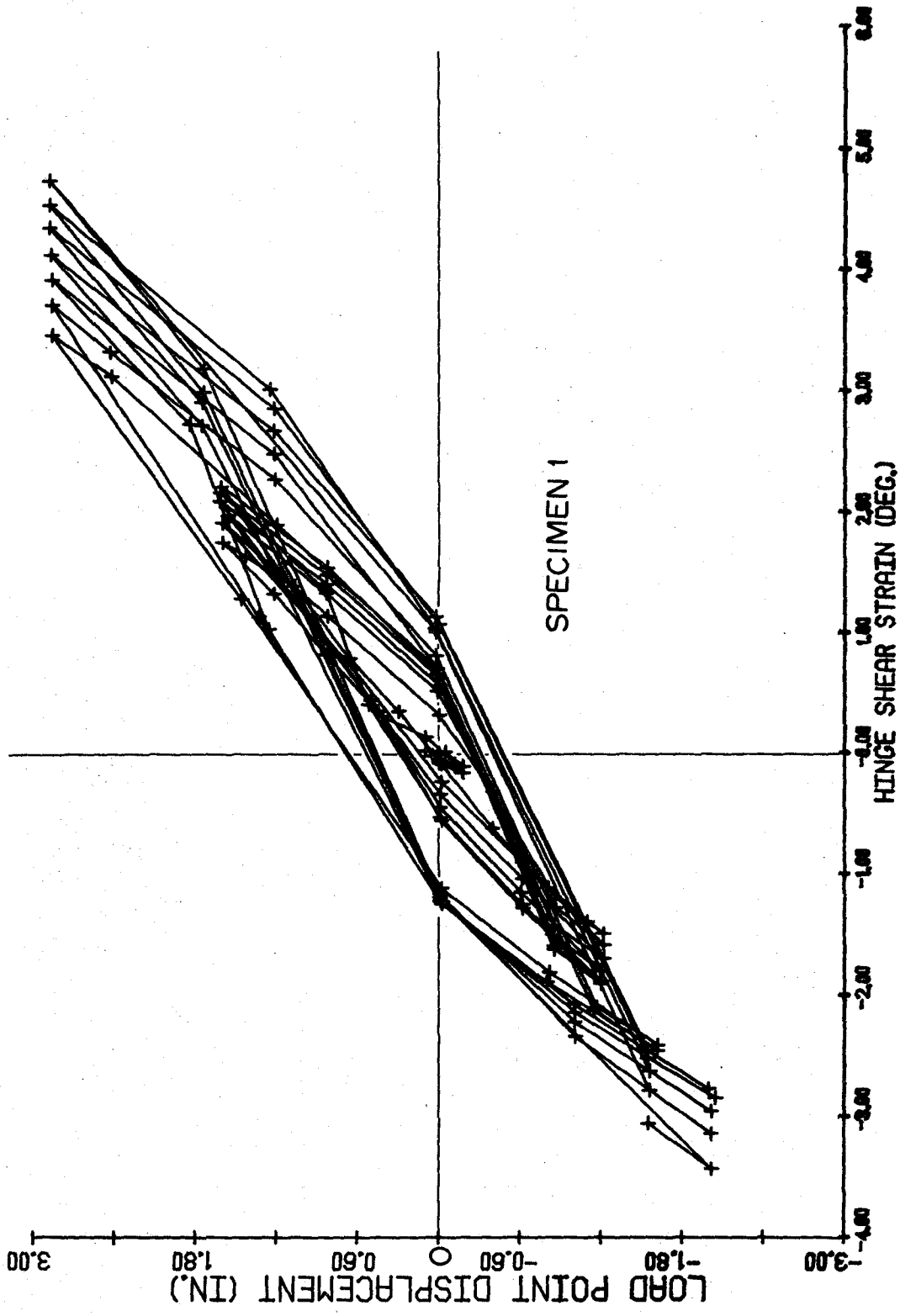

Fig. 3.3(b). Beam Load Point Displacement vs. Hinge Shear Strain - Specimen 1.

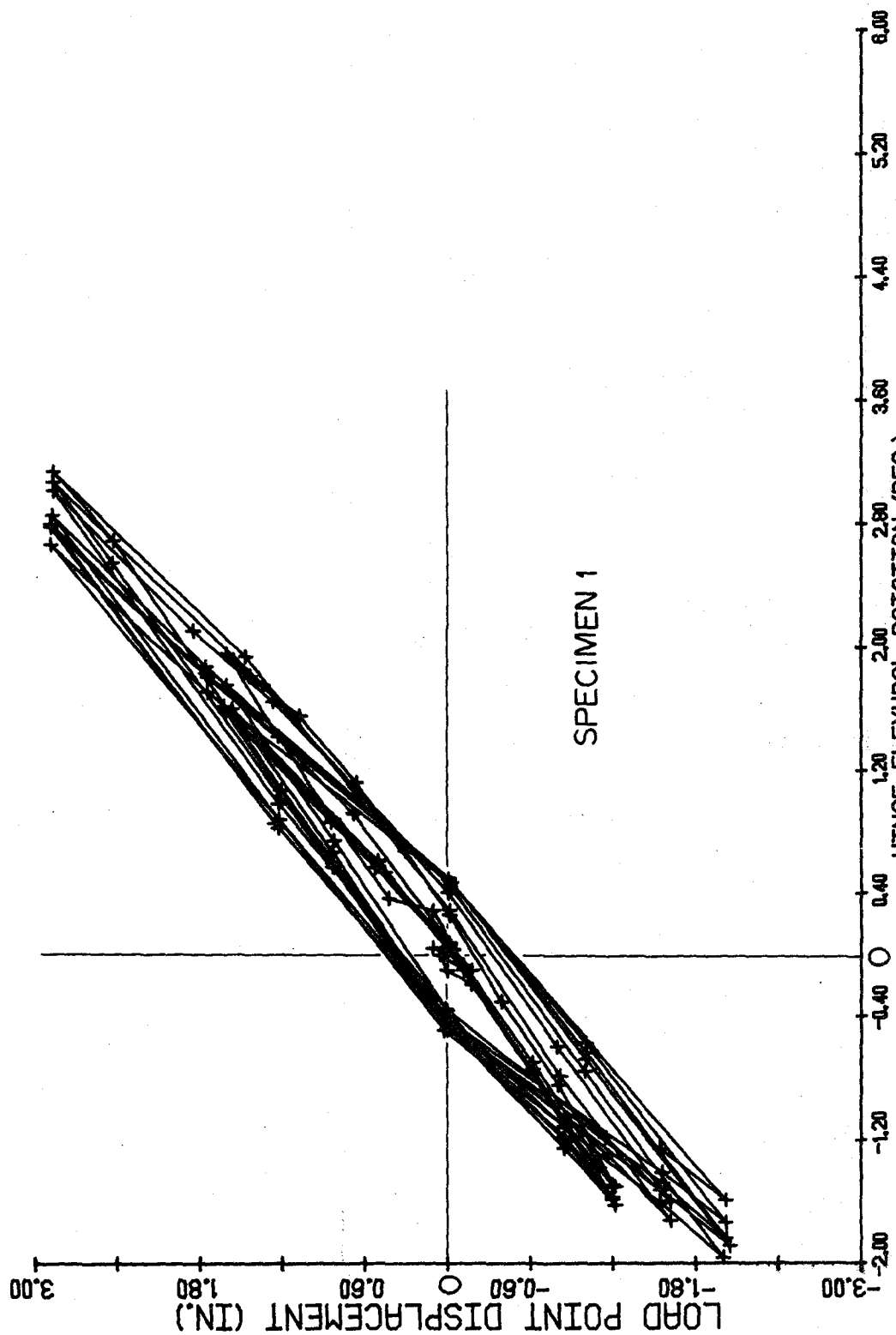

Fig. 3.3(a). Beam Load Point Displacement vs. Hinge Flexural Rotation - Specimen 1.

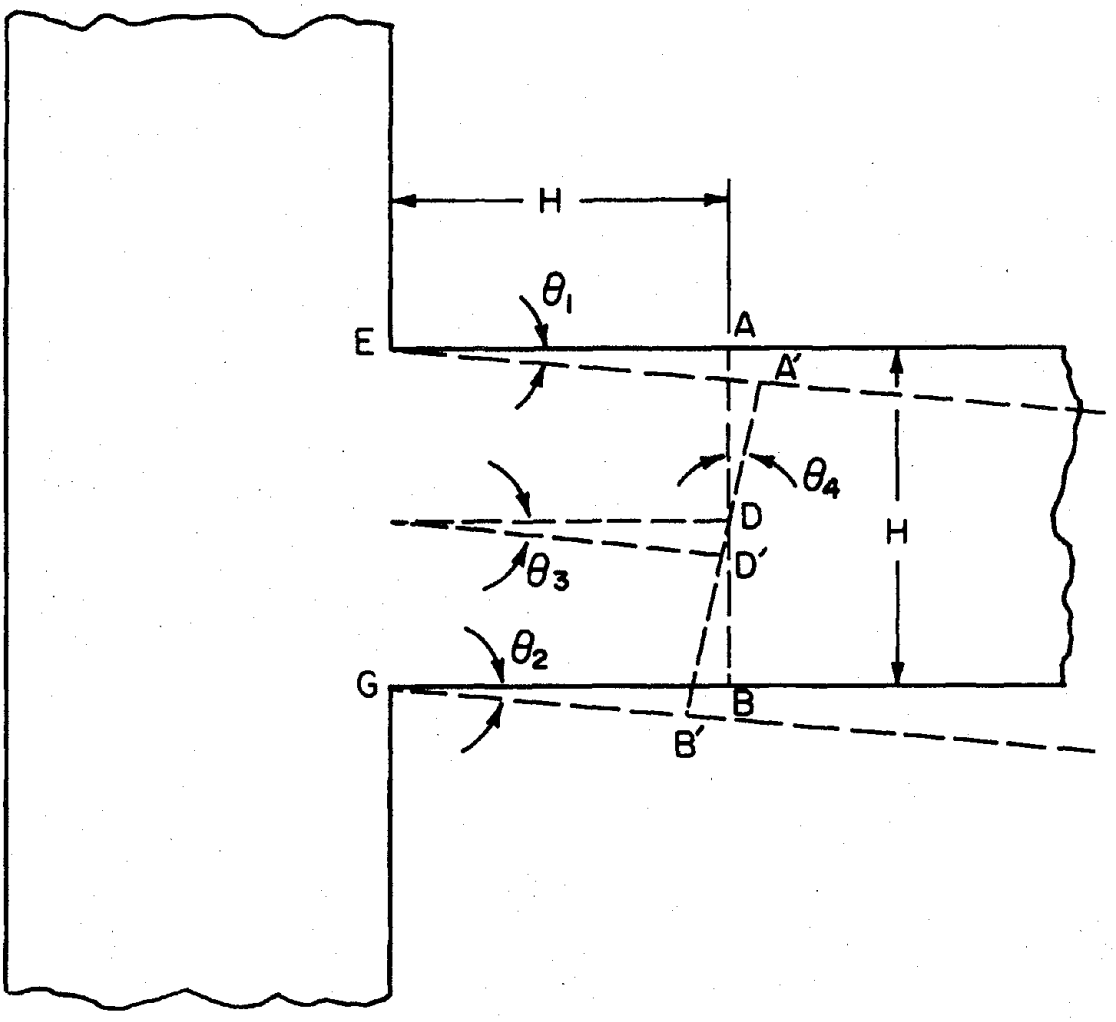

Fig. 3.2. Deformation of Plastic Hinging Zone.

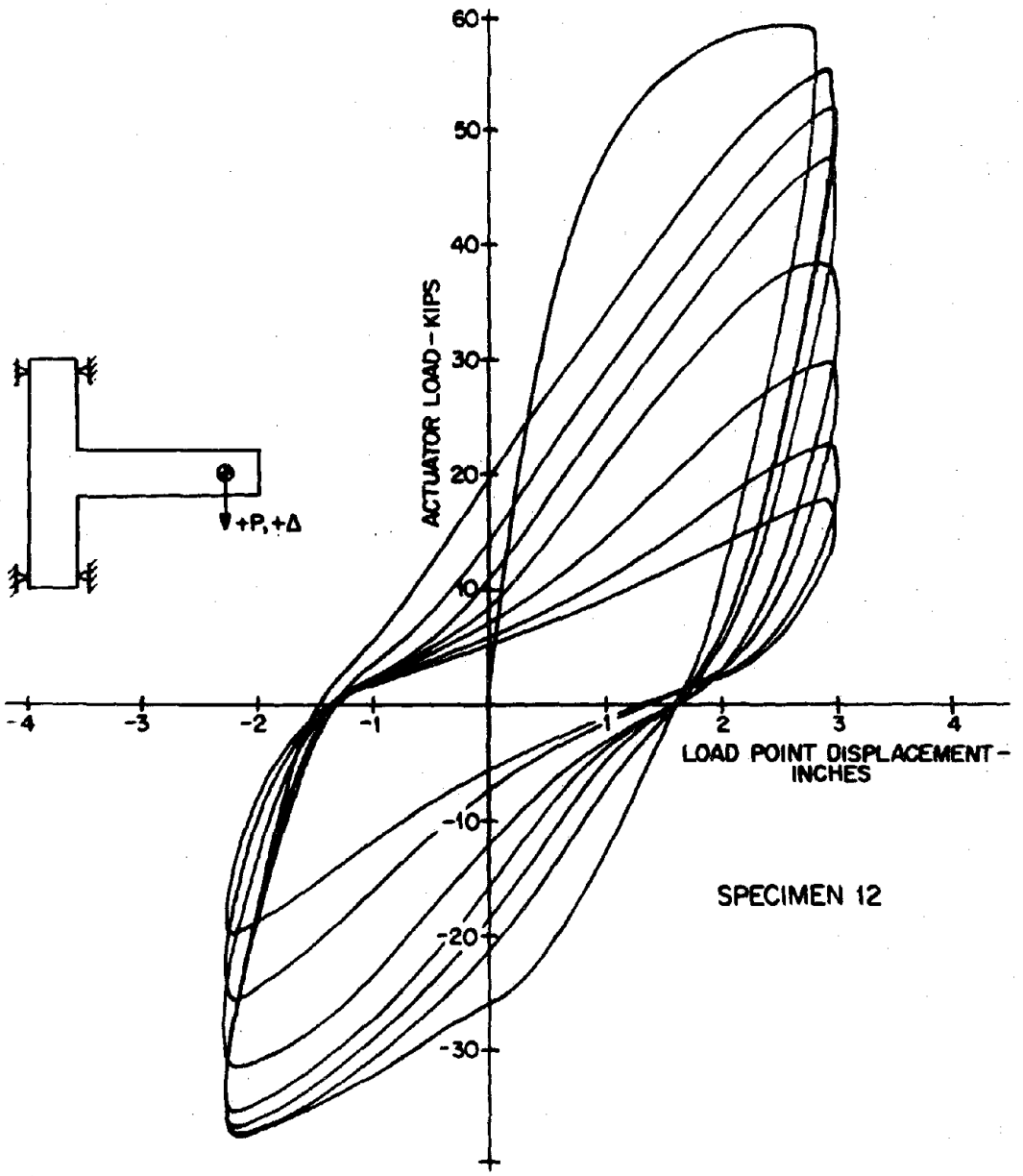

Fig. 3.1(ℓ). Load vs. Deflection Response of Specimen 12.

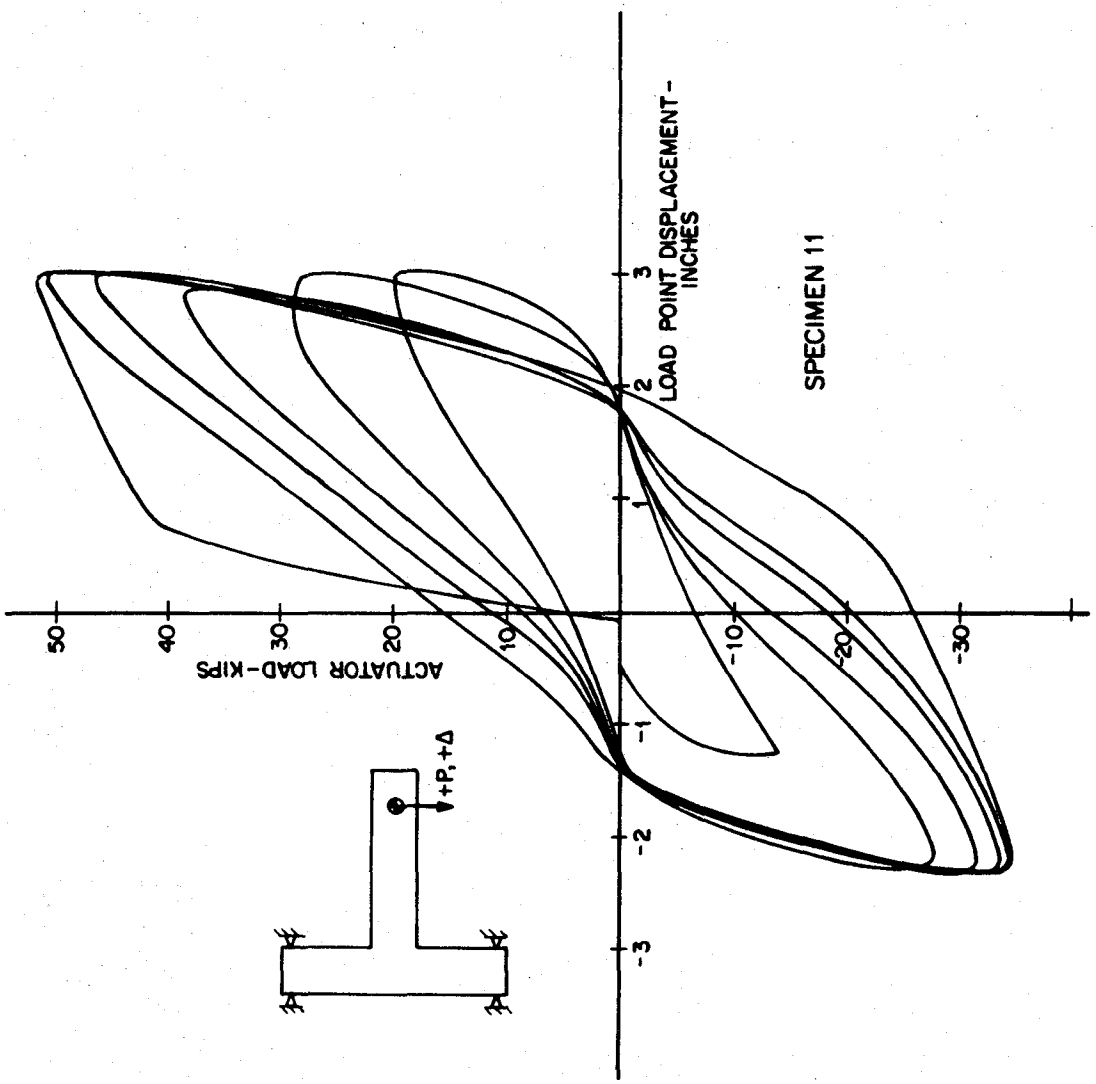

Fig. 3.1(k). Load vs. Deflection Response of Specimen 11.

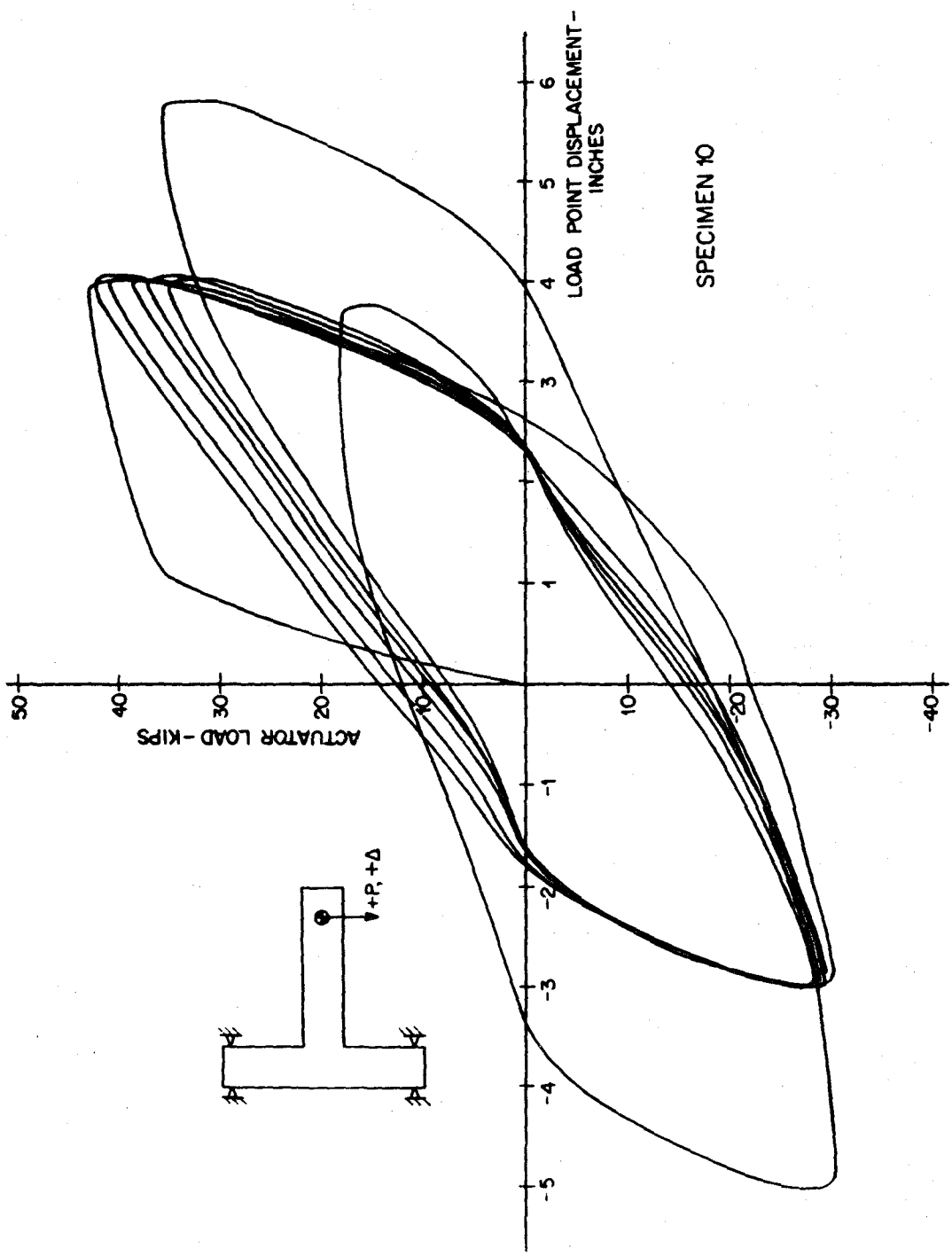

Fig. 3.1(j). Load vs Deflection Response of Specimen 10.

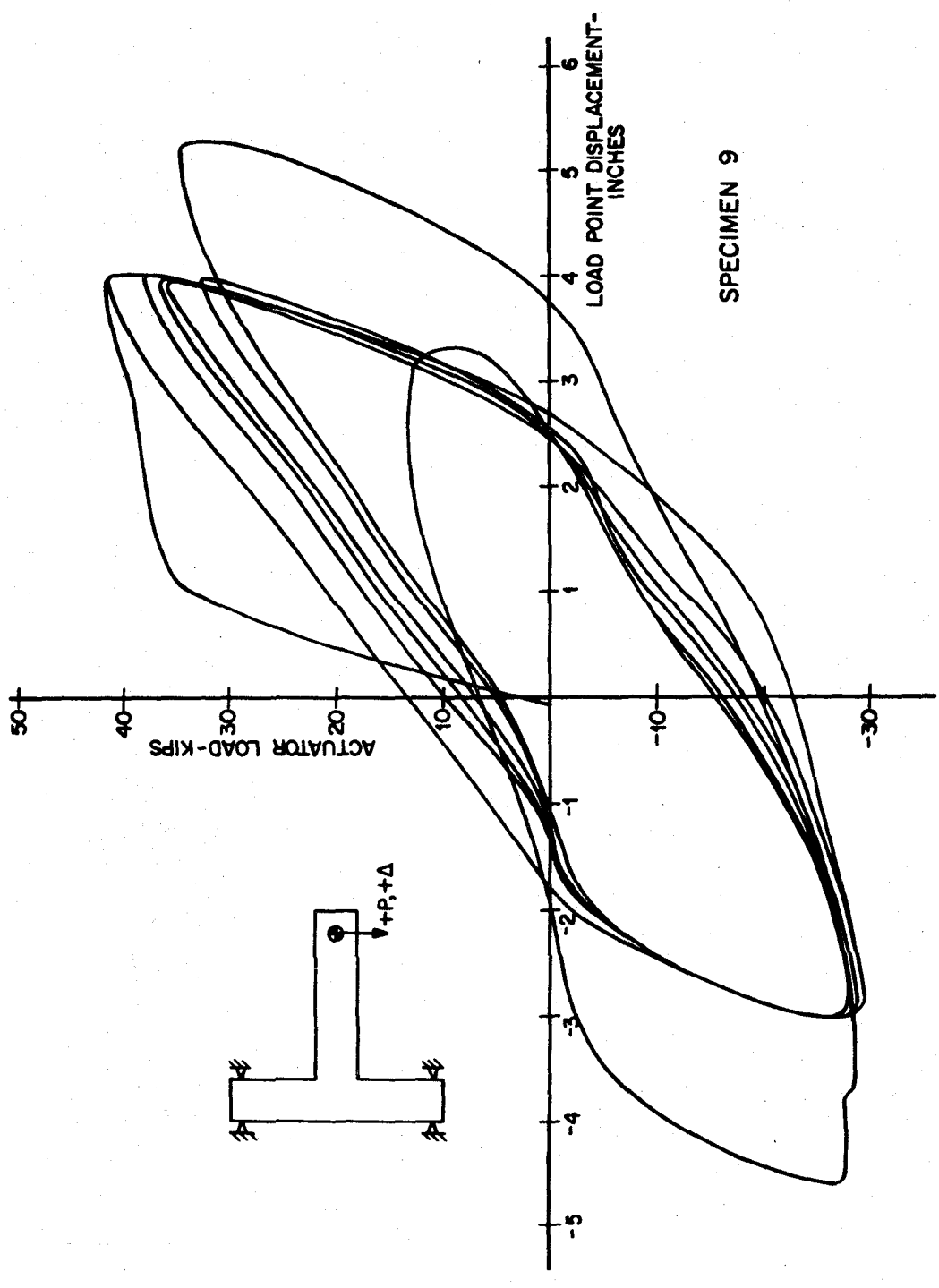

Fig. 3.1(i). Load vs. Deflection Response of Specimen 9.

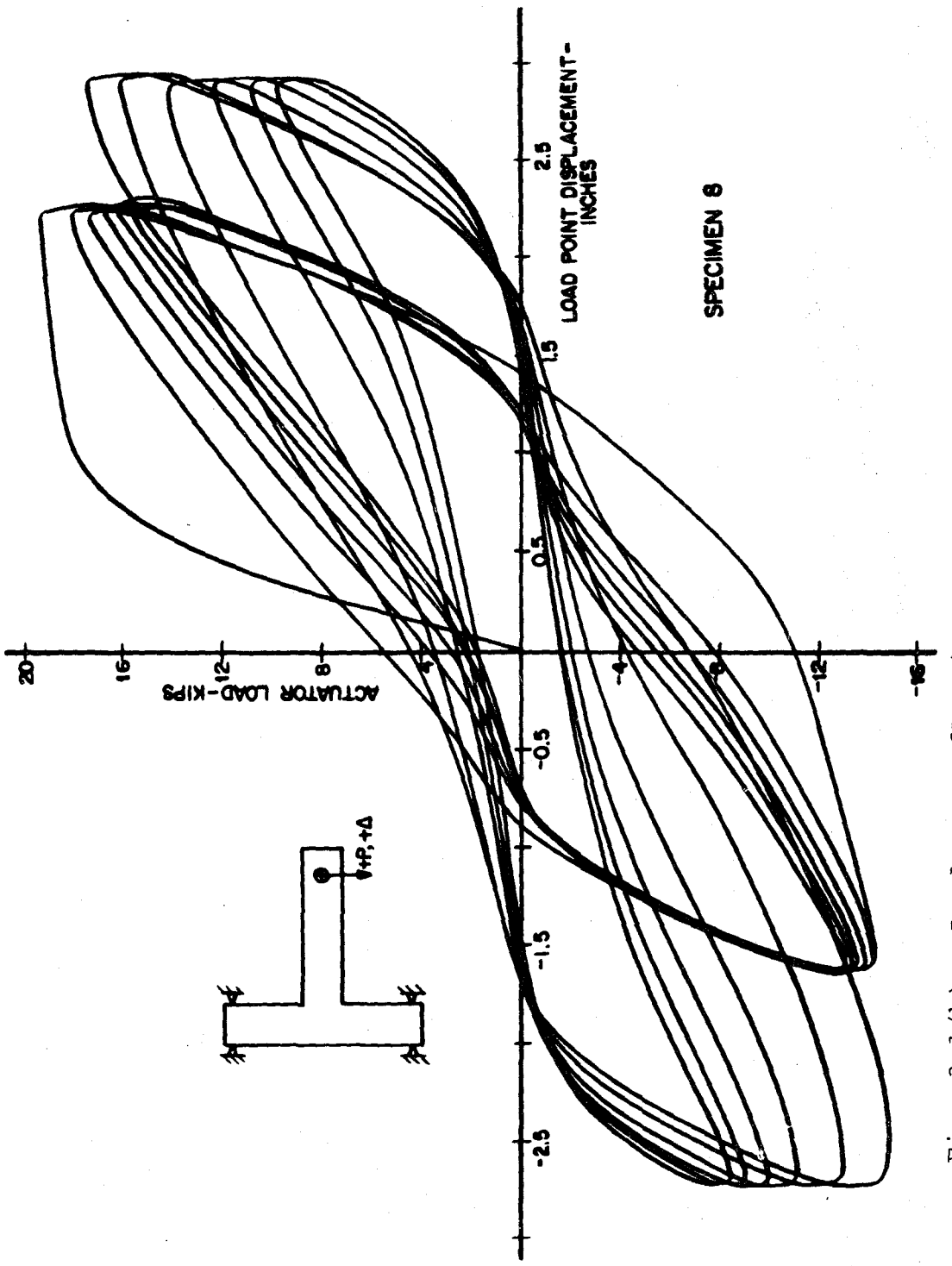

Fig. 3.1(h). Load vs. Deflection Response of Specimen 8.

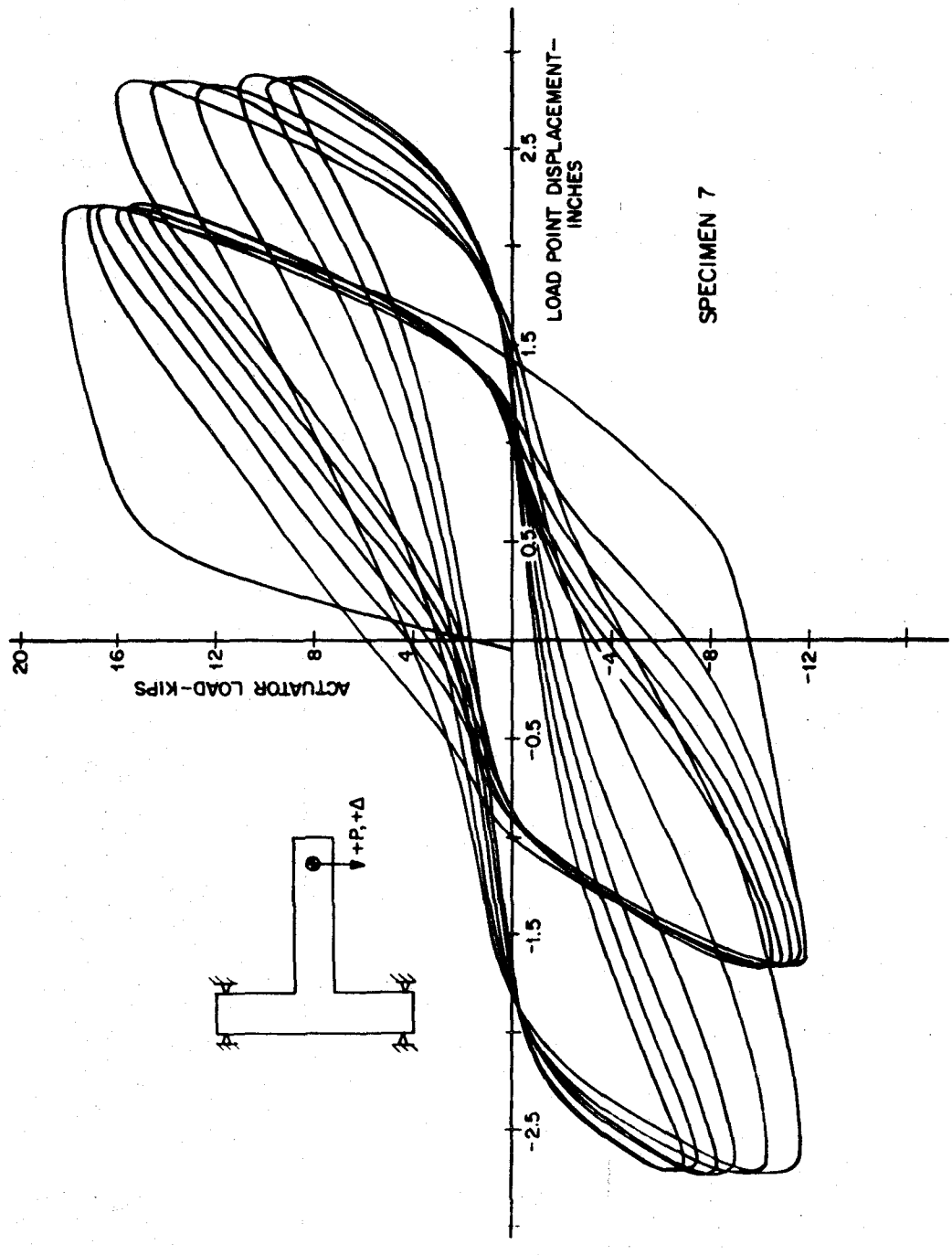

Fig. 3.1(g). Load vs. Deflection Response of Specimen 7.

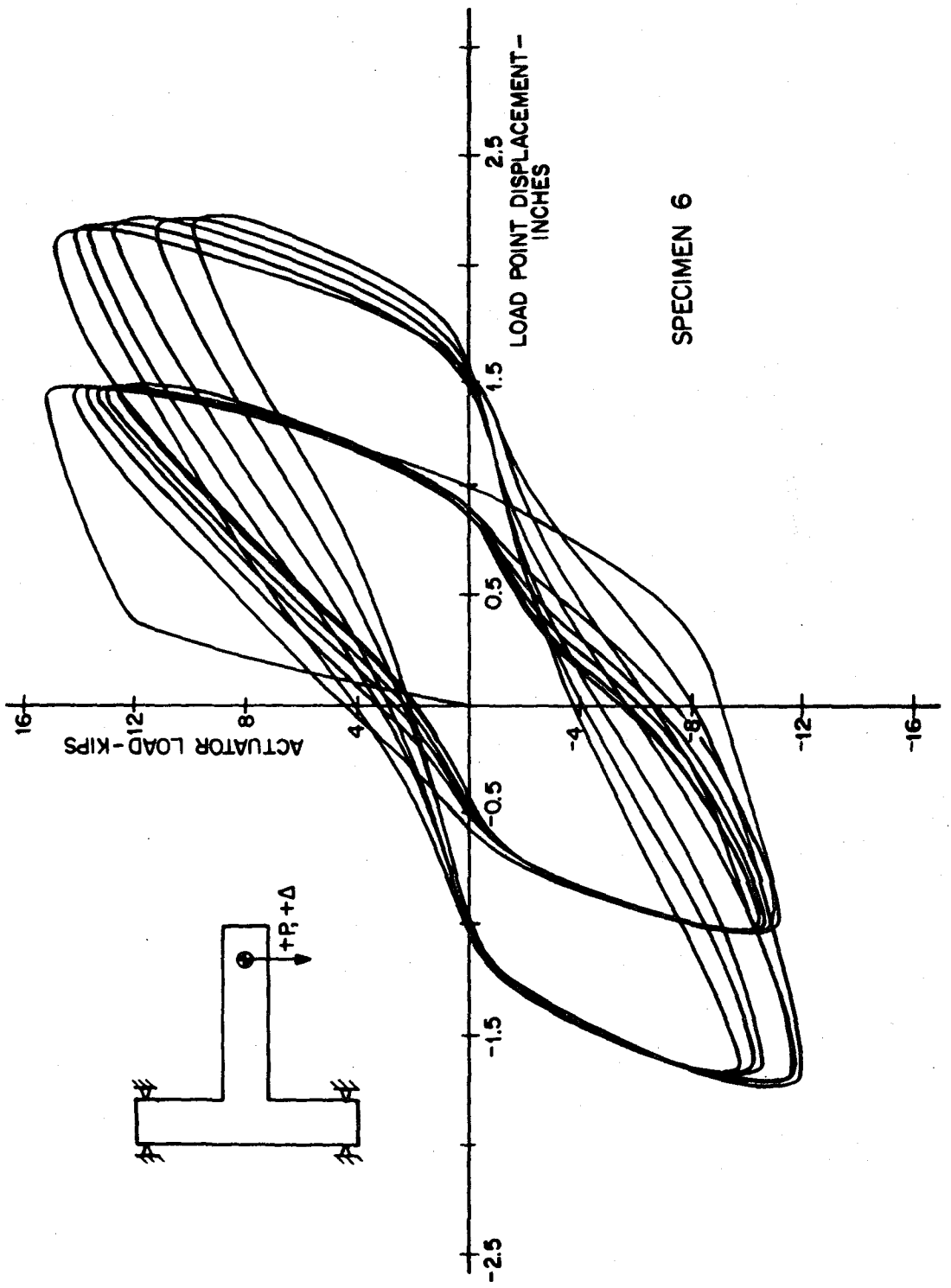

Fig. 3.1(f). Load vs. Deflection Response of Specimen 6.

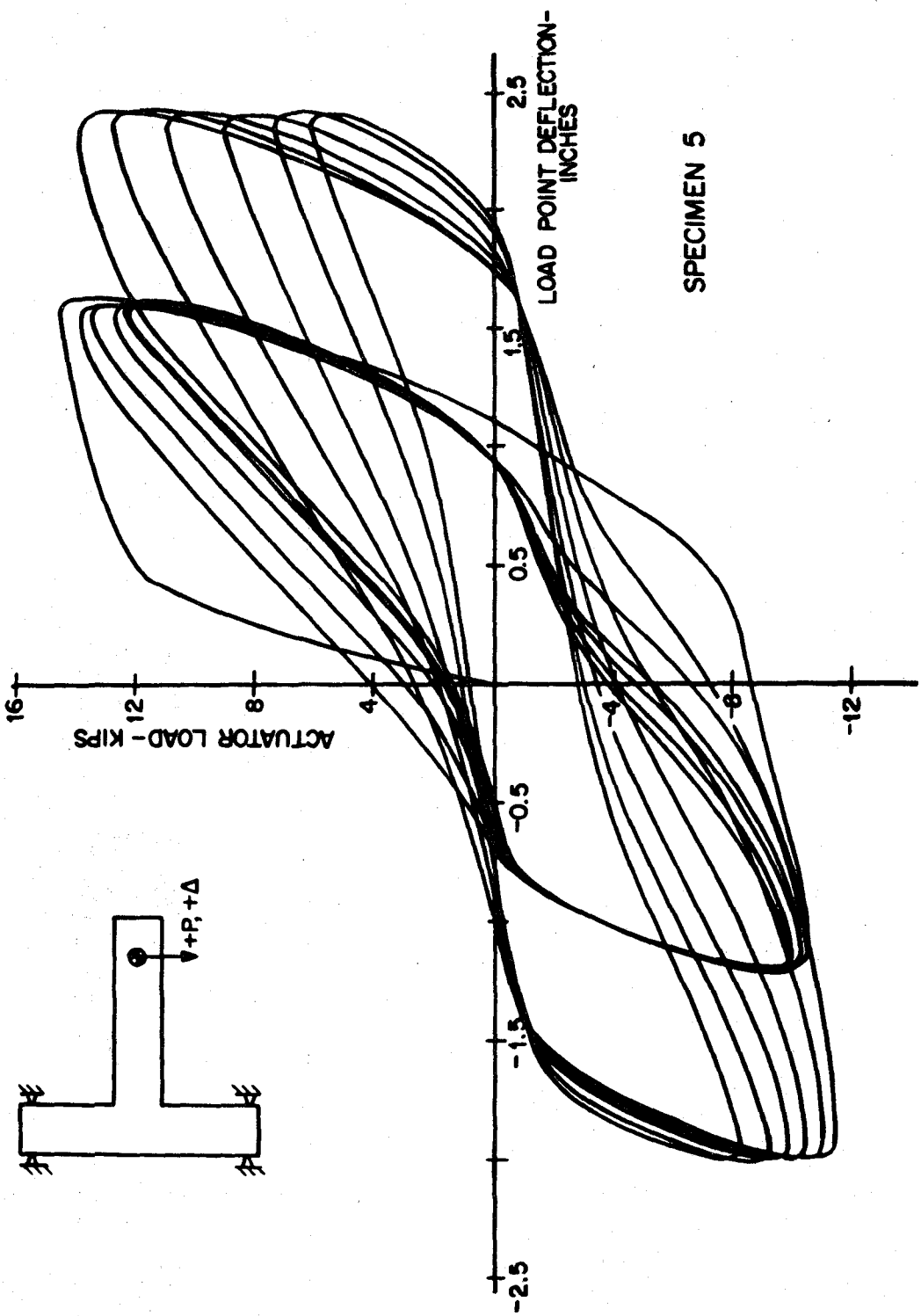

Fig. 3.1(e). Load vs. Deflection Response of Specimen 5.

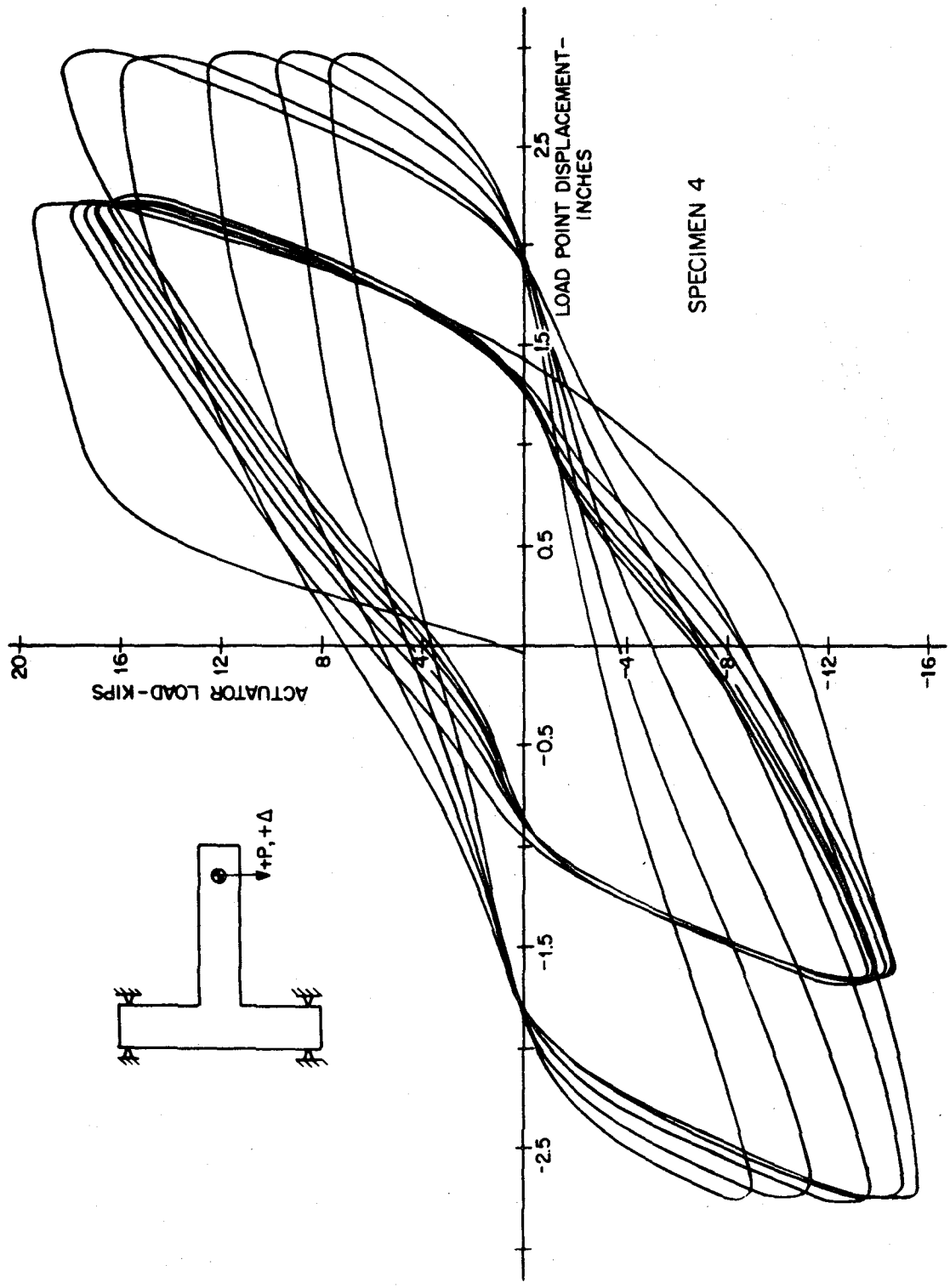

Fig. 3.1(d). Load vs. Deflection Response of Specimen 4.

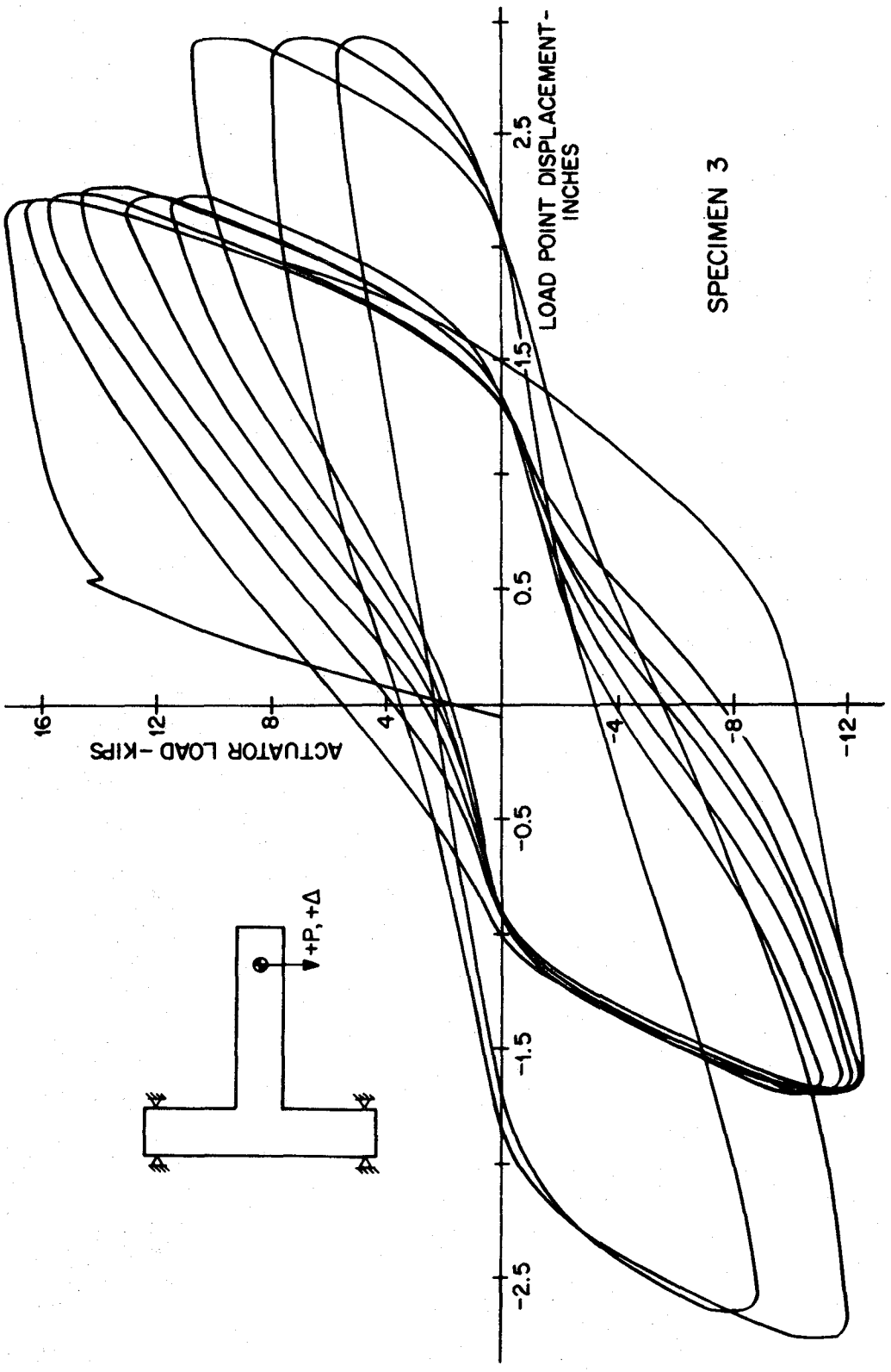

Fig. 3.1(c). Load vs. Deflection Response of Specimen 3.

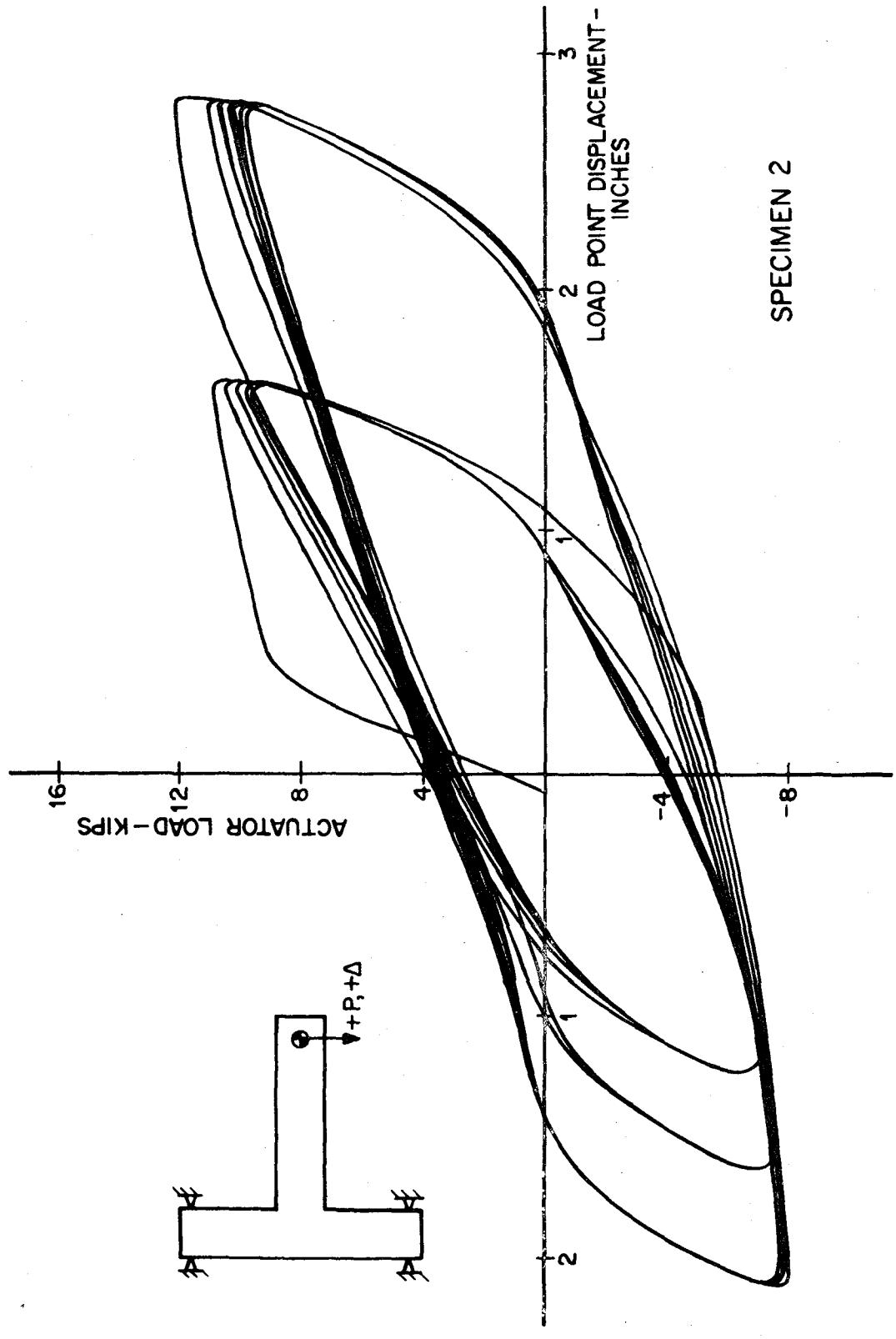

Fig. 3.1(b). Load vs. Deflection Response of Specimen 2.

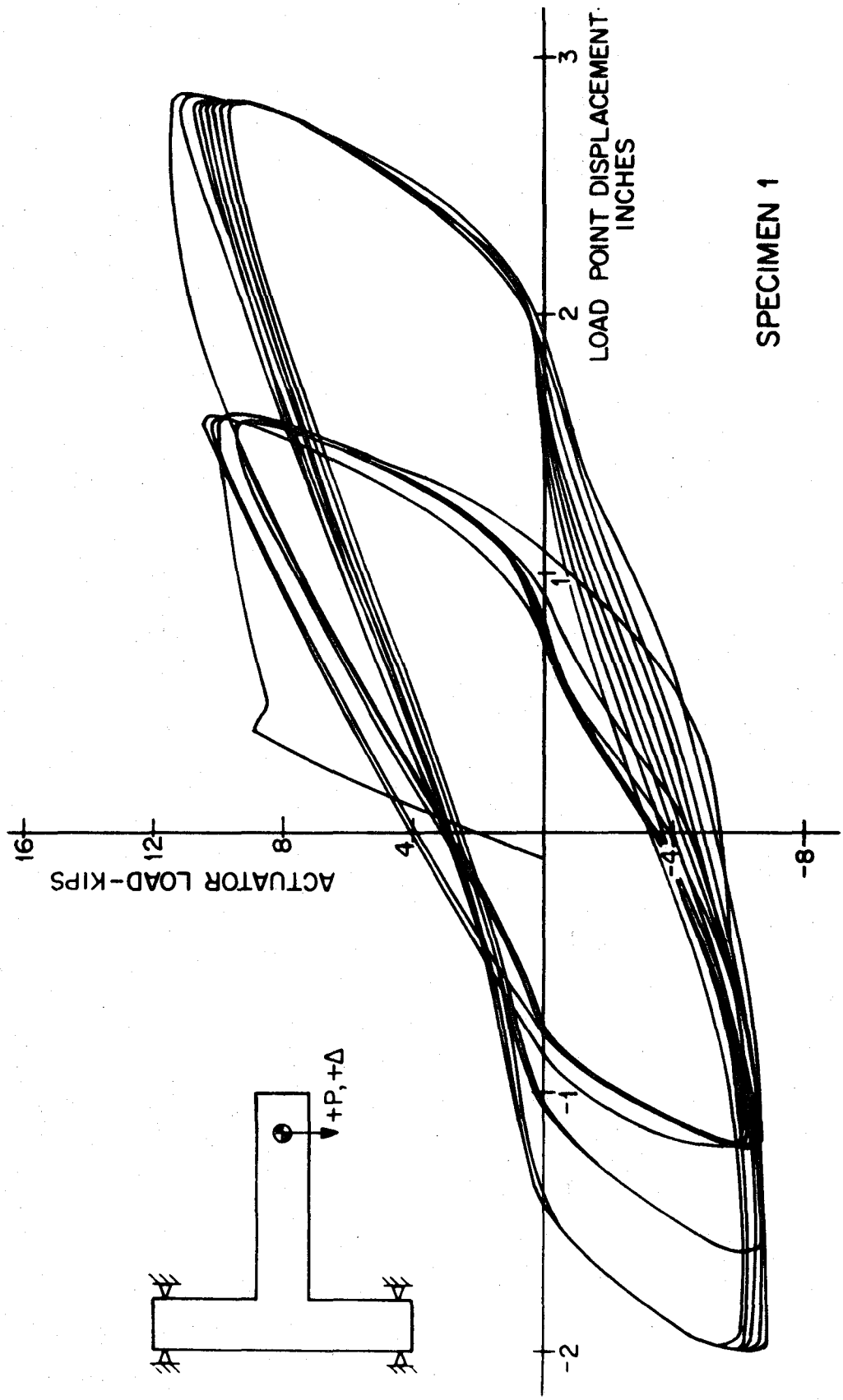

Fig. 3.1(a). Load vs. Deflection Response of Specimen 1.

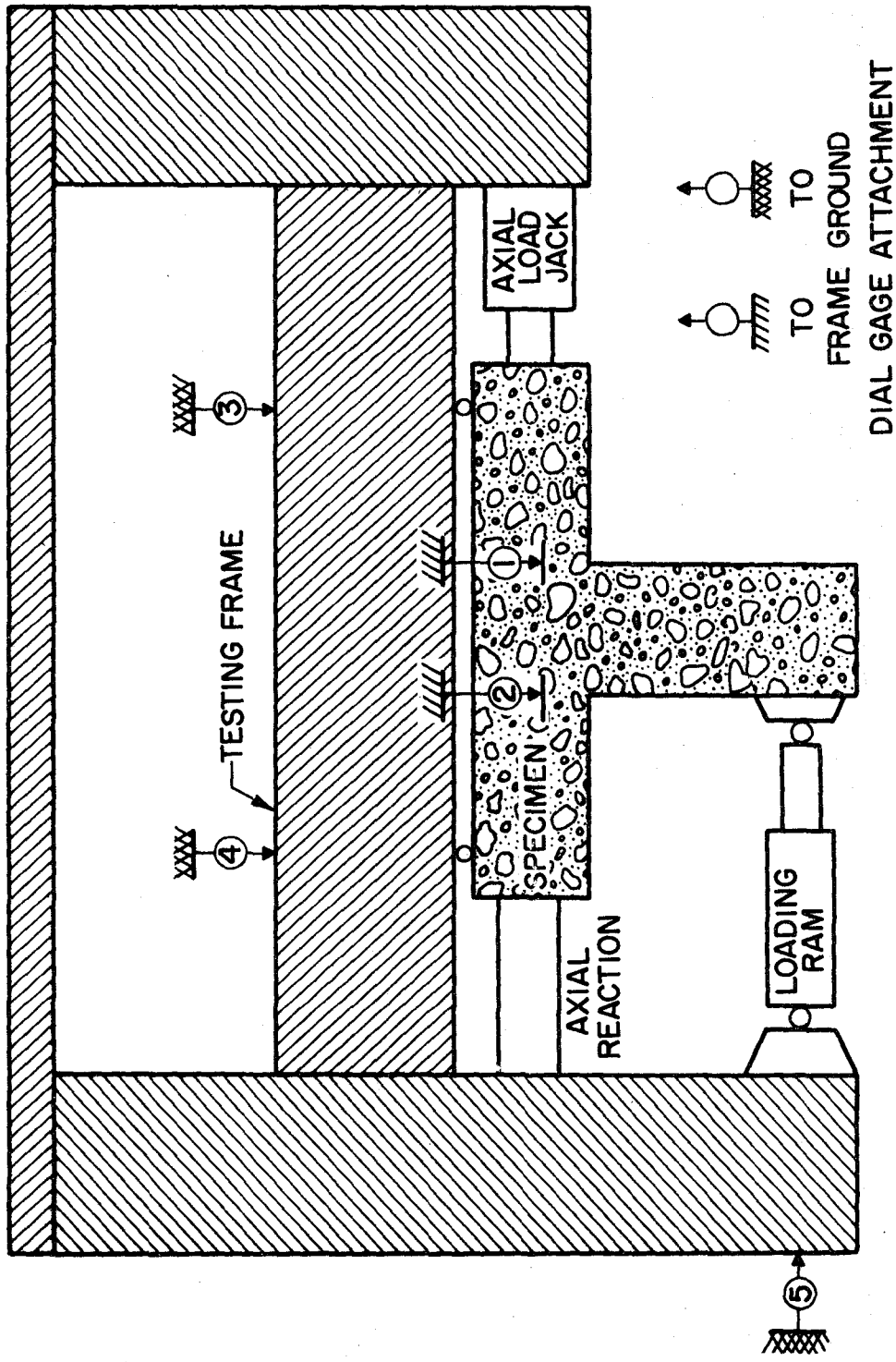

Fig. 2.7. Location of Dial Gages - Group I Specimens.

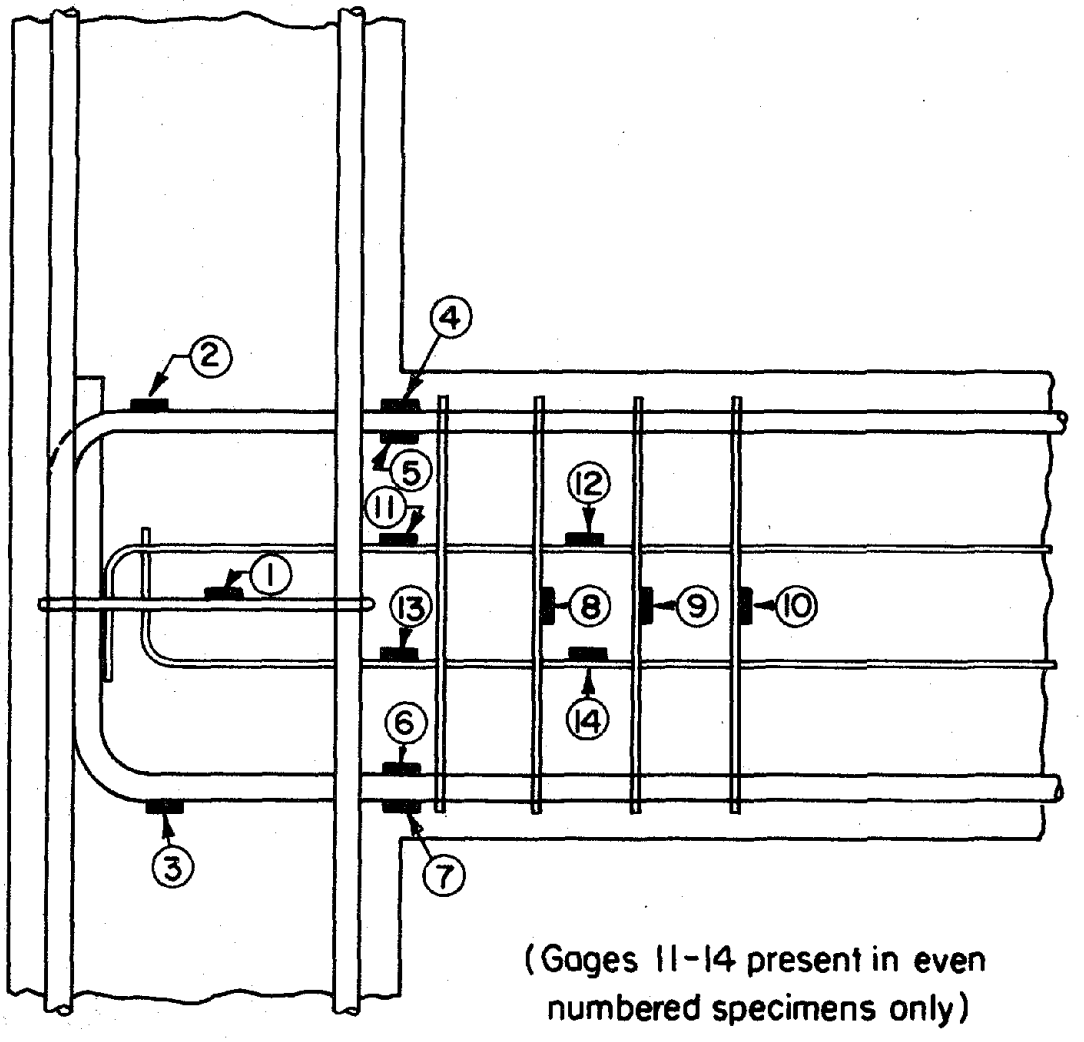

Fig. 2.6. Location of Strain Gages.

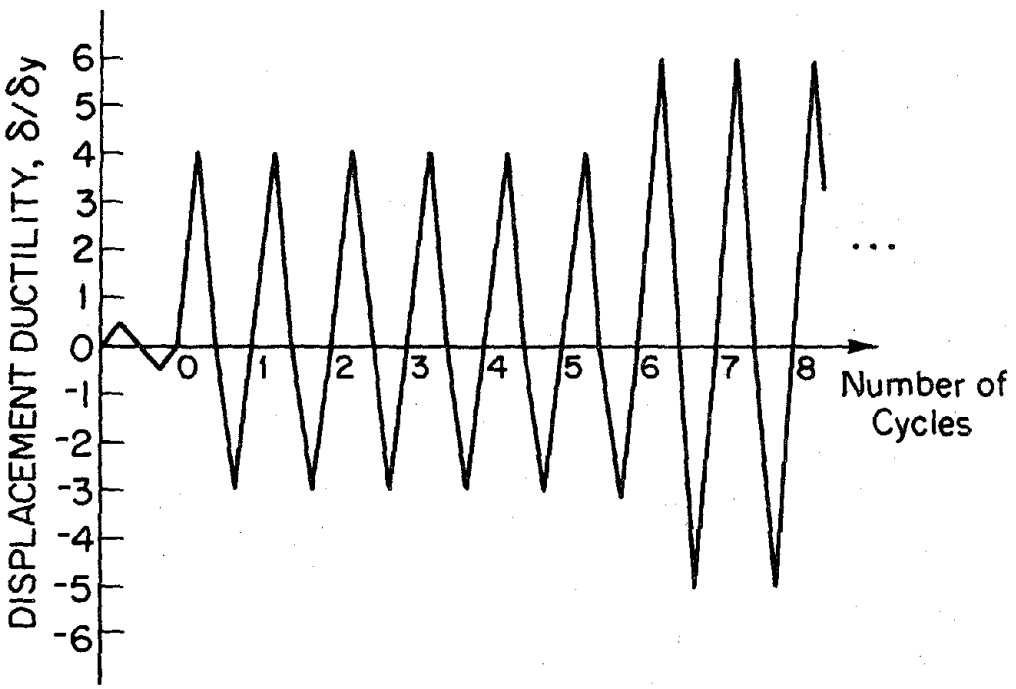

Fig. 2.4. Typical Loading Schedule.

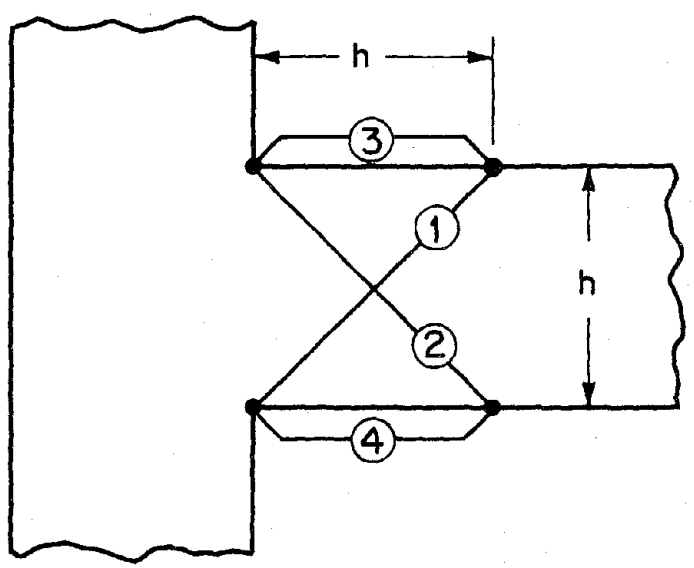

Fig. 2.5. LVDTs Positioned over Beam Hinging Zone.

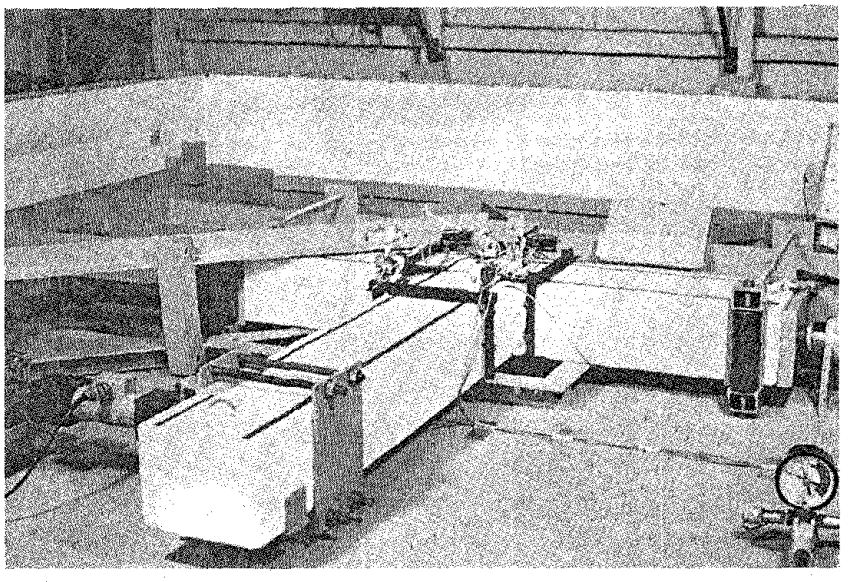

Fig. 2.2. Specimen in Testing Frame (Group I).

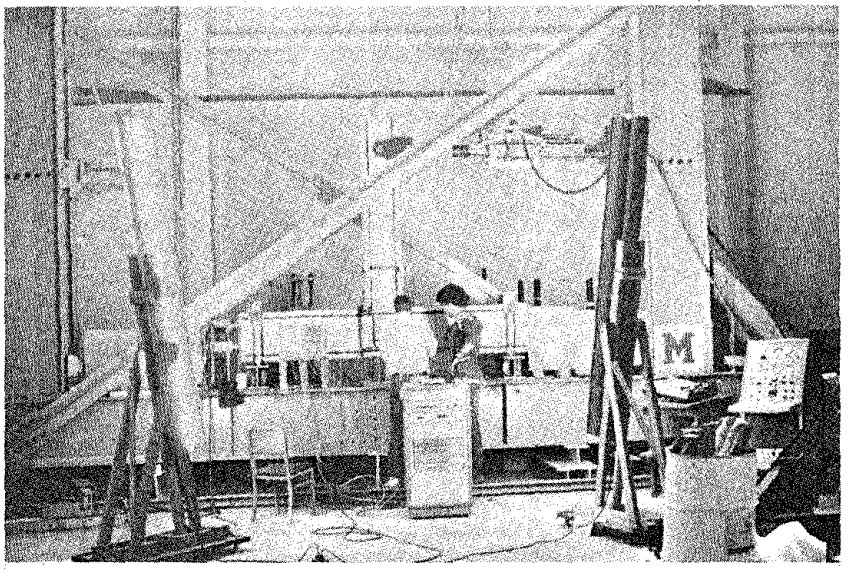

Fig. 2.3. Specimen in Testing Frame (Group II).

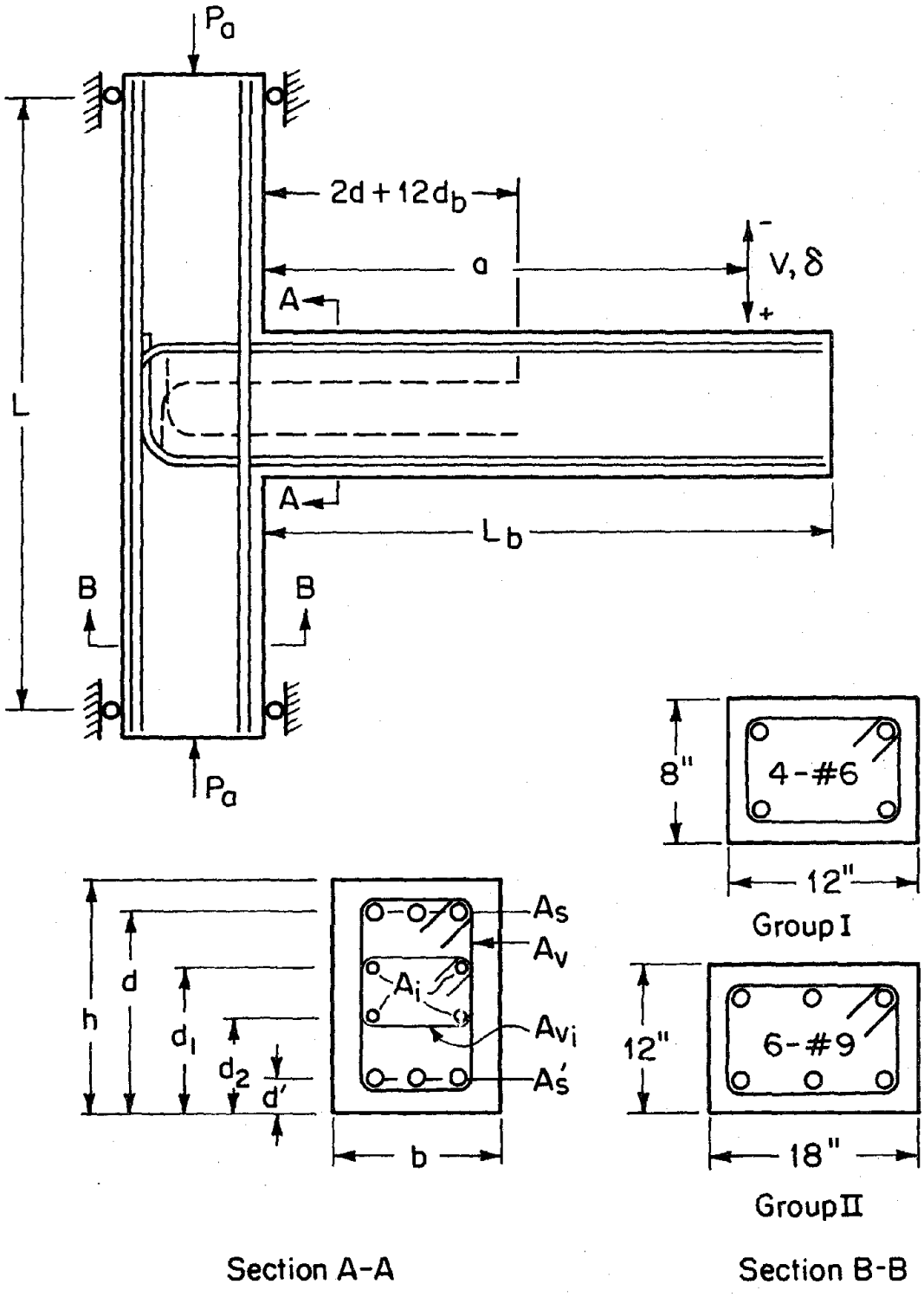

Fig. 2.1. Specimen Configuration and Dimension Designation.

FIGURES

38. Wang, C., and Salmon, C.G., Reinforced Concrete Design, 2nd ed., New York: Intext Educational Publishers, 1973.

39. Wight, J.K., and Sozen, M.A., "Strength Decay of RC Columns under Shear Reversals," Journal of the Structural Division, ASCE, Vol. 101, No. ST5, May, 1975, pp. 1053-1065.

40. Yamada, M., and Furui, S., "Shear Resistances and Explosive Cleavage Failure of Reinforced Concrete Members Subjected to Axial Load," Final Report, Eighth Congress, International Association of Bridge and Structural Engineering, New York, New York, 1968, pp. 1091-1102.

29. Meinheit, D.F., and Jirsa, J.O., "The Shear Strength of Reinforced Concrete Beam-Column Joints," Civil Engineering Structural Research Laboratory, Report No. 77-1, University of Texas, Austin, Texas, January, 1977.

30. Minor, J., and Jirsa, J.O., "Behavior of Bent Bar Anchorages," American Concrete Institute Journal, Vol. 72, No. 4, April, 1975, pp. 141-149.

31. Morita, S., and Kaku, T., "Local Bond Stress-Slip under Repeated Loading," Final Report, International Association of Bridge and Structural Engineering Symposium, Lisbon, September, 1973.

32. Paulay, T., "Coupling Beams of Reinforced Concrete Shear Walls," Journal of the Structural Division, ASCE, Vol. 97, No. ST3, March, 1971, pp. 843-862.

33. _____, "Simulated Seismic Loading of Spandrel Beams," Journal of the Structural Division, ASCE, Vol. 97, No. ST9, September, 1971, pp. 2407-2419.

34. Popov, E.P., Bertero, V.V., and Krawinkler, H., "Cyclic Behavior of Three Reinforced Concrete Flexural Members with High Shear," Earthquake Engineering Research Center, Report No. EERC 72-5, University of California, Berkeley, California, October, 1972.

35. "Recommendation for Design of Beam-Column Joints in Monolithic Reinforced Concrete Structures," Reported by ACI-ASCE Committee 352, J. Jirsa, Chmn., American Concrete Institute Journal, Vol. 73, No. 7, July, 1976, pp. 375-393.

36. Structural Engineers Association of California Seismology Committee, Recommended Lateral Force Requirements and Commentary, San Francisco: Structural Engineers Association of California, 1974.

37. Uzumeri, S.M., and Seckin, M., "Behavior of Reinforced Concrete Beam-Column Joints Subjected to Slow Load Reversals," Publication No. 74-05, Department of Civil Engineering, University of Toronto, March, 1974.

19. Hisada, T., Ohmori, N., and Bessho, S., "Earthquake Design Considerations in Reinforced Concrete Columns," Kajima Institute of Construction Technology Report No. 1, Tokyo, Japan, January, 1972.

20. Ikeda, A., "Load-Deformation Characteristics of Reinforced Concrete Columns Subjected to Alternating Loading," Report of the Training Institute for Engineering Teachers, Yokohama National University, March, 1968.

21. International Conference of Building Officials, Uniform Building Code, 1976 Edition, Whittier, California: International Conference of Building Officials, 1976.

22. Ismail, M.A.F., and Jirsa, J.O., "Bond Deterioration in Reinforced Concrete Subject to Low Cycle Loads," American Concrete Institute Journal, Vol. 69, No. 6, June, 1972, pp. 334-343.

23. Jirsa, J.O., "Factors Influencing the Hinging Behavior of Reinforced Concrete Members under Cyclic Overloads," Paper No. 147, Session 3D, Fifth World Conference on Earthquake Engineering, Rome, 1973.

24. Kanoh, Y., et al., "Shear Strength of Reinforced Concrete Beams under Many Cyclic Alternating Loading," Research Report of the Agricultural Institute of Japan, August, 1969.

25. Lee, D.L.N., Wight, J.K., and Hanson, R.D., "RC Beam-Column Joints under Large Load Reversals," Journal of the Structural Division, ASCE, Vol. 103, No. ST12, December, 1977, pp. 2337-2349.

26. Ma, S.M., Bertero, V.V., and Popov, E.P., "Experimental and Analytical Studies on the Hysteretic Behavior of Reinforced Concrete Rectangular and T-Beams," Earthquake Engineering Research Center, Report No. EERC 76-2, University of California, Berkeley, California, May, 1976.

27. Marques, J.L.G., and Jirsa, J.O., "A Study of Hooked Bar Anchorages in Beam-Column Joints," American Concrete Institute Journal, Vol. 72, No. 5, May, 1975, pp. 198-209.

28. Megget, L.M., and Park, R., "Reinforced Concrete Exterior Beam-Column Joints Under Seismic Loading," New Zealand Engineering, Wellington, New Zealand, Vol. 26, No. 11, November 15, 1971, pp. 341-353.

9. Brown, R.H., and Jirsa, J.O., "Reinforced Concrete Beams under Load Reversals," American Concrete Institute Journal, Vol. 68, May, 1971, pp. 380-390.

10. Burns, N.H., and Siess, C.P., "Plastic Hinging in Reinforced Concrete," Journal of the Structural Division, ASCE, Vol. 92, No. ST5, October, 1966, pp. 45-64.

11. _____, "Repeated and Reversed Loading in Reinforced Concrete," Journal of the Structural Division, ASCE, Vol. 92, No. ST5, October, 1966, pp. 65-78.

12. Clough, R.W., "Effect of Stiffness Degradation on Earthquake Ductility Requirements," Structural Engineering Laboratory, Report No. 66-16, University of California, Berkeley, California, October, 1966.

13. Gosain, N.K., Brown, R.H., and Jirsa, J.O., "Shear Requirements for Load Reversals on RC Members," Journal of the Structural Division, ASCE, Vol. 103, No. ST7, July, 1977, pp. 1461-1476.

14. Goto, Y., "Cracks Formed in Concrete around Deformed Tension Bars," American Concrete Institute Journal, Vol. 68, No. 4, April, 1971, pp. 244-251.

15. Hanson, N.W., and Conner, H.W., "Seismic Resistance of Reinforced Concrete Beam-Column Joints," Journal of the Structural Division, ASCE, Vol. 93, No. ST5, October, 1967, pp. 533-560.

16. Hanson, R.D., and Degenkolb, H.J., "The Venezuela Earthquake, July 29, 1967," Earthquakes, American Iron and Steel Institute, New York, New York, 1975, pp. 201-319.

17. Hassan, F.M., and Hawkins, N.M., "Anchorage of Reinforcing Bars for Seismic Forces," Reinforced Concrete in Seismic Zones, American Concrete Institute, Detroit, Michigan, 1976.

18. Hawkins, N.M., Kobayashi, A.S., and Fourney, M.E., "Reversed Cyclic Loading Bond Deterioration Tests," Structures and Mechanics Report SM 75-5, University of Washington, Seattle, Washington, November, 1975.

SELECTED BIBLIOGRAPHY

1. American Concrete Institute, Committee 318, Building Code Requirements for Reinforced Concrete (318-71), Detroit, Michigan: American Concrete Institute, 1971.

2. _____, Commentary on Building Code Requirements for Reinforced Concrete (318-71), Detroit, Michigan: American Concrete Institute, 1971.

3. American Society of Civil Engineers - American Concrete Institute, Task Committee 426, N. Hawkins, Chairman, "The Shear Strength of Reinforced Concrete Members," Journal of the Structural Division, ASCE, Vol. 99, No. ST6, June, 1973, pp. 1091-1187.

4. Berg, G.V., "The Skopje, Yugoslavia Earthquake, July 26, 1963," Earthquakes, American Iron and Steel Institute, New York, New York, 1975, pp. 89-144.

5. Bertero, V.V., and Popov, E.P., "Hysteretic Behavior of Reinforced Concrete Flexural Members with Special Web Reinforcement," Proceedings of the U.S. National Conference on Earthquake Engineering, Ann Arbor, June, 1975, pp. 316-326.

6. Bertero, V.V., Popov, E.P., and Wang, T.Y., "Hysteretic Behavior of Reinforced Concrete Flexural Members with Special Web Reinforcement," Earthquake Engineering Research Center, Report No. EERC 74-9, University of California, Berkeley, California, August, 1974.

7. Bresler, B., and Bertero, V.V., "Behavior of Reinforced Concrete under Repeated Loading," Journal of the Structural Division, ASCE, Vol. 94, No. ST6, June, 1968, pp. 1567-1590.

8. Bresler, B., and MacGregor, J.G., "Review of Concrete Beams Failing in Shear," Journal of the Structural Division, ASCE, Vol. 93, No. ST1, February, 1967, pp. 343-370.

Preceding page blank

SELECTED BIBLIOGRAPHY

ing topics is necessary.

1. The effect of varying the ratio of the area of intermediate longitudinal reinforcement to the area of main tension reinforcement should be considered. It is possible that an optimum ratio exists for any given shear stress range.

2. Various arrangements of intermediate longitudinal reinforcement should be tried to determine what bar arrangement provides the most significant increase in member energy dissipation.

3. Criteria should be developed to specify the size (stiffness) of stirrup ties in a beam plastic hinging zone, when used at the maximum allowable spacing of d/4, as a function of the size of the longitudinal bars.

4. The effect of different loading histories on specimen deterioration rate should be studied to determine if the load history used to test any particular specimen has an effect on the amount of total energy which that specimen can dissipate during repeated reversed loading.

specimens were not able to endure enough cycles of repeated reversed loading to satisfy a consensus of load-carrying criteria.

3. Vertical web reinforcement in a plastic hinging zone must be selected using criteria other than strength and maximum allowable spacing. Tests of specimens containing identical longitudinal reinforcement, but different strength and stiffness web reinforcement (Specimens 3 and 7) demonstrated that web reinforcement larger than that required for strength and maximum allowable spacing criteria was beneficial in preventing hinging zone deterioration.

4. No amount of vertical web reinforcement was as effective as supplementary longitudinal reinforcement in distributing damage throughout the hinging zone and limiting shear strength decay.

5. The presence of intermediate ties around supplementary reinforcement did not significantly affect overall specimen response in the specimens tested.

6.3 Recommendations for Additional Research

Although this research project verified the ability of intermediate longitudinal reinforcement to delay physical and shear strength decay, it left unanswered some questions regarding the significance of certain reinforcement and member details in determining overall member behavior. In this light, research on the follow-

which varied with shear stress level.

2. The effect of intermediate longitudinal reinforcement on beam response was dependent on maximum shear stress level. It was possible to define the contribution of the intermediate longitudinal reinforcement for three levels of shear intensity:

a) For beams with maximum shear stresses less than $3\sqrt{f'_c}$, web reinforcement designed in accordance with existing seismic standards prevented significant strength and stiffness decay during repeated reversed loading. Although a 5% increase in energy dissipation over twelve cycles of load was realized by using intermediate longitudinal reinforcement in the beam plastic hinging region, the increase was considered superfluous.

b) For beams with maximum shear stresses between $3\sqrt{f'_c}$ and $6\sqrt{f'_c}$, intermediate longitudinal reinforcement significantly increased both the total energy dissipation and the stability of hysteretic response. Beams containing intermediate longitudinal reinforcement were able to dissipate an average of 27 percent more input energy than beams having identical main reinforcement and vertical ties only.

c) For beams with maximum shear stresses greater than $6\sqrt{f'_c}$, the inclusion of intermediate longitudinal reinforcement increased total energy dissipation by 30 percent. Even with this improvement, however, the

ties were not sufficiently strong to confine the buckled section to one stirrup interval, and in all cases buckling deformation spanned three to four stirrup intervals.

In a specimen which contained web reinforcement much larger than that required for shear strength considerations (Specimen 7), buckling of longitudinal reinforcement was prevented even though concrete had spalled off so completely by the last load cycle that lower longitudinal reinforcement was totally uncovered for the full length of the hinging region.

6.2 Conclusions

Based on the results of the tests discussed here and in conjunction with research done by others, it is possible to draw the following conclusions:

1. The repeatability of hysteretic response of concrete members during repeated reversed inelastic flexure was closely linked to the maximum shear stress level experienced by the member. Members with maximum shear stress levels less than $3\sqrt{f'_c}$ showed primarily flexural response with little tendency to develop significant planes of shear slippage. In contrast, members with maximum shear stress levels greater than $6\sqrt{f'_c}$ reacted primarily in shear, with severe damage resulting along planes of shear slippage formed under reversed flexure. Members with maximum shear stresses between $3\sqrt{f'_c}$ and $6\sqrt{f'_c}$ responded with a mixture of shear and flexural action

with members having only vertical ties.

The length of the beam plastic hinging zone was not significantly affected by the inclusion of intermediate longitudinal reinforcement. In all specimens the length of the plastic hinging region was approximately equal to the effective beam depth, although cracking was more uniformly distributed through this region when intermediate longitudinal reinforcement was present. When essentially identical specimens were tested with different shear spans, the specimen with the shorter shear span developed a shorter plastic hinge, indicating a general tendency toward shear-related failure for specimens with higher shear stresses.

Buckling of compression reinforcement was a significant factor in limiting the load-carrying capacity of the majority of the specimens tested. One of the main concerns of codes which specify close spacing of ties in locations of probable inelastic hinging is to prevent buckling of compression reinforcement during repeated large scale load reversal. The nature of buckling noted in the specimens tested indicated that stirrup stiffness was more important than stirrup spacing in preventing buckling of compression reinforcement. Ties acted as lateral springs to prevent or delay buckling after concrete had spalled off and exposed the longitudinal bars. When buckling occurred,

Several characteristics of behavior were common to all specimens. During inelastic flexure, vertical and inclined cracks formed in the beam at various points in the region of high moment near the face of the column and elsewhere along the beam. Upon reversal of load, these cracks remained open until the residual plastic strains in reinforcement were overcome. Continued reversed loading caused vertical and inclined cracks to form in the side of the beam previously in compression. Cracks from opposite sides of the beam then joined, forming planes of weakness sometimes nearly perpendicular to the longitudinal axis of the member. Additional cycles of loading reversal caused slippage along planes of weakness, with accompanying degradation of concrete, local bending and loss of bond along main reinforcement, spalling of cover concrete, and eventual inability to carry load because of shear strength loss or buckling of main compression reinforcement. Most planes of shear slip did not cross vertical ties.

Intermediate longitudinal reinforcement crossed all planes of shear slippage and, together with vertical ties, confined the beam core more effectively than did vertical ties by themselves. Intermediate bars, by improving crack distribution and providing better confinement, prolonged stable hysteretic behavior and increased energy dissipation significantly in comparison

reinforcement to main tension reinforcement was approximately 0.25 (ranging from 0.23 to 0.33) for all specimens having supplementary reinforcement. All specimens contained normal web reinforcement designed in accordance with Appendix A of the ACI Building Code Requirements for Reinforced Concrete (1). Beam-column joints contained shear reinforcement as specified by ACI-ASCE Committee 352 recommendations (35) except in specimens containing intermediate longitudinal reinforcement. The shear contribution of intermediate reinforcement was neglected in proportioning joint transverse reinforcement.

Specimens were held in the test frame by simple supports near the ends of the column section. The beam tip was slowly deflected to four times positive yield deflection in the assumed positive direction (downward) and three time positive yield deflection in the negative direction for six cycles. This was followed by several load cycles at larger displacements until beam failure or until twelve cycles of load had been applied. Load and load point deflection were continuously monitored during testing. Shear and flexural deformations in the beam plastic hinging region were measured at discrete points during loading, as were beam-column joint rigid body rotations, test frame deflections, and strains at various locations on longitudinal and transverse reinforcement.

CHAPTER 6

SUMMARY AND CONCLUSIONS

6.1 Summary of Research Program

The primary objective of this research program was to determine the ability of intermediate longitudinal reinforcement to prolong stable hysteresis action in reinforced concrete members subjected to repeated reversed flexure. A secondary objective was to study the response of exterior beam-column joints supporting such members.

To satisfy the research objectives, eight half-size and four full-size T-shaped beam-column subassemblies were constructed. Variables in the twelve specimens included longitudinal reinforcement ratio, web reinforcement ratio, shear span to depth ratio, and the inclusion of intermediate longitudinal reinforcement in half the specimens. Intermediate longitudinal reinforcement consisted of four bars placed in two layers at approximately the third points between tension and compression reinforcement. These bars were anchored by standard 90 degree hooks in the beam-column joint and extended into the beam a distance equal to twice the beam effective depth plus a development length of twelve bar diameters. The ratio of the area of intermediate

to satisfy a consensus of criteria for suitable performance under repeated reversed loading.

12 with similar conclusions.

Bertero tested several T-shaped specimens with high shear stresses and concluded that although very sophisticated and potentially expensive reinforcement details could virtually eliminate stiffness decay resulting from repeated reversed loading, beams should not be designed to carry shear stresses larger than $6\sqrt{f'_c}$ in regions where seismic activity is anticipated. Gosain, in contrast, adopted a performance specification criterion not tied to any particular shear stress level. He theorized that a structure could be expected to perform well under seismic loading if the individual members could provide five cycles of stable inelastic flexure to displacements of $\pm 5\Delta_y$. For the shear span to depth ratio at which Specimens 11 and 12 were tested (4), this translates to a modified work index requirement of 18.75. (See explanation of modified work index calculation given in conjunction with Table 5.1).

Test results previously presented in Tables 3.1 and 5.1 indicate that Specimens 11 and 12 did not meet Bertero's proposed maximum shear stress criterionand failed to provide Gosain's measure of sufficient energy dissipation. It is possible to draw two conclusions from the test results for these specimens. First, it is apparent that intermediate longitudinal reinforcement increased energy dissipation significantly, regardless of the method of comparison. Second, neither Specimen 11 or 12 was able to perform well enough

load to hinging zone shear strain shown in Figs. 5.12 and 5.13. The results shown in these two figures give some indication of the amounts of degradation in moment at a constant maximum displacement which can be attributed to losses in shear and flexural stiffness. It is evident in comparing the relationship of maximum positive shear load to hinge shear strain that a much larger percentage of load loss at a given displacement was due to shear stiffness loss in Specimen 3 than in Specimen 4.

Specimens with α greater than 6.0

This group included Specimens 11 and 12, both of which suffered severe stiffness and strength deterioration during repeated loading. These specimens were reinforced identically except that Specimen 12 contained intermediate longitudinal reinforcement. As with all other specimen pairs discussed, energy dissipation was substantially increased by the inclusion of intermediate bars. Specimen 12 was able to survive two more cycles of loading than Specimen 11 at comparable displacement ductilities. However, neither specimen was judged adequate in retaining strength and stiffness.

The determination of minimum performance criteria for specimens of this type has been addressed by several researchers. Bertero and Popov (5) and Gosain et al. (12) considered this problem from diametrically opposed viewpoints, but their recommendations may be applied to Specimens 11 and

reinforcement. In order to determine the contribution of these ties in prolonging the integrity of the hinging zone, Specimen 8 was reinforced identically to Specimen 4 except that it did not contain additional ties around intermediate bars. Normalized energy dissipation was nearly identical for the two specimens, as shown in Table 5.1. This similarity of performance is explained by the fact that the modes of deterioration which the supplementary ties could have prevented, such as buckling of intermediate reinforcement and expansion of the hinging region perpendicular to the plane of bending, were not significant factors in the overall deterioration of these particular specimens. Other researchers (5) have found such ties beneficial, however, and their use is encouraged.

The correlation between shear stiffness retention and satisfactory energy dissipation can be observed by considering the relationship of load point displacement vs. hinging zone shear strain for Specimens 3 and 4 (Figs. 3.13 and 3.18 respectively). As shown in Fig. 3.13, maximum positive shear strain in the hinging zone of Specimen 3 increased significantly with each cycle of positive displacement. The comparable plot for Specimen 4, Fig. 3.18, shows a more stable relationship between displacement and shear strain in the hinging zone.

The comparison between Specimens 3 and 4 may be extended by examining also the relationships of beam shear

and may or may not have crossed vertical ties. Intermediate bars were able to restrict the width of cracks at any inclination by providing a tensile force across the crack. In turn, the shear friction force (3) along the crack was sufficient to prevent or delay sliding along the crack, causing damage to occur in the previously uncracked larger blocks. Because cracking was more uniformly distributed through the zone of inelastic flexure by intermediate reinforcement, average crack width remained small and sliding degradation along each crack was inhibited.

The patterns of cracking shown in the three pairs of specimens discussed above illustrate the ability of intermediate longitudinal reinforcement to provide excellent confinement. Intermediate bars also limited crack widths and limited the mobility of concrete blocks in the hinging zone, preventing a concentration of physical degradation along vertical planes of weakness. Consequently, the matrix of concrete blocks in the core was forced to carry flexural and shear stresses instead of being allowed to slide along cracks formed in previous load cycles. As the tests proceeded, new cracks formed in the restrained concrete blocks until a point of concrete degradation was reached at which the beam core's strength and stiffness were significantly reduced.

As indicated in Appendix A, Table A.1, Specimen 4 contained supplementary ties around intermediate longitudinal

The appearance of the plastic hinging region of Specimen 7 following removal of loose and broken concrete is shown in Fig. 3.25 and the appearance of Specimen 8 after its corresponding disassembly is shown in Fig. 3.34. It is undeniable that the large web reinforcement used in Specimen 7 controlled inclined cracks, as the beam core in the hinging zone of this specimen was almost undamaged. However, as shown previously by Jirsa (23), no size web reinforcement can prevent the formation of a vertical plane of weakness in a beam such as occurred in this specimen at the face of the column. Further, a comparison of the failure modes of Specimen 7 and the other specimens in this test series indicates that sliding along this plane was aggrevated by the increased shear stiffness of the hinging region.

In contrast, the nature of damage in the hinging region of Specimen 8, shown in Fig. 3.30, exemplifies the ability of intermediate reinforcement to prevent a concentration of deterioration in one location. The process of crack distribution occurs in two stages with initial formation of large blocks and subsequent segmentation into smaller blocks. Goto (14) showed that primary cracks form at some relatively uniform spacing along a deformed bar in tension. Cracks of this type, seen in all specimens tested, propagated through the depth of the beam at various inclinations. Depending on their angle of inclination to the beam centerline, these cracks crossed intermediate longitudinal bars

loading by the removal of all broken and loose concrete. The character of the remaining blocks is shown in Figs. 3.14 and 3.17. It is evident in these photographs that blocks almost as large as the beam core remained intact in the hinging region of Specimen 3, a specimen which performed poorly. In contrast, segmentation of the hinging zone of Specimen 4, which performed well, was so complete that almost all blocks could be removed from this region.

Because the increased confinement provided by intermediate bars appeared to be a major factor in increasing energy dissipation, Specimen 7 was constructed with No. 3 grade 60 stirrups to determine if a larger amount of web reinforcement would provide confinement and behavior comparable to that obtained by use of intermediate reinforcement. Figure 3.24 illustrates the nature of crack distribution in Specimen 7 after three inelastic displacement cycles. Although the large web reinforcement employed in this specimen did produce a good distribution of cracking and was able to confine the hinging region beam core well, the overall behavior of the specimen was not as good as the behavior of Specimen 8, a comparable specimen which contained No. 2 web reinforcement and No. 3 intermediate longitudinal bars in addition to conventional shear reinforcement. The reasons for the relative performance of these two specimens (Specimens 7 and 8) may be inferred by examining the nature of beam deterioration at the conclusion of testing.

this shear stress level.

Specimens with α between 3.0 and 6.0

Behavior of specimens with maximum first-cycle shear stresses between 3.0 $\sqrt{f'_c}$ and 6.0 $\sqrt{f'_c}$ (Specimens 3 through 10) is of major interest in this study. Specimens with intermediate longitudinal reinforcement were able to dissipate an average of 27% more energy than comparable specimens which contained only vertical web reinforcement as required by the ACI Building Code seismic provisions.

Perhaps one of the most significant contributions of intermediate longitudinal reinforcement was to inhibit opening of vertical and inclined cracks in the beam plastic hinging region and to create a better distribution of cracking within this region. Consider the relative appearance of Specimens 5 and 6, shown in Figs. 3.20 and 3.22(b) respectively, after twelve cycles of loading. These specimens contained identical reinforcement except for the presence of intermediate longitudinal bars in Specimen 6, which forced the concrete in the hinging zone of that specimen to be subdivided into much smaller blocks than were formed in Specimen 5. This relative behavior was also evident in Specimens 3 and 4, which were identically reinforced except that Specimen 4 contained intermediate longitudinal bars and supplementary ties. The hinging regions of these two specimens were dismantled following the completion of

specimens is suggested by the linearity of the displacement vs. flexural rotation relationship shown in Fig. 5.11 for Specimen 2. A similar relationship for Specimen 1 is shown in Fig. 3.3(a). Comparison of the two figures shows that they are identical in all significant respects, with flexural rotation proportional to displacement for all cycles of deflection.

Although the addition of intermediate longitudinal shear reinforcement did not affect yield load significantly (yield load for both specimens was estimated as 8.8 kips), it did increase maximum shear load in the first load cycle for Specimen 2 by approximately 5% in comparison to maximum shear in Specimen 1. Specimen 2 also dissipated 8% more total energy than Specimen 1 through 12 load cycles. As previously noted, however, both specimens were stable at the termination of loading. It is doubtful that the inclusion of supplementary intermediate longitudinal reinforcement could have contributed enough energy dissipation to cause significant improvement in the performance of the actual structure under seismic loading. Both specimens in this group would satisfy any conservative criteria for strength and stiffness retention under repeated reversed loading. In this light, it must be concluded that shear reinforcement required by the seismic provisions of the ACI Building Code (1) is sufficient to ensure stable beam performance under maximum anticipated seismic excitation for

maximum first-cycle beam shear stress. Behavior of specimens within each of the following three groups tended to indicate the ability of web reinforcement and supplementary longitudinal reinforcement to delay strength and stiffness decay during repeated reversed loading.

Beam shear stress values of $3\sqrt{f'_c}$ and $6\sqrt{f'_c}$ were used as the points of separation for the three groups. Specimens in the group having beam shear stress levels less than $3\sqrt{f'_c}$ (α less than 3.0) were stable throughout the loading routine used during testing, regardless of the shear reinforcement used. Specimens in the group with shear stress levels between $3\sqrt{f'_c}$ and $6\sqrt{f'_c}$ ($3.0 < \alpha < 6.0$) suffered stiffness and strength decay of varying severity, with significant improvement shown for specimens containing supplementary longitudinal reinforcement. Specimens with maximum beam shear stresses greater than $6\sqrt{f'_c}$ (α greater than 6) experienced severe stiffness and strength decay and were unable to survive six load cycles to displacement ductilities of $4\Delta_y$. The behavior of specimens in the final group was judged to be less than acceptable, regardless of reinforcement configuration.

Specimens with α less than 3.0

This group included Specimens 1 and 2, both of which showed ductile and stable behavior for the duration of loading. The primarily flexural response of these two

of the stiffening effect of floor sections or other members contiguous to ductile frame members.

It is possible to make the following general observations which summarize the characteristics of buckling observed in these tests:

1) Concrete in the plastic hinging region must have deteriorated sufficiently to allow the axial shortening of longitudinal reinforcement which must accompany buckling.
2) Cover concrete and concrete near the longitudinal bars must have deteriorated sufficiently to allow lateral bar motion.
3) Small stirrups may allow bars to buckle outward or may allow deterioration of concrete adjacent to bars with concurrent lateral buckling.
4) Loss of torsional stiffness allows beam twist and bar buckling at reduced axial load which can occur with relatively minor deterioration of concrete near longitudinal bars.

5.4 Behavior of Specimens with Various Beam Shear Stress Levels

When considering the generalized behavior of the specimens examined in this test series, it is convenient to consider the specimens in three groups based on

buckling. Figure 5.9 illustrates deformation of this nature which occurred in Specimen 4. This type of failure may occur after severe spalling of cover concrete has taken place in the vicinity of compression reinforcement and it is not necessarily prevented by stirrups of any size or spacing. Larger stirrups can help to delay this failure mode, however, by preventing spalling from penetrating to the depth of longitudinal reinforcement. The nature of spalling is illustrated in Fig. 5.10. As suggested by this figure, a large stirrup may prevent the spall from extending into the beam to the depth of the longitudinal steel centroid, or to a depth which allows bar lateral motion.

The loss of shear strength after several load reversals in four members led to a twist of the members about their longitudinal axes. This twisting caused lateral bending of longitudinal reinforcement and created a situation where bars could buckle at a lower load than if the ends of the potential buckling section were restrained from relative motion. It must be noted, however, that this type of buckling might be confined to specimens tested under laboratory conditions where no means of inhibiting beam twist is provided because of the method of load application. In a normal structure, the probability of beam twisting is very small because

of compression reinforcement was a major cause of loss of load-carrying ability in Specimens 3 and 4. In contrast, buckling was prevented by the very stiff hinging zone ties used in Specimen 7, even though severe spalling of cover concrete took place in the vicinity of lower reinforcement.

The length of the buckled section was also significant in another respect. In all cases of severe buckling, the length of bar displacement was approximately equal to beam depth, a dimension which varied within a narrow range. Two observations may be made based on this fact, in conjunction with the pattern of degradation exhibited by the specimens tested. First, because of the widely varying bar sizes involved in buckling, it is apparent that longitudinal bar size was not the major determinant of buckling mode shape. Second, the retention of cover concrete was a major factor in preventing buckling. No buckling took place in any specimen until nearly all cover concrete had spalled off in the area of instability.

It is also possible to consider a situation in which longitudinal reinforcement does not buckle outward against the confining tie. Several of the specimens showed buckling of this nature, in which the longitudinal bar section moved laterally along the stirrup during

by considering a situation where a bar buckles by deforming in a direction perpendicular to the stirrups over a length equivalent to some multiple of the stirrup spacing. The possible buckled shape for instability spanning one and three stirrup intervals is shown in Fig. 5.8. In this figure, it is assumed that concrete adjacent to the bars at the end of the buckled section is sufficient to provide an essentially fixed-end condition and no translation of ends relative to each other is considered.

For the case of buckling extending over one stirrup interval, a theoretical buckling load can be easily found based on the stirrup spacing, the stress-strain properties of the steel, and the moment of inertia of the bar cross section. When buckling is considered to extend over a number of stirrup intervals, as seen in Fig. 5.8(b), a new theoretical buckling load will result based on the new assumed buckled length, the steel properties, and the stiffness of the lateral springs which represent the confining force of the ties. Because of the increased length of deformation in the second situation, a lower buckling load is probable, depending on the stiffness of lateral springs. The effect of lateral spring (tie) stiffness is indicated by the relative performance of Specimens 3, 4, and 7. Buckling

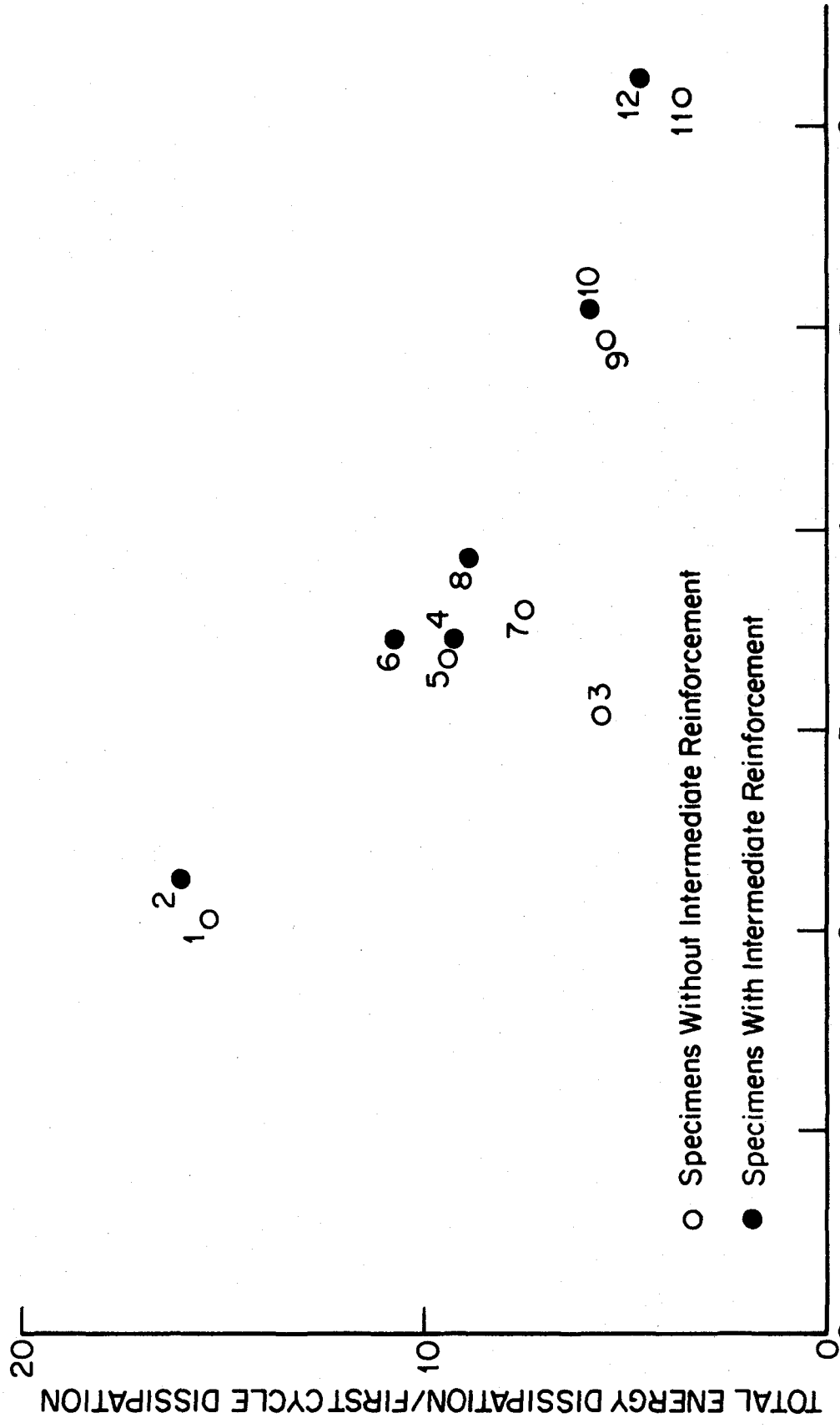

Fig. 5.4. Normalized Energy Dissipation vs. Maximum First-Cycle Shear Stress.

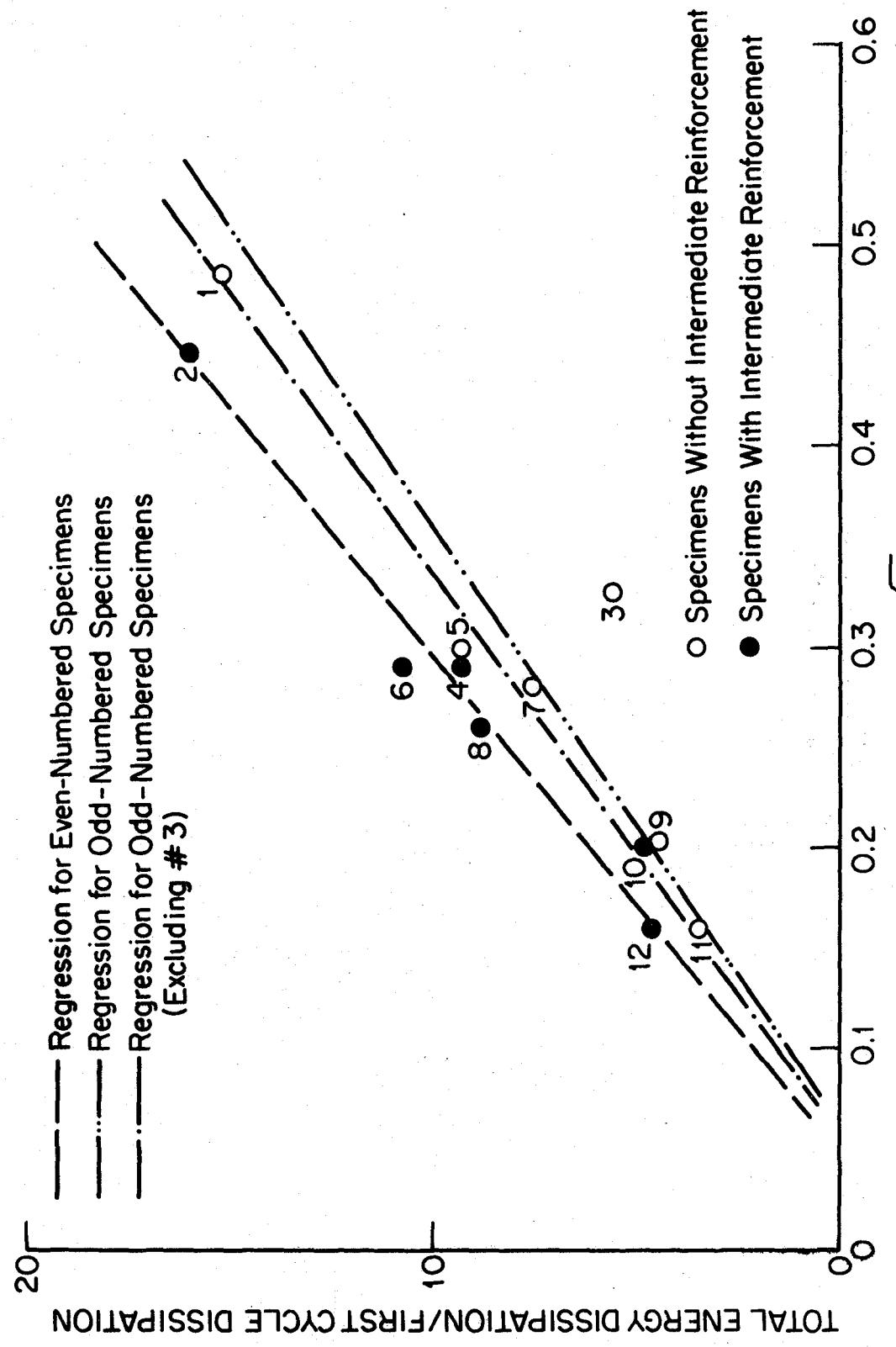

Fig. 5.5. Normalized Energy Dissipation vs. Reciprocal of Maximum Shear Stress.

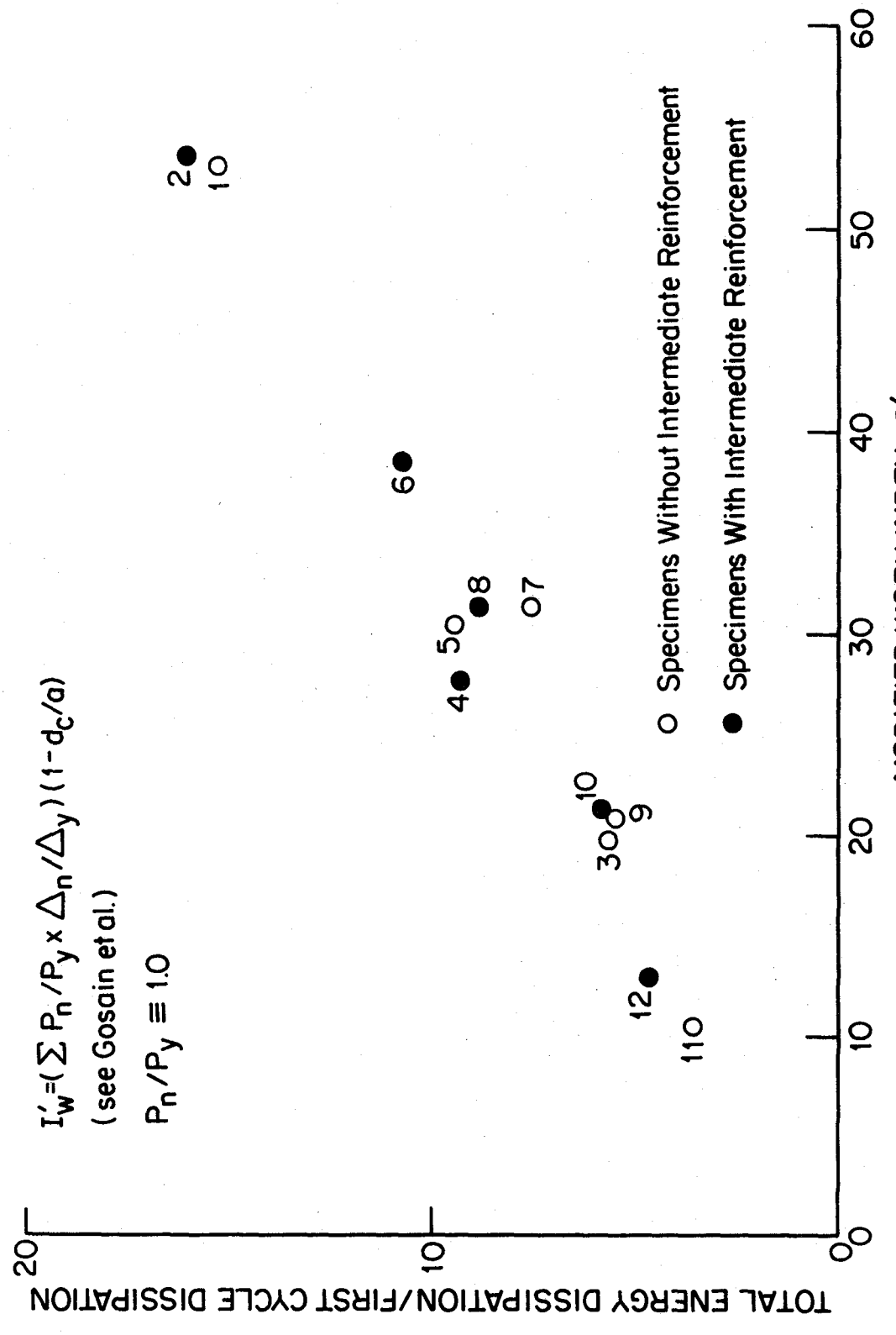

Fig. 5.6. Normalized Energy Dissipation vs. Modified Work Index for Twelve Specimens.

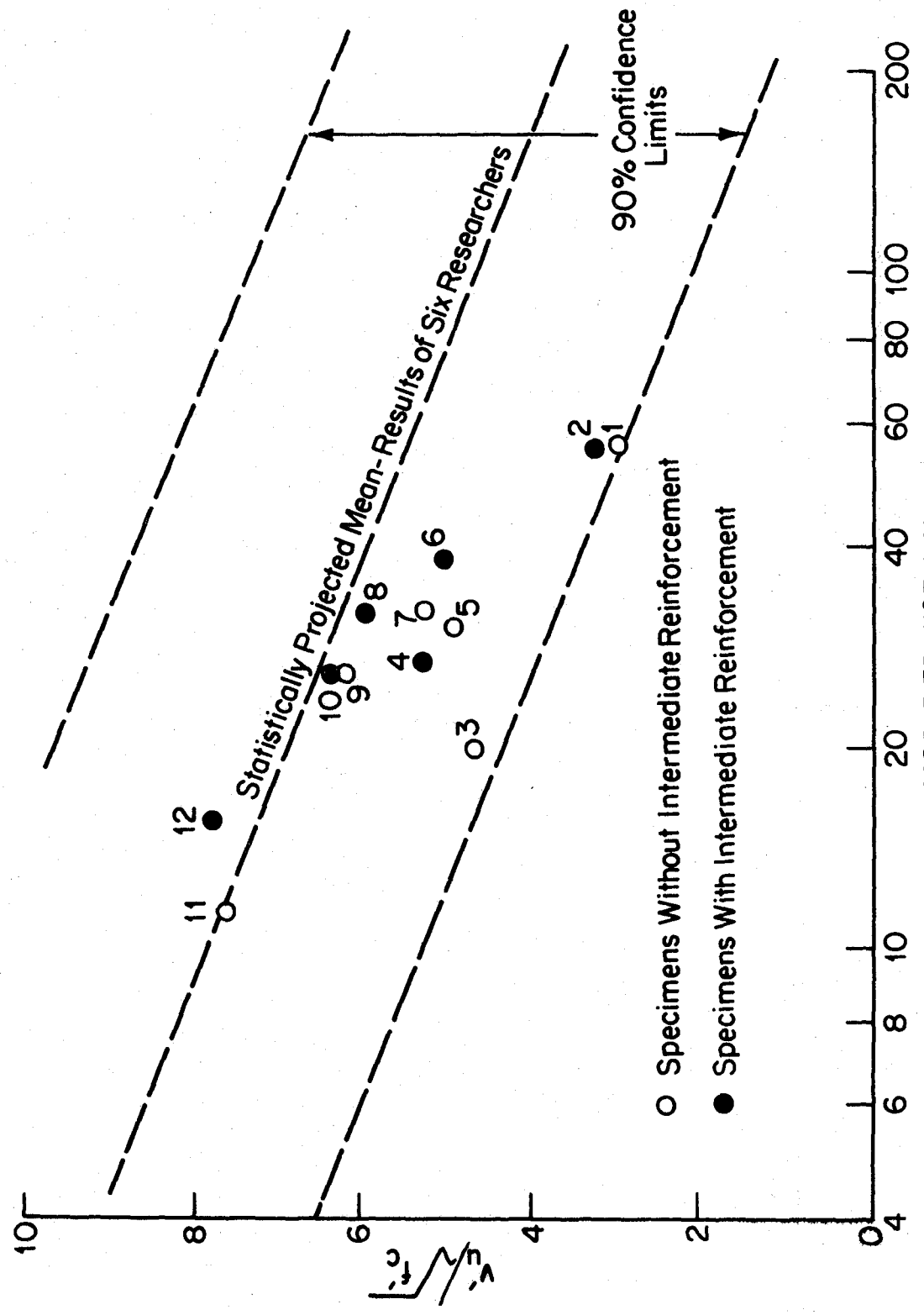

Fig. 5.7. Test Results Compared to Results Obtained by Six Other Researchers.

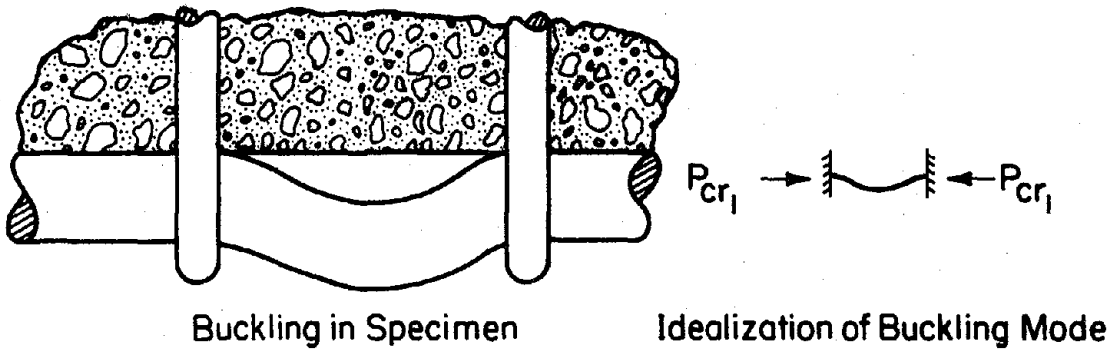

Fig. 5.8(a). Buckling Spanning One Stirrup Interval.

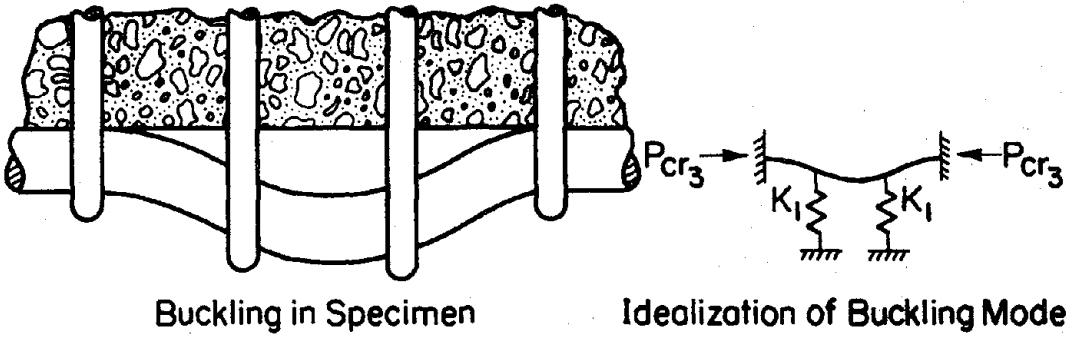

Fig. 5.8(b). Buckling Spanning Three Stirrup Intervals.

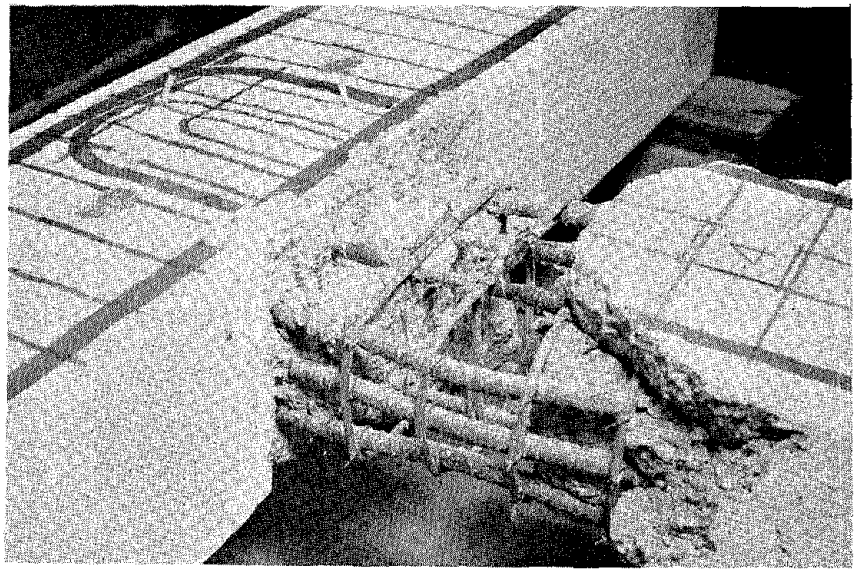

Fig. 5.9. Buckled Shape of Compression Reinforcement Showing Lateral Displacement of Buckled Section - Specimen 4.

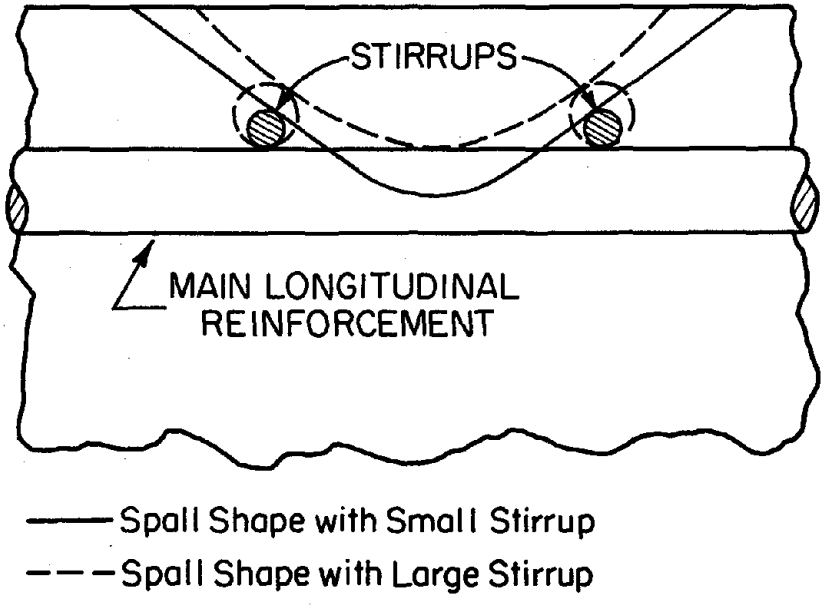

Fig. 5.10. Characteristics of Spalling Illustrate Benefits of Large Stirrup in Denying Penetration of Core Concrete.

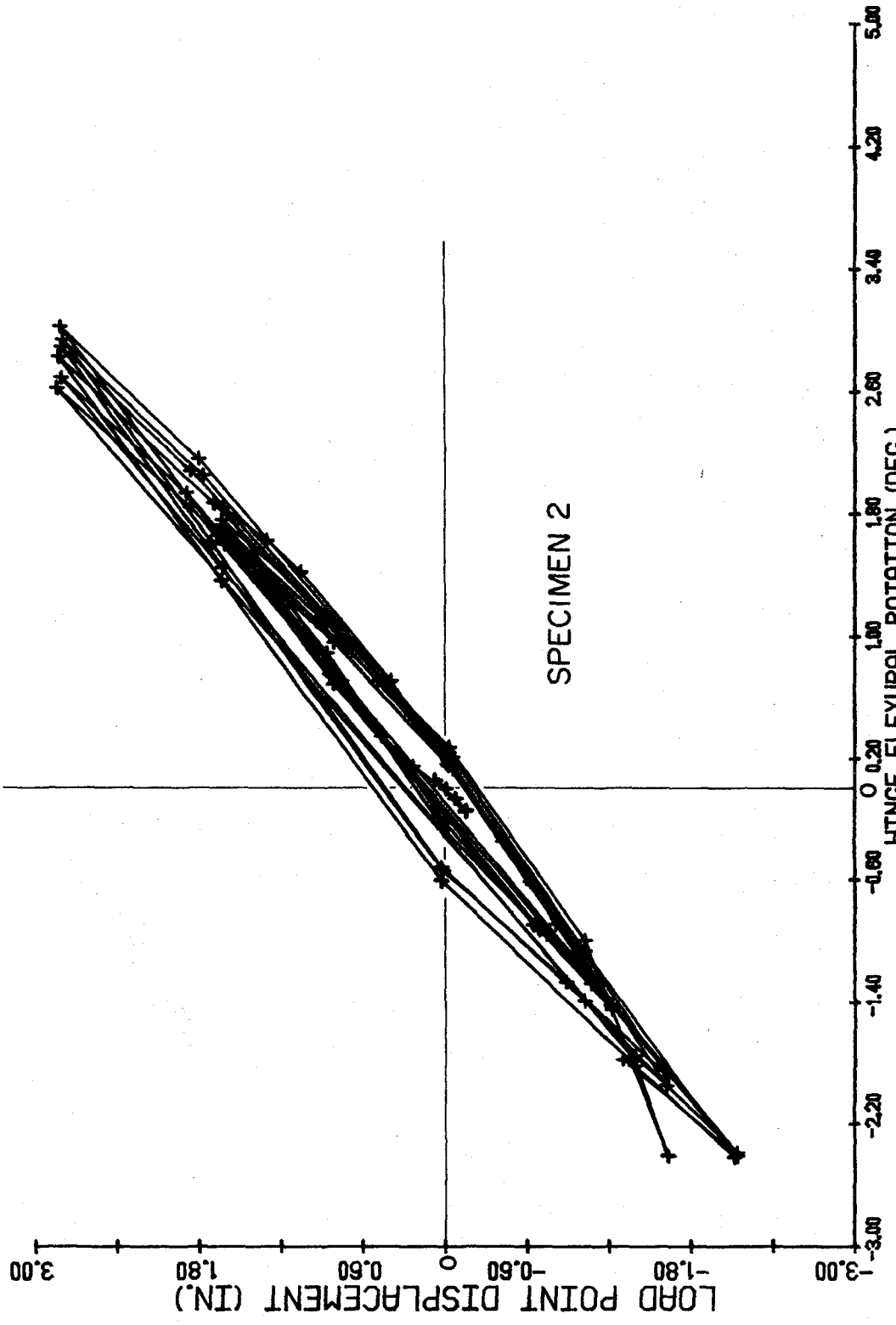

Fig. 5.11. Load Point Displacement vs. Hinge Flexural Rotation - Specimen 2.

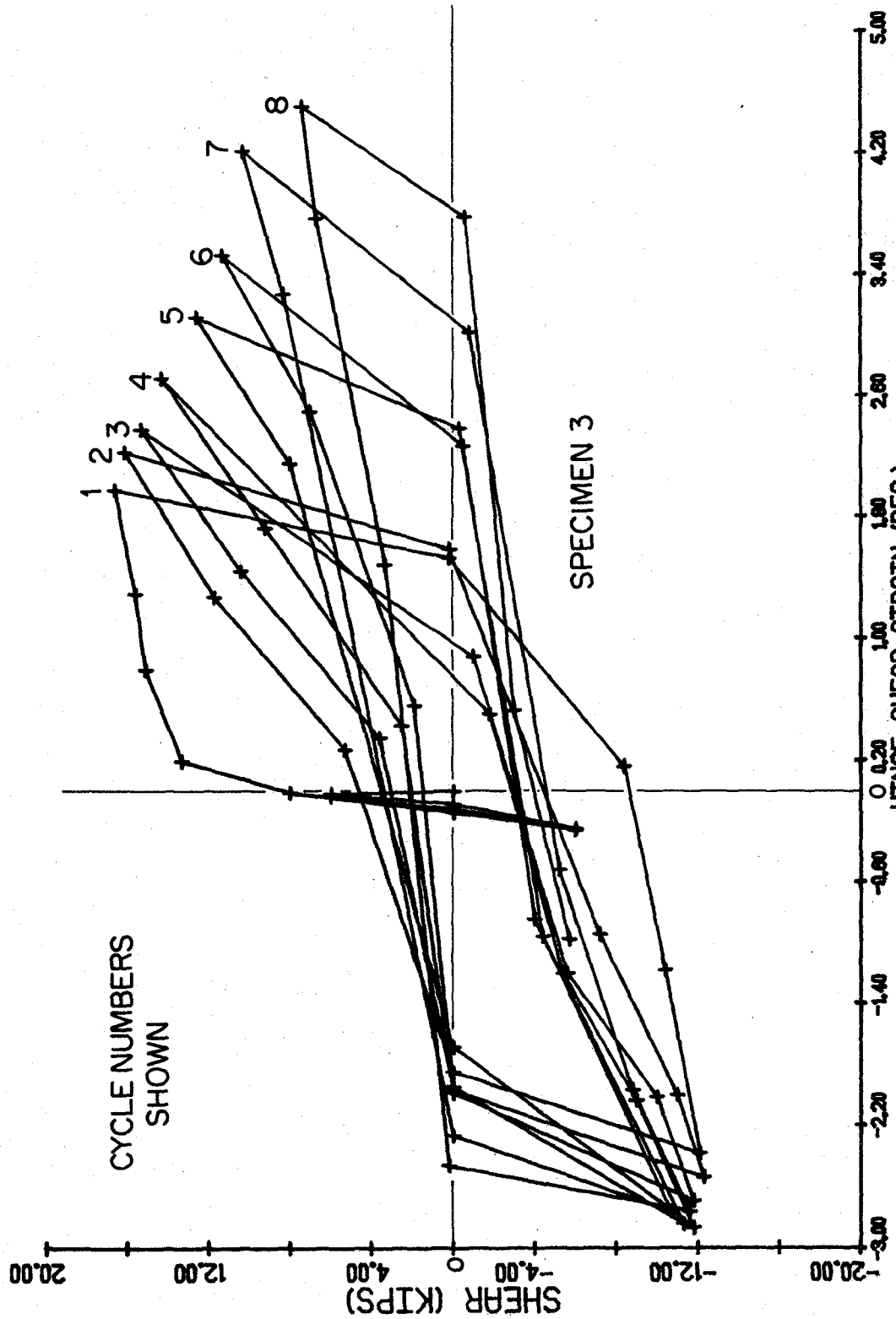

Fig. 5.12. Beam Shear Load vs. Hinge Shear Strain - Specimen 3.

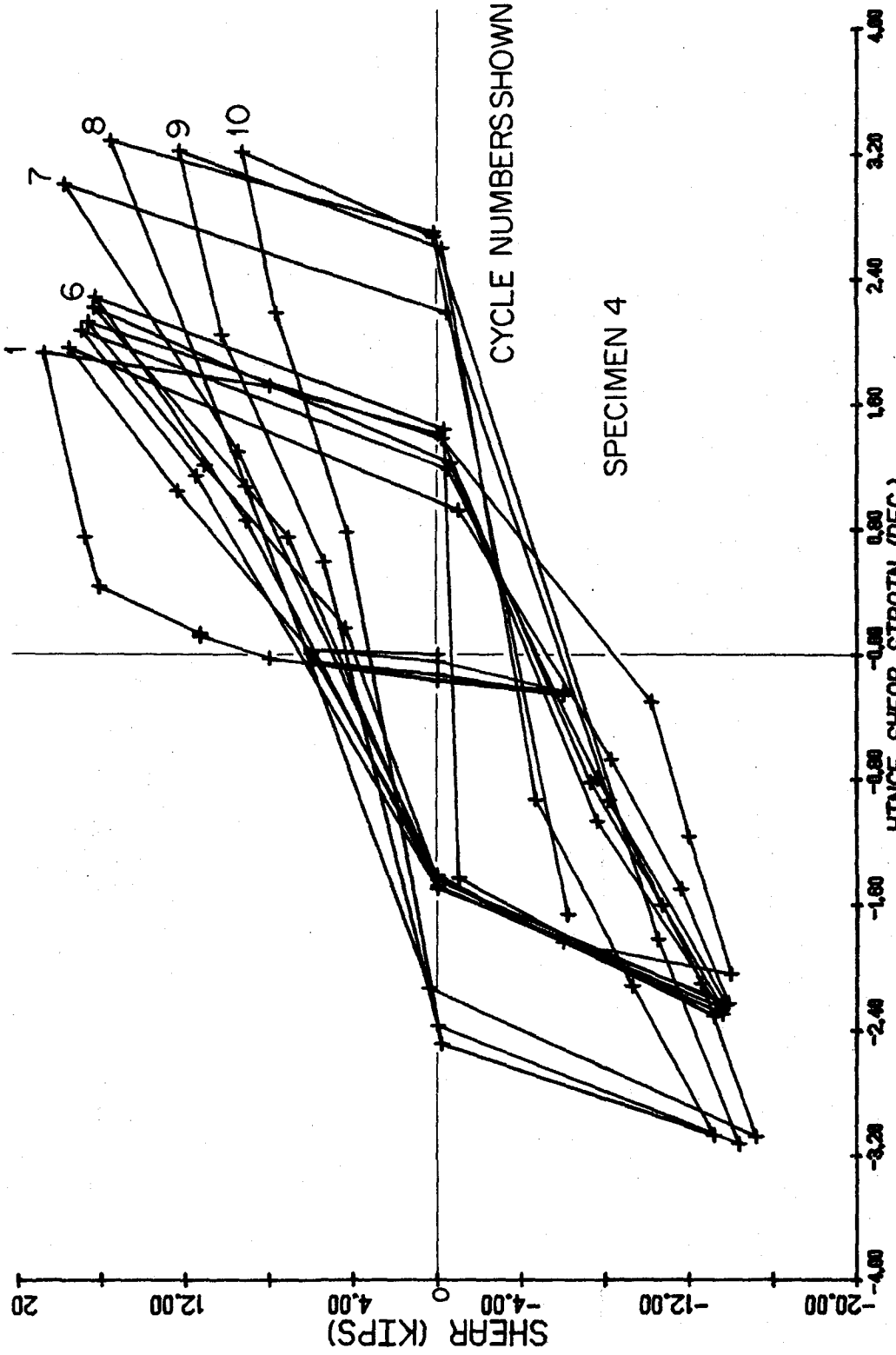

Fig. 5.13. Beam Shear Load vs. Hinge Shear Strain - Specimen 4.

APPENDICES

APPENDIX A

DETAILS OF SHEAR REINFORCEMENT

Shear reinforcement was designed as discussed in Appendix C. All web reinforcement in beams and columns consisted of closed, one-piece ties as required by ACI 318-71 (1) for structures located in zones of frequent seismic activety. Intermediate longitudinal beam shear reinforcement was anchored in the beam-column joint by standard 90 degree hooks with twelve-bar-diameter extensions. This reinforcement extended into the beam a distance equal to twice the beam effective depth plus an extension of twelve bar diameters. Figure A.1 illustrates the shear reinforcement placement in the specimens, with exact bar size and spacing given in Table A.1.

TABLE A.1

SHEAR REINFORCEMENT DETAILS

Specimen Number	Number, size, and spacing of web reinforcement at location shown in Fig. A.1					Bar Ext. (f)
	(a)	(b)	(c)	(d)	(e)	
1	9-#2@2"	9-#2@4"	3-#3@1.75"*	5-#3@2.25"*	7-#2@2.25"	
2	9-#2@2"+	9-#2@4"	3-#3@1.75"*	5-#3@2.25"*	7-#2@2.25"	20.5"
3	9-#2@2.5"	6-#2@5"	5-#3@1.5"*	5-#3@2.25"*	7-#2@2.25"	
4	9-#2@2.5"+	6-#2@5"	5-#3@1.5"*	5-#3@2.25"*	7-#2@2.25"	25"
5	9-#2@2"	9-#2@4"	3-#3@1.75"*	5-#3@2.25"*	7-#2@2.25"	
6	9-#2@2"+	9-#2@3"	3-#3@1.75"*	5-#3@2.25"*	7-#2@2.25"	20.5"
7	9-#3@2.5"*	6-#2@5"	5-#3@1.5"*	5-#3@2.25"*	7-#2@2.25"	
8	9-#2@2.5"	6-#2@5"	5-#3@1.5"*	5-#3@2.25"*	7-#2@2.25"	25"
9	9-#3@3"	7-#3@6"	4-#4@2"*	9-#3@4"	2-#3@8"	
10	9-#3@3"+	7-#3@6"	4-#4@2"*	9-#3@4"	2-#3@8"	30"
11	9-#3@3"	7-#3@5.25"	4-#4@2"*	9-#3@4"	2-#3@8"	
12	9-#3@3"+	8-#3@4.5"	4-#4@2"*	9-#3@4"	2-#3@8"	30"

*Grade 60 Reinforcement

+Also includes #2 intermediate ties around supplementary longitudinal reinforcement at same spacing.

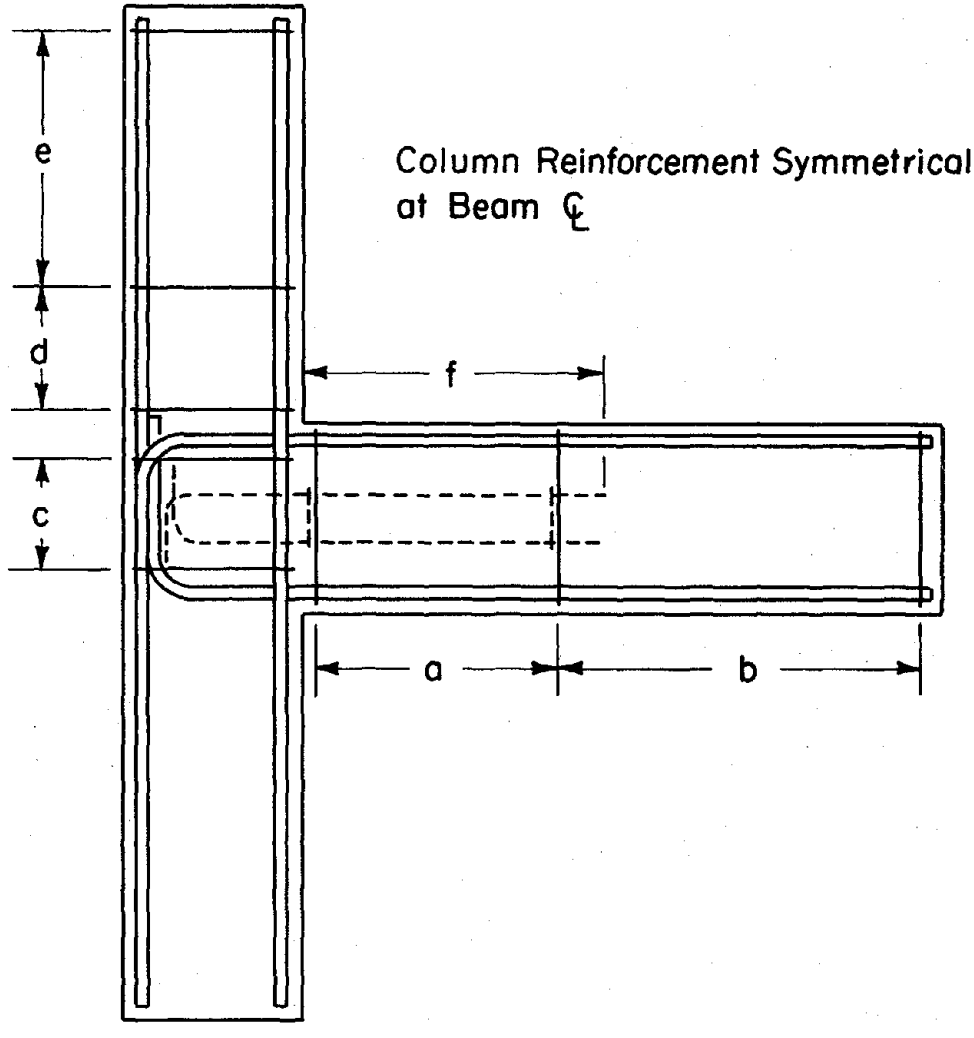

Fig. A.1. Shear Reinforcement Details.

APPENDIX B

SPECIMEN FABRICATION AND EXPERIMENTAL SETUP

B.1 Specimen Fabrication

All test specimens were constructed in G. G. Brown Laboratory by student research assistants and laboratory technicians. Fabrication sequence was the same for all specimens regardless of size.

Reinforcing steel cages were assembled first. One-piece closed ties were used throughout the specimen and served to position main longitudinal reinforcement in both the column and beam portions of the specimen. Ties for Group I specimens were bent by a commercial fabricator while ties for Group II specimens were bent in the laboratory using a Hossfeld #2 reinforcing bar bender. In either case, bending technique and dimensions of the finished ties conformed to applicable specifications of Chapter 7 of the ACI Building Code.

Column reinforcement was identical for all specimens of a given size. Fabrication of column cages served as the basis of construction for the remainder of the total cage. Beam main reinforcement was mated to the completed column cage and installation of beam ties completed reinforcement fabrication. A completed steel cage is shown in Fig. B.1. Eighteen gauge annealed wire was used to fasten reinforcement components together.

Specimens were cast in a horizontal position in

reuseable wooden forms. Four forms were constructed for each size specimen to allow casting of four specimens simultaneously. Forms were constructed of 3/4 in. exterior grade plywood which was reinforced with 1-1/2 in. square fir wales and waterproofed with orange shellac. Form sections were joined with 1/4 in. machine bolts. Completed forms were caulked at all seams with oil base clay and coated with viscous oil to ease form removal from finished specimens.

Steel cages were placed in the forms and supported with small concrete cubes. This insured proper concrete cover and held steel in position during casting. The beam-column joint region of an assembled form with steel cage in place is shown in Fig. B.2.

Concrete was mixed by the Ann Arbor Construction Company according to the mix design specified in Appendix D. The concrete was transported to the laboratory in a mixer truck and water was added to the mix at the casting site to obtain a slump of approximately 4 inches.

Concrete was placed in the forms and consolidated with a hand held electric vibrator. Excess concrete was struck off with wooden screeds and smoothed with a metal float. After the concrete had attained its initial set, it was covered with wet burlap and plastic sheeting to retain moisture. Specimens were maintained in a wet condition for 7 days after casting and then their cover-

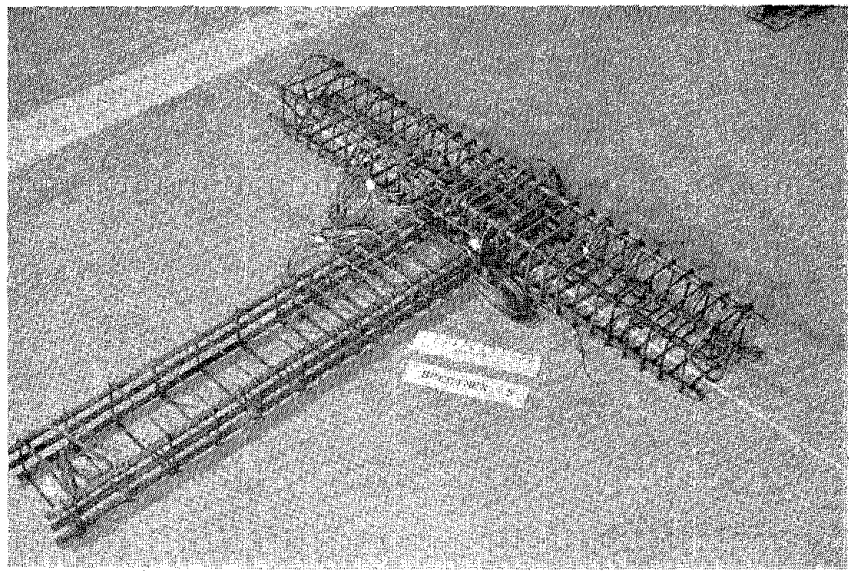

Fig. B.1. Completed Reinforcement Cage.

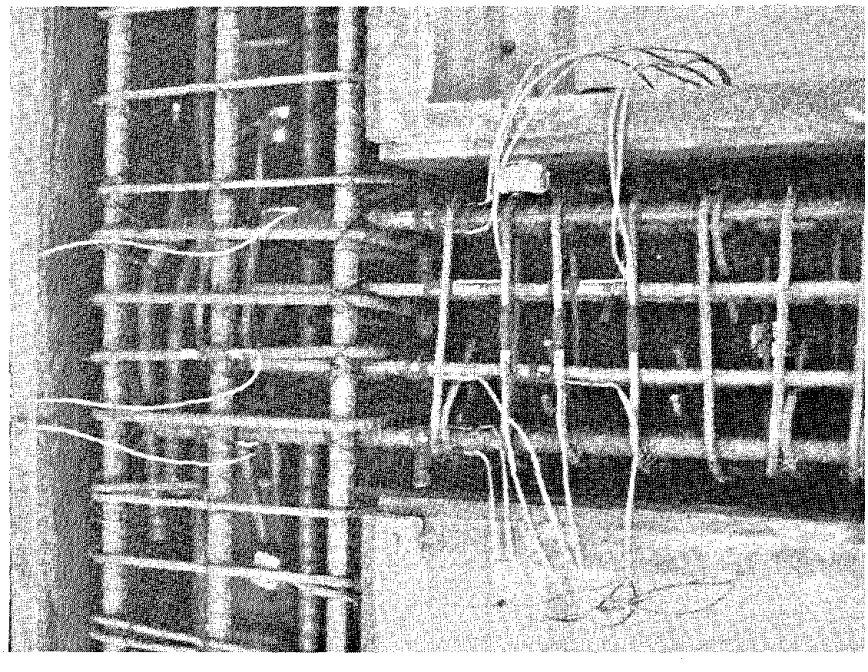

Fig. B.2. Beam-Column Region of Assembled Form with Reinforcement in Place.

TABLE B.1

CASTING AND TESTING TIMETABLE

Specimen Number	Date Cast	Date Tested
1	25 Nov 1975	13 Feb 1976
2	25 Nov 1975	24 Mar 1976
3	25 Nov 1975	19 Apr 1976
4	25 Nov 1975	6 May 1976
5	8 Dec 1976	3 Mar 1977
6	8 Dec 1976	21 Feb 1977
7	8 Dec 1976	12 Jan 1977
8	8 Dec 1976	10 Feb 1977
9	5 May 1977	28 Jul 1977
10	5 May 1977	3 Aug 1977
11	5 May 1977	17 Aug 1977
12	5 May 1977	23 Aug 1977

ing was removed, allowing specimens to cure uncovered until they were tested. A schedule of casting and testing dates is shown in Table B.1.

Standard 4 x 8 in. concrete test cylinders were cast at the same time each series of four specimens was cast. Four cylinders were cast for testing after 28 days and three cylinders were cast to be broken in conjunction with the test of each specimen. The four cylinders to be tested at 28 days were placed in a 100% humidity curing room while the remainder of the cylinders were cured in a manner identical to that used for the test specimens. Details of cylinder casting, testing, and concrete strength are shown in Appendix D.

When dry, all specimens were painted with flat white paint to aid in crack detection during testing. An oil base paint was used for specimens in Group I and latex paint was used for specimens in Group II. Flat black enamel was used on the upper surface of each specimen to show location of reinforcement.

B.2 Specimen Loading

Specimens 1 through 8 were tested in a horizontal position while Specimens 9 through 12 were tested with the beam portion of the specimen in a vertical position. In this and following appendices Specimens 1 through 8 will be referred to as Group I and Specimens 9 through 12

will be referred to as Group II. Respective test setups are shown in Figs. 2.2 and 2.3. Loading procedure was uniform for both test positions.

Prior to the application of any loads, the column portion of the specimen was firmly clamped into the test frame with roller bearings held by threaded rods. These rods were pretensioned to a stress near their yield stress to prevent any motion of the specimen relative to its supports during loading. Axial load was applied to the secured specimen with Templeton-Kenly R506SB 100 kip capacity hydraulic jacks. A Templeton-Kenly manual pump was used to drive the jacks. One jack was used to apply a 40 kip axial load for specimens in Group I. Specimens in Group II required two jacks in parallel to provide a 100 kip axial load. A Templeton-Kenly #7097 inline pressure gauge was used to monitor jack loads.

Shear was applied to the beam portion of the specimen by Gilmore solenoid-controlled hydraulic rams. A 20 kip capacity ram was used for Group I specimens while a 50 kip capacity ram was required for the larger Group II specimens. Both rams were secured to the respective specimens through essentially moment-free connections. Displacement of ram ends was manually controlled through a Gilmore console which included a Gilmore 431 Servo Amplifier, 416D Control Module, 416A Position

Signal Amplifier, and 416B Load Signal Amplifier to control the 20 kip actuator and a Gilmore 660 Servo Controller to govern the 50 kip ram. These control amplifiers also provided outlets to monitor a load cell and position transducer for each ram.

B.3 Data Acquisition

Data was acquired during testing from four major sources: (1) a load cell and position transducer attached to the loading ram, (2) LVDT's positioned over the beam hinging region, (3) electric resistance strain gages attached to longitudinal and shear reinforcement and (4) dial gages positioned to show overall specimen deformation.

Load vs. Displacement

A Honeywell 530 X-Y plotter was used throughout testing to monitor and record load (vertical axis) being applied by the beam loading ram and displacement (horizontal axis) of the loading ram tip. Signals to drive the plotter were provided by the Gilmore actuator control console discussed in section B.2, which served as the power supply and main signal conditioning unit for the load cell and displacement transducer of the loading ram.

LVDTs

Linear variable displacement transducers (LVDTs) were used to monitor the shearing and flexural deformations of the beam in the plastic hinging region. This region was assumed to extend over a distance equal to the beam overall depth from the face of the column. The location of these LVDTs is shown in Fig. 2.5. A listing of LVDT manufacturer and model number is shown in Table B.2.

Brackets to hold the LVDTs in position were fabricated from 1 x 1 x 1/8 in. angle stock. Four hex-head bolts held each bracket fixed to the specimen by friction. The ends of each LVDT assembly were held in bearings to insure accurate measurement of displacements.

Alternating current LVDTs were used for Group I specimens. A Sanborn 211-A preamplifier served as the power supply and initial signal conditioner for these transducers. Final output voltage was measured with a Hewlett-Packard digital voltmeter and manually recorded. Direct current LVDTs were used for all specimens in Group II. A Lambda LOD-Z-152 power supply was used to supply 15 VDC input power. Output voltage from these transducers was fed through a Visig 211 Signal Conditioning Module to the Vidar voltmeter. It was then processed by teletype and paper tape in the same way strain gage data was recorded.

TABLE B.2

LVDT CHARACTERISTICS AND MANUFACTURER

LVDT Number	Specimen Number	Manufacturer and Model Number
1	1-8	HP Sanborn 585-DT-250
2	1-8	Schaevitz 300 HR
3	1-8	HP Sanborn 585-DT-500
4	1-8	Schaevitz 500 HR
1-4	9-12	Schaevitz 1000 DC-D

Strain Gages

Electrical resistance strain gages were bonded to reinforcement at various points. The position of these gages in the specimen is shown in Fig. 2.6. A digital monitoring system manufactured by Accurex Autodat Corporation was used to measure strains. This system consisted of Visig 611 Signal Conditioning Modules, a Vidar 606-03 Master Scanner, a Vidar 502B-01 Integrating Digital Voltmeter and a Vidar 5404 D-DAS System Controller. A 3320-5JE Teletype was used to punch individual strain gage readings onto paper tape. The Vidar console and Teletype are shown in position for operation in Fig. B.3. The paper tape punching was compatible with the computer system paper tape reader at the University of Michigan Computer Center, allowing strain readings to be copied directly into a computer disk file after test completion.

Sufficient input channels were not available to accept all strain gage signals from Specimens 2 and 4. For these specimens, four gages were monitored using a BLH Model 20 Strain Indicator and intermediate switchbox. The resultant observed strain readings were manually recorded.

Dial Gages

Two micrometer dial gages were used to determine

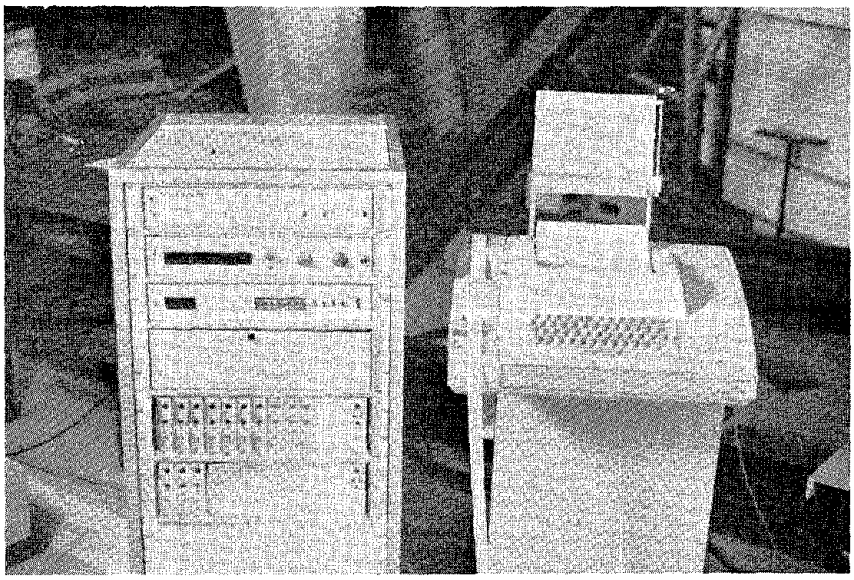

Fig. B.3. Vidar Console and Teletype in Position for Operation.

rigid body distortion of the beam-column joint relative to the testing frame for all specimens during testing. Three additional dial gages were used during testing of Specimen 3 to measure overall distortion of the small loading frame used for all Group I specimens. The location of gages is shown in Fig. 2.7. The large loading frame used in conjunction with Group II specimens was considered rigid and no auxiliary dial gages were used to measure its distortion.

APPENDIX C

SPECIMEN DESIGN

C.1 General

Specimens were designed with three objectives in mind: (1) to insure that all inelastic flexural deformations took place in the beam section of the specimen, (2) to insure that no shear failures occurred in the column or in the beam outside the zone of inelastic flexure, and (3) to insure that the design ultimate moment of the beam section could be provided by available testing equipment. In addition, some dimensions of Group I specimens were dictated by the size of the testing frame used to hold these specimens.

The American Concrete Institute Building Code Requirements for Reinforced Concrete (ACI 318-71) (1) was used as a guide for reinforcement details. In this appendix only, when a governing value of stress or dimension is referenced, the applicable paragraph of the Code will be given in parentheses. A similar procedure will be used to reference applicable sections of the ASCE-ACI Committee 352 recommendations (35) regarding details of beam-column joint shear reinforcement, with the exception that the section number referenced will be preceded by "R". Unless otherwise specified, the definitions of terms used in equations in this appendix are the same as those used in the applicable

provisions of the ACI code and Committee 352 recommendations.

Specimens were designed for ultimate moments which would induce, using shear spans within a range dictated by test frame dimensions, maximum total shear stresses of from 2 $\sqrt{f'_c}$ to greater than 6 $\sqrt{f'_c}$. For this discussion of design, Specimen 3 will be used as an example to illustrate the typical calculations which governed the design of reinforcement details.

C.2 Column Analysis

An interaction diagram was calculated for each column size employed, assuming f_y = 78 ksi (an average value obtained from previous tests of column longitudinal reinforcement) and f'_c = 4000 psi, the concrete design strength. By assuming various neutral axis locations, a maximum concrete strain of 0.003, and a Whitney stress block (10.2.7) approximation of concrete compressive force, various points on the column axial load vs. flexural moment capacity curve were calculated and a smooth curve was drawn to connect these points. The interaction diagrams for the column sections used in Group I and Group II specimens are shown in Fig. C.1.

For convenience, a test column axial load less than 40 percent of the balanced load was chosen to allow design of the column as a flexural member (A.6.3). The choice of

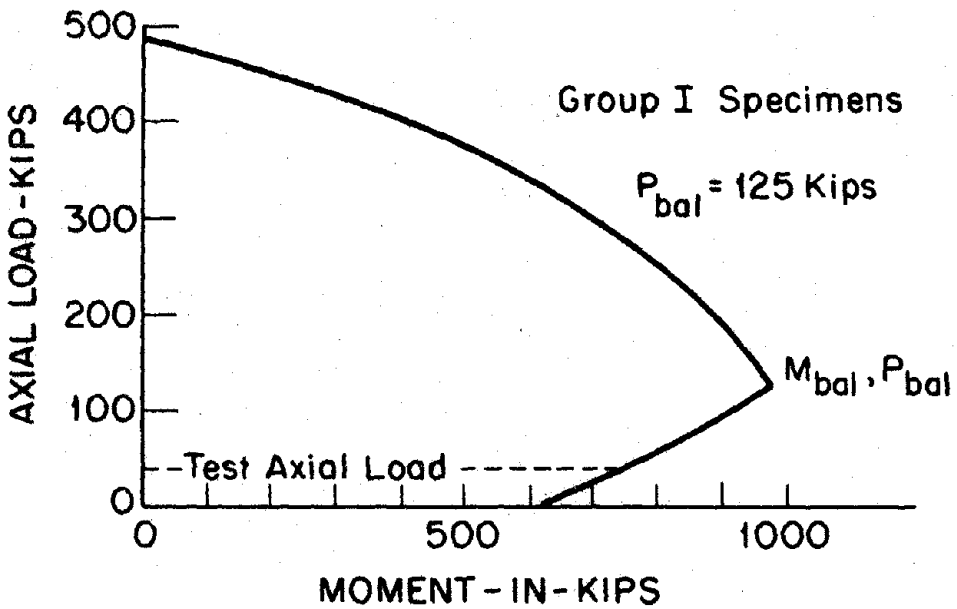

Fig. C.1(a). Interaction Diagram for Group I Specimens.

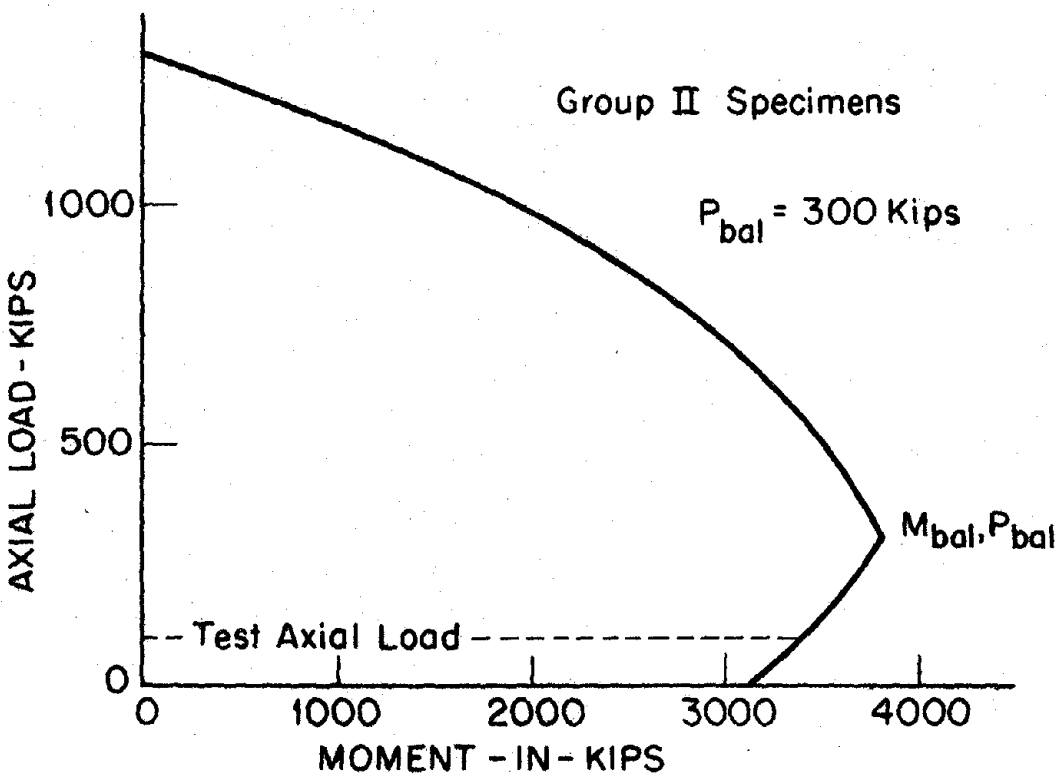

Fig. C.1(b). Interaction Diagram for Group II Specimens.

a 40 kip axial load for Group I columns and a 100 kip axial load for Group II columns satisfied this criterion, as well as providing a restraining force twice as large as the maximum capacity of the loading ram used to test the respective specimens to insure minimum column motion during testing. At these chosen test axial loads, in order to satisfy the requirement that the sum of the moment strength of the columns be greater than the moment strength of the beam (A.6.2) it was necessary that beam design moment capacity be less than 1500 in-kips for Group I and less than 6800 in-kips for Group II specimens.

C.3 Design of Column Shear Reinforcement

Column shear reinforcement was designed for shear which would have resulted from application of maximum available ram force. The centerlines of the specimen segments were used for static analysis of this condition. Because the maximum anticipated beam shear span was 47 in. (41.5 in. to the face of the column), the maximum possible column shear force was

$$V_{col} = 20 \left(\frac{47}{60}\right) = 15.7 \text{ kips}, \qquad \text{(C.1)}$$

which translates to a maximum column shear stress of:

$$v_u = \frac{V_{col}}{\phi\ b\ d} = \frac{15{,}700}{(0.85)(8)(9.64)} = 239 \text{ psi} \qquad \text{(C.2)}$$

where

v_u = gross shear stress in the column, psi.

b = overall column width, in.

d = effective depth of column, in.

ϕ = capacity reduction factor = 0.85 for shear.

The shear stress which the concrete can carry is calculated as (11.4.3):

$$v_c = 2\left(1 + 0.0005 \frac{N_u}{A_g}\right) \sqrt{f'_c} \qquad (C.3)$$

$$= 2\left(1 + 0.0005 \frac{40{,}000}{88}\right) \sqrt{4000}$$

$$= 155 \text{ psi.}$$

where

v_c = shear stress carried by concrete in the column, psi.

N_u = gross column axial load, lbs.

A_g = gross cross sectional area of column, sq. in.

Assuming the use of No. 2 grade 40 stirrups, the required spacing is computed as (11.6.1):

$$s = \frac{A_v f_y}{(v_u - v_c)b} = \frac{0.10(40{,}000)}{(239 - 155)(8)} = 6 \text{ in.} \qquad (C.4)$$

where

A_v = area of web reinforcement within a distance s along the beam, sq. in.

f_y = specified yield stress of web reinforcement, psi.

s = spacing at web reinforcement bars, in.

Spacing is also governed by code provisions which require

maximum spacing to be limited to no more than one-quarter of the member effective depth (A.5.9) near member ends. In addition, other provisions suggest that beam-column joint reinforcement be carried into the column adjacent to the joint for some distance (R 4.2.2.2). Because column shear was not a controlling factor, two compromises were reached for column shear reinforcement. In the case of Group I specimens, bars of the same size and grade as those that were used for beam-column joint reinforcement were used at a spacing of d/4 for a distance equal to column depth from the beam-column joint. Smaller ties (No. 2) were placed in the remainder of the column at the same d/4 spacing. For Group II specimens, No. 3 ties were spaced at d/4 for a distance 2d from the beam-column joint and at d/2 elsewhere in the column. There was no significant shear cracking in the columns of either Group I or Group II specimens.

C.4 Design of Beam Reinforcement

Beam longitudinal reinforcement was chosen so that maximum design moment in any beam would not exceed the capacity of the loading ram. This limiting value was (41.5)(20) = 830 in-kips for Group I specimens and 60(50) = 3000 in-kips for Group II specimens.

Beam shear reinforcement was chosen to resist the shear required in each specimen to produce the design ultimate beam moment. The allowable shear stress for concrete

was taken as 2 $\sqrt{f'_c}$, 126 psi for the design concrete compressive strength of 4000 psi (11.4.1). Using Specimen 3 (design ultimate moment of 703 in-kips) as an example, beam ultimate shear stress was calculated as (11.2.1):

$$v_u = \frac{V_u}{\phi\ b\ d} = \frac{(703/41.5)}{(0.85)(8)(10.1)} = 0.247 \text{ ksi} \qquad (C.5)$$

Now, the steel requirement for strength is calculated as (11.6.1):

$$A_v = \frac{(v_u - v_c)b\ s}{f_y} \qquad (C.6)$$

Assuming a No. 2, grade 40 stirrup and solving for required spacing:

$$s = \frac{A_v\ f_y}{(v_u - v_c)b} = \frac{(0.10)(40)}{(0.247 - 0.126)(8)} = 4.13 \text{ in}$$

Other provisions (A.5.9) of the design code required a tie spacing in the beam no greater than d/4 within a distance of 4d from the column face, so spacing, rather than strength, was the controlling factor for web reinforcement placement in the beam hinging zone in this and all other specimens. One compromise was made, however, in determining how far into the beam the ties would be continued at the spacing at d/4. Because the Uniform Building Code (21) and the SEAOC Code (36) required this spacing for a distance of 2d from the face of the column, it was decided that ties at a d/4 spacing would only be continued a distance of 2d into the beam to allow observation of damage

which took place as a result of abberation from the more conservative ACI code. Elsewhere in the beam, ties were spaced to satisfy strength requirements as well as the maximum spacing requirement of d/2 (A.5.9).

C.5 Beam-Column Joint Shear Reinforcement

Recommendations of ASCE-ACI committee 352 (35) were used as a design standard of proportion beam-column joint shear reinforcement. The forces assumed to be acting at the joint are shown in Fig. 4.7. Joint shear stress carried by the concrete was calculated as (R 4.2.3.2):

$$v_c = 3.5\ \beta\ \gamma\ \sqrt{f'_c(1 + 0.002\ N_u/A_g)} \qquad (C.7)$$

where

β = joint type correction factor = 1.0 for Type 2 joint

γ = joint classification correction factor = 1.0 for joints considered here.

For Specimen 3, this becomes

$$v_c = 3.5\ (1.0)(1.0)\ \sqrt{4000(1 + 0.002\ \frac{40,000}{88})} = 306 \text{ psi.}$$

Using a value of f_s = 60,000 psi for the ultimate stress in top longitudinal beam reinforcement in conjunction with the static column shear of 11.7 kips calculated as the reaction force present when this steel stress is used to calculate ultimate beam moment, the joint shear stress can be calculated as (R 4.2.3.1):

$$v_j = \frac{V_u}{\phi A_{cv}} = \frac{T_s - V_{col}}{\phi A_{cv}} \qquad (C.8)$$

$$= \frac{79.2 - 11.7}{(0.85)(7)(9.64)} = 1.18 \text{ ksi}$$

where

v_j = nominal joint shear stress

A_{cv} = effective area of beam-column joint which is considered to resist shear force

And that spacing of stirrups was calculated as before:

$$s = \frac{A_v f_y}{(v_u - v_c) b_c}$$

Using a No. 3 grade 60 stirrup, spacing becomes:

$$s = \frac{(0.22)60}{(1.18 - 0.31)(7)} = 2.2 \text{ in.}$$

Because it is also essential that total shear force in the joint be resisted by the steel and concrete, an alternate method of computation based on total force was used to calculate the required number of joint stirrups. Here, using the allowable concrete stress and the effective joint area,

$$V_c = (0.31)(7)(9.64) = 20.9 \text{ kips}$$

and, for the total forces acting on the joint

$$V_u = \frac{T_s - V_{col}}{\phi} = \frac{79.2 - 11.7}{0.85} = 79.4 \text{ kips} \qquad (C.9)$$

where

T_s = the total design tensile force in beam tension reinforcement.

Now, the shear to be carried by the steel is

$$V_s = V_u - V_c = 79.4 - 20.9 = 58.5 \text{ kips} \qquad (C.10)$$

and the total number of ties in the joint will be calculated as

$$n = \frac{V_s}{A_v f_y} = \frac{58.5}{(0.22)(60)} = 4.4 \qquad (C.11)$$

Therefore, 5 ties must be used in the joint of this specimen.

This procedure was repeated for analysis of all odd-numbered specimens. For design and testing considerations, the same number of joint ties were used in specimens with intermediate longitudinal reinforcement as were used in the comparable specimen which did not contain such supplementary beam reinforcement.

C.6 Development of Reinforcement

All longitudinal reinforcement was anchored in the beam-column joint by 90 degree standard hooks (7.1). The tensile stress which the hooks were capable of developing was calculated as (R 4.2.5.2):

$$f_h = 700(1 - 0.3\, d_b)\ \psi\ \sqrt{f'_c} \qquad (C.12)$$

where

f_h = tensile stress developed by a standard hook, psi.

ψ = anchorage effectiveness coefficient = 1.0

d_b = nominal diameter of reinforcing bar, in.

For the No. 6 and No. 5 bars used as beam longitudinal reinforcement in Group I specimens, the hooks were allowed to carry the following stresses:

For No. 6 bar,

$$f_h = 700(1 - 0.3(0.75))\ (1.0)\sqrt{4000} = 34{,}300 \text{ psi}$$

For No. 5 bar,

$$f_h = 700\ (1 - 0.3(0.625))\ (1.0)\sqrt{4000} = 36{,}000 \text{ psi}$$

The required straight embedment length prior to the beginning of the bar hook was then calculated as (R 4.2.5.2):

$$l_s = 0.04\ A_b\ (\alpha\ f_y - f_h)/\psi\sqrt{f'_c} \qquad \text{(C.13)}$$

where

A_b = area of reinforcing bar, sq. in.

l_s = minimum straight lead embedment length from critical section to beginning of bar hook, in.

α = stress multiplication factor to account for strain hardening in steel strained past yield.

For the bars used in Group I specimens, this length was computed as:

For No. 6 bar,

$$l_s = 0.04(.44)\ (60{,}000 - 34{,}300)/\sqrt{4000} = 7.15 \text{ in.}$$

For No. 5 bar,

$$l_s = 0.04(.31)\ (60{,}000 - 36{,}000)/\sqrt{4000} = 4.71 \text{ in.}$$

Figure C.2 illustrates the details of reinforcement

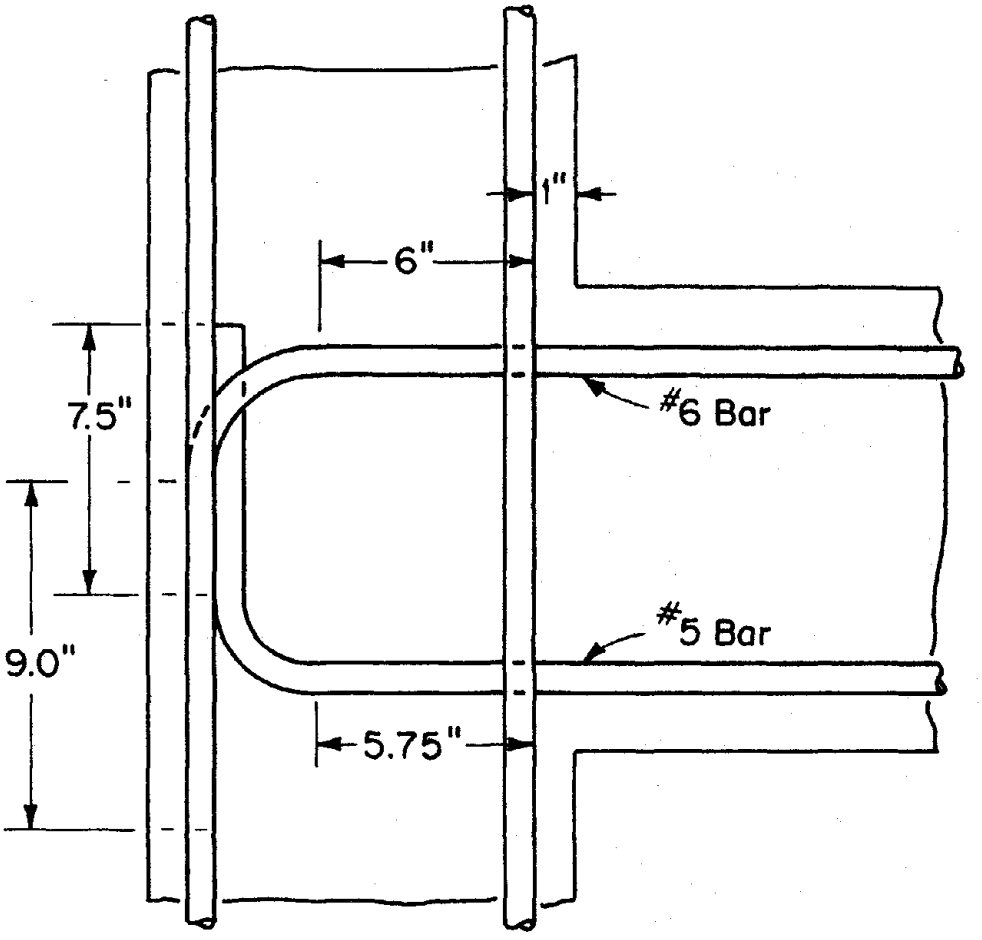

Fig. C.2. Details of Reinforcement Anchorage - Group I Specimens.

development which existed in Group I specimens. All ACI Code specifications were satisfied, although straight lead embedment requirements for the top (No. 6) bars did not meet the requirements of Committee 352 recommendations, which suggest measurement of straight lead embedment from the outside of column longitudinal reinforcement (as shown in Fig. C.2), rather than from the face of the column as specified by ACI 318-71.

Intermediate longitudinal reinforcement was also anchored in the joint case. Because these bars were always smaller than the main longitudinal reinforcing bars used in each beam, the required embedment was easily obtained.

APPENDIX D

MATERIAL PROPERTIES

D.1 Reinforcing Steel

Accurate records of reinforcing steel characteristics were considered essential for accurate modelling of member moment capacity. A representative sample of each beam reinforcing bar used in specimen fabrication was tested in uniaxial tension to determine gross yield and ultimate strength. Measured strengths for all samples tested are given in Table D.1. Additional representative samples of reinforcement were chosen for stress-strain analysis. For the latter case, a mechanical extensometer was attached to the bar with an initial 2" gage length and strain was monitored in conjunction with monotonically increasing load to determine the modulus of elasticity, yield strain, strain at onset of strain hardening, and modulus during strain hardening for all longitudinal reinforcement. Figure D.1 shows a typical reinforcing bar with the extensometer attached in preparation for testing. Results of all stress-strain tests are listed in Table D.2 and typical steel stress vs. strain curves for two sizes of reinforcing bars are shown in Figs. D.2 and D.3.

TABLE D.1

REINFORCEMENT YIELD AND ULTIMATE STRENGTH

Bar Designation	Bar Size	Specimen, Location	Strength, psi Yield	Ultimate
None	#2	6,2 Intermediate	48,200	72,400
None	#2	1,2 Beam Stirrup	42,600	71,000
None	#3	8,4 Intermediate	55,500	76,400
None	#3	1-4 Joint Tie	75,500	103,000
1	#5	3 Main Reinf.	52,600	84,200
2	"	3 " "	53,200	87,700
3	"	1 " "	52,900	85,800
4	"	4 " "	51,600	81,300
5	"	2,4 " "	49,400	76,100
6	"	2,4 " "	54,500	91,000
7	"	1,3 " "	47,700	77,400
11	#6	3 " "	48,000	79,300
12	"	1,2,3 " "	49,800	83,900
13	"	1,3 " "	49,100	81,800
14	"	4,2 " "	48,900	82,000
15	"	3,4 " "	49,100	82,000
22	#5	5-8 " "	53,200	83,900
23	"	5-8 " "	52,300	85,500
24	"	5-8 " "	53,600	88,100
25	"	5-8 " "	52,600	85,200
26	"	5-8 " "	52,900	81,600
28	"	5-8 " "	52,600	85,500
29	"	5-8 " "	52,900	85,800
30	"	5-8 " "	51,300	81,600
None	#6	5-8 Main Reinf.	52,700	85,500

TABLE D.1 (Cont'd)

Bar Designation	Bar Size	Specimen, Location	Strength, psi Yield	Ultimate
4-1	#4	10,12 Intermediate	59,500	88,000
4-2	"	10,12 Intermediate	58,000	86,500
4-3	"	10,12 Intermediate	57,000	85,000
None	"	9-12 Joint Ties	None	103,000
7-1	#7	9,11 Main Reinf.	51,000	92,800
7-2	"	10,12 " "	46,700	83,200
7-3	"	10,12 " "	50,000	86,800
7-4	"	9,11 " "	46,800	83,500
7-5	"	9,11 " "	48,000	83,500
7-6	"	9,11 " "	50,700	87,200
7-7	"	10,12 " "	50,700	92,800
7-8	#7	10,12 Main Reinf.	50,300	86,700
8-1	#8	10,12 Main Reinf.	59,500	103,800
8-2	"	10,12 " "	60,760	104,400
8-3	"	9,11 " "	59,600	102,500
8-4	"	10,12 " "	60,100	103,800
8-5	"	9,11 " "	60,100	103,800
8-6	"	10,12 " "	61,400	105,000
8-7	"	9,11 " "	60,100	104,400
8-8	#8	9,11 Main Reinf.	60,100	105,000
None	#9	9-12 Col. Reinf.	69,500	104,500
None	"	"	67,500	100,000
None	"	"	72,000	106,000
None	#9	9-12 Col. Reinf.	69,000	101,000

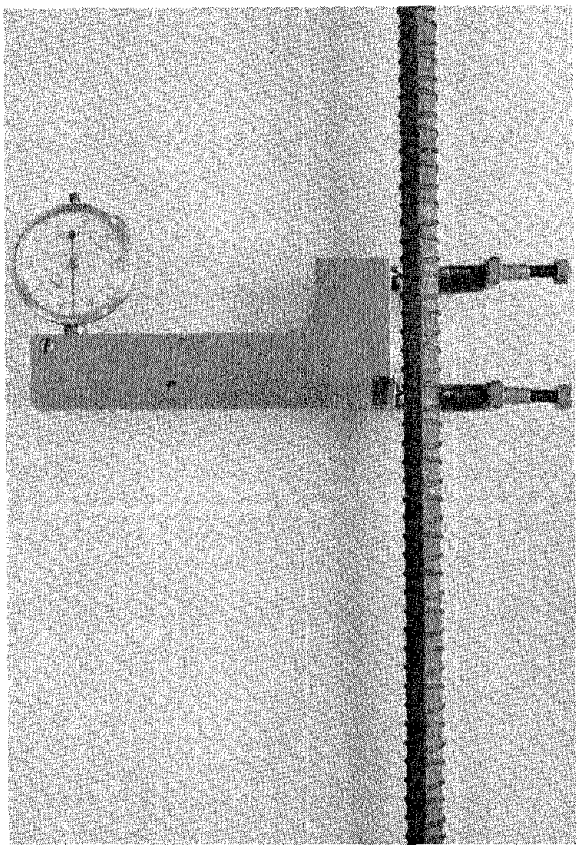

Fig. D.1. Extensometer Attached to Reinforcing Bar.

TABLE D.2

TABULATION OF REINFORCEMENT PROPERTIES

Bar Size	Specimen, Location	E_s	ε_y	E_{sh}	E_{sh}	ε_{max} (failure)	σ_{max} Failure (ksi)
#3	4,8-Intermediate 9-12-Beam Ties	29.2	1.85	14.2	0.91	Not Measured	75.4
#4	10,12 Intermediate	27.0	1.95	14.5	1.13	120	89.3
#4	9-12 BC Joint Tie	27.5	2.4	4.0	1.22	245	101
#5	1-8 Main Reinf.	26.2	2.0	12.2	0.94	175	84.2
#6	1-8 Main Reinf.	28.2	2.0	9.7	1.01	160	84.8
#7	9-12 Main Reinf.	27.8	1.8	9.3	1.09	160	87.1
#8	9-12 Main Reinf.	32	2.2	5.0	1.7	200	104

Moduli expressed in units of ksi x 10^3; strains expressed in units of in/in x 10^{-3}.

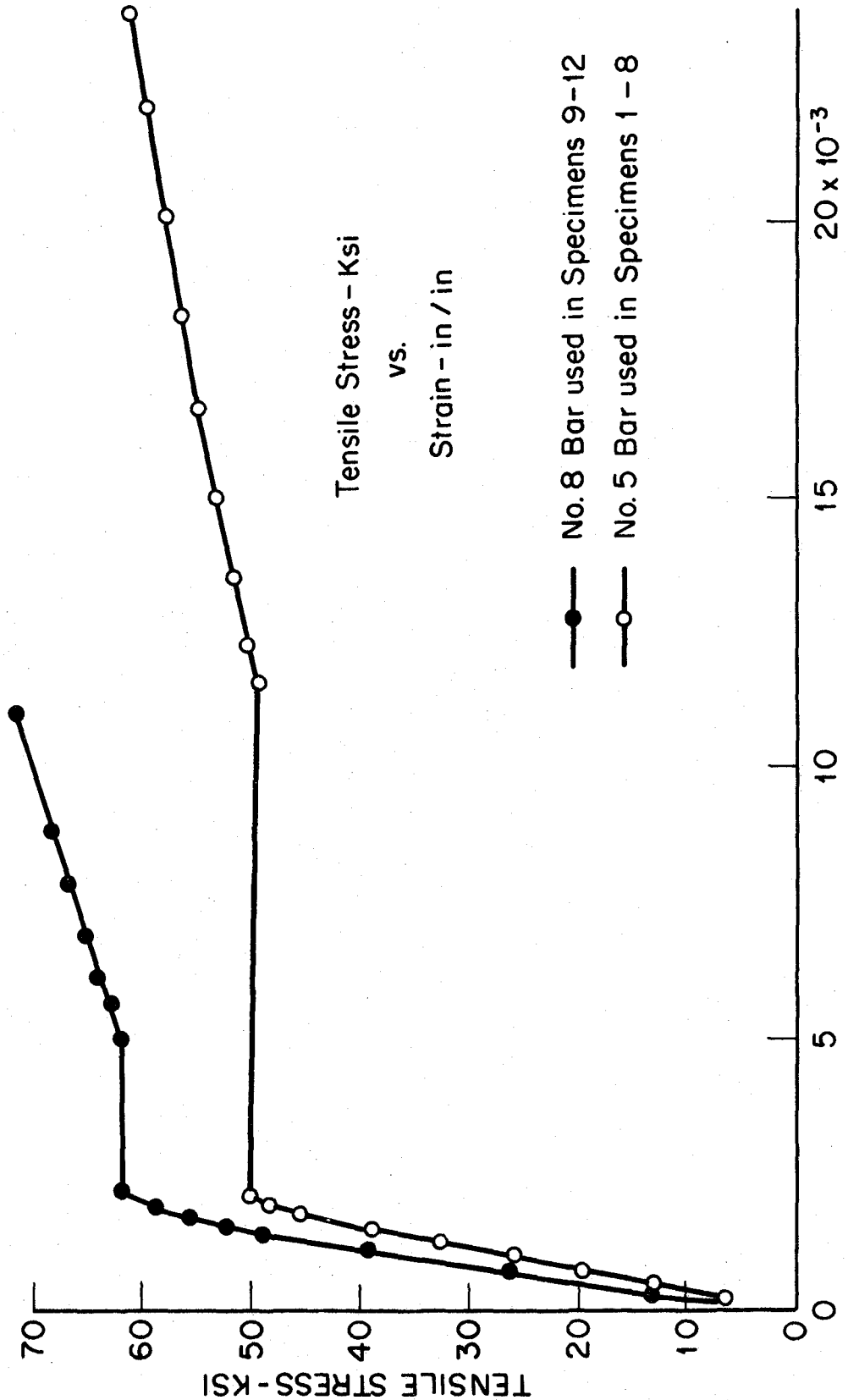

Fig. D.2. Stress vs. Strain Relationship for Reinforcement Used in Specimens Indicated.

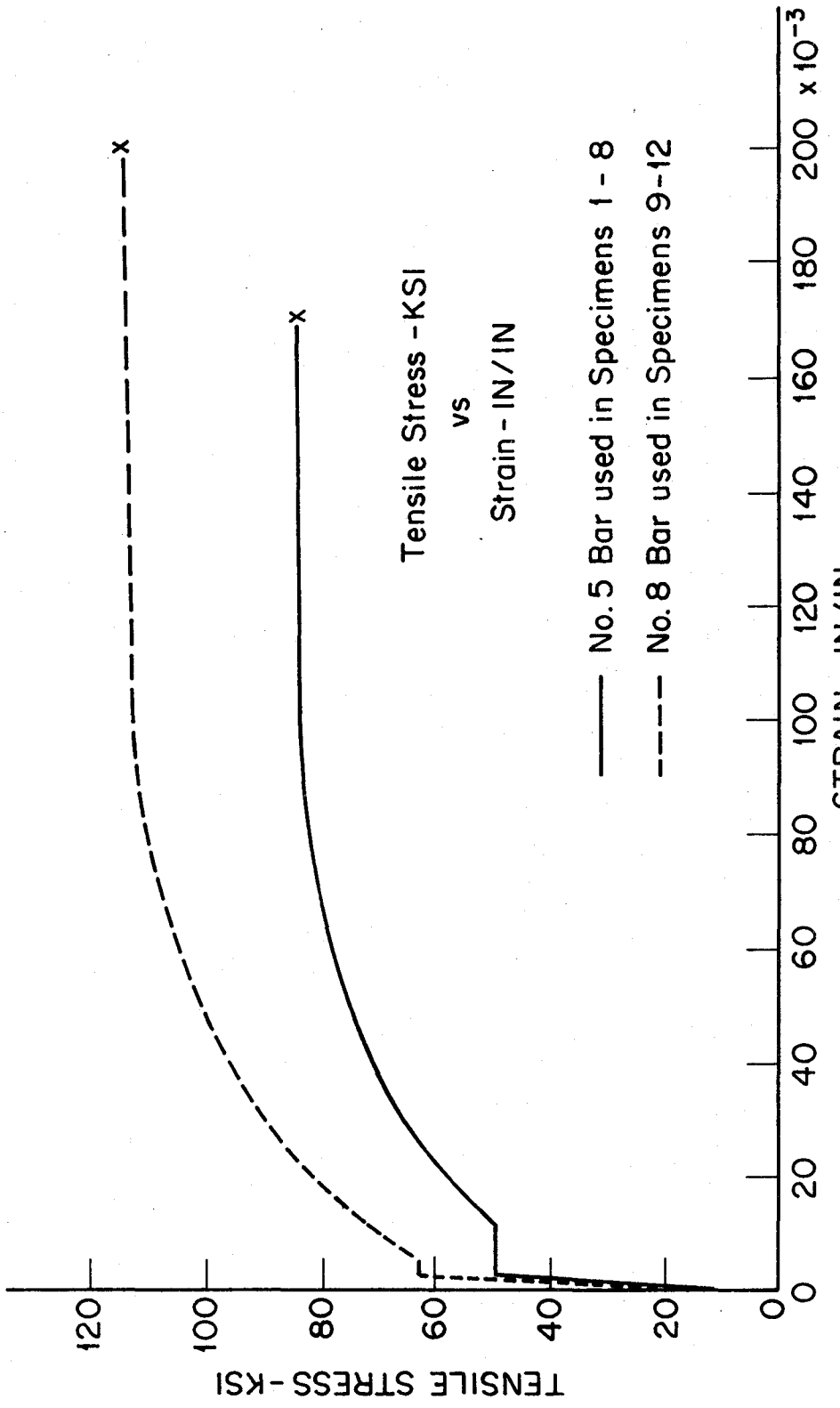

Fig. D.3. Stress vs. Strain Relationship for Reinforcement Used in Specimens Indicated.

D.2 Concrete

Concrete mix design was chosen to provide approximately 4000 psi maximum compressive strength at 28 days. Final mix design proportions, based on previous designs used by others for similar specimens and on two trial mixes, were as follows for one cubic yard of concrete:

Coarse aggregate (3/8" pea pebble)	1225 lb.
Fine aggregate	1785 lb.
Cement (Type I Portland)	493 lb.
Water	252 lb.

Additional water was added to produce a slump of approximately 4" at the time of casting. Three standard 4" x 8" cylinders were cast and cured simultaneously with each specimen and were subjected to uniaxial compressive loading on the same day the beam-column subassembly was tested. An extensometer was attached to each test cylinder to determine the initial modulus of elasticity of the concrete and the strain at maximum stress. Strains were recorded at uniform stress levels for all cylinders tested in conjunction with a given specimen and strains were averaged at each stress level to obtain the stress-strain curve for concrete in each specimen. A typical concrete stress vs. strain curve is shown in Fig. D.4.

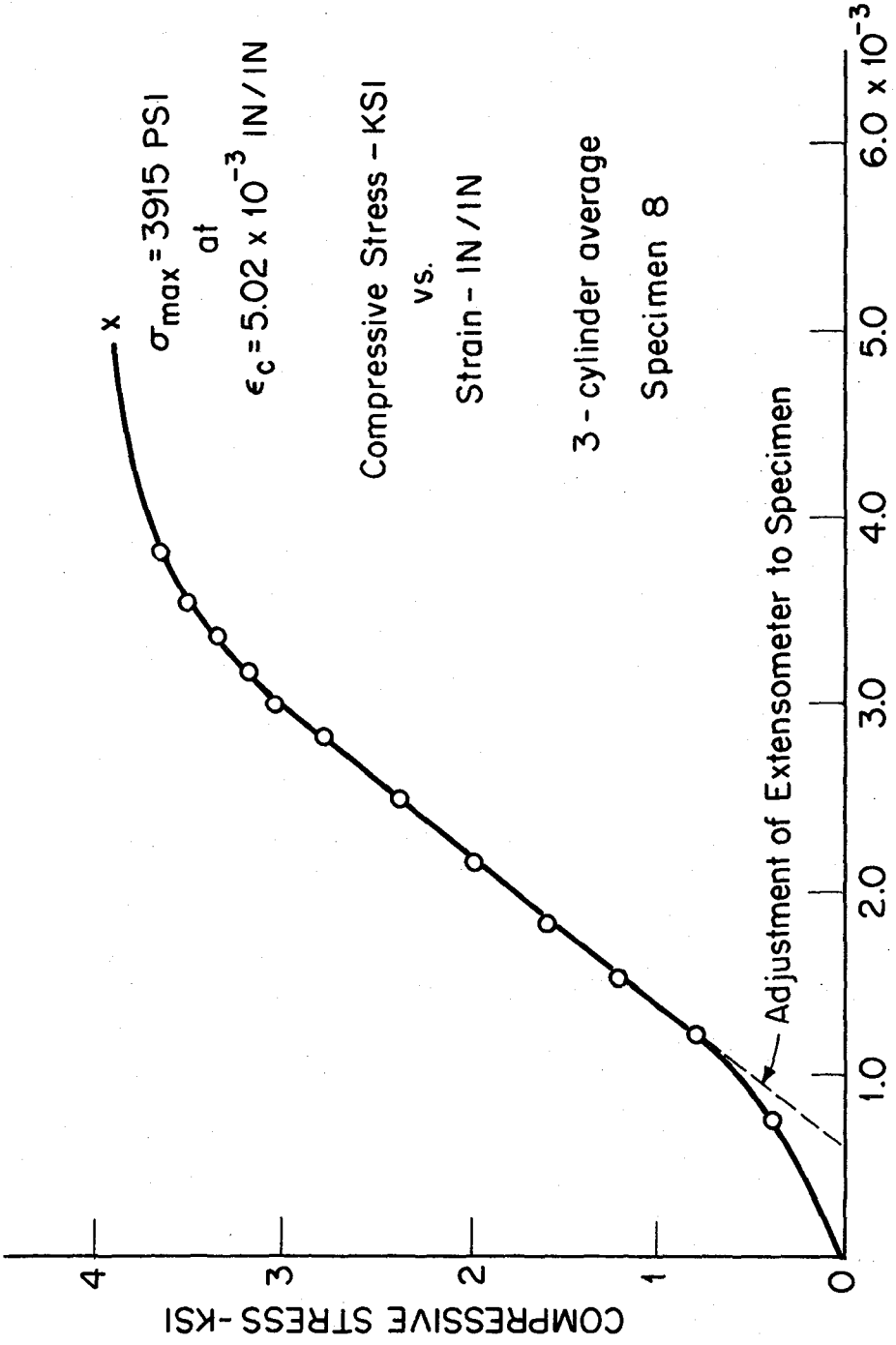

Fig. D.4. Typical Stress vs. Strain Curve for Cylinders Tested in Conjunction with Structural Tests.

TABLE D.3

RESULTS OF CONCRETE CYLINDER TESTS

Specimen Number	Cylinder Number	Strain at Maximum Stress in/in x 10^{-3}	Maximum Stress, psi
1	1	3.67	4960
	2	2.75	4850
	3	3.33	5050
2	1	3.25	5120
	2	3.29	5100
	3	3.29	4930
3	1	3.67	4970
	2	3.33	4890
	3	3.75	4970
4	1	Strains	4800
	2	not taken	5010
	3		5050
5	1	5.67	3400 *
	2	3.25	3960 *
6	1	4.42	3980
	2	3.63	4140
	3	3.85	4120

*test cylinders badly cracked: results of test cylinders for Specimen 6 used in all critical calculations for this specimen.

TABLE D.3 (Cont'd)

RESULTS OF CONCRETE CYLINDER TESTS

Specimen Number	Cylinder Number	Strain in Maximum Stress in/in x 10^{-3}	Maximum Stress, psi
7	1	4.79	3790
	2	4.92	3640
	3	4.28	4080
8	1	5.80	4010
	2	4.48	3790
	3	4.79	3950
9	1	4.13	4680
	2	2.75	5370
	3	2.58	5330
10	1	Strains not taken	5330
	2		5180
	3		5120
11	1	Strains not taken	5050
	2	3.50	4420
	3	2.50	4710
12	1	2.69	4660
	2	1.25	5000
	3	1.95	4770
	4	Strains not taken	4610

APPENDIX E

COMPILATION OF ENERGY DISSIPATION

Beam load and load point displacement were continuously monitored during loading of each specimen as discussed in Appendix B. A planimeter was used to measure the area within the load vs. displacement curve produced by the X-Y plotter for each load cycle and this area was converted to energy dissipated during each cycle according to the scale used for load and displacement recording. Each load cycle was considered to begin and end at the point of zero displacement of the beam tip preceeding positive displacement. Values of all per-cycle energy dissipations (areas) are given in Table E.1.

TABLE E.1

ENERGY DISSIPATION - IN-KIPS/CYCLE

Specimen Number	Load Cycle Number											
	1	2	3	4	5	6	7	8	9	10	11	12
1	23.9	19.4	18.6	15.9	15.9	14.9	35.9	32.0	40.2	32.9	30.9	29.8*
2	24.6	19.1	17.6	16.9	16.3	15.6	37.1	34.1	37.5	37.7	36.2	34.5*
3	55.8	41.8	36.5	34.4	30.0	26.6	49.6	36.7				
4	59.4	46.1	42.6	40.3	38.7	37.1	73.2	70.3	57.2	44.9	34.5	
5	33.9	25.7	22.2	19.7	18.4	17.6	42.2	37.6	31.2	26.3	22.0	18.6
6	30.6	23.5	21.1	19.5	18.6	18.0	40.8	38.4	33.8	30.5	27.2	25.0*
7	54.5	39.4	35.9	30.6	27.6	25.2	48.9	42.8	33.2	26.9	22.4	19.3
8	57.3	42.2	37.1	33.8	31.6	28.9	60.0	53.9	41.3	32.2	26.4	22.8
9	232	184	166	154	145	139	247					
10	233	187	174	163	155	148	298					
11	205	160	142	118	98.4							
12	205	176	153	138	120	85.8	64.3					

*Specimens 1, 2, and 6 underwent 14 cycles of loading with energy dissipations as follows for the thirteenth and fourteenth load cycles:
Specimen 1: 28.5; 27.2
Specimen 2: 3.40; 32.6
Specimen 6: 20.4; 18.3

APPENDIX F

APPLICATION OF STRAIN GAGES

Special annealed Constantan foil high elongation strain gages were applied to selected reinforcing bars in each specimen. Usually the bars were prepared to accept the gages by filing off deformations and surface scale in a small area where the gage was to be applied. However, the main reinforcement in Specimens 1, 2, 3 and 4 was prepared by milling a flat area approximately 3/8 in. x 2 in. to accept the gage. After filing or milling, fine emery cloth was then used further to smooth the surface. The surface was also chemically cleaned with an acid cleaner and neutralizer.

Gages were positioned on the cleaned area with clear cellophane tape prior to application of adhesive. All gages, adhesive and accessories used in the application process were manufactured by Micro-Measurements Corporation. Gage EP-08-250BG-120 was selected for use on all sizes of reinforcement. When the gages had been correctly positioned, one end of the cellophane holding strip was raised and epoxy adhesive M-Bond AE-10 was applied to the back of the gage. The gage and tape were then returned to position on the bar and held in place for 24 hours by curved pressure pads and spring clips.

Belden #22 AWG three-lead cable was attached to each gage. Two leads were connected to one of the gage

tabs and the remaining lead was attached to the other tab. This procedure compensated for lead wire length. The lead wire was secured to the reinforcing bar to insure that no tension would be placed on the gage connection.

All gages were then waterproofed with M-Coat A polyurethane coating, M-Coat D acrylic lacquer and two coats of M-Coat B nitrile rubber coating. Each coat was allowed to dry thoroughly before successive coating was applied. Gages were then mechanically protected by applying M-Coat FB butyl rubber sealant and M-Coat FN neoprene rubber sheets. Cloth friction tape was wrapped over the rubber protective sheets to insure that they would not be disturbed during handling and fabrication.